Correlation between Parameters of the Tribosystem and Automotive Disc Brake Squeal

zur Erlangung des akademischen Grades eines
DOKTORS DER INGENIEURWISSENSCHAFTEN (Dr.-Ing.)
von der Fakultät für Maschinenbau
der Universität Paderborn

genehmigte
DISSERTATION

von
Dipl.-Phys. Martin Bernhard Hiller
aus Tübingen

Referent:	Prof. Dr.-Ing. habil. Jörg Wallaschek
Korreferent:	Prof. Dr.-Ing. habil. Kai Willner
Tag des Kolloquiums:	20.12.2006

‘Forty-two’ yelled Loonquawl. ‘Is that all you’ve got to show for seven and a half million years’ work?’

‘I checked it very thoroughly,’ said the computer, ‘and that quite definitely is the answer. I think the problem, to be quite honest with you, is that you’ve never actually known what the question is.’

Douglas Adams, The Hitch Hiker’s Guide to the Galaxy

Abstract

The friction coefficient and the pad/disc stiffness, perpendicular to the friction force direction, are considered important parameters for disc brake squeal. This is based on theoretical considerations of the brake squeal excitation mechanisms and brake system modeling. However, this is without experimental verification on a real brake system.

Because this work focuses on the disc/pad tribosystem parameter's influence on brake squeal, the friction coefficient and the pad's normal stiffness have been investigated. Experiments using different brake pads were carried out.

By analyzing the gathered data, the friction coefficient proved to have the most single correlation to the brake squeal propensity, however counter-examples to the general trend exist. The general trend of an increasing squeal propensity with increasing friction coefficient is mainly supported by the European Metallic type friction materials, which also tend to generate very high friction coefficient values during dynamometer testing.

In contrast to the friction coefficient, the pad's normal stiffness is not in-situ measurable with sufficient precision, so a model of the pad normal stiffness based on compressibility measurements was developed. Using this model a clear trend of an increasing squeal propensity with increasing friction coefficient and increasing stiffness can be found. The local trends for the different friction material tests add up to a similar global trend, but also produce counter-examples.

Linear squeal propensity regression models based on the friction coefficient and the stiffness were built and used to calculate the squeal propensity for each test. The deviations between the squeal propensity measurements and the calculated squeal propensities from the models are in a suitable range to reproduce general trends. However, the models are not able to precisely estimate the squeal propensity. This might indicate the existence of additional (unconsidered) parameters.

Data mapping functions have been used to calculate characteristic values based on the friction coefficient and the pad normal stiffness, one per brake application or one per test.

The correlation between the squeal propensity and these characteristic values, showed that the measured squeal propensity trends can be maintained throughout data pooling. By using specific characteristic values for squeal propensity models on the brake application and test timescale, the squeal propensity models are not worse than the measurement data based on squeal propensity models.

To judge the usefulness of the squeal behavior models, a ‘Model Quality Rating Measure’ was introduced. By using the squeal propensity regression models, the squeal propensity of each test was calculated. The deviations between the calculated and the measured squeal propensities were used to assess the model’s applicability. Additionally, the Quality Rating was used to arrange the different models by usefulness.

One of the squeal propensity models with the smallest deviations between measured and calculated squeal propensity for each test was built using a single characteristic value per test. It was based on the percentage of friction coefficient values above 0.5 during the test and on the modeled stiffness with a brake line pressure of 60 bar. This supports the assumption that higher friction coefficient values drastically influence brake squeal and that the squeal propensity is dependent on the pad normal stiffness, perpendicular to the friction force direction.

Acknowledgments

This PhD thesis is the result of my three year long activities as a research associate in the corporate research and development sector of Robert Bosch GmbH, in the department of Fluid Mechanics and Tribology in Gerlingen-Schillerhöhe, Germany.

Many people contributed to this dissertation in innumerable ways, and I am grateful to all of them. At this point I would like to thank all those who contributed, but are not explicitly listed below, as without the 'little helpers' no such work could be done successfully.

Many thanks go to Prof. Dr. Jörg Wallaschek for the supervision of my work. His sometimes unconventional but always visionary impacts helped to form both my thesis and myself. I do not remember a single discussion during which we did not make significant progress with the issue at hand.

I also would like to thank Prof. Dr. Kai Willner, who kindly accepted to write the second expert's survey. His remarks in the final stage of this work greatly contributed to form a coherent dissertation.

I would like to thank all members of the graduation committee for a mostly pleasant examination for a doctorate, namely Prof. Dr. Jürgen Gausemeier, Prof. Dr. Hans Jürgen Maier besides the already mentioned Professors.

I am deeply indebted to Dr. Ulrich Stolz, my supervisor at Bosch, for various fruitful discussions and his huge knowledge and experience in the field of brake tribology. More than once he kept me from setting unachievable goals, encouraging me to change them to be more realistic and scientifically desirable ones. I am very appreciative of his generosity with time, advice, and support, to name but few of his contributions.

I am very grateful to the Robert Bosch GmbH for giving me the opportunity to carry out this work. I would like to thank Dr. Klaus Dobler, former head of the Engineering Mechanics department at Robert Bosch GmbH, whose support made this work possible, Dr. Winfried Keiper for his support during his time as head of Bosch's brake NVH department at the (European) Chassis-Systems business unit and for his continued support

as head of the research department ‘Structural Mechanics’. I would also like to thank Dr. Peter Blaschke, former head of the brake NVH department at Bosch’s American Chassis Systems business unit for the opportunity to do parts of the research in Farmington Hills, MI, USA and for his further support as head of Bosch’s brake NVH department at the Chassis Systems business unit in Europe.

I would especially like to thank Karl-Heinz Hach for sharing his immense knowledge of brake systems and brake dynamometer testing with me and his support with my experiments. He is the prime example of a helping hand, taking a back seat, but without him such a work would not have been possible.

I also want to thank Dr. Mohamed Khalid Abdelhamid, head of the dynamomter group at Bosch’s American NVH department for his support during the last years, especially during my time in the United States and for the careful proof-reading of this thesis.

For providing specially designed friction materials I thank Phil Ferdani and Dr. Alastair Bissett from Federal Mogul. I want to thank them also for the discussions about brake material tribology, which have been very enlightening for me.

For sharpening various expressions, great thanks go to Tyson Burnett.

During my time in the brake business I met or talked to a large variety of people at Bosch all over the world. They all contributed in some way to this work, providing information or support or by making my time more enjoyable. I want to thank my (partly former) colleagues from the United States’ business unit, Dr. Ralph Allgaier, Charles J. Evans Jr., Mingan Tan, Michael Chang, Alex Wang, Steve McGinnis, Jim Malosh, and all students. From the Japanese business unit, I would like to thank Nick Dodson, from France Thibault Hoguet and Thierry Pasquet. From Abstatt’s business unit I thank Sabine Ansmann, Uwe Bretz, Thomas Dewald, Eric Dutt, Thilo Eickhoff, Martin Hering, Manuela Koch, Uwe Langhauser, Julian Staack, Volker Scheef, Alexander Geilfuss, and Manfred Hohenstein. I also want to thank Sven Nielsen, Harald Schorr, Dr. Marcus Simon, Jürgen Vdovak and all other people at Schillerhöhe’s tribology research group, at the prototyping department and my fellow doctorial student colleages.

At last I want to thank my parents, family and friends. Their love and support kept me going even in hard times. Ulrike, Niklas and Christian Harms made each cloudy day a little bit brighter. Our cat Maxi kept sitting on the finished and unfinished pages of this work, thus reminding me it is still just paper. The most heartfelt thanks go to Eva Renz for her patience with me and this thesis and for making my life with her worth living - every single day.

Martin Hiller, *March 2oo7*

Contents

Variables

Symbol	Description	Unit
a	Acceleration	m/s^2
A	Area	m^2
c	Stiffness	N/m
c_{b}	Brake pad bulk stiffness	N/m
$c_{\text{b,0}}$	Normal force independent part of the pad bulk stiffness	N/m
c_{c}	Contact stiffness	N/m
c_{leading}	Stiffness of leading spring in [49]	N/m
c_{trailing}	Stiffness of trailing spring in [49]	N/m
d	Compliance	m/N
E	Young's modulus (direction see index)	N/m^2
f	Numerator of stiffness model	N^2/m^2
freq	Squeal frequency	Hz
F_{r}	Friction force	N
g	Denominator of stiffness model	N/m
m	Mass	kg
m^*_{vehicle}	Amount of vehicle mass to be decelerated by the brake	kg
M	Torque	$N \cdot m$
M_{B}	Braking torque	$N \cdot m$
n	Number of measurements	
N	Normal force	N
O	Occurrence, number of data points for which noise was detected	
p	Brake line pressure	N/m^2
$p_{\text{threshold}}$	Threshold brake line pressure	N/m^2
P	Suspected propensity (Bernoulli's law)	
r_{eff}	Brake's effective friction radius	m
r_{dyn}	Dynamic running radius of vehicle wheel	m

Symbol	Description	Unit
R^2_{adj}	Adjusted multiple coefficient of determination, cp. [65]	
SI	Squeal index, squeal propensity	
ΔSI	Difference between 'measured' and modeled squeal propensity	$\%$-*age* $points$
SSE	Sum of squared errors (cp. [65])	varies
t	Time	s
T	Brake disc temperature	$^\circ C$
v	Vehicle velocity	m/s
z	Displacement in axial direction (cp. fig. 2.1(a))	m
α	Characteristic value on different timescales	varies
χ_j	parameter j, the absolute differential dz depends on	varies
ζ	Coefficient from regression model	varies
η	Brake's efficiency	
Γ	Transformation to map data onto a different timescale	
ε	Absolute deviation between SI measurement and true, but unknown squeal propensity	
Θ	Moment of inertia	$kg \cdot m^2$
κ_i	Compressibility during i-th cycle	μm
λ	Coefficient of linear increase of stiffness with normal force	$1/m$
μ	Coefficient of friction	
σ	Standard deviation, statistic error of parameter according to index	varies
τ	Time between two measurement points (equal to 1/(sampling rate))	s
Φ	Angle between trailing spring and friction force in [49]	$degrees$
Ψ	Statistical confidence level	
ω	Angular velocity	$1/s$

Indices

Index	Type	Describtion
ˆ	upper	Parameter value or dependence calculated by a regression model
¯	upper	Average value of parameter
˜	upper	Mean value of particular parameter space
b	lower	Parameter related to the friction material bulk
ba	lower	Measured or calculated parameter value on the ‘one value per brake application’ timescale
B	lower	Parameter related to the brake
c	lower	Parameter related to the contact at the friction interface or stiffness
dynamometer	lower	Parameter related to a brake dynamometer
flywheel	lower	Parameter related to mechanical inertia simulation with flywheels
fin	lower	Final value at end of brake application
i	lower	Number of measurement, characteristic value or data mapping
ini	lower	Initial value at begin of brake application
kin	lower	Kinetic (e. g. energy)
measured	lower	Measurand or parameter calculated based on measured data
model	lower	Parameter related to a model
motor	lower	Parameter related to the electric motor powering a dynamometer
M	lower	Parameter related to brake torque
p	lower	Parameter related to brake line pressure
pad	lower	Parameter related to pad
piston	lower	Parameter related to piston
real	lower	Theoretical or (unknown) true value
rt	lower	Measured or calculated parameter value on the ‘real-time’ timescale
rot		Parameter related to a rotatory motion
sim	lower	Parameter related to dynamometer inertia simulation
T	lower	Parameter related to brake disc temperature
v	lower	Parameter related to vehicle velocity
vehicle	lower	Parameter related to vehicle

Index	Type	Describtion
tt	lower	Measured or calculated parameter value on the ‘one value per test’ timescale
wt	lower	Weighted model
x	lower	Tangential direction, as shown in fig. 2.1(a)
x,y	lower	Lateral, within the x-y-plane
y	lower	Radial direction, as shown in fig. 2.1(a)
z	lower	Axial direction, as shown in fig. 2.1(a)
μ	lower	Parameter related to friction coefficient

Abbreviations

Abbreviation	Description
ABS	Antilock Braking System
EM	European Metallic Friction Material
ESP	Electronic Stability Program
FE	Finite Element
FEM	Finite Element Method
FM	Friction Material
FRF	Frequency Response Function
GfT	Gesellschaft für Tribologie (Society of Tribology, *German*)
LACT	Los Angeles City Traffic (vehicle testing)
LDV	Laser Doppler Vibrometer
LM	Low-Steel Low-Metallic Friction Material
MQRM	Model Quality Rating Measure (as introduced in chapter 5.4)
NAO	Non-Asbestos Organics Friction Material
NS	No-Steel Low-Metallic Friction Material
OEM	Original Equipment Manufacturer
SAE	Society of Automotive Engineers
SI	Squeal Index
SM	Semi-Metallic Friction Material
SPL	Sound Pressure Level
SUV	Sport Utility Vehicle

1. Introduction

Brake squeal phenomenon has been studied for nearly 70 years now. During this time many researchers have contributed to solving parts of the problem, but until now, no comprehensive solution is available.

For the brake industry, an intrinsic completely noise free brake system would be a significant competitive advantage. Based on the consideration of the brake squeal excitation mechanism, brake squeal generation is dominated by factors, which are part of two different fields: structural mechanics and tribology. The recent research efforts more and more focus on simulation methods, like the Finite Element Method. These methods investigate the structural components of the vibrating system in detail, e. g. the resonant frequencies. However, parameters of the tribosystem, like the friction coefficient, are only of secondary importance in these considerations.

On the other hand, different models with few degrees of freedom are mainly used to explain the excitation mechanisms or to state general trends. Some of these models estimate the friction coefficient and the stiffness perpendicular to the friction force direction to be dominant parameters for the brake system instability.

So far, no experimental proof has been given, if the friction coefficient and the stiffness are dominant parameters in brake squeal generation. Also, it is unclear if the stiffness from small degree of freedom models can be easily related to the normal stiffness of the brake system. For the investigated brake system, the stiffness perpendicular to the friction force direction is mainly influenced by the brake pads. This stiffness will further also be called (pad) normal stiffness. Unfortunately, it is not yet possible to measure the normal stiffness of the pad during brake dynamometer testing. However, if it is possible to model the pad normal stiffness, e. g. based on compressibility measurements, the correlation between squeal behavior and pad normal stiffness can be investigated.

This work focuses on the tribological influence on brake squeal. From a tribological point of view, it has to be experimentally verified, if the most important parameters of the

brake/disc tribosystem, the friction coefficient and the pad's normal stiffness, influence brake squeal. Additionally it has to be investigated, whether these parameters are able to dominate the squeal behavior in a way, that allows finding correlations.

A preferable way to estimate important contributors to brake squeal is to model the squeal behavior and assess its dependence on the different input parameters. By so doing, the influence of each single parameter and each parameter combination can be tested, different tests can be compared and an overall picture of the squeal behavior dependence on tribosystem parameters can be produced.

To judge the usefulness of the squeal behavior models, a 'Model Quality Rating Measure' (MQRM) must be found that allows the assessment and ranking of different models according to their usefulness and applicability. Based on MQRM, it has to be determined, whether a parameter influence on, and a correlation to, the squeal behavior exists and how dominant this influence is.

Brake noise testing generates a huge amount of data. Therefore, it is common practice in the brake industry to pool the real-time data and calculate characteristic values. A single so-called nominal friction coefficient is calculated from a whole dynamometer test procedure's data. It is unclear, if these characteristic values correlate to the squeal behavior and which characteristic values are best for this purpose. However, by modeling the squeal behavior based on characteristic values derived from real-time data, this can be investigated.

2. Literature Review

In this chapter the present state of knowledge concerning the scope of this work is presented. After a short overview of the brake assembly, tribological aspects of brake systems are shown.

Subsequently, a closer look is given to friction in general, leading consequently to automotive disc brake friction materials in particular. The second focus of this work is on elastic properties, their measurement and the role of the contact between brake pad and disc on these elastic properties.

Thereafter, the brake squeal phenomenon is presented. This includes the squeal excitation mechanisms and dependencies of brake squeal on various parameters and a section about brake squeal measurement. The brake squeal analysis section is the connection to the brake testing block. Here, different types of dynamometers as well as different dynamometer operational modes and testing procedures are presented.

2.1. The Brake Assembly

2.1.1. Brake Components

The brake system can be divided into three subsystems. The mechanical subsystem, further called the brake assembly, the hydraulic subsystem including the brake booster, master cylinder and ABS pump, and the electronic subsystem with the control units of ABS, ESP etc.

In this section the brake assembly and its common modeling approaches will be presented. For details on the other subsystems see Bosch's Automotive Handbook [16].

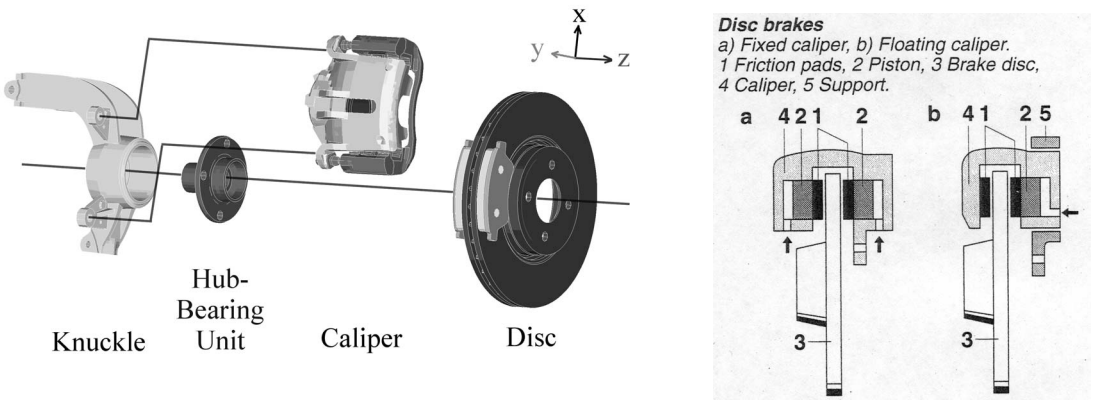

(a) Overview **(b)** Brake calipers (cp. [16])

Figure 2.1.: *Brake Assembly*

2.1.2. Overview and Coordinate System

An overview of the brake assembly is presented in figure 2.1 (a). The disc is mounted on the hub bearing unit, which is carried by the knuckle. There are two categories for brake calipers, fixed and floating calipers, as shown schematically in figure 2.1 (b). In the case of a fixed caliper, the housing is rigidly connected to the knuckle and at least one piston on each side of the brake disc forces the pad against the disc. For the floating caliper, one or more pistons exert direct pressure on the inside friction pad. The floating caliper then pushes the outer pad against the disc. Both, pad and floating caliper, are guided by the anchor bracket. While fixed calipers are attached directly to the knuckle, for floating calipers the anchor bracket is attached to the knuckle [16].

To ease the discussion of numerous motions, forces or elastic properties a coordinate system will be presented here, as the directions of all these forces and motions are crucial to the value. So, for this work, the z-direction is the axial direction, which is normal to the disc surface. The tangential direction is indexed by x, and y is the radial direction as shown in figure 2.1 (a). In-plane and out-of-plane are often used in the literature to describe disc modes or motions within the xy-plane (in-plane) or perpendicular thereto (out-of-plane). The edges of the brake pad are usually named inner edge (small radial distance) and outer edge (large radial distance) in the y direction and depending on the direction of disc motion leading edge (where a specific disc segment first touches the pad) and trailing edge (where the segment touches the pad last). From the pad point of view,

the rotation of the disc takes place from the leading edge to the trailing edge. The two different pads are called inner or piston side pad and outer or finger side pad, respectively. The inner pad, as the name suggests, is the pad on the piston side of the disc, which is (for the floating caliper) the side more inside the wheelhousing.

2.1.3. Brake Disc

During the application of the brake, kinetic energy is mainly transformed into heat to decelerate a vehicle. The main part of this generated heat is stored in the brake disc. According to Kemmer [58], pearlitic gray cast iron with 3 - 4 wg. % carbon has been settled upon as the most widely used brake disc material, due to low cost, good machineability and well-balanced properties (high heat conductivity and vibration damping due to the flaky graphite, reasonable heat capacity and thermal stability).

According to Bargel and Schulze [6] the flake graphite is also the reason for different behaviors under tensile and compressive stress. The compressive strength (~600 MPa to 720 MPa, according to Deike et al. [30]) is 3 to 4.5 times higher than the tensile strength (~150 MPa to 300 MPa, [30]). This behavior forms a stress dependent Young's modulus, which decreases with increasing tensile stress. The compressive stress, usually generated by brake applications, is less load dependent and in the range of 78 GPa to 113 GPa (values according to Deike et al. [30]).

The brake disc consists of the friction ring, where the contact between brake pads and disc takes place, and the hat section, where it is mounted on the hub bearing unit. For lighter vehicles the friction ring is solid, while for heavier or high performance cars and trucks vented discs, two friction rings are connected via vanes for better heat dissipation, are used.

2.1.4. Brake Pads

Besides transforming kinetic energy into heat, there are various needs, which should be met by the friction couple, namely by the brake pads and disc, in a disc brake. These needs include low wear rates, good machineability, stability of the coefficient of friction and low price among other things, as described by Blau [13], Kemmer [58] or Nguyen and Taylor [69]. Changes to improve the friction couple are mostly made within the brake pad.

Table 2.1.: *Typical ranges of the more common constituents of brake pads (cp. [13])*

Category	*Constituent*	*Range [vol%]*	*Typical value [vol%]*
Binder Materials	Phenolic resin	10 - 45	20 - 25
Fillers and Reinforcements	Barium sulphate	0 - 40	20 - 25
Fillers and Reinforcements	Fibers	5 - 30	n. s.
Fillers and Reinforcements	Cashew particles	3 - 30	15 - 20
Friction Modifiers	Graphite	0 - 15	5 - 7
Friction Modifiers	Metal sulphides	0 - 8	0 - 5
Friction Modifiers	“Friction dust”	0 - 20	n. s.
Abrasives	Abrasives	0 - 10	2 - 3

The mechanical strength of brake pads is mainly achieved by a metallic backplate. In a complex process 10 - 20 different ingredients in powder form are pressed on the backplate [69]. This part of the brake pad is normally referred to as friction material (FM) or lining [58], while the mix of ingredients is called formulation within the brake industry. To improve adhesive strength and damping of the friction material, an underlayer with a different composition is inserted between the backplate and the friction material before pressing. On the reverse side of the backplate often a shim (also called insulator) is attached to the backplate to decrease emitted noise.

According to Blau [13] the ingredients may be grouped based on their expected functions into abrasives, friction modifiers, fillers and reinforcements or binder materials. A lot of different materials are used within each category as summarized by Blau [13] or, within a more recent review of automotive brake friction materials, by Chan and Stachowiak [23]. Typical compositions of industrial friction materials are shown in table 2.1. While nearly all of the constituents are self-explanatory, ‘Friction dust’ commonly consists of processed cashew shell resin and may have a rubber base which includes some additives used to reduce spontaneous combustion or help particle dispersion.

A common classification of disc brake pads is based on its ferrous and non-ferrous metal content as shown in table 2.2. In some publications (e. g. by Chan and Stachowiak [23]) the No-Steel Low-Metallic friction material type is also termed Non-Asbestos Organics friction material (NAO), which is a quite confusing term, because asbestos have been banned in friction materials nearly throughout the whole world since the 1990s. According to Wiaterek [20, chap. 23] in Japanese friction material philosophy NAO refers

Table 2.2.: *Friction material type classification (analog to [22])*

Category	*Abbr.*	*Metal content [wt %]*	*Metal type*
Semi-Metallic	SM	≥ 40	ferrous
Low-Steel Low-Metallic	LM	≤ 15	ferrous and non-ferrous
No-Steel Low-Metallic	NS	≤ 15	non-ferrous
European-Metallic	EM	$15 - 40$	ferrous and non-ferrous

to friction materials with organic binders and without steel wool.

A broad survey of needs, composition, production and quality assurance of brake pads is also given by Oehl and Paul [70].

2.2. Brake System Tribology

In this section, the tribological system of disc brakes is presented. After looking at the definition of tribology and the tribological system, the contact situation in disc brakes, friction and the elastic properties of brake friction materials are discussed.

2.2.1. Tribological System of Disc brakes

The first definition of tribology was stated by Jost [56]: “Tribology is the science and technology of interacting surfaces in relative motion and related subjects and practices.”

According to DIN 50 323 tribology embraces the science and associated technology devoted to the interaction of surfaces in mutually opposed states of motion (cp. tribological concepts in [16]). It focuses on the entire range of friction, wear and lubrication, and also includes the effects at the contact surfaces of solids as well as those between solids and gases.

As shown in figure 2.2 and described also by Czichos and Habig [28], a tribological system or tribosystem consists of the material elements, the properties of these elements and the reciprocal effects between the elements. The elements’ properties and their reciprocal effects form the structure of the tribosystem. As the composite stress factor, e. g. forces, motion and temperatures, acts upon this structure it is transformed into useful quantities and loss quantities. This classification depends also on the particular system - in figure 2.2 the friction is listed as a loss quantity, but for the brake system friction is

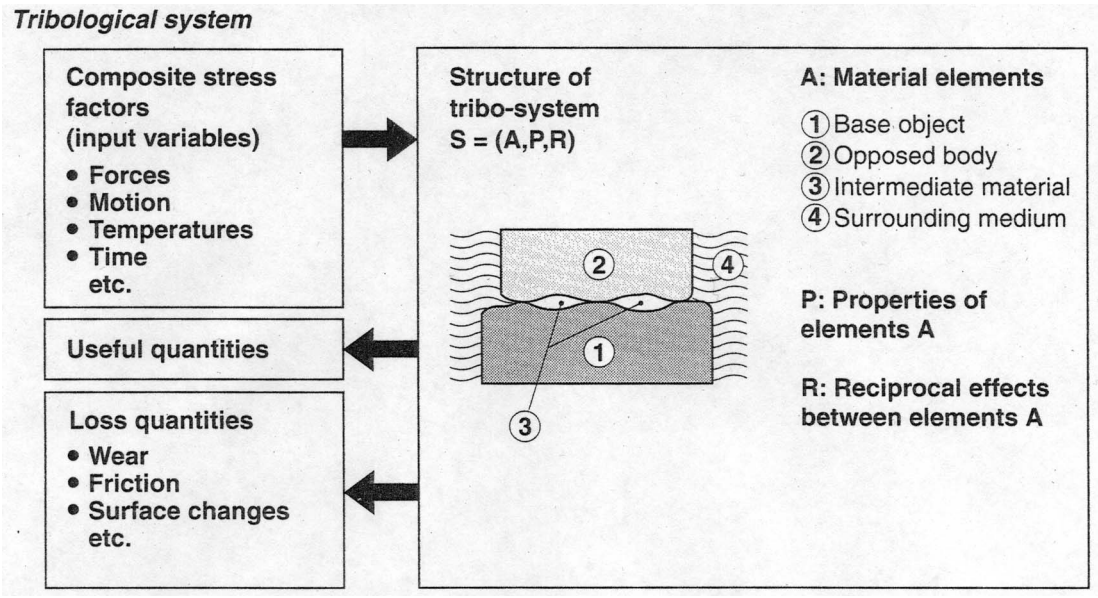

Figure 2.2.: *The tribological system (cp. [16])*

both wanted and useful. Because tribological stresses are surface stresses, the previously-mentioned properties must also be viewed as surface characteristics.

2.2.2. Contact Situation of Disc Brakes

Hertz was the first to solve the normal contact problem in 1881. According to Mao et al. [64] Hertz' theory is for perfectly smooth surfaces of elastic homogeneous and non-conforming bodies and the surfaces are assumed to be frictionless, so that only a normal pressure is transmitted between them.

Since then, various authors have expanded the understanding of contact mechanics, which is far beyond the scope of the present work. A summary and further references are presented by Willner [96].

Real surfaces are generally rough. Therefore the real area of contact, where the asperities of the opposing rough surfaces are in contact, is only a fraction of the nominal macroscopic area of contact. According to Bowden and Tabor [17], if two solids are placed in contact, the upper surface will be supported on the summits of the irregularities, and large areas of the surfaces will be separated by a distance, which is large compared with the molecular range of action. They expect that in most practical cases, for all types and shapes of surface irregularities, the real area of contact will be very nearly propor-

tional to the load. They found a linear load dependent area of real contact for steel and silver surfaces by measuring load dependent electrical resistances.

While theoretical calculations of the true area of contact are acceptable for static contact, there is no reliable theoretical or experimental method of determining this area during sliding, according to Ibrahim [54]. Thomas [87] stated that the assumption, most engineering surfaces would have a Gaussian summit height distribution, should be used with caution and that the technical important process of grinding should not produce a Gaussian height distribution. Nevertheless, Thomas stated that the Gaussian assumption is rather robust, and even for undeniably non-Gaussian surfaces it yields statistical predictions which are in good agreement with experiments.

Even though the theoretical details of these contact models are not necessary for this work, the relationship between the contact stiffness and the normal load is crucial for the stiffness model of the tribosystem presented later. Thomas and Sayles [88] showed a load dependent contact stiffness dependence for a Gaussian height distribution of elastic asperities using the model of Greenwood and Williamson [47]. This contact stiffness c_c shows a linear dependence on the normal force N with λ_c as a factor:

$$c_c = -\frac{dN}{dz} = \lambda_c \cdot N \tag{2.1}$$

Sherif [82] confirmed for elastic contact, that on principle, the contact stiffness increases with increasing load. He investigated the contact model of Greenwood and Williamson as well as the one of Onions and Archard, which is based on the results of the theory of Whitehouse and Archard. The behavior of contact stiffness variation with normal load is in both cases similar to that of a stiffening spring.

According to Persson [75] every height distribution, in which the number of asperities of a given height decreases rapidly with increasing height leads to an approximate exponential force vs. axial-displacement relationship, thus leading to a λ changing quite slowly with axial displacement. Thomas and Sayles [88] showed a constant λ to be a good approximation as the axial displacement is only varied to a minor extent by the usual applied normal forces during brake applications. This is especially true for for the typical practical vibration condition of a relatively small periodic normal force variation superimposed on a large static normal preload.

For disc brakes, multiple authors have done research on the contact situation in recent years. Based on their experimental research Eriksson and Jacobson [38] introduced the

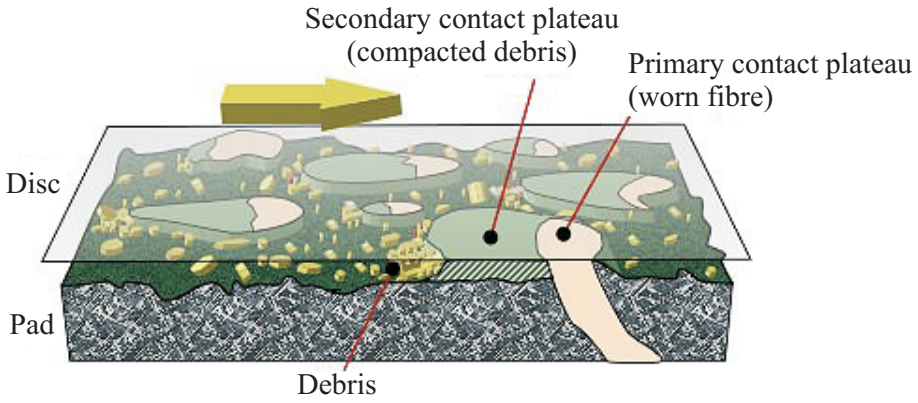

Figure 2.3.: *Schematic of the contact situation between an organic brake pad and a brake disc (cp. [38])*

theoretical concept of the disc brake contact situation processes, schematically shown in figure 2.3: The primary plateaus are first formed, due to better wear resistance of some ingredients (mostly fibers) with regards to the three-body abrasion generated by wear debris [40]. Debris, in the form of small particles, piles up against the primary plateaus, as observed in-situ by monitoring the contact of pads running against a glass disc [40]. The normal pressure, shear forces and the frictional heat combines to compact the debris, forming secondary plateaus. The lateral size of the secondary plateaus varies with the brake pressure, as described in [40] and [35]. The top layer of the secondary plateaus is less than 1 μm thick, more homogeneous (compared to the rest of the 5 - 10 μm thick secondary plateau) and has nanoindentation hardness values, which are in the same range as the fibers, according to Eriksson and Jacobson [38].

Österle and Bettge [71] investigated a brake friction material using topographic examination methods such as a confocal laser scanning microscope and an interference microscope as well as micro-analytical and surface layer characterizing methods like scanning electron microscopy, light microscopy and Focused Ion Beam. They contradicted Eriksson and Jacobson [38] that the characterization of contacting surfaces as plateaus protruding from the surface is generally valid. However, they did confirm a lower roughness on the contacting surfaces compared to the area surrounding them.

Kemmer [58] experimentally investigated the friction layer between pad and disc and modeled it as a granular medium. In his simulations he found the contact stiffness of the granular friction layer to be directly dependent on the particles' diameter, the shear modulus of the particles' material, the friction coefficient for the interactions among the

particles, the normal force, and inversely dependent on the friction layer's thickness. With his experiments, he showed that for one friction material, higher pressures lead to smaller wear debris particles.

In various publications (e.g. [2],[46],[61] or [74]), the Finite Element Method (FEM) is used to model disc brakes, mostly to investigate brake noise. In these studies, often an extra look is taken on the contact situation by modeling the contact with different elements. The stiffness or Young's modulus at the contact is assumed to depend on (local) forces, while for the rest of the friction material commonly constant elastic properties are used.

2.2.3. Friction

Various authors, e. g. Bowden and Tabor [17], Dowson [32], Ibrahim [54] and Kemmer [58] have summarized the history of friction. The very first recorded theory, that 'Friction produces double the amount of effort if the weight be doubled', is attributed to da Vinci [29], as described in [17] and [32]. In the following decades and centuries, numerous researchers have improved our understanding of the friction phenomenon, e. g. Amontons [4] and Coulomb [26].

While the exact history of friction and the achievements of each researcher can be read in the cited sources, the most recent 'definition' of friction by the GfT (Society of Tribology) states friction as an interaction between contacting bodies, which acts opposite to relative motion [45]. Commonly, the terms friction and friction force are used in an equal sense, while friction is the interaction and the friction force is the force resulting from this interaction.

The friction coefficient μ is commonly defined as factor between the friction force F_r and normal force N [15], namely

$$\mu = \frac{F_r}{N}$$

Today, it is common knowledge, although often disregarded, that friction is not an intrinsic property of the two contacting materials, but a material- *and* a system property [15]. According to Blau [15] the number of potential friction-affecting factors is large and models for friction have used geometric arguments (surface roughness and asperity interlocking), mechanical properties-based arguments (shear based properties of the solids and of the substances between the surfaces), fluid dynamics approaches, considerations of electrostatic forces between surface atoms, and chemical compatibility arguments.

Czichos and Habig [28] classify the friction mechanisms into adhesion with shearing, plastic deformation, plowing or abrasion, and elastic deformation with hysteresis and damping. They further state that only under idealized simplified conditions there is a correlation between friction mechanism and macroscopic friction force. In operational systems the elemental friction mechanisms superpose in temporal and regional changing fractions. This leads, according to Czichos and Habig [28], to an inability of theoretical prediction of friction behaviors, which is also confirmed by Ibrahim [54] for many dry extended contacts.

Blau [15] advises that the use of the friction coefficient is not appropriate in some cases. He finds the term ambiguous for the 'stick-slip' phenomenon or in micro- or nano-tribology, where the coefficient of friction during scratching becomes a strong function of the tip geometry. An example of the friction phenomena in nano-tribological investigations with an atomic force microscope is given in [51].

For disc brake systems, the tribometer design is within the torque measurement category, according to the classification given by Blau [14]. For most brake dynamometers no direct measurement of the normal- or the friction force are implemented. The coefficient of friction is calculated from brake torque M_B and brake line pressure p measurements as specified in the SAE J2521 standard [94] and shown in equation 2.2:

$$\mu = \frac{M_B}{2 \cdot (p - p_{\text{threshold}}) \cdot r_{\text{eff}} \cdot A_{\text{piston}} \cdot \eta} \tag{2.2}$$

The threshold pressure $p_{\text{threshold}}$ is usually assumed to be 0.5 bar for disc brakes, the effective friction radius r_{eff} is defined as the radius to the center of the piston, whose area is A_{piston} and the efficiency η is assumed to be 100 %, according to the SAE J2521 specification [94].

For automotive disc brakes, the friction behavior has been investigated by various authors. A typical phenomenon for brakes is an increasing mean coefficient of friction per brake application during the first brake applications with new brake pads and disc (cp. e. g. [58]) or after a period of inactivity [92], called run-in behavior. Therefore, the number of brake applications conducted with same controlled parameters, until a stable mean coefficient of friction per brake application is reached, is called run-in period. Kemmer [58] found a lower friction coefficient resulting from interventions against the tribological interface, such as removing the particles between the pad and disc with compressed air, which fully recovers to the previous value after a repetition of the run-in period.

During the run-in period a third body is formed. According to Kemmer [58] a transfer film is attached to the disc while a friction film forms on the friction material surface. Trapped between these layers are wear particles mainly originating from the brake pads, which are called a friction layer [58] and form the films (and plateaus [40]). The friction film was also investigated by Filip et al. [43], who found no simple correlation between composition of the friction film and friction material formulation. Gudmand-Høyer et al. [48] found no transfer layer for stops with moderate energy and power ('low duty'), while there was a larger transfer layer after a test with 'high duty' stops. Österle et al. [72] investigated friction and transfer films and showed that oxidation processes play an important role in the development of the third body on a surface of friction-producing couples. From his modeling of the friction layer as granular medium, Kemmer [58] found inverse dependencies of the friction coefficient on the wear particle diameter, shear modulus and normal force. While an increasing coefficient of friction among the particles, friction layer thickness (for thin layers), disc roughness angle and height of pad plateau led to higher friction coefficients. Kemmer [58] showed experimentally for one pad material that smaller wear debris particles within the interface, which were generated with higher brake line pressure during a run-in period, led to a higher coefficient of friction.

According to Eriksson et al. [37] the coefficient of friction is higher for decreasing brake line pressure than for increasing normal load during an experiment with continuously changing brake line pressure. Eriksson [34] states that the reason for the run-in behavior and the increase of the friction coefficient during a brake application, normally with decreasing velocity and thus called in-stop friction increase, is mainly correlated to the formation and shape adaption of the contact plateaus. Eriksson and Jacobson [39] confirmed the velocity dependence by making brake applications with increasing velocity. They concluded, that the coefficient of friction depends on the absolute value of velocity rather than on the velocity change. Stolz et al. [86] showed by conducting acceleration brake applications that the in-stop friction increase is usually not dependent on temperature or a brake time effect, but is velocity dependent.

Dörsch [31] investigated the periodic change of local contact variables. Using an infrared thermo-camera he observed nearly periodic radial oscillating temperature rings on the brake disc. The oscillating frequency and peak temperature increased with increasing energy per brake application. The radial size and peak value of the ring temperature is also a function of the pad hardness. The oscillation of temperatures indicates an oscillating contact radius, which is supported by the measured in-phase oscillating brake

torque. The measurement of local friction coefficients with a specially designed machine, enabled him to detect increasing friction coefficients on the pad during the run-in period. He also found areas with a similar local coefficient of friction in the circumferential direction, while the coefficient of friction in the radial direction differs over the investigated area. However, as the local friction coefficient could not be measured in-situ during brake application, the test was interrupted and the brake pads' friction coefficient was measured with an external analyzer. As the friction coefficient is not only a material- but also a system property the measured local friction coefficients might differ from the local friction coefficients during brake application.

Kemmer [58] showed, that the history of a brake system, which consists of the collectivity of all previous brake applications, modifies the tribological interface in a deterministic way. The condition of the tribological interface determines the friction characteristics, e. g. the value of the friction coefficient. For randomly varied brake line pressure, initial and final velocity and initial temperature statistical regression models are not able to describe the behavior of the friction coefficient satisfactorily, because of friction coefficient changes due to brake history, resulting in so-called history effects [58]. Nevertheless, parameter dependency tendencies can be obtained from such models.

2.2.4. Elastic Properties of Disc Brake Friction Materials

The elastic properties of friction materials are anisotropic, temperature and history dependent, and nonlinear, according to Richmond et al. [77]. They showed uniaxial stress/strain curves (in the z-direction) of friction materials in tension and compression. In tension, the material behaves as if it has a very low yield stress, but then hardens isotropically. In compression, the results are very different, the material has a much higher strength, becomes progressively stiffer as the normal force is applied and the load versus deflection curve shows a hysteresis.

For brake pads, non-destructive testing is preferred, mainly because the brake pads are normally tested before dynamometer tests are conducted. Therefore, the estimation of material properties usually differs from the standardized tests, e. g. described by Bargel and Schulze [6].

The procedure used for defining pad axial stiffness (ISO 6310) uses a widely known compressibility machine, and is mainly used as an important factor for brake pedal feel, e. g. as investigated in [50]. The brake pad is placed between a flat surface on its disc

Table 2.3.: *Elastic properties of brake friction materials (cp. [18])*

Physical value	*Range*	*Unit*
Compressive strength (z-direction)	30 - 100	MPa
Compressive strength (x-direction)	20 - 70	MPa
Young's modulus E_x (Grindosonic)	2 - 15	GPa
Young's modulus E_x (Ultrasound)	5 - 25	GPa
Young's modulus E_z (Compressibility)	0.3 - 3	GPa

side and an adapter, which has the dimensions of the piston in the x and y directions. While applying force, the compressive deformation is measured. From the measured deformation, the (mainly) axial Young's modulus or a stiffness in axial direction can be calculated [5]. Augsburg et al. [5] found an increasing axial pad stiffness with increasing normal force preload and with increasing frequency of a normal force oscillation.

Rinsdorf [79] also conducted measurements of the quasi-static elastic properties of brake friction materials. By cutting out samples from the brake pad he was able to estimate the compressive Young's moduli in axial and tangential directions in a similar way as described above. Additionally, he estimated the tangential Young's modulus with a four point bending test and found them to be 20 % less compared to moduli from compressive or tensile tests. One explanation for this difference is the inhomogeneity of the friction material, which influences the bending test a lot more than the compressive or tensile material testing.

By using an ultrasonic test method, elastic moduli at a frequency of 1 MHz can be determined. By fixing the samples between a transmitter and a receiver the Young's and shear moduli in all directions can be calculated from the time it took for the waves to pass through (cp. [5] and [19]). During conducted ultrasonic measurements a transversal isotropic material behavior is observed and a ratio between the lateral Young's moduli $E_{x,y} = E_x = E_y$ and the axial Young's modulus is $E_{x,y}/E_z \approx 3.8$, according to Brecht [18]. He also presented the natural frequency technique, where the Young's modulus is measured by using a mechanical impulse to induce a bending vibration in a bar-shaped

sample (Grindosonic). This very simple method calculates the lateral Young's modulus based on a linear isotropic material law. Brecht [18] investigated the temperature influence on the lateral Young's modulus, which has the lowest value of approximately 8 GPa at 400 °C during increasing temperature and the highest value of approximately 16 GPa at 300 °C (decreasing temperature).

Schmalfuß [81] investigated the frequency dependence of brake pad damping with a hydropulse compressibility machine in the frequency range up to 100 Hz. For a sinusoidal external normal force oscillation, she found a decreasing energy dissipation per cycle with increasing preload, which is the mean value of the normal force. With increasing oscillation frequency, the energy dissipation per cycle increases.

An overview of typical ranges of elastic friction material properties at room temperature is given by Brecht [18] and shown in table 2.3.

2.3. Brake Squeal

In the last couple of years brake noise has become the leading cause of customer complaints regarding brake systems. From a commercial point of view, solving the brake noise problem would save a lot of money and be a competitive advantage. Brake noise does not compromise the function and safety of the brake, but it has become a major comfort problem, because todays vehicles are becoming increasingly quieter. After classifying the type of brake vibrations a short survey of the brake squeal mechanisms is given in this section. The section closes with a summary of parameter dependencies of the squeal phenomenon for both, modeling and experimental approaches.

2.3.1. Types of Brake Vibrations

According to Wallaschek et al. [95] brake vibrations and noise are usually named according to how they sound (or feel) and are classified as following:

- Judder is a low frequency (< 100 Hz) forced vibration, excited by cyclic non-uniformities of the friction force. The vibration frequency is proportional to the wheel speed and often the amplitude of vibration varies due to the resonance amplification of suspension or vehicle structure modes.
- Groan, moan and howl are characterized by one or more single frequency pure tones, whose frequencies are generally independent of wheel speed, temperature

and pressure. The key feature of this type of vibration is that the energy flow into the system gets synchronized in phase with a vibration mode of the structure, resulting in a positive feedback loop. Groan and moan are usually associated with lower frequencies (100 Hz - 500 Hz) than howl (500 Hz - 1 kHz).

- Low-frequency squeal is associated with frequencies between 1 kHz and 3 kHz. High-frequency squeal covers the range from 3 kHz to 20 kHz. It is generally accepted that brake squeal (as well as groan, moan and howl) are a result of self-excited oscillations. Squeal frequencies are in general nearly invariant, because they are strongly coupled to the resonances of the brake system.

- Wire-brush is a superposition of high frequency oscillations with randomly varying amplitude. According to Crolla and Lang [27] it is often observed prior to the occurrence of squeal.

- Squelch is a superposition of several high-frequency vibrations resulting in a low-frequency amplitude modulation of the envelope. While the frequencies of the carrier waves are in general time-invariant, the lower modulation frequency is continually variable.

2.3.2. Squeal Mechanisms

The first sets of investigations on brake squeal were conducted by Mills [66]. As described by Kinkaid et al. [59], Mills attempted to correlate friction pairs, showing a decreasing friction coefficient with increasing sliding velocity, to the occurrence of drum brake squeal without arriving at any definitive conclusions. Since then, a lot of research on the field of brake squeal mechanisms has been done, which will be summarized in this section.

Although some of the shown squeal mechanisms are said to be not important for squeal, some researchers (e. g. Chen et al. [25] and Mottershead and Chan [68]) concluded that it is likely that there is no unique mechanism, which is solely responsible, but that squeal may be triggered by any one of a number of mechanisms. Figure 2.4 shows a categorization tree for friction induced vibrations in brakes as proposed by Hultén [53]. Please note, that this classification is not without controversy: For stick-slip to occur a higher static than dynamic friction coefficient is necessary, but e. g. coupling mechanisms can occur even if the friction coefficient is not constant.

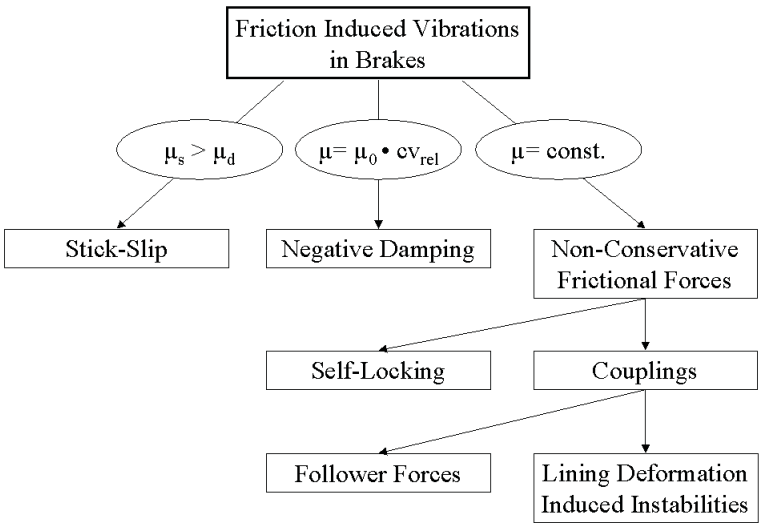

Figure 2.4.: *Categorization tree for friction induced vibrations in brakes (cp. [53])*

Stick-Slip

Stick-slip is the classical example for a self-excited vibration, which means the system is fed as much energy per cycle as needed to maintain the vibration, e. g. as for a mechanical clock [63].

Rinsdorf [79] showed the existence of a critical belt velocity for a one-degree-of-freedom model, a single mass oscillator with damping on a moving belt with friction interface. For belt velocities above the critical value, the mass does not achieve the belt velocity, due to the damping. Therefore the motion dies out and no stick-slip occurs. For belt velocities equal to or less than the critical value, a periodic stick-slip behavior is observed after a tune-in cycle. This critical velocity decreases with increasing damping and vibration frequency and increases with increasing normal force and difference between static and dynamic coefficient of friction.

After verifying similar trends with multi-body systems, FEM and experiments Rinsdorf [79] concluded that stick-slip only occurs for low-frequency noise at very low velocities. From his diagrams one can estimate a friction interface velocity below 0.2 m/s (correspond to less than 2 km/h vehicle velocity for the brake used in this work) for realistic masses, damping, normal forces and friction coefficients.

Hammering

Rhee et al. [76] proposed a simple mechanical impact model for noise excitation, which they called hammering. If the noise frequencies identified in a vehicle test of the same brake also match those from modal analysis of the brake components or the brake assembly, brake noise and vibration might be activated by a 'hammering' type of mechanism, not dissimilar to the analysis where a hammer or shaker is used to induce brake component vibration. Hammering during braking may be initiated by the rocking action of the pads when they slide across the disc surface against 'hills and valleys', which are formed by thermal distortion (so-called hot-spots) or by any other mechanical distortion. These mechanical distortions can include uneven disc wear (resulting in disc thickness variations) or massive friction material transfer to the disc. The impacted pads might in turn hammer the caliper or disc, and thus start a chain reaction of hammering among the brake components.

The authors concluded that the model is not inconsistent with the flutter type theories, although it differs from them in that it depicts the physical process by which the noise and vibration are activated. Moreover, stick-slip can also be treated as a secondary mechanism of hammering, since a relative velocity of zero between the components is needed. Hammering is not included in many of the recent models or investigations of brake squeal.

Negative μ-Velocity Slope

A single mass oscillator can also become unstable due to a decreasing friction coefficient μ with increasing velocity v, usually called negative slope (of the friction-velocity characteristic). The $\partial\mu/\partial v < 0$ characteristic can be taken as negative damping and if the resulting excitation energy exceeds the energy loss due to damping, instability will occur [3]. Hultén [53] states however, that the destabilizing effect of the 'Negative μ-Velocity Slope' is less than the stabilizing effect of the material damping of the parts.

Kinematic Constraint Instability

The combination of friction forces with certain geometries can lead to self-locking, often called kinematic constraint instabilities in literature. If there, at any circumstance, exists a contact pattern that can give self-locking (first introduced in the sprag-slip model by Spurr [85]), the self-locked parts will deform until the geometry and/or the contact pattern changes enough to result in a slip phase [53]. The slip phase persists until conditions for

a new self-locking cycle exist. According to Flint and Hultén [44] kinematic constraint models are very simplistic and by themselves not well suited to model a complex disc brake.

Flutter Type Instability (Modal Coupling)

Chen et al. [25] summarized the mechanisms and causes of squeal. From their studied references, they concluded that at low frequency (below the first in-plane mode of the disc), squeal of a disc brake system is usually caused by modal coupling between rotor and other brake components such as knuckle, caliper, anchor bracket, pad or even wheel. Modal coupling between in-plane and out-of-plane modes of the disc, or modal coupling between a disc out-of-plane mode and a pad mode is usually responsible for high frequency squeal. Modal coupling requires the proper vibration phase relationship between two modes.

Binary flutter is a term for the state oscillation, in which energy is exchanged between two modes of vibration in a way that feed additional energy into the system [44]. According to Flint and Hultén [44] follower forces as well as lining deformation *can* lead to binary flutter, however, modal coupling *can* also result without (the consideration of) follower forces, if two-degrees of freedom are coupled by any other interaction.

Follower forces change their directions as the geometry changes (e. g. due to vibration), therefore, strictly spoken, normal and friction forces are follower forces [3], even as models rarely consider. A rotation of the rotor segment will result in friction force components perpendicular and normal force components parallel to the original (unrotated) surface [53]. This coupling between rotational degrees of freedom and radial and tangential force components and the non-conservative character of the described follower forces can lead to instability [3]. According to Mottershead and Chan [68] for a FE model considering follower forces, flutter instabilities in brake systems occur primarily as a result of symmetry, when two normal modes coalesce at a critical frequency. In the general case of flutter in structures, it is necessary to cause two modes to coalesce by the application of load.

Hultén [52] developed theories regarding drum brake squeal, termed lining-deformation-induced instability, which are basically an extension and refinement of the binary flutter mechanism. For drum brakes four mechanisms lead to generation of traveling waves, which can couple and lead to instabilities [53].

Flint and Hultén [44] investigated the effect of follower forces, as well as lining-deformation-induced couplings with a disc brake model. While the effect of follower forces is shown to be marginal, the lining-deformation-induced couplings can be of significant importance, as a factor in generating instabilities. They also state, that the obtained results from the model show good agreement with squeal measured in a vehicle test, using the modeled brake system.

Allgaier [3] showed for a disc brake related pin-on-disc system, that the system instability was due to the coupling of a pin and a disc mode, while Lang and Newcomb [60] showed the modal coupling squeal correlation for a drum brake.

2.3.3. Squeal Dependence on various Parameters

Automotive brake squeal depends on numerous variables. In engineering science there is commonly a strict distinction between controlled variables, called parameters, and physical parameters being quantified by measurements, called measurands. As the definition of the latter is commonly accepted for ‘parameter’ numerous definitions exist for different areas, e. g. mathematics, computer science, engineering etc. Not all variables used in this work are well-defined parameters or measurands. Some parameters, e. g. brake line pressure, are controlled and measured, while others like temperature are only controlled during some brake applications or in some dynamometer modes (cp. section 2.4.1). To simplify this issue, all variables in this work will be called parameters. Furthermore, ‘parameter’ is used in the mathematical sense, being an argument of a function or, on a more abstract level, an input variable (for modeling dependencies). Besides the purely theoretical distinction, the readability of this work greatly improves by not having to classify each variable in each context.

Bergman, Eriksson and Jacobson investigated the influence of various parameters on brake squeal, summarized in the doctoral theses of Bergman [7] and Eriksson [34]. They also introduced the squeal index (SI), which is the number of registered squeal events divided by the number of measurements, basically the squeal propensity.

Bergman et al. [11] showed a general reduction of squeal index as the nominal contact area was halved, for all three tested surface geometries. By removing 5 % of the nominal contact area along the radial outer edge of the pad, the ocurrence of squeal was reduced by 40 %.

Bergman et al. [9] further showed, that (for their brake) there were no squeals gener-

ated when the coefficient of friction was below a critical value and a very small friction increase could lead to a dramatic increase in squeal generation propensity.

In publications [8] and [12] the influence of solid lubricants on friction and squeal was investigated. Within the investigated three different organic pad matrix compositions, there existed a strong relationship between the friction coefficient and the squeal index, although no general trend for all three pad matrix compositions could be found. It is clearly shown that none of the solid lubricant additives Cu_2S, PbS or Sb_2S_3 by itself possesses any general squeal or friction reducing properties. For their test, they concluded that for a given friction material a higher friction coefficient will lead to the generation of more squeal events. During a deeper investigation of Cu_2S within a single pad matrix material, they found that the addition of Cu_2S consistently reduced the number of generated squeals with a minimum of 4 - 8 vol % Cu_2S.

Eriksson et al. [35] found an increasing size of contact plateaus with increasing brake line pressure. For their conducted tests, there seemed to be a correlation between the properties of the contact plateaus and the squeal generation. One type of pad, where the contact plateaus grew with increasing brake pressure, was less prone to generate brake squeal than the modified pads with almost non-growing plateaus. Österle et al. [73] also found smaller contact spots on a train brake pad after interrupting the test in a squealing state, compared with the contact plateaus estimated after the pads were silent.

Eriksson et al. [36] further investigated the initialization and inhibition of disc brake squeal. For this purpose they grit blasted a sector of the disc and concluded from their experiments, that squeal is generated almost instantaneously when the contact conditions are right and is maintained only if the contact conditions continuously promote it. Also a high and evenly distributed friction coefficient is needed to initialize brake squeal, however it can be maintained with only a small part of the pad experiencing a coefficient of friction high enough for squeal to be initialized.

Eriksson et al. [41] also showed that the tested pads show a larger in-stop friction increase at low relative air humidity. Humidity has a stabilizing effect on the friction coefficient for relative humidities between 20 % and 80 %. For relative air humidities above 80 % the mean coefficient of friction per pad and test increased for some pads, while it decreased for some other pads with respect to further increasing relative air humidity. The correlation between air humidity and brake squeal generation was limited. One pair of the tested pads displayed significantly higher squeal generation in dry atmosphere than in humid. None of the pads showed lower squeal generation in dry conditions.

Eriksson and Jacobson [39] investigated the influence of speed and pressure variations at velocities below 4 revolutions per second (corresponding to vehicle speeds below approx. 26 km/h). Within the limits of their test, an increasing squeal index with an increasing mean coefficient of friction per test was clearly visualized. Their investigation also suggests that the friction level is more important than the local slope of the μ-v curve for squeal generation. During their tests, the separation between the friction curves for increasing and decreasing velocity was very small, which means that the coefficient of friction depends on the absolute velocity only. For some pads a hysteresis was observed in the μ-p curves, which indicates that the sign of the pressure change slope is important for the friction coefficient. However, a relationship between its hystereses and squeal generation could not be revealed. Nevertheless, squeal generation had some correlation with brake line pressure, which can not be explained by a variation of the friction coefficient with pressure. The coefficient of friction seemed to influence the level of the lowest brake line pressure to generate squeal. This indicates that a critical friction force is needed for the system to become unstable or just that the system in general is less prone to squeal at low pressures, making the critical friction coefficient higher in these cases.

Brecht [18] tested two brake pad pairs of the same friction material with different Young's moduli. By slicing the friction material from a cube in perpendicular directions, two pad pairs were manufactured which had exchanged Young's moduli in normal and lateral direction ($E_{x,y,1} = E_{z,2} = 14.5$ GPa and $E_{x,y,2} = E_{z,1} = 3.8$ GPa respectively). During a noise test the pad material number 2 with the higher Young's modulus in the normal direction generated 15 times more noise events with a significant higher sound pressure level compared to the pad material with the higher lateral Young's modulus. He concluded that the directional friction material properties have great effect on noise levels and judder.

Canali and Tamagna [22] investigated the noise dependence on several pad and disc related parameters. They concluded that noise performance can be strongly affected by modifying just one material of the friction couple, and therefore, the selection would be better if disc and pad were defined together. In their tests, the magnitude of the friction coefficient for different brake pads with similar discs has shown a great influence on noise generation. Besides the friction coefficient, Young's modulus and tensile strength are properties of brake pad materials that presented the most significant slope coefficients in multiple regression analysis, while hardness and porosity have a lower significance.

Allgaier [3] discussed the two-degree-of-freedom model of Hamabe et al. [49]. The

model consists of a mass on a frictional belt, which is attached to two orthogonal springs. For this model, the equations of motion are coupled. Allgaier [3] concluded, that for unstable behavior a coupling of both possible directions of motion due to stiffnesses of the structure is obligatory. For the exemplarily discussed case unstable behavior results when the product of the friction coefficient and the stiffness perpendicular to the belt exceeds a critical value.

Dunlap et al. [33] constructed a lumped parameter model to gain an understanding of the relationships between the stiffness of the disc, the stiffness of the brake pad, the coefficient of friction and the resulting normal and tangential direction response levels. The model was used to generate a stability diagram of pad stiffness versus the coefficient of friction for constant values of rotor stiffness. Based upon the diagram, reductions in pad normal stiffness or increased rotor stiffness for the same friction coefficient will move the operating point to a more stable region.

Based on more than one hundred literature references Chen et al. [25] concluded, that friction processes at contact surfaces can be considered to introduce an instant dynamic loading condition, which alters resonant modes of the friction system to form an instantaneous squealing mode. From analytical and complex eigenvalue analysis, it is certain that higher friction coefficients will lead to higher squeal propensities. However, tests exist during which squeal actually arises at relative lower friction coefficients instead of higher ones. Using a whole brake system model with complex mode analysis, it is shown that adding damping to a pad always helps to reduce high frequency squeal. Caution needs to be exercised at low frequency, at which point the effect of adding damping may be detrimental since brake pads may mainly act as a coupling media between other brake components [25].

Shin [83] investigated the dynamical interaction between the pad and the disc for in-plane and out-of-plane vibrations with two simple two-degree-of-freedom models. For in-plane vibration of pad *and* disc dampening has to be increased to prevent instability. Even worse, from his non-linear investigation of the in-plane model behavior he concluded that increasing the dampening of a pad or disc alone may make the system noisier. His out-of-plane vibration model shows, that the system is more stable as the stiffness of the system increases. Also, in this case he states that both stiffness parameters of the pad and the disc are equally important, and they must be large enough to suppress the effect of negative stiffness $\mu \cdot \ c_c$.

From a Finite Element analysis of a brake system, Liles [62] summarized, that higher

friction coefficients increase the occurrence of squeal. In general, shorter friction materials in a tangential direction decrease squeal occurrence and, as friction materials wear the probability of squeal increases. The occurrence of squeal is decreased with stiffer lining assemblies. The likelihood of squeal can be decreased using a slightly softer rotor and increased structural dampening reduces squeal. Liles also noted that some statements may apply only for the brake system investigated in his research effort.

On a linear pin-on-disc model, Tuchinda [93] showed, if the contact stiffness increases to a certain level, two modes merge to form one complex mode which becomes linearly unstable. However, as the contact stiffness further increases the complex mode splits into two modes, which become asymptotically stable again.

Conclusively, it can be said that the friction coefficient and the lining stiffness have been mentioned quite often in recent brake squeal investigations. Therefore, they can be assumed to play some role in brake squeal generation.

2.4. Brake Testing

The main focus of this overview of brake testing will be on dynamometer testing including data acquisition, data analysis, and the resulting plots. Nevertheless, other techniques used in this work, like frequency response function and compressibility testing, are also discussed.

2.4.1. Dynamometer Testing

Even today, if a significant number of vehicle tests is needed to be performed for final verification of the brake design, dynamometer tests are used early in the development stage, when representative vehicles are not available or during problem resolution stages, when a better controlled design of experiment is needed, according to Chen et al. [24]. In automotive brake testing, three different types of dynamometers are commonly used, which are summarized by Weiss [20, ch. 25]. One type, the chassis dynamometer, is used to test the whole vehicle under well controlled environmental conditions. Inertia dynamometers, the second type, are used to test the single brake assembly up to the whole mechanical brake system, often also including suspension [24]. Reduced-scale or reduced-sample friction testing, as used by Sanders et al. [80] and Kemmer [58], is within the third brake dynamometer type. They are used to generate accurate friction material data for use in

brake system design and lining screening, because friction materials can be tested easily without vehicle specific fixtures and brake hardware [80]. Reduced-scale dynamometers are not practical for brake noise testing as squeal does not depend solely on the friction material behavior. Nevertheless, according to Sanders et al. [80] the agreement between the test results of an inertia and a reduced-scale dynamometer test based on constant energy density scaling is excellent.

Dynamometers are used in different operational modes. During a test procedure, the time between the brake applications is either firmly specified (time controlled mode) or the next brake application is started when a specific (e. g. disc) temperature is reached (temperature controlled mode), independent of the cooling time in the latter case. For special test procedures, a combination of both operational modes is also possible. In the same manner, the control parameter during a brake application is either brake line pressure (pressure controlled) or the brake torque (torque controlled), besides the initial and final velocity and in the case of temperature control also initial temperature. During cooling time, the disc is usually slowly rotated to prevent the pads from becoming stuck on the disc and to ensure a uniform cooling of the disc. For temperature controlled brake applications also heating brake applications are carried out, if required. The control parameters of these heating brake applications are normally specified in the test procedure (e. g. in SAE J2521 [94]), but may vary between different test procedures. Also, it is obvious that the frequency of the heating stops depend on the fed energy, as well as on the type and amount of cooling and may therefore vary between different applications of the same test procedure. As described before (cp. p. 14 and [58]) the brake history may alter the friction behavior, so one would expect an impact of cooling time and velocity as well as heating brake application frequency and control parameters on friction (and also on noise) behavior.

For a dynamometer, two types of brake applications are generally differentiated. If the initial velocity is higher than the final velocity, the brake application is usually called deceleration or stop brake application (even if the final velocity is not equal to zero), while a drag brake application is at constant velocity. In some special cases, also accelerating brake applications are used, where the final velocity is higher than the initial speed [86]. For drag, acceleration and sometimes also stop brake applications, a predefined brake application time is used, during which the velocity is changed linearly or kept constant (for drag brake applications). For more realistic conditions, inertia dynamometers test the braking system under inertia simulation conditions [24], for which the brake application

time automatically results.

For most vehicles, the kinetic energy, resulting from the moving vehicle mass is much larger than the kinetic energy from rotating parts like brake disc, wheel, driving shaft, etc. As the dynamometer does not conduct a longitudinal uniform motion in order to rotate the brake disc, the inertia simulation is either done mechanically, via inertia discs attached to the driving shaft, or electrically, where the electric motor generates the needed torque. For calculation of the needed dynamometer inertia a transformation of the translatory vehicle inertia system to the rotatory dynamometer inertia system is done, using an energy equivalence. So starting with

$$E_{\text{kin,vehicle}} = E_{\text{rot,dynamometer}}$$

neglecting vehicle rotatory energy terms and using the amount of vehicle mass m^*_{vehicle}, which is decelerated by the brake

$$\frac{1}{2} \cdot m^*_{\text{vehicle}} \cdot v^2_{\text{vehicle}} = \frac{1}{2} \cdot \Theta_{\text{sim}} \cdot \omega_B^2$$

results. As the brake rotational speed ω_B is linked to the vehicle velocity v_{vehicle} through the wheel's dynamic running radius r_{dyn}

$$v_{\text{vehicle}} = \omega_B \cdot r_{\text{dyn}}$$

the resulting rotatory inertia to be simulated by the dynamometer Θ_{sim} is

$$\Theta_{\text{sim}} = m^*_{\text{vehicle}} \cdot r^2_{\text{dyn}} \tag{2.3}$$

According to Thun [91] the mechanical inertia simulation is normally done with practical scaled flywheels while the fine adjustment is achieved by raising or lowering the velocity to assure energy equality. With an electric inertia simulation not only the conditions in a dynamometer are reproduced more precisely, but also changes in the axle load during a brake application can be simulated [91], resulting in a vehicle equivalent power characteristic during braking. The simulation of the additional torque can be done based on the angular acceleration or based on the measured brake torque. The latter case is generally preferable, because the first leads to a feedback which limits the dynamics of the inertia simulation [91]. So for the commonly used combination of electric inertia simulation and flywheels, the vehicle equivalent needed dynamometer inertia Θ_{sim} has to

be the sum of the inertias from the flywheel Θ_{flywheel} and the electric inertia simulation Θ_{motor}:

$$\Theta_{\text{sim}} = \Theta_{\text{flywheel}} + \Theta_{\text{motor}}$$

The (measured) brake torque M_B causes an angular brake disc acceleration $\dot{\omega}_{\text{B,sim}}$ dependent on the vehicle equivalent needed dynamometer inertia Θ_{sim}

$$M_{\text{B}} = \Theta_{\text{sim}} \cdot \dot{\omega}_{\text{B,sim}}$$

Similarly, the brake torque needed to decelerate the dynamometer driving shaft and flywheels, without applying any electric inertia simulation, is

$$M_{\text{flywheel}} = \Theta_{\text{flywheel}} \cdot \dot{\omega}_{\text{flywheel}}$$

Using the required power equality, in terms of the same angular acceleration

$$\dot{\omega}_{\text{B,sim}} = \dot{\omega}_{\text{flywheel}}$$

the electric inertia simulation must generate a torque M_{motor} to alter the brake torque, in order to achieve vehicle equivalent angular acceleration values

$$M_B + M_{\text{motor}} = \Theta_{\text{flywheel}} \cdot \dot{\omega}_{\text{B,sim}}$$

Using the equations presented above, the torque, which has to be applied by the dynamometer motor can be derived:

$$M_{\text{motor}} = M_B \cdot \left(\frac{\Theta_{\text{flywheel}}}{\Theta_{\text{sim}}} - 1 \right) \tag{2.4}$$

Basically, each vehicle manufacturer as well as each full brake system supplier has his own dynamometer test procedures and the standardization is quite poor. Today, two procedures are widely used and commonly accepted - the AK master (SAE J2522) for performance tests and the SAE J2521 [94], which was derived from it [24], for noise purposes. The SAE J2521 consists of an initial conditioning module after which the evaluation section is repeated three times with an optional fade and recovery module at the end. The evaluation module contains drag and stop brake applications as well as drag brake applications in forward and reverse vehicle direction. A summary of the experience with the procedure is given by Thompson and Fudge [89]. They state, that the procedure has the potential to represent noise trends of the vehicle. Nevertheless, an integral part of

the release procedure of a new brake system is vehicle testing in Los Angeles (LACT) for US vehicles and in Mojacar for European vehicles, according to Mody et al. [67].

Even if every noise during a vehicle test is recorded with a data acquisition device, the majority of the release procedures of a new brake system - at least in Europe - are based solely on the subjective noise ratings of the drivers during a vehicle test [67]. In recent years there have been efforts to develop an objective noise rating based on measured data to overcome this dilemma [67]. During dynamometer testing the noise and vibration behavior is recorded with one or more microphones and often also additional accelerometers attached to the caliper. Modern noise recording systems (as built by Brüel & Kjær, STAC or Roush) process the gathered data automatically and generate reports, e. g. as specified in the SAE J2521 [94]. A standard SAE J2521 result report includes a sound pressure level versus frequency plot for estimation of the dominant squeal frequencies. Also, a plot of frequency versus brake application number is usually included to see when the noise occurred. The test report normally closes with plots showing the distributions of the measured noise as functions of test procedure section, brake line pressure, temperature and initial vehicle velocity. If more specific plots are favored, like in this work, one must post-process the data individually. Bergman et al. [10] used self-designed data acquisition and analyzing tools for the analysis of their experiments.

With respect to the comparability of dynamometer test results, Thompson et al. [90] state that despite the development of measurement standards such as SAE J2521 the correlation of noise measurements between laboratories remains an issue. The possible sources of variation are differences in rates of brake apply, temperature limits, cooling air applications, and alike. From their experiments they achieved a satisfactory correlation, even if that was not a true data point to data point correlation in the classical sense. According to Thompson et al. [90] correlation is achieved, if there is a general correspondence that indicates similar trends. Tests at two laboratories indicating noise at exactly the same amplitude and frequency is very unlikely.

2.4.2. Elastic and Modal Properties Testing

As described earlier (see p. 14), there are different ways to estimate the elastic properties of friction materials. In this work, the compressibility testing procedure is used to estimate the elastic properties.

The procedure used for the compressibility tests is specified in the ISO 6310 Standard

[55]. Compressibility is the deformation of the specimen after applying a specific force. During the procedure a brake pad is compressed between a massive steel plate and an adapter, which has the piston diameter. For the so-called cold compressibility at ambient temperature, the procedure is as follows: After an one second dwell time with a preload, which correspondents to 5 bar brake line pressure, the force is linearly (normally at a pressure rate of 80 bar/s) increased up to the maximum level. The maximum normal force is also held for one second before the force is linearly decreased to the preload again. This cycle is repeated usually six times according to ISO 6310 [55], even though there are examples where only three cycles were conducted, e. g. by Hecht-Basch et al. [50]. The deformation behavior of the first cycle allows conclusions about the quasi-plastic deformation behavior of the friction material, while in general the 6th cycle is used to estimate the elastic properties. For the so-called hot compressibility the steel plate is heated up to 400 řC. The pad is pressed against it for 10 minutes, using the usual preload. Thereafter, two cycles, as described above, are performed. Normally a maximum force corresponding to 160 bar brake line pressure is used, but there are also examples where different values (e. g. 100 bar [50]) are used.

Because of the nature of the compressibility test, the deformation is a sum of deformations of friction material, underlayer and backplate. The uneven pressure distribution on the backplate due to the use of the piston adapter also leads to bending of the pad. Therefore the test is not suitable for estimation of the pure friction material Young's modulus in normal direction, but a quite good approximation for the coupling between normal deflection and normal force - at least for the piston side pad. For the estimation of a normal Young's modulus one would prefer to use two steel plates to be pressed against each other, possibly even two brake pads facing each other between the plates. Such a test is in the Japanese Industrial Standard specification, according to Kaido and Sasaki [57].

According to Siller [84], the frequency response function (FRF) is perhaps the single most used tool in the field of modal analysis to describe the input-output relation of a system. Although its applications go far beyond the vibrations field, structural engineers use it almost invariably as a first step for assessing the dynamic features of a structure [84]. After exciting the structure by an impulse hammer or a shaker, the displacement, velocity or acceleration is measured. The usually complex and frequency dependent response function is calculated from the relation between excitation and measured value. The absolute value of the response function plotted versus the excitation frequency is called FRF spectrum. Abdelhamid [1] showed the measurement system used for a typical noise and vibration measurement. The system used in this work was similar, except a manual im-

pulse hammer was used for excitation. In this work, the shown FRF spectra are only used to show similarities of parts, which are identical in construction, and therefore no modal analysis is done. One should note that a resonance peak in the FRF spectrum not necessarily indicates exact one mode vibrating at that frequency, as also the superposition of more than one mode with close frequencies is possible. In general, the free-free modes of the parts are not the same for the operating brake assembly. For further informations on FRF and modal analysis, one is referred to the work of Ewins, e. g. in [42].

3. Scope of the Present Work

In this chapter, the motivation and goal of this work are presented. As described earlier, the phenomenon of brake squeal has been intensively investigated so far and is found to be a quite complex matter. Therefore, this work focuses on the tribological aspects of brake squeal, while the structural parameters are tried to be kept constant. Irreversible intrinsic processes of the brake, like pad wear and friction history effects, additionally complicate the brake squeal investigation.

3.1. Motivation

As seen in the literature review in the previous chapter, a lot of research and progress in the area of brake noise has been done during the past 70 years. In experimental studies, various parameters have been investigated and the coefficient of friction has been an important tribological parameter concerning brake squeal. Nevertheless, examples exist, proving that the friction coefficient on its own can not be the only relevant tribological parameter for the brake squeal generation. On the other hand, modeling approaches mainly focus on structural parameters mostly assuming a relatively simple friction law. From these models often the friction coefficient and the stiffness perpendicular to the friction force are estimated as main contributors to brake squeal. Models with only few degrees of freedom are well qualified to study the mechanisms of brake squeal, but their usefulness as model for the complete dynamic brake system is questionable. The stiffness of the spring perpendicular to the friction force in two-degree-of-freedom models, for example as discussed by Hamabe et al. [49], is often called contact stiffness, which is valid for these models, but need not necessarily correspond to the contact in the real brake. In these models, c_c is the coupling term of the out-of-plane displacement and the normal force. In a similar way, the friction coefficient couples the normal force and the perpendicular friction force. The structural coupling of in-plane and out-of-plane degrees of freedom closes

this loop, possibly resulting in instability. From this point of view, the stiffness in these models would correspond to the stiffness of the disc, pad, piston, and caliper assembly and the contacts between the components. In a series of stiffnesses, the overall stiffness is dominated mainly by the lowest stiffness value. In this case, the low stiffness values are the brake pad stiffness and the contact stiffness between disc and pad. Nevertheless, no systematic experimental validation of the often proposed friction coefficient and stiffness hypothesis has been done with a real brake system yet.

The friction behavior of the brake tribosystem is often reported by a single value per test, even if no constant friction coefficient during the whole experiment is explicitly assumed. Because the friction coefficient is not only a material but also a system parameter, it usually changes when the system changes. Even if, for brake performance issues, reporting a nominal friction coefficient might be sufficient, a closer look with respect to noise behavior is needed. So far, it is unknown to which depth data pooling preserves possible squeal information and if some functions (like averaging, maximizing, etc.) are better qualified to maintain correlations between tribosystem parameters and brake squeal than others.

3.2. Goals

The main focus of this work is to clarify the question if it is possible to describe squeal behavior with the most squeal relevant parameters of the tribosystem, consisting of brake pad and disc. Additionally, the question, on which timescale dependencies have to be reported to find the best correlations, will be investigated.

As described before, the friction coefficient and the stiffness normal to the friction force have been assumed to be the dominant contributors to brake squeal. The overall normal stiffness of the tribosystem is a series connection of the disc and pad stiffnesses and the contact stiffness between them. By using the identical caliper during all tests, the stiffness of piston and caliper is kept constant. Using these considerations, the elastic and the friction properties of the tribosystem are the main tribological contributors to brake squeal.

Consequently, this work focuses on the influence of these tribosystem parameters on brake squeal. By using different friction materials, the friction level and the elastic properties are modified. On the other hand, by using the same caliper and identical discs the ‘structure’ is kept as constant as possible. Always the same dynamometer is used and the

investigated brake system is set-up without a knuckle to reproduce the same conditions best possible.

Although often ignored, elastic properties and friction behavior in the brake tribosystem are not constant. Therefore, the conducted tests are analyzed on three different timescales. The measurement of brake torque, brake line pressure, vehicle velocity, brake disc temperature and brake noise is recorded several times during a brake application. This timescale (where data is taken very often during a brake application) is called real-time timescale and discussed in detail in this work.

For second timescale investigated, the real-time data is reduced to one value per brake application. The real-time data is reduced more for brake applications lasting longer, and the reduced value strongly depends on the data reduction method. Different data pooling functions will be investigated, exploring the correlations between brake squeal and reduced friction coefficient and pad normal stiffness.

Thirdly, only a single value per test will be considered to investigate friction coefficient and stiffness influences on brake squeal.

Today, no in-situ measurement of the elastic properties of the brake tribosystem is known. Therefore, a compressibility measurement of every pad is conducted prior to each dynamometer test. It results in one stiffness value for each brake pad per test. To be able to find dependencies on the timescale of one value per brake application and within the real-time data, a model of the elastic properties, based on measured data had to be developed.

To investigate the impacts of tribological parameters on brake squeal, the data is modeled on all three timescales, using regression models. If the models are statistically significant, the correlations can be explored, and if no (reasonable) models can be built, there might be no correlation at all.

To judge the model's usefulness and correlation between squeal and the tribological parameters a measure is introduced. Using the models, the overall squeal propensity for each test is calculated and compared to the 'measured' squeal propensity. Using the deviations, the models are arranged by usefulness. In this way, one is able to assess the applicability of each model and the possible correlations between squeal and the tribological parameters can be estimated.

In chapter 4, the data generation approach and the conducted experiments are described. Also, calculations and models, like the squeal propensity calculation or the pad normal stiffness model, are presented.

Subsequently, in chapter 5 the basic principles of different timescales, model building, data pooling and model evaluation are discussed.

In chapter 6, the analyses and models on all three timescales are presented and the tribological impact on brake squeal generation is investigated.

In chapter 7, a general discussion is presented, reviewing the presented models and analyses to clarify the tribological influences on brake squeal, the usefulness of data pooling and the model's potentials and limits. The summary and outlook is presented in the last chapter.

4. Data Generation and Conditioning

In this chapter the conducted experiments are presented. After outlining the experimental approach, a deeper look on the experimental set-up, data acquisition and data post-processing is done. Using the generated data, the squeal propensity calculation is discussed and the pad normal stiffness model, built on compressibility data, is presented.

4.1. Experimental Approach

The friction coefficient of the pad and disc couple can be varied by changing the control parameters, like brake line pressure, velocity and temperature or by changing the pad or disc. In general, the friction coefficient changes due to control parameter changes are limited and, based on the previous discussed history effects, not independent of the order of brake applications. In this work a change in the average coefficient of friction $\bar{\mu}$ and in the average normal pad stiffness $\bar{c}$ is mainly done by using different friction materials.

To investigate the influences of μ and c on brake squeal an equally spaced grid of pads in the μ-c parameter space is desirable. Unfortunately, the coefficient of friction as well as the normal stiffness of the brake pad can only be controlled to a certain extent, because these are not parameters which are directly accessible.

In a first series of tests, eight brake pad friction materials were tested. Five of them were specified and manufactured for the brake, used in this works' experiments. To be more precisely, friction materials A and B were from an original equipment manufacturer (OEM), and the remaining three friction materials (C - E) were from different manufacturers in the automotive aftermarket. Although most likely different in formulation, the five lining materials were European-Metallic type and due to the specification for the brake, similar in friction level and pad normal stiffness. Thus, these friction materials were com-

Table 4.1.: *General information about the tested friction materials*

FM	*FM class*	*Shape*	*Vehicle*	*Specialty*
A, B	EM	original	original	pads from OEM
C - E	EM	original	original	aftermarket pads
F	SM	cut to fit	US No. 1	
G	LM	cut to fit	US No. 2	one radial slot each
H	EM	cut to fit	US No. 2	one radial slot each
I, J	NS	original	none	designed experiment
K, L	NS	original	none	designed experiment, identical formulation
M, N	NS	original	none	designed experiment, identical formulation
O - Q	NS	original	none	designed experiment
R, S	NS	original	none	designed experiment, identical formulation
T	NS	original	none	designed experiment

plemented by three friction materials from two American sports utility vehicles (SUV) each from a different friction material class, resulting in a Low-Steel Low-Metallic (G), a European-Metallic (H) and a Semi-Metallic (F) lining material. The European-Metallic and the Low-Steel Low-Metallic friction materials were taken from the same vehicle and each one had, different from all other pads used in this work, one radial slot in the middle of the friction material's tangential direction. Throughout all tests the same caliper was used, so the original pads from the SUV were cut into the same smaller shape to fit in.

For the second row of tests No-Steel Low-Metallic friction materials (identifiers I - T) from a designed experiment were developed by Federal-Mogul, a brake pad manufacturer. These friction materials are based on a formulation from an US vehicle and use the same ingredients for all friction materials, varying only in the particular amounts. Table 4.2 summarizes the relative volume amounts within each category for all different friction materials to give an impression of the formulation similarity. While most brake pad ingredients should be self-explanatory, two categories need a few more words of explanation: Premix consists of rubber and 'friction dusts', and inorganics are fibers and fillers. All in all, there are nine different friction materials based on the same formulation basis, which indicates that six formulations of the 12 tested pad pairs in this set were pairwise identical. Table 4.1 contains a more detailed overview.

The general goal of both sets of tests was to cover a wide range of the μ-c parameter space with the used friction materials, equally spaced if possible. In figure 4.1 one

Table 4.2.: *Summary of the relative volume amounts for each category for all friction materials of the second row of dynamometer tests*

FM	*Amount [vol%]*						
	Binder	*Premix*	*Organic Fiber*	*Metal Fiber*	*Inorganic*	*Lubricant*	*Abrasive*
I	15.58	25.00	2.86	3.86	41.36	7.36	4.00
J	21.28	15.00	4.57	5.62	39.52	4.00	10.00
K, L	15.15	16.68	1.00	3.55	44.75	9.92	8.95
M, N	21.17	16.72	2.94	3.23	41.08	10.00	4.87
O	17.74	25.00	1.00	2.95	33.31	10.00	10.00
P	22.00	15.00	1.00	4.82	46.06	5.60	5.52
Q	20.69	22.40	1.00	2.00	45.91	4.00	4.00
R, S	17.25	15.00	5.00	3.64	41.84	7.27	10.00
T	17.71	15.00	4.86	0.00	50.00	5.89	6.54

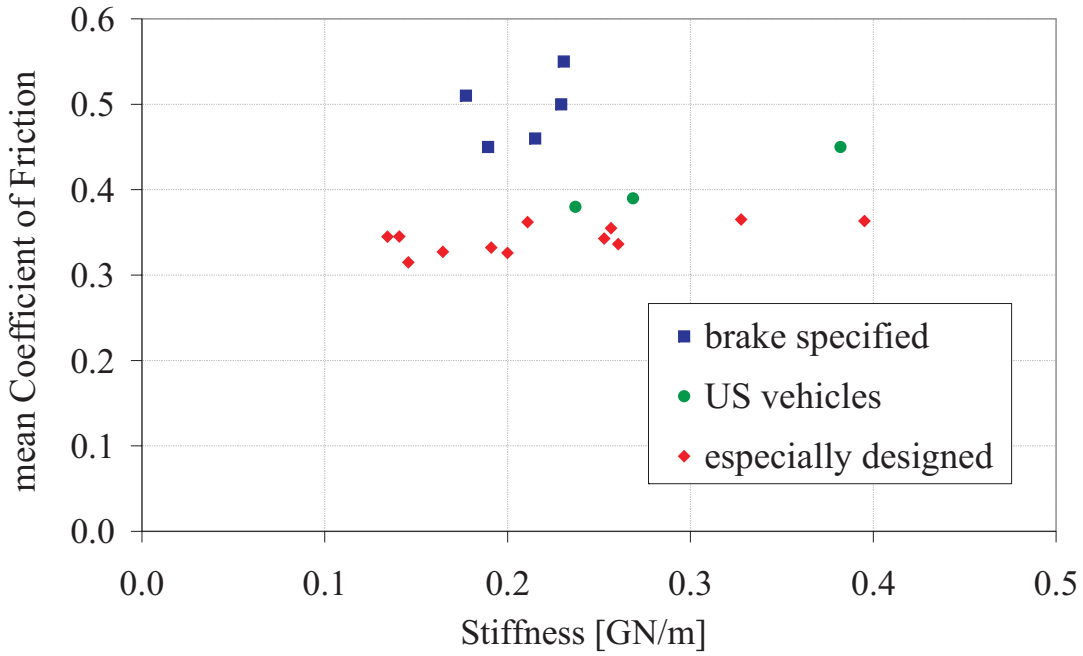

Figure 4.1.: *Mean friction coefficient and stiffness for tested pad pairs, more detailed description see chapter 6.3*

marker indicates the position in the μ-c parameter space for each conducted test, squares indicating tests with pads produced for the used brake system, circles tests with the pads of American SUV and diamonds for the latter mentioned specially developed brake pads. Figure 4.1 shows the large range of covered stiffnesses at nearly the same mean friction coefficient for the developed brake pads. The calculation of the stiffness values shown in figure 4.1 is presented more detailed in chapter 4.4.2.

4.2. Setup and Implementation

4.2.1. Test Equipment

For brake noise testing, an inertia dynamometer manufactured by ITT Automotive Europe GmbH, including a control unit of Jurid, was used. The dynamometer has a fixed flywheel, which has a mechanical inertia of $\Theta_{\text{flywheel}} \approx 22\ kg \cdot m^2$ and an electrical inertia simulation via the 64 kW direct current electric motor. The dynamometer was originally designed for friction evaluation purposes and has a maximum rotational speed of 1700 revolutions per minute. The maximum permanent permitted motor torque is 920 Nm, even if temporary peak torque values up to 1472 Nm can be realized. These peak torque values can be used during stop brake applications with rotational speed below 665 revolutions per minute. The brake line pressure is generated with a relay valve, transferring the incoming pneumatic pressure into hydraulic pressures up to 70 bar. The brake cooling air volume is adjustable up to $15\ m^3/min$, which corresponds to an average air speed of approx. 32 m/s. To minimize background noise within the testing cabin, 70 % of the maximum cooling air volume was used in this work and the cooling air temperature was adjusted to approximately 5 °C. The measurement of the rotational speed is done by an inductive sensor, generating 1024 impulses per revolution. This signal is also taken for the electric inertia simulation, as described in chapter 2.4.1. The brake line pressure sensor has a measurement range of $0 - 200\ bar$ and is attached into the brake line near the caliper connection point. Telemetry is used to transfer signals from rotational measurements to the control unit. The transferred signals are up to four temperature sensors (k-type, 0 - 1000 °C) and the torque measuring shaft with a range of -2000 Nm to 2000 Nm. Due to the limited cabin space, the microphone was placed closer to the brake than specified in the SAE J2521 [94]. From the center of the friction ring, the microphone was placed 10 cm in radial, 10 cm in axial and 35 cm in upward direction (perpendicular to the floor),

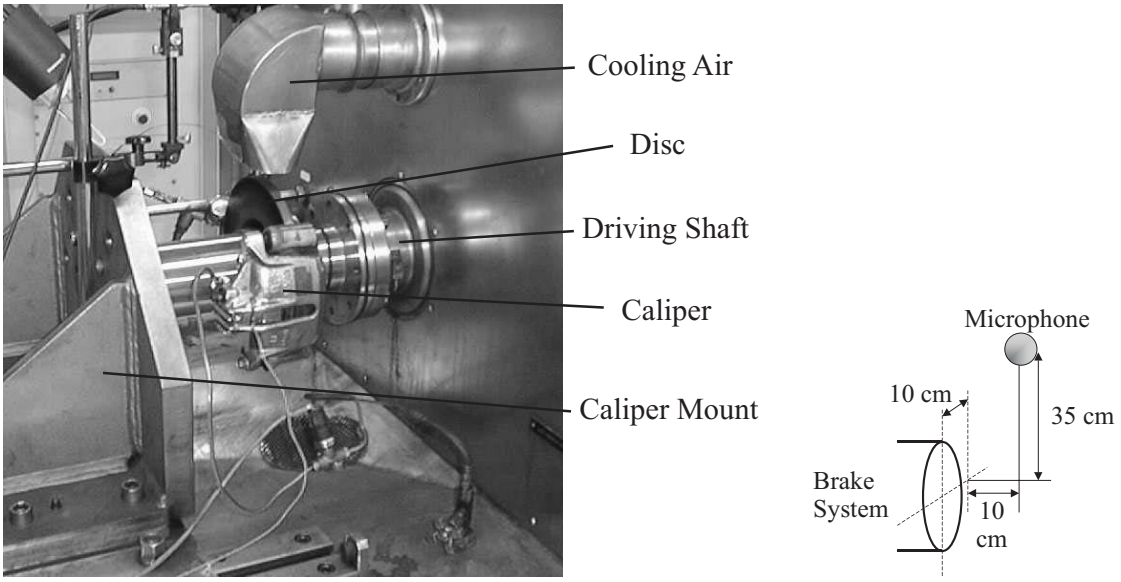

(a) Dynamometer setup

(b) Microphone position

Figure 4.2.: *Dynamometer setup and microphone position*

as shown in figure 4.2 (b). Due to the smaller distance between microphone and brake disc, the measured sound pressure level (SPL) is expected to be higher than that of a standard SAE J2521 setup, and absolute values should not be compared to those of other tests. Nevertheless, the microphone position has been retained unchanged throughout the whole experiments. So, relative changes in SPL are significant within this work and can be expected most likely to be similar to results from a SAE J2521 setup. The brake setup on the used dynamometer is shown in figure 4.2 (a).

All compressibility tests were conducted on a Jurid compressibility machine. To minimize measurement errors by reason of pad misalignment, a positioning device was used during the tests. All compressibility tests had a maximum brake line pressure of 100 bar, which results in a normal force of approximately 18.1 kN and in a nominal contact pressure of approximately 5.03 MPa. Under ambient conditions, six compression cycles for every pad were carried out. The minimum brake line pressure (normal preload) between each cycle was 1.1 bar for the first set of pads and 5 bar for the second row of experiments with the especially designed friction materials. The lower preload pressure during the first series of experiments was used to test how precise the contact deformation at

small normal loads could be measured. As the measurement turned out to be very error prone, 5 bar preload was used for the second row of tests. With the latter parameters the compressibility was measured according to the ISO 6310 Standard, described in chapter 2.4.2.

In order to determine modal frequencies of parts (structural properties) the frequency response function (FRF) testing was done with the SignalCalc Mobilyzer Dynamic Signal Analyser from the Data Physics Corporation. A one-dimensional accelerometer was attached to the specimen and the system was excited manually with an impulse hammer. For the brake pads, the accelerometer was attached to the backplate as far as possible on the leading or trailing edge. On the disc, two locations were needed to measure axial- and radial frequency response functions. For the axial measurement the accelerometer was attached to the friction ring near the outer diameter of the disc, while for the estimation of the radial FRF the accelerometer was attached to the radial outer edge of the disc. All accelerometer positions during FRF testing and a typical set of parts, used in this work, are shown in figure 4.3. The excitation done by the impulse hammer, was very close to the accelerometer positions, consequently resulting in an axial excitation for axial disc FRF measurement and a radial excitation for the radial disc FRF. Five impulses per measurement were sufficient to get reproducible results. The disc was measured in free-free condition and while they were mounted on the dynamometer. The pads were measured in free-free condition only.

In addition, a couple of measurement devices were used on a more irregular basis to estimate general trends in specimen behavior. A 1-D Laser Doppler Vibrometer (LDV) was used to estimate the out-of-plane mode shapes of pad and disc. Pad wear was measured with a contact measurement length gage from Heidenhain.

4.2.2. Brake

For this work, a Bosch brake assembly from an European compact car was used. The parts are shown in figure 4.3. During all tests, the identical left-front floating caliper was used. It was not modified compared to the original condition, only an accelerometer was attached (cp. fig. 4.3, marker 5) to measure brake vibration during dynamometer testing. To keep the overall structural setup simple and minimize possible structural changes during testing, a dynamomter setup without knuckle has been used. The brake caliper was attached directly to the caliper mount via a flange, which is shown in figure 4.2 (a). Due

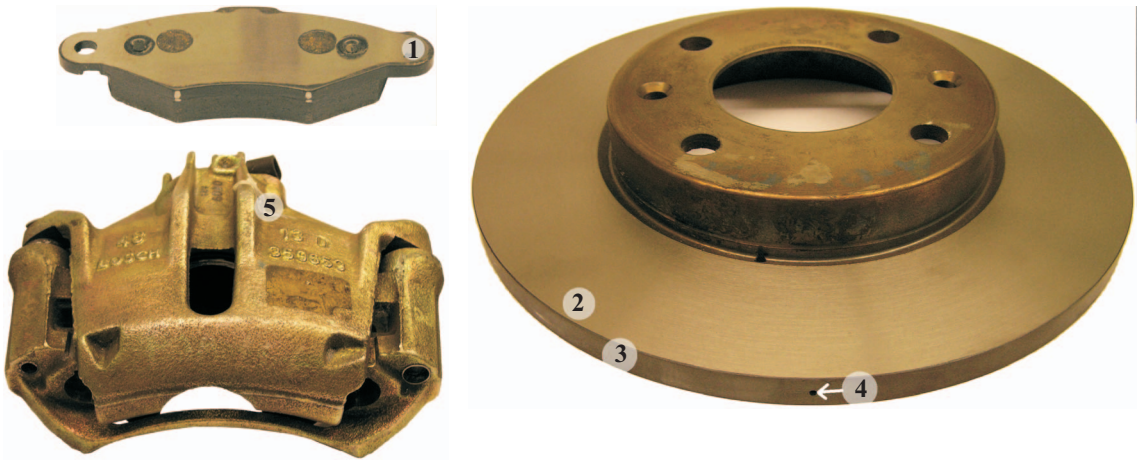

Figure 4.3.: *Parts used: marker 1 denotes the position of the 1D accelerometer during FRF measurement on pad, marker 2 for axial FRF and marker 3 for radial FRF on disc. Marker 4 points at the radial bore hole in the middle of the friction ring, where the thermocouple was inserted. Marker 5 denotes the position where the accelerometer during dynamometer testing was attached.*

to the disc wear it was necessary to use more than a single brake disc for all tests. On the other hand, using a new disc for each test increases the structural variety in an unwanted way, which is more difficult to control, even though the discs are identical in design. To make a compromise, six discs, identical in construction, have been used alternately. Prior to each new test, the friction ring surfaces were finely machined to remove wear scars, disc thickness variations, transfer films and thermal surface changes. However, as little material as possible was removed to minimize structural changes. Through the friction ring of each disc, a 1.1 mm diameter radial bore hole was drilled to situate the thermocouple during dynamometer testing. The temperature measurement point in radial direction was approximately in the middle of the friction ring. To test only the friction material influence, the shims of all the used brake pads were removed, not to tamper squeal generation by the use of different or no shims. This removal also led to a higher overall squeal occurrence, which is beneficial for the squeal propensity investigations. Similar in shape, the pads were finely machined coplanar to minimize errors of the compressibility measurement due to waviness, surface roughness or taper.

For the ‘tested vehicle’ it has been calculated, that 75 % of the gross vehicle weight rating are decelerated by the two front axle brakes, which leads to a needed dynamometer inertia $\Theta_{\text{sim}} = 45\ kg \cdot m^2$, according to equation 2.3. All relevant parameters of the

Table 4.3.: *Vehicle and brake assembly properties*

Physical value	*Symbol*	*Range*	*Unit*
Gross vehicle weight rating	m_{vehicle}	1587	kg
Relative front axle load distribution		75 %	
Half front axle load	m^*_{vehicle}	595	kg
Simulated dynamometer inertia for the brake	Θ_{sim}	45	$kg \cdot m^2$
Dynamic running radius	r_{dyn}	0.275	m
Brake disc lateral diameter		0.247	m
Friction ring axial thickness		0.013	m
Effective friction radius	r_{eff}	0.103	m
Brake piston diameter		0.048	m
Brake piston area	A_{piston}	0.0018	m^2
Nominal lateral brake pad area	A_{pad}	0.0036	m^2

vehicle and its brake assembly used in this work's experiments are summarized in table 4.3. If throughout this document terms associated with a vehicle are used, it is referred to this vehicle. The values used in dynamometer testing can be calculated using the stated constants in table 4.3. For example, at a vehicle velocity of 69 km/h the rotational disc speed is approx. 665 revolutions per minute (rpm). During dynanmometer testing this was simulated by a rotational speed of the dynamometer driving shaft of approx. 665 rpm.

4.2.3. Procedures

To improve readability, the description of the measurement procedures is separated from the presentation of the results. In this section the procedures are presented, while the results will be discussed in the following sections.

Two kinds of measurement procedures have been used: various procedures used to

Table 4.4.: *Target values of dynamometer test matrix to investigate electrical inertia simulation*

Section No.	*application No.*		$\Theta_{vehicle}$ $[kg \cdot m^2]$	v_{ini}	v_{fin}	*p* $[bar]$	T_{ini} $[°C]$
	From	*To*		$[km/h]$			
1	1	5	45	80	10	20	100
2	6	10	25	80	10	20	100
3	11	15	45	80	10	30	100
4	16	20	25	80	10	30	100

estimate general trends or ensure measurement correctness, while the main experiments have been conducted according to a ‘standard operating procedure’.

Dynamometer Inertia Simulation

To produce comparable results using different friction materials (and resulting different friction levels), the reliability of the electrical inertia simulation has to be investigated first. For this purpose a dynamometer test matrix, the parameters of which are shown in table 4.4, was conducted. This test matrix consists of four sections, each with five repeated brake applications with identical controlled parameters. The whole test consists of pressure controlled stop brake applications from 80 km/h to 10 km/h at an initial disc temperature of 100 °C. Two simulated inertias, the needed target dynamomter inertia value of 45 $kg \cdot m^2$ and the approximate value of the collective mechanical inertia of 25 $kg \cdot m^2$ (flywheel, driveshaft and brake disc), are tested at two different brake line pressures to vary stop time. Using the measured brake torque and rotational deceleration the simulated inertia can be calculated (cp. equation 4.2, p. 65).

Disc and Pad Deflection Shapes

Out-of-plane deflection shapes of a brake disc and a brake pad have been measured in free-free condition, using a Polytec one-dimensional scanning Laser Doppler Vibrometer (LDV). While an assignment of these deflection shapes to measured resonant frequencies from pad FRF testing is possible, the high resonant frequency density complicates such a classification for the brake discs. The brake disc mode shapes are shown in appendix B.1 to obtain a general impression which deflection shapes occur in free-free condition for the discs used in this work.

Standard Operating Procedure

The whole standard operating procedure for each friction material consisted of six successive steps:

1. After brake pads are finely machined coplanar, compressibility measurements of both pads with six cycles up to 100 bar brake line pressure at ambient temperatures are conducted. Before proceeding to the next step, the pads are given a waiting period of at least 24 hours. This is common practice in brake industry, to recover the viscous behavior of the elastic properties. Although the usefulness of this method has not been proved here, the waiting period has no known negative effects.

2. FRF measurements of brake disc and pads in free-free condition are carried out. Each measurement consistes of five excitations by an impulse hammer. For the brake disc measurements in axial and radial direction are done separately.

3. The disc is mounted on the driving shaft of the dynamometer and additional disc FRF measurements are conducted. All fixing screws of disc and caliper are lubricated and locked with a torque of 110 Nm.

4. The setup of the parts on the dynamometer is completed by fixing the caliper, including the brake pads. Disc FRF measurements with applied brake line pressure are conducted.

5. The dynamometer test procedure, which is discussed more closely below, is run fully automated.

6. After the dynamometer test ends, the brake pads are removed from the caliper and a FRF measurement of the mounted brake disc is conducted.

7. The disc is dismounted and FRF measurements of brake disc and pads in free-free condition are carried out in the way described in step 2.

All noise-related data in this work has been gathered according to this standard procedure. Most of the other data, like the brake disc free-free out-of-plane deflection shapes, was measured differently.

Standard Dynamometer Test Matrix

An overview of the target values of the used standard dynamometer test matrix is given in table 4.5. The test procedure consists of 564 pressure controlled brake applications grouped into nine sections. The whole dynamometer test is run in temperature controlled mode, applying heating drag brake applications at 50 km/h vehicle speed and 20 bar brake line pressure (as specified in the SAE J2521 specification) or unpressurized cooling at 10 km/h vehicle velocity, if required. The brake time of all deceleration brake applications arises from the inertia simulation.

The first 150 stop brake applications have identical control parameters and form the run-in section. During this section, the frictional run-in behavior can be observed and a conditioning of the tribosystem for the following brake applications is achieved.

Sections two to four, seven and nine are taken from the SAE J2521 procedure unchanged. The standardization of these sections makes it possible to compare them to other SAE J2521 tests, even if it can be assumed that the first section modifies the friction behavior of the second section.

The sections two and three are used to change the run-in brake line pressure to get a more balanced conditioning of the tribosystem.

Sections four, seven and nine are generally used to evaluate the friction behavior during a SAE J2521 test. This section was originally taken from the AK Master dynamometer procedure and incorporated into the SAE J2521. The standardization of the section makes it possible to compare the friction behavior of the conducted tests to standard SAE J2521 test results.

The sections five and six are based on the SAE J2521 procedure. The goal of the modification is to balance the amount of drag and stop brake application data, resulting in a balanced noise test matrix. This is done by using the same initial temperature steps for both sections. Compared to the SAE J2521 the temperature steps in this test matrix are larger for the drag brake applications, and the stop brake applications have a higher maximum temperature level. The average stop brake time is higher as the mean drag brake application duration. However, as the drag brake application section has two additional (unpressurized) drag brake applications at each temperature step, the best possible balanced amount of measurement data points results.

The drag section consists of brake applications at two different (but constant) velocities with seven different brake line pressures at 11 different initial temperatures. Each

Table 4.5.: *Target values of standard dynamometer noise test matrix used in this work*

Section		*Appl. No.*		v_{ini}	v_{fin}	p	T_{ini}
No.	*Name*	*From*	*To*	$[km/h]$		$[bar]$	$[°C]$
1	Run-In	1	150	80	30	20	100
2	Break-In	151	180	80	30	30	100
3	Bedding	181	212	80	30	15, 30, 15, 18, 22, 38, 15, 26, 18, 34, 15, 26, 15, 22, 30, 46, 26, 51, 22, 18, 42, 15, 18, 46, 30, 15, 34, 22, 18, 30, 18, 38	100
4	μ-Eval.	213	218	80	30	30	100
5	Drag	219	372	alternate 3 10	3 10	0, 30, 5, 25, 10, 20, 15 for 8 seconds	50, 100, 150, 200, 250, 300, 250, 200, 150, 100, 50
6	Stop	373	504	50	0	30, 5, 25, 10, 20, 15, 30, 5, 25, 10, 20, 15	50, 100, 150, 200, 250, 300, 250, 200, 150, 100, 50
7	μ-Eval.	505	510	80	30	30	100
8.A	Pressure (pads A - H)	511	558	alternate 50 3	0 3	5, 5, 10, 10, 15, 15, 20, 20, 25, 25, 30, 30, 35, 35, 40, 15, 45, 35, 50, 30, 55, 25, 60, 20	100, 200
or							
8.B	Pressure (pads I - T)	511	558	alternate 50 3	0 3	5, 10, 15, 20, 25, 30, 35, 40, 45, 50, 55, 60	100, 200
9	μ-Eval.	559	564	80	30	30	100

brake application lasts eight seconds and all control parameter combinations result in 154 drag brake applications.

There are main differences between the conceptional goals of the SAE J2521 and the test matrix used in this work. The SAE J2521 covers the parameter space continuously

not to miss a noise event. The matrix for this work generates large amounts of data at specific points in the parameter space, which is needed to do scientific significant statistical analyses. Therefore the drag brake applications in this test matrix are conducted with constant brake line pressure.

The order ot brake applications is shown in the parameter list in table 4.5, which should be read as:

- The first brake application of section five is at constant 3 km/h vehicle velocity with 0 bar brake line pressure and an initial disc temperature of 50 °C.
- The following second brake application is at 10 km/h vehicle velocity with 30 bar brake line pressure, also at 50 °C initial disc temperature.
- The third brake application is at 3 km/h with 5 bar brake line pressure again and still at 50 °C initial disc temperature.
- This pattern is continued in the the way for the first 14 brake applications.
- After 14 brake applications the initial disc temperature is changed from 50 °C to 100 °C. At this initial temperature the next brake applications are conducted exactly as described above. After another 14 brake applications the initial temperature is increased again, and so on.

All stop brake applications of section six have an initial vehicle velocity of 50 km/h and end at standstill. During each initial disc temperature block, two cycles of brake applications with different brake line pressures are conducted, as shown in table 4.5. Overall, section six has 132 stop brake applications with varying durations, due to the inertia simulation.

The pressure section was added to investigate noise behavior at higher brake line pressures. The SAE J2521 covers the brake line pressure range of interest to the automotive industry, where brake noise e. g. during an emergency stop is not very important. However, this work investigates the influences of pad, disc and contact assembly stiffness and the friction coefficient on the squeal propensity. With the nature of the brake assembly to become stiffer with increasing normal load, a larger brake line pressure range leads to a larger variation in the stiffness range (cp. chapter 4.4.2).

Section eight consists of drag and stop brake applications with pressures between 5 bar and 60 bar at two initial disc temperatures. During a stop brake application only

a part of the brake torque has to be applied by the electric motor of the dynamometer (electric inertia simulation) as the other part is brought up by the flywheel. For drag brake applications the generated motor torque has to be equal to the brake torque in order to maintain velocity. This limits the maximum applicable brake line pressure.

For the first series of tests (pad materials A - H) the friction level was higher than for the second series which had specially designed brake pad materials. To use the largest brake line pressure range available for both sets of tests, two alternative sections have been used. Both sections have two initial temperature blocks with alternating stop and drag brake applications. For the second series of tests (pad materials I - T, section 8.B in table 4.5) the brake line pressure steps are constantly increasing from 5 bar to 60 bar, using the same pressure for two successive brake applications - one stop and one drag application. In section 8.A, for the first set of tests, the maximum brake torque of 920 Nm was met for brake line pressures little above 35 bar, due to the partly very high friction coefficients. Consequently, the brake line pressure of the drag brake application following the 40 bar stop brake application was reduced. Instead of the drag brake applications at 40, 45, 50, 55, and 60 bar of the second test series, drag brake applications at 15, 35, 30, 25, 20 bar were carried out, respectively (shown in table 4.5). The brake line pressure during the stop brake applications was the same for both sections (8.A and 8.B). The ten different drag brake applications of the two versions of section eight lead to small changes in the investigated parameter space and might lead to history dependent variations in the friction behavior. On the other hand, the friction behavior has been measured and for the present investigation the benefit of the enlarged parameter range justifies the small test parameter variation.

All sections in the test matrix can be classified into three groups, according to their purpose:

- The run-in and conditioning group, consisting of sections one to three, namely the first 212 brake applications.
- The friction evaluation sections four, seven and nine, which also can visualize changes in friction level (even not at noise relevant control parameters). They also serve as intermediate conditioning sections.
- The remaining sections five, six and eight form the actual measurement group, from which the most statistical data analyses were performed. These 334 brake applica-

tions generate a sufficiently large number of data points per test (approx. 10^5). Brake applications of these measurement sections will further also be called measurement brake applications.

The need to keep the structural changes as small as possible limits the pad wear. To deal with his issue the test matrix is shorter as the SAE J2521 procedure because no sections are repeated. The dynamometer test procedure used in this work generated sufficient data for analyses, but is on the other hand short enough not to generate large pad wear.

4.2.4. Data Acquisition

A STAC SPMulticompact Brake Noise Analyser was used to record all signals during dynamometer testing. With the standard software 'EventScan' data is recorded while a trigger signal is applied. During the recording periods up to eight 'slow' channels can be taken with a sample frequency of 25 Hz. Additionally, the time signals of two 'fast' channels with a sampling rate of 51.2 kHz can be recorded. All channels record voltages between -10 V and 10 V. By applying predefined calibration factors to the voltage signals, it is possible to save the data already converted into the units of interest.

During the dynamometer testing, the two fast channels recorded time signals of microphone and accelerometer, the first converted into Pa, the latter into m/s^2. The signals of brake line pressure, brake torque, disc temperature and velocity have been taken from the dynamometer control unit and recorded by the slow channels. The time lag (due to telemetry, mechanical and electronic delays) of these signals has been estimated to be less than 30 ms. Nevertheless, in the worst case there could be a false assignment of the directly measured fast channels to the delayed slow channels. As the signal change of brake line pressure, brake torque, disc temperature and velocity within 40 ms between two measurement points is less than the estimated errors for the signals (in this work), this worst case effect can further be neglected.

Prior to the first set of tests, a calibration of the dynamometer was done to ensure correctness of the measurement values and estimate systematic and statistical errors. The calibration of the accelerometer and microphone was done (and checked periodically) by the manufacturers. The accelerometer error for frequency was well within the 50 Hz validation interval (cp. subsection 4.2.5). Although the absolute amplitude of the accelerometer was of minor importance, a maximum dB error of 1.8 % up to 7 kHz and

4.0 % up to 10 kHz (based on the measured value) was estimated. For the microphone an amplitude error of 1 dB has been specified for frequencies below 10 kHz and 2 dB above 10 kHz. The frequency precision was higher as the 50 Hz intervals used for analysis.

A closer look has to be taken on the slow channel signals, which are partly used to calculate secondary values, like the friction coefficient. The two most important parameters for these calculations are brake line pressure and brake torque.

The pressure was calibrated in two steps. First, an external pressure gage was used to calibrate the pressure control. Then, the pressure was controlled by the dynamometer with different target values and the response was recorded with the STAC system. During these tests a systematic error was found. The rate of the pressure rise was not constant as specified. It decreased drastically when the target pressure value was almost reached. As as a result, applying a target pressure took more time than expected, but no pressure overshooting occured. Thus, on the 25 Hz measurement scale the pressure is observably lower than the target value during the first measurement points, because the measurement is started when the pressure reaches 90 % of its target value. In the pressure range of interest (0 bar - 60 bar) the standard deviation of the measured brake line pressure values is without functional dependence to the pressure target value as shown in figure 4.4 (a). The statistical error was estimated from these tests to $\sigma_p < 0.09$ bar.

The brake torque calibration was done by placing masses on a shaft-mounted lever arm. In this way, well defined torque steps were applied to the torque sensor and the measured value could be recorded and used for error estimation. The torque was ramped up in steps of 200 Nm and down again, before the procedure was repeated on the opposite end of the lever arm, resulting in a torque in opposite direction. The measured torque as function of applied torque shows a hysteresis behavior, mainly during the torque direction change. During the experiments for this work, only positive vehicle velocities were tested, so this effect is of minor importance here. All brake torque in this work is treated as absolute values, knowing that a friction force acts in opposite direction to the (positive) velocity. The standard deviation for the brake torque along the direction of interest is shown versus applied brake torque in figure 4.4 (b), as absolute value with point-markers related to the left y-axis and as relative value with '+'-type markers related to the scale on the right y-axis. An increasing standard deviation of the measured torque with increasing applied torque can be seen, while the standard deviations during increasing and decreasing applied torque match. The relative standard deviation of the brake torque is less than 1.6 % of the brake torque, resulting in a statistical error of $\sigma_M < 0.016 \cdot M_B$.

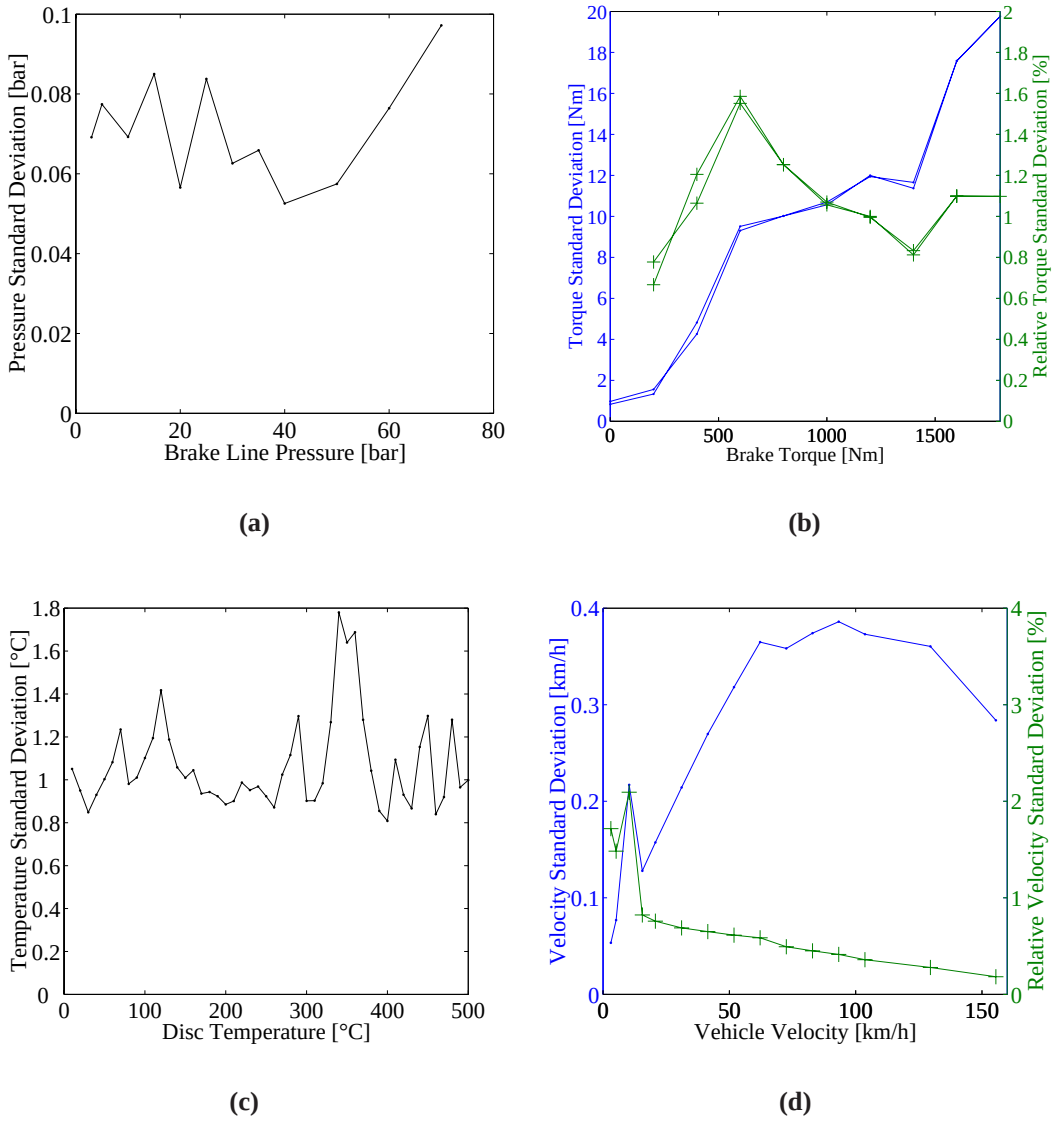

Figure 4.4.: *Standard deviations of measurement signals, taken during calibration experiments, for error estimation. Curves marked by '+' are scaled according to the right hand axis.*

The friction coefficient calculation was done according to equation 2.2 from the SAE J2521 standard (cp. equation 2.2 on page 12), using a constant $p_{\text{threshold}} = 0.5$ bar. The errors resulting from $p_{\text{threshold}}$, the piston area A_{piston} and the efficiency η are mainly dependent on the chosen value or caliper and are test matrix dependent. As neither these chosen values nor the caliper or the matrix is varied for the different tests, the resulting errors can

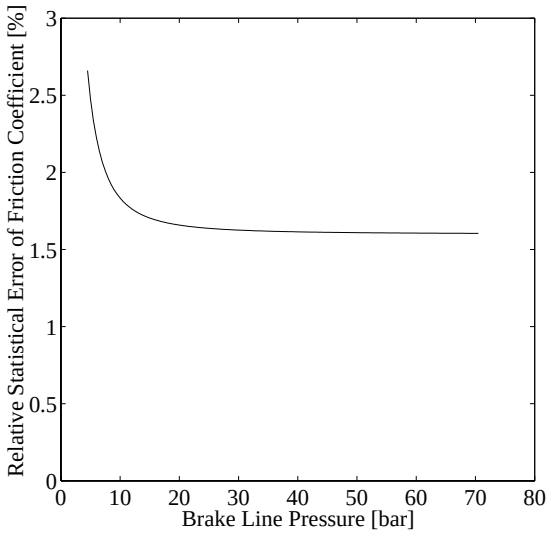

(a) Relative statistical error of the friction coefficient versus brake line pressure

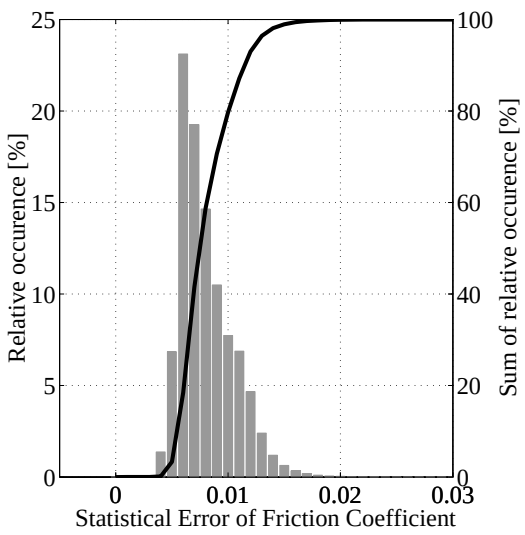

(b) Absolute statistical error distribution of the friction coefficient for all tests conducted in this work. The histogram refers to the left y-axis while the right y-axis is for the line plot

Figure 4.5.: *Statistical error of the friction coefficient*

be assumed to be systematical errors of the measurement. In this case, the errors affect all tests in the same way, the results are comparable within this work and these errors can further be neglected here. The effective friction radius r_{eff} also leads to a systematic error, further discussed below.

According to the Gaussian error propagation [21], the resulting statistical error of the calculated friction coefficient is solely dependent on the friction coefficient, the brake line pressure, the statistical error of the brake line pressure and the coefficient of the relative statistical torque error according to equation 4.1:

$$\begin{aligned} \sigma_\mu &= \sqrt{\left(\frac{\partial \mu}{\partial M_B}\right)^2 \cdot \sigma_M^2 + \left(\frac{\partial \mu}{\partial p}\right)^2 \cdot \sigma_p^2} \\ &= \mu \cdot \sqrt{\frac{\left[0.016 \cdot (p - p_{\text{threshold}})\right]^2 + (0.09\ bar)^2}{(p - p_{\text{threshold}})^2}} \end{aligned} \tag{4.1}$$

To show the estimated statistical errors of the friction coefficient, the relative statistical

error versus brake line pressure plot is presented in figure 4.5 (a), while the statistical error distribution for all tests of this work is shown in figure 4.5 (b). It can be seen, that in 80 % of all friction coefficient measurements the statistical error is less than 0.01.

Although the systematic errors of pressure and torque can be neglected during a brake application, the errors of a torque based friction coefficient estimation depends also on the effective friction radius. Due to the caliper shape deformation, the effective friction radius increases with increasing brake line pressure. And, as shown before (cp. chapter 2.2.3), the effective friction radius might change periodically with brake time. This effect would be stronger for larger brake line pressures [31], as it is associated to the degradation of the real contact area. These mechanisms lead to a systematic friction radius error. Based on Dörsch [31], the real contact area for disc brakes is composed of numerous small regions in radial direction, where contact exists. The change of real contact regions therefore influences the resulting friction radius only to a minor extent, as no oscillation of a single contact spot over the whole radial pad area was observed by Dörsch [31]. Based on his findings, the amplitude of the oscillation can be expected to be not significantly larger as 0.3 cm, resulting in a friction coefficient error which is most likely below 3 %.

With the above calculations and considerations the relative overall error of the friction coefficient is estimated to be less than 6 %. This constant relative overall error for the friction coefficient causes different absolute friction coefficient errors, each depending on the measured friction coefficient level. This would make it necessary e. g. to set friction coefficient dependent histogram interval ranges, which is not done in this work. Instead, the interval length is chosen appropriately, knowing that for low friction coefficients the resolution could be better and for high coefficients of friction there is a tolerable chance of measurement error effects.

The temperature shows a nearly constant statistical error of $\sigma_T < 1.8$ °C, as shown in figure 4.4 (c). However, in this work, only the disc temperature in the axial middle of the friction ring is measured to show a general temperature level. The relationship between the temperature at the friction interfaces and the measured disc temperature is not straight forward. For a quasi-static condition with constant heat generation at the friction interfaces a constant temperature gap results, which is about an order of magnitude larger than σ_T. For changing heat generation at the friction interfaces a time lag of the measured temperature occurs due to the heat conduction. As a result, lower final rotor temperatures at the end of the brake application are measured at higher brake line pressures for brake applications with constant overall dissipated energy. Dependent on the brake application

power, even different temperature variations in time are possible, which means the friction interface temperature versus time curves might have no functional relationship to the measured disc temperature curves.

Similar to the brake torque the statistical error of the measured vehicle velocity is velocity dependent. The relative error is below 2.1 %, while the absolute value is $\sigma_v < 0.4$ km/h. In figure 4.4 (d) the absolute error value corresponds to the scale on the left y-axis and is indicated by the point-markers, while the '+'-type markers indicate the relative velocity error (right y-axis).

4.2.5. Postprocessing and Analysis

The used software of the STAC SPMulticompact Brake Noise Analyser stores four different files per brake application on the hard disc, of which two files per brake application are used for analysis. In one file, the time signals of microphone and accelerometer are stored with a sampling frequency of 51.2 kHz, while the other file contains the data of the slow measurement channels. So, approximately 900 MB of raw data per test is generated.

The requirements on a data analysis tool were complex:

- It should be able to handle the large amount of data
- Every step from raw data to the final analysis should be comprehensible (with no unwanted data filtering, averaging, etc.)
- Different statistical analyses (e. g. regression analysis) and customized plots should be possible
- And to have it all done by a single software was preferable.

To fulfill these needs Mathworks' Matlab, a mathematical programming language, was chosen. With Matlab, all data postprocessing was done by developing new program modules, partly based on former work of American Bosch colleagues.

During a first step, the two files for a particular brake application are read, calculations are done and one Matlab file per brake application is saved, including the processed data. Besides unit conversions, the calculations consist of the friction coefficient calculation (according to equation 2.2), the stiffness calculation (explained in chapter 4.4.2) and the processing of the microphone and accelerometer signals to find brake noise.

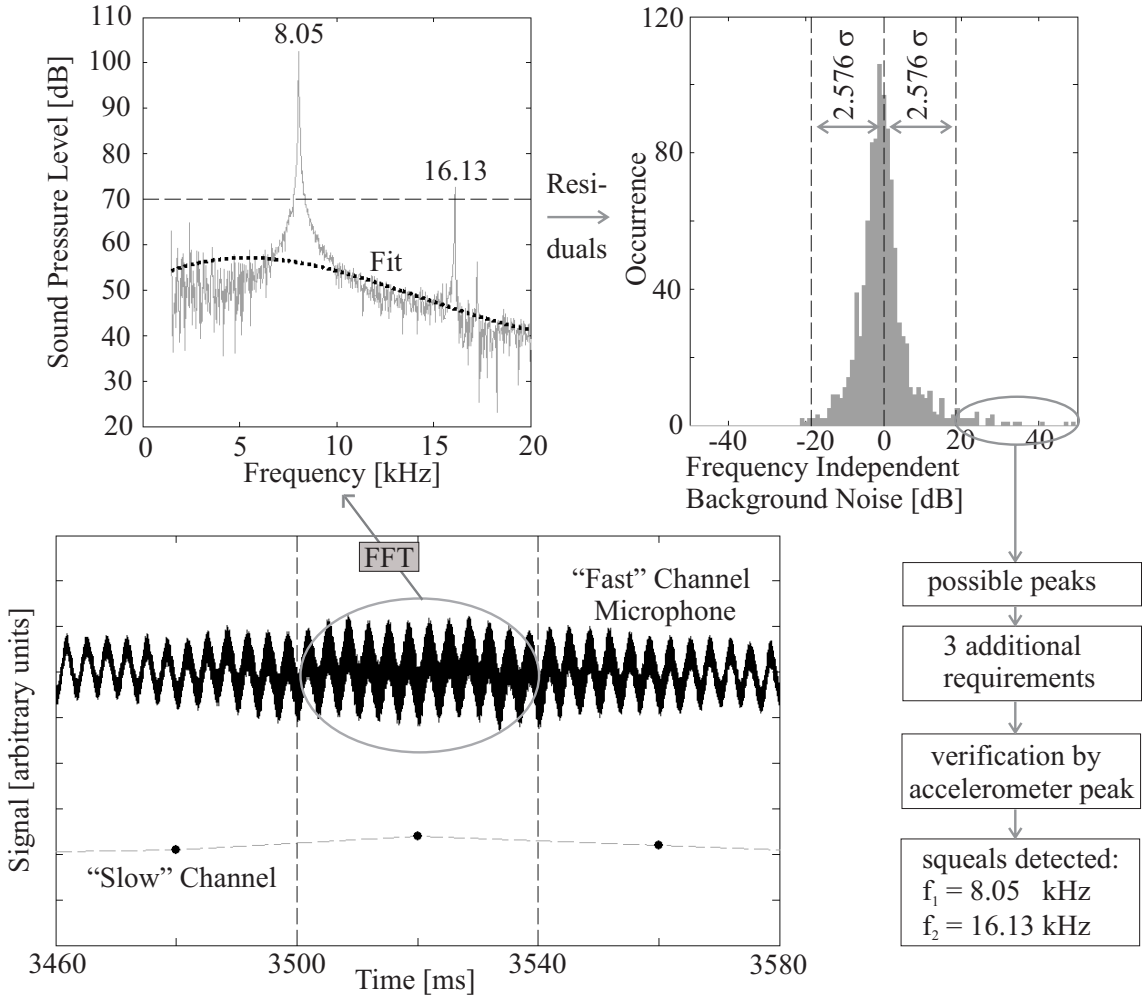

Figure 4.6.: *Schematic process of the noise detection function. Starting in the lower left corner, the microphone signal is segmented. Using a third order polynomial fit the background noise of the signal is estimated (upper left figure). All peak heights, which exceed 2.576 · σ are checked to detect brake noise, as seen on the right hand side*

The steps of the squeal detection function are shown in figure 4.6. First, the microphone and accelerometer signals are divided into sections, each 40 ms (2048 measurement points) long and with the data acquisition of the slow channels occurring in the middle of the time interval. With the one dimensional fast Fourier transformation, two power spectra are calculated from each section, one for the microphone and one for the accelerometer. Then a third order polynomial is fitted onto each dB-scaled spectrum to estimate the frequency dependent mean background noise. The standard error of the fit residuals serves

as frequency independent additional background noise. A peak in the spectrum has to fulfill all of the four requirements:

- The sound pressure level (SPL) in the microphone spectrum at the peak frequency has to be above 70 dB.
- The sound pressure levels at the neighboring frequencies have to be lower than the SPL at the peak frequency.
- The sound pressure level at the peak frequency has to be at least 10 dB above the frequency dependent background noise.
- The sound pressure level at the peak frequency has to be at least 2.576 times the frequency independent additional background noise higher than the frequency dependent mean background noise. If the third order polynomial fit residuals of the measured sound pressure level is Gaussian distributed, this would correspond to 0.5 % of peaks with the highest SPL, because 99 % of a normal curve lie within $\pm 2.576 \cdot \sigma$.

At last, if a peak in the microphone spectrum fulfills all four requirements, a peak in the accelerometer spectrum fulfills the last three and the frequencies of both peaks are within 50 Hz, brake noise is detected. Then, the squeal frequencies and sound pressure levels are included as noise in the postprocessed data for the particular brake application. If two noise events occur in the microphone spectrum within 100 Hz they are and treated as one.

In this first step of postprocessing, one data set is calculated for every brake application, where each measurement point of the slow channels is connected to the noise information consisting of one or more squeal frequencies and related sound pressure levels. In a second postprocessing step, all data sets (brake applications) of one test are merged together to form one data matrix per test. During this merging process all information, e. g. brake application number and brake application time, is maintained. The resulting data set with a sampling rate of 25 Hz is further called real-time data.

Based on this real-time data set various data analyses and plots will be presented. They are presented in the following sections and explained in more detail there. In general, only measurement points where the related brake line pressure is above 90 % of the target value for that brake application are considered. Even with this limitation, systematic

errors might occur at the beginning of the brake application (due to pressure, see chapter 4.2.4). During the last measurement points, the real pad normal forces are usually higher as calculated based on the measured brake line pressure. As the brake line pressure is lowered at the end of a brake apply, effects like the brake fluid's viscosity or the friction between pad edges and caliper wronlgy lead to higher calculated friction coefficients. To solve this matter, the first and last three measurement points within this 90 % target pressure section are also not considered for data analysis and display.

The mathematics used to calculated the regression analyses can be found in the book of Mendenhall and Sincich [65], while Matlab's help provides a lot of additional information on the other used functions and methods, including further references and formulas.

4.3. Application

In this section, results from the application of the previously described measurements are presented. More precisely, the brake pad FRF measurements, the pad out of plane LDV measurements, the dynamometer electric inertia simulation test and the exemplary pad wear estimation are discussed. The squeal related dynamometer results are not discussed here as they are presented in chapter 6.

4.3.1. Structural Analysis

Figure 4.7 (a) shows a typical pad Frequency Response Function (FRF) result plot. The location of excitation and the measurement of the response function was as denoted by marker 1 in figure 4.3 (p. 42). The complex values are plotted as absolute value and phase reversal. A peak in the logarithmic spectrum indicates a resonant frequency. It can be seen that not all peak values for all resonances are equal and that only a part of the resonant frequencies are readily identifiable. To obtain an impression of the deflection shapes, which arise at different resonant frequencies, figure 4.7 (b) contains a summary of LDV measured out-of-plane deflection shapes of a brake pad with a friction material similar to those of the R type brake pads. For clarity all bending modes are presented in a quasi three-dimensional display, while the torsional deflection shape (second from the bottom) is shown from a top view position. Because the resonant frequencies and the according deflection shapes are dominated by the shape of the brake pad backing plate, similar deflection shapes most likely will occur at similar resonant frequencies - even for

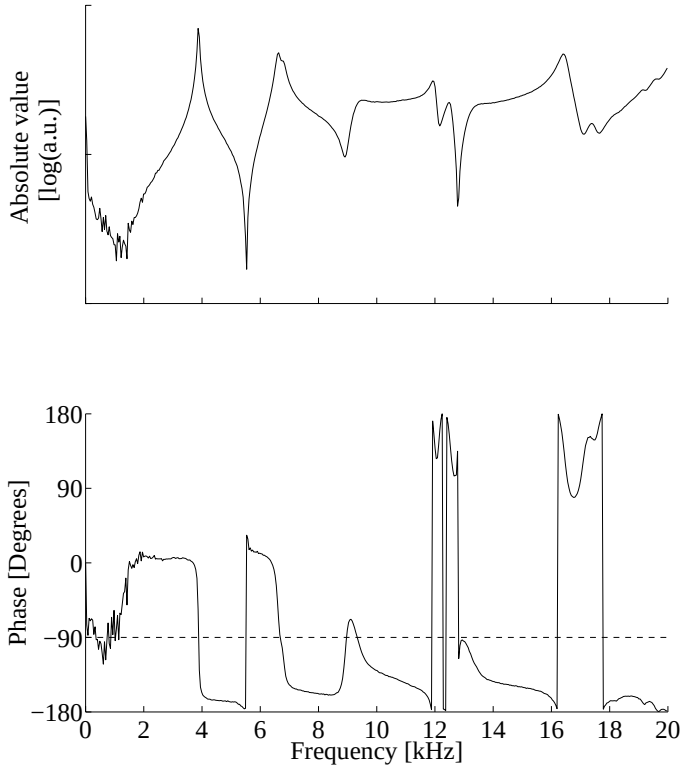

(a) Frequency Response Function of pad A.2 in free-free condition, top: absolute value, bottom: phase reversal

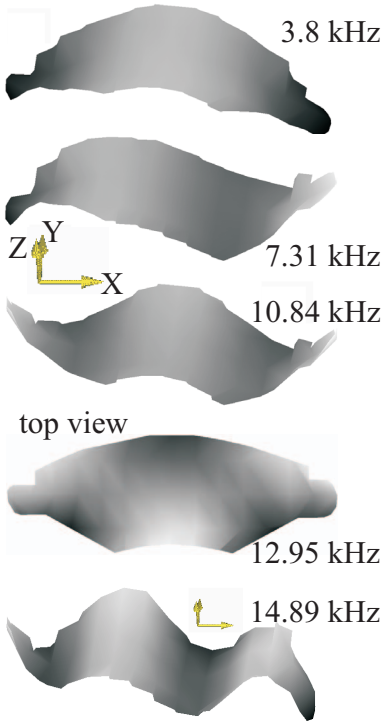

(b) Out-Of-Plane deflection shapes from LDV measurements of a brake pad similar to the used R-type brake pads, top three and bottom bending modes in 3D display, torsional mode in top view

Figure 4.7.: *Exemplary results of Frequency Response Function testing of brake pads*

different lining materials.

Table 4.6 summarizes the resonant frequencies from the pad FRF measurements. Similar trends throughout all brake pads are visible, even if there are some differences in detail. The brake pads of the US vehicle no. 2, which had a radial slot through the friction material and had to be cut into the standardized shape for the used caliper, all show a significantly lower first resonant frequency and also an additional resonance frequency around 5.6 kHz or 5.9 kHz. For frequencies above 10 kHz not all resonant frequencies of all pads could be clearly assigned to each other. Some brake pads show “additional” or largely shifted resonant frequencies, even if the overall tendency appears to be similar for

Table 4.6.: *Resonant frequencies of brake pads from FRF measurements in free-free condition prior to dynamometer testing*

FM	*Resonant Frequency [Hz]*						
	# 1	*# 2*	*# 3*	*# 4*	*# 5*	*# 6*	*# 7*
A.1	3866		6673	9318	11922	12492	16480
A.2	3866		6632	9481	11922	12492	16398
B.1	3581		6795	10050	11841	14364	16927
B.2	3581		6632	9928	12085	13835	16805
C.1	3337		6429	9521	11759	13062	14974
C.2	3255		6266	9277	10457		15218
D.1	3621		5900	8260	11149	14771	17131
D.2	3703		6307		11556	15706	17741
E.1	3499		6755	9725	11597	13672	16602
E.2	3499		6714	9684	11597	13265	16032
F.1	3499		6836	10783	12166	15666	18799
F.2	3540		6755	10620	11515	15259	
G.1	2686	5656	6388	10132	11312	15096	
G.2	2686	5615	6470	10173		15177	16846
H.1	2767	5900	6958	10050	12410	15422	16154
H.2	2808	5941	7161	10376	12410		16113
I.1	3459		6592	9928	11678	13916	17660
I.2	3459		6632	9928	11841	13835	15910
J.1	3906		7365	11027		15625	17782
J.2	4028		7690	11068		13102	16276
K.1	3621		6877	10213	12044	14242	16724
K.2	3581		6755	10091	11922	13916	
L.1	3621		6877	10173	11515	14486	16846
L.2	3621		6877	10213	12044	14608	

all pads.

The resonant frequency density of the brake discs is much higher compared to the brake pad. Additionally, it is necessary for each brake disc to conduct two measurements, one to estimate the out-of-plane and another to estimate the in-plane resonant frequencies. Figure 4.8 shows the FRF plots of brake disc four in free-free condition prior to the first dynamometer test. Due to the large amount of measured resonant frequencies (all brake discs, FRF measurements prior and after each test, free-free and mounted

Table 4.6.: *Resonant frequencies of brake pads from FRF measurements in free-free condition prior to dynamometer testing,* **continued**

FM	*Resonant Frequency [Hz]*						
	# 1	*# 2*	*# 3*	*# 4*	*# 5*	*# 6*	*# 7*
M.1	3988		7528	10905		15706	18473
M.2	3906		7284	10457		15340	17131
N.1	3947		7487	10905	13265	15096	17049
N.2	3947		7487	10986		15544	18392
O.1	3540		6795	10457		15177	16683
O.2	3499		6795	10335		14323	16439
P.1	4110		7650	11353	13875	15747	
P.2	4110		7690	11068	13520	15951	
Q.1	3540		6632	10132	13997	15869	17212
Q.2	3540		6673	10173	14323		16764
R.1	3743		7121	10579		14974	17660
R.2	3743		7080	10417		15137	17537
S.1	3743		7121	10498		15137	17782
S.2	3743		7202	10579		15503	17822
T.1	3784		7161	10620	12858	14730	16439
T.2	3784		7161	10539		15381	17863

condition), no explicit listing of the resonant frequencies is given in this work. As an example, the out-of-plane deflection shapes of the disc number six are given in appendix B.1, knowing that conclusions to the deflection shape based on the resonant frequencies of the other discs are not easy.

For each brake disc the resonant frequencies change, due various reasons: mounting and pressure application, wear during a dynamometer test or machining between two dynamometer tests. Exemplary, these changes are shown for one brake disc, but the results are representative for all brake discs used. Figure 4.9 (a) contains the resonant frequencies of brake disc number four before and after the first and last test in free-free condition on the left hand side and in free-free and mounted condition at different brake line pressures on the right hand side. In both diagrams a white line indicates a resonant frequency from the in-plane FRF measurement while a black line represents a resonant frequency from the out-of-plane measurement.

The measured resonant frequencies before and after the first and last test in free-free

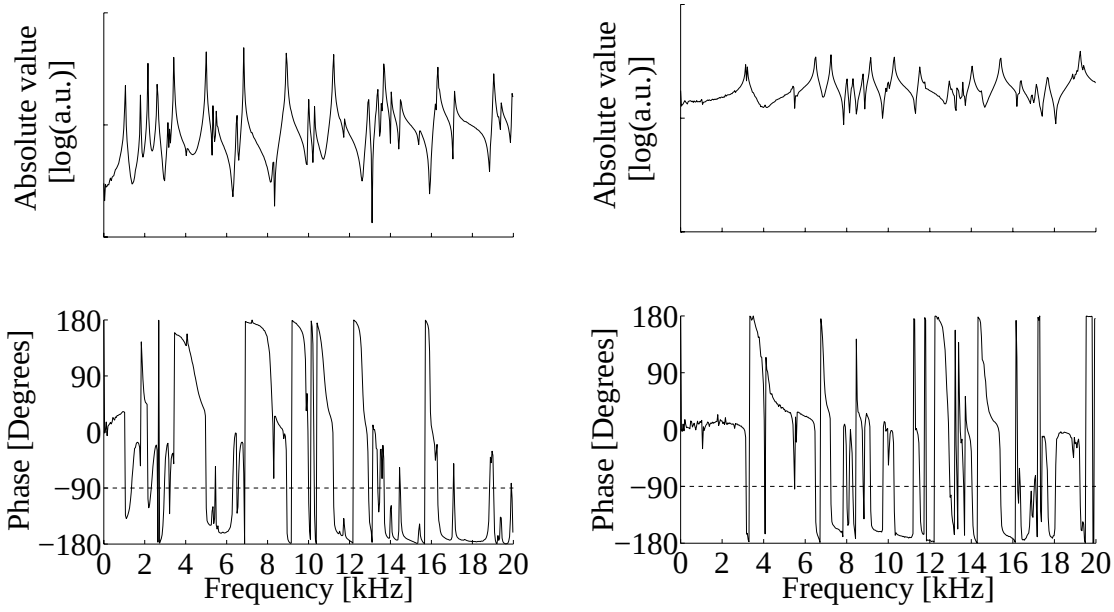

(a) axial **(b)** radial

Figure 4.8.: *Frequency Response Function results of brake disc four as an example, top: absolute value, bottom: phase reversal, each from measurements along (a) axial or (b) radial direction*

condition have no large deviation compared to the resonant frequency change between free-free and mounted condition and further with increasing brake line pressure.

For the mounted condition, some resonant frequencies change, while others are nearly unchanged compared to the free-free condition. With increasing brake line pressure, the resonant frequencies visibly shift, appear or disappear. The lowest applied pressure (5 bar) significantly has more detected resonant frequencies than in the mounted (but unpressurized) condition. At the highest applied pressure of 40 bar the most resonant frequencies occurred.

In the comparison of the different brake discs in figure 4.9 (b) some resonant frequencies are similar for all brake discs, e. g. the axial 3.4 kHz, the radial 7.2 kHz and the 8.8 kHz resonant frequency, which was detected in both directions. These resonant frequencies (among others) are also detectable before and after all conducted tests, they do not significantly change or disappear. Additionally, different resonant frequencies have been measured for the different discs. In general, throughout all disc FRF measurements

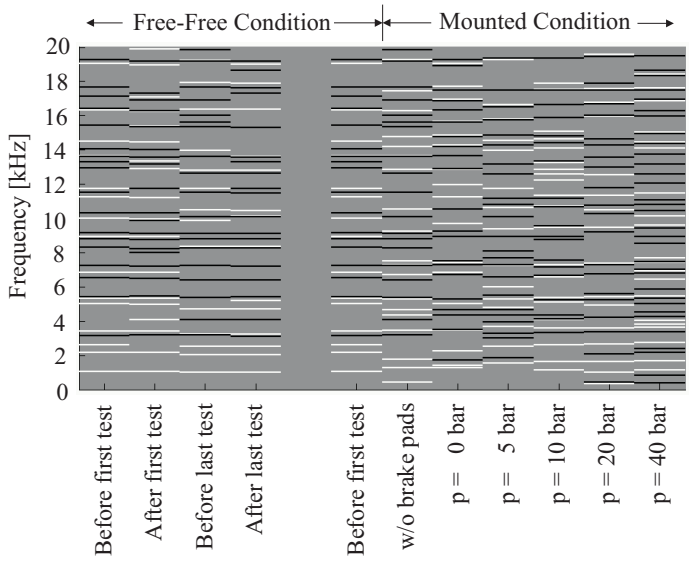

(a) Disc 4: resonant frequency comparison in free-free condition before and after first and last test (left) and resonant frequency comparison of free-free and mounted conditions at different brake line pressures (right), with brake pads of type O friction material

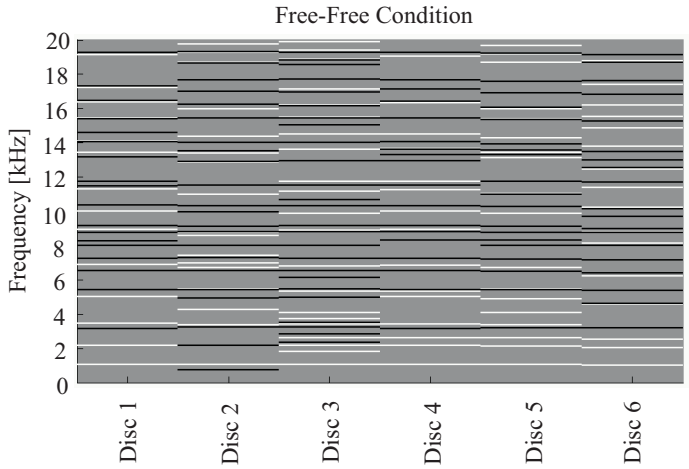

(b) Resonant frequency comparison in free-free condition before first dynamometer test for all discs used

Figure 4.9.: *Frequency Response Function testing of brake discs result summary, black lines represent resonant frequencies from out-of-plane FRF testing (axial) while white lines indicate resonant frequencies from in-plane FRF testing (radial)*

resonant frequencies appear, disappear or reappear between FRF measurements with the same disc (cp. figure 4.9). In some cases, this might be due to the errors of the measurement and the peak estimation. The variation of the resonant frequencies in free-free condition of all used brake discs (figure 4.9 (b)) is less than the resonant frequency variation due to mounting or pressure appliance.

In conclusion the following can be stated:

- The estimation of the disc resonant frequencies by Frequency Response Function measurements shows the deviation between the six identically constructed brake discs to be negligible. The resonant frequency differences of the discs are smaller than the change of the resonant frequencies between free-free and mounted condition of the same disc. Further, the differences between discs are small compared with resonant frequency changes due to applied brake line pressure. Additionally, based on not explicitly shown analyses, no correlation between squeal frequencies and a particular disc could be found. This suggests, that the use of six identically constructed discs did not change the particular system in a drastic way.

- The resonance frequencies from pad FRF measurements are in the same range for all but two friction materials. These are friction materials G and H, which had a centered radial slot dividing the lining. They differ mainly in the first two resonant frequencies.

- In summary it can be concluded from the FRF measurements that for each test similar structural systems resulted, but changes mainly due to the pads with different friction materials are inevitable. Unfortunately for this work, the pad normal stiffness influences its resonant frequencies, so small changes there are unavoidable as the pad stiffness has to be varied.

4.3.2. Inertia Simulation

Before the first dynamometer test, the validity of the inertia simulation was verified. Starting from the definition of the velocity change equations, the actual inertia $\Theta_{sim,i}$ and the overall inertia Θ_{sim} are derived for a constant measurement sampling rate (which leads to

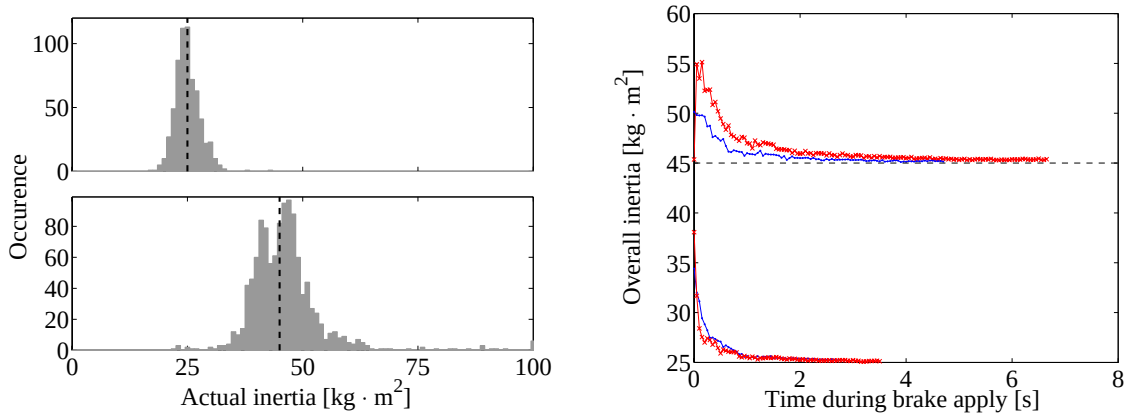

(a) Distribution of actual measured inertia

(b) Overall inertia versus brake application time

Figure 4.10.: *Results of the inertia simulation dynamometer test procedure*

a constant time between two measurement points τ). They are shown in equations 4.2:

$$
\begin{aligned}
v_{\text{vehicle}} - v_{\text{vehicle,ini}} &= \int_0^t a_{\text{vehicle}}\, dt' = \int_0^t \frac{M_B(t')}{r_{\text{dyn}} \cdot m^*_{\text{vehicle}}}\, dt \\
&\approx \frac{\sum_i (M_{B,i} \cdot \tau_i)}{r_{\text{dyn}} \cdot m^*_{\text{vehicle}}} \overset{\tau=\tau_i=\text{const.}}{=} \frac{\tau}{r_{\text{dyn}} \cdot m^*_{\text{vehicle}}} \cdot \sum_i M_{B,i} \\
(2.3): \quad \Theta_{\text{sim}} &= m^*_{\text{vehicle}} \cdot r^2_{\text{dyn}} = \frac{\tau \cdot r_{\text{dyn}} \cdot \sum_i M_{B,i}}{v_{\text{vehicle}} - v_{\text{vehicle,ini}}} \\
\Theta_{\text{sim,i}} &= \frac{\tau \cdot r_{\text{dyn}} \cdot M_{B,i}}{v_i - v_{i-1}}
\end{aligned}
\tag{4.2}
$$

So for each data point i the actual inertia can be calculated from the measured brake torque $M_{B,i}$ and the velocity change $\Delta v = v_i - v_{i-1}$ between actual and previous measurement. In the same manner, the overall simulated inertia from the beginning of the brake application can be calculated based on the velocity change and the sum of the brake torque.

Figure 4.10 contains the results of the electrical inertia simulation test procedure (cp. table 4.4). While the distribution of the actual inertia $\Theta_{\text{sim,i}}$ is nearly Gaussian around the target values (figure 4.10 (a)), the overall inertia Θ_{sim}, calculated from the beginning of

the brake application, converges to the target value, as shown in figure 4.10 (b).

The standard deviation of the actual measured inertia value $\sigma_{\Theta=25\ kg \cdot m^2}$ is 2.69 kg $\cdot\ m^2$ for the lower tested inertia target value and $\sigma_{\Theta=45\ kg \cdot m^2} = 11.13\ kg \cdot m^2$ for the higher tested inertia target value. Even as these values seem large, the actual simulated inertia is only of minor importance. Because the inertia simulation is done to ensure vehicle equivalent energy dissipation during all brake applications, mainly the precision of the overall inertia is crucial.

It is important to note, that the difference between measured overall inertia and the target inertia value decreases with increasing braking duration. For stop brake applications with shorter duration (due to higher pressure) the deviation decreases faster, so the overall inertia difference at the end of the stop is less than $0.5\ kg \cdot m^2$ for all stops. However, the fact that each overall inertia at the end of the brake application is higher as the target value might indicate a systematic inertia simulation error. For this work, this effect will be neglected, because no correlation to a vehicle (and therefore to an exact absolute inertia simulation) is done, and for the dynamometer testing the overall inertia deviation of approximate 1 % is tolerable.

So, the electrical inertia simulation is sufficient to ensure similar and vehicle related conditions for all tests, independent of the friction level.

4.3.3. Pad Wear

The pad wear was tested exemplarily on a pad pair of friction material type A. After a complete run of the standard dynamometer test matrix (cp. table 4.5 on page 47) the inner pad had a wear volume of 423 mm^3 while the outer pad had 516 mm^3. On seven different measurement points per brake pad different wear values were measured - taper wear occurred for both pads. On both sides, the taper wear has a decreasing wear depth from outer to the inner diameter, which is superimposed with a decreasing taper wear depth from leading to trailing edge. On the outer pad both (lateral and radial) wear depth gradients are equal, which results in a nearly linear taper wear from the outer diameter on the leading side to the inner diameter on the trailing side. The wear depths on the outer pad decreased from 0.22 mm (leading edge, outer diameter) to 0.07 mm (trailing edge, inner diameter). For the inner pad, the wear depth gradient in radial direction is two times the lateral gradient. So, the maximum wear depth of the inner pad is at the outer diameter in the middle between leading and trailing edge. It has a wear depth of 0.18 mm, while

the lowest wear depths occur at the inner diameter (0.07 mm on the trailing and 0.10 mm on the leading side).

4.4. Postprocessing

Using the measured data two sorts of calculations are done, whose results will further be used for the squeal propensity models. In this section, the squeal propensity calculation and error estimation is presented. In the second part of this section the stiffness model is discussed. As it is not possible to measure the pad normal stiffness during dynamometer operation with sufficient precision, a model is built, using the data from compressibility testing.

4.4.1. Squeal Propensity Calculation

In general, it is not possible to measure the squeal propensity. The squeal propensity is calculated based on the frequency of occurrence of the two possible discrete conditions ‘squealed’ and ‘did not squeal’. This is similar to flipping a coin to estimate the propensity that it comes up heads. However, similar to flipping a coin many repeated statistically independent experiments are needed. For brake squeal, each measurement is considered to be independent - a realistic assumption, if brake squeal occurs any time the set of parameters is right, which was stated e. g. for the contact conditions by Eriksson et al. [36].

As the parameters can not be measured exactly, the data has to be clustered to calculate the squeal propensity. Within each cluster, the squeal propensity must be constant, so very small intervals have to be chosen. For each cluster the ratio between the number of data points, where a brake noise was detected and the number of all data points within the cluster is defined as the squeal propensity, also called squeal index (SI). The particular value of the squeal index is further related to the middle of the data cluster interval.

By estimating the squeal propensity from occurrence measurements, the precision of the calculation will most likely strongly depend on the number of measurements for each parameter set. Based on some assumptions, the squeal propensity error interval can be evaluated. These assumptions are: there is the same squeal propensity for all data points within a cluster (or the squeal propensity differences within each cluster can be neglected), the squeal propensity depends on the parameter (set) and the squeal propensity

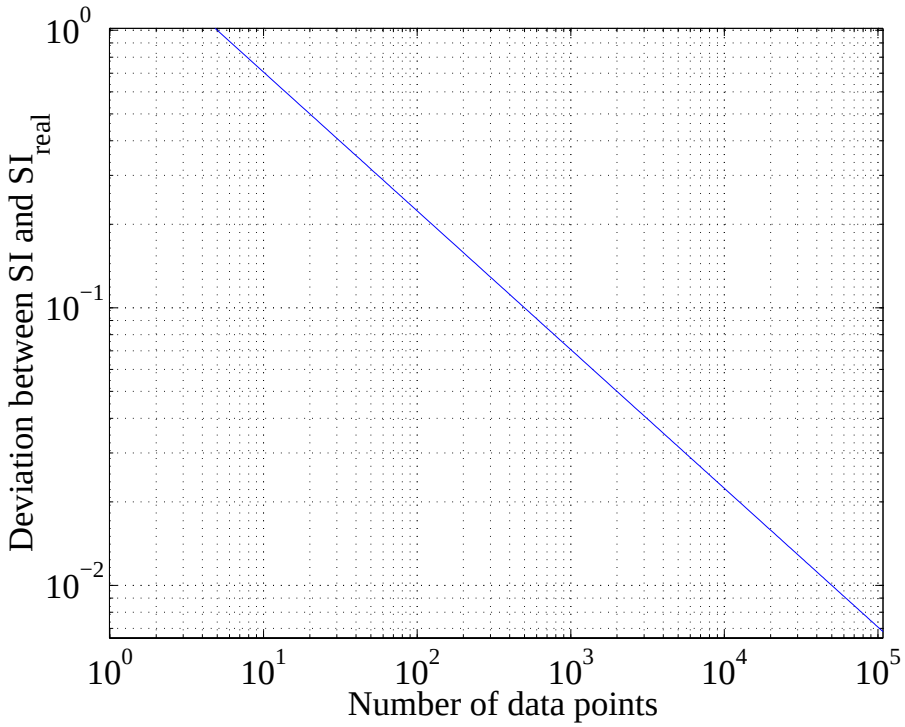

Figure 4.11.: *Maximum deviation ε between measured and true (but unknown) squeal propensity as function of number of data points for a confidence level $\Psi = 95\,\%$*

distribution is static.

Bernoulli's law of large numbers states, that the relative occurrence of squeal (SI) will converge onto the true (but unknown) squeal propensity (SI_{real}) as the number of independent measurements n goes toward infinity [78]:

$$\lim_{n\to\infty} P(|SI_n - SI_{\text{real}}| < \varepsilon) = 1, \quad \forall \varepsilon > 0$$

The absolute deviation ε between relative occurrence SI_n and true squeal propensity SI_{real} provides a good measure for the error. For values of n less than infinity, the weak law of large numbers allows a limit estimation of the propensity P, that the true squeal propensity is within a specific deviation ε from the measured relative occurrence:

$$\begin{aligned} P(|SI_n - SI_{\text{real}}| < \varepsilon) &\geq 1 - \frac{SI_{\text{real}} \cdot (1 - SI_{\text{real}})}{n \cdot \varepsilon^2} \\ \Leftrightarrow \quad P(|SI_n - SI_{\text{real}}| \geq \varepsilon) &\leq \frac{SI_{\text{real}} \cdot (1 - SI_{\text{real}})}{n \cdot \varepsilon^2} \end{aligned} \tag{4.3}$$

In statistics, most calculations and their interpretations are based on a confidence level Ψ, measuring the likelihood that the quantity being estimated falls in the confidence interval $[-\varepsilon,\ \varepsilon]$. This constraint leads to

$$\begin{aligned} & P(|SI_n - SI_{\text{real}}| < \varepsilon) \geq \Psi \\ \Leftrightarrow \quad & P(|SI_n - SI_{\text{real}}| \geq \varepsilon) \leq 1 - \Psi \end{aligned} \tag{4.4}$$

Comparing equations 4.3 and 4.4 an estimate for the error measure ε can be derived. The value of ε depends on the number of data points n, the confidence level Ψ and the true squeal propensity SI_{real}. For each given confidence level Ψ an error measure ε exists, so that the right hand sides of equations 4.3 and 4.4 are equal:

$$\begin{aligned} & \frac{SI_{\text{real}} \cdot (1 - SI_{\text{real}})}{n \cdot \varepsilon^2} = 1 - \Psi \\ \Rightarrow \quad & |\varepsilon| = \sqrt{\frac{SI_{\text{real}} \cdot (1 - SI_{\text{real}})}{n \cdot (1 - \Psi)}} \end{aligned} \tag{4.5}$$

Because $SI_{\text{real}} \cdot (1 - SI_{\text{real}}) \leq 0.25$ for all true but unknown squeal propensities and $\varepsilon > 0$, the error estimation as a function of the confidence level Ψ and the number of data points results in equation 4.6. The error estimation based on $\Psi = 95\ \%$ is shown in figure 4.11.

$$\varepsilon \leq \sqrt{\frac{1}{4 \cdot n \cdot (1 - \Psi)}} \tag{4.6}$$

Strictly spoken these error considerations are only valid, if the squeal propensity exclusively depends on the investigated parameter or set of parameters. However, if a parameter or subset of parameters has a strong impact on the squeal propensity, it is still applicable as approximation. This can be assumed to be mainly true for the coefficient of friction or the stiffness, but not in general e. g. for the brake line pressure or velocity. Without this assumption it is not possible to estimate the error bounds using an acceptable amount of dynamometer tests.

4.4.2. Stiffness Model

Measuring the pad normal stiffness during dynamometer operation is not possible with sufficient precision. Due to circumferential disc thickness variations, pad and disc wear and other effects, it is most unlikely to measure comparable and reliable compressibility

values with a sufficient precision during dynamometer testing, especially at low brake line pressures. However, compressibility measurements prior to dynamometer testing supply data of pad normal deformation versus applied normal force. As the pad normal stiffness is mainly influenced by pressure, the compressibility data is used to model the stiffness during dynamometer testing. In this section, the stiffness modeling approach is presented. After presenting the approach, the results and the model's limitations are discussed.

Modeling Approach

Before dynamometer testing the compressibility of each brake pad was measured. In general, compressibility κ is the deformation of the brake pad under a brake line pressure change from the preload to the maximum pressure level. Assuming that the brake pad normal stiffness c_κ is independent of the normal force N (Hooke's Law), the constant stiffness can be calculated according to

$$c_\kappa = \frac{\Delta N}{\kappa} = \frac{A_{\text{piston}} \cdot \Delta p}{\kappa}$$

The stiffness calculated in such a manner (based on the compressibility test data of the sixth cycle) was used in figure 4.1 (p. 38) to visualize the points where the different friction materials lie in the μ-c parameter space.

As discussed in chapter 2 the deformation versus normal force curve of brake friction materials is non-linear and has a hysteresis. As shown in figure 4.12 during the normal force increase the successive curves match (even for different maximum contact pressures). While the absolute compressibility value and the slope of the curve during decreasing normal force are dependent on the maximum normal force value. Since during dynamometer testing the brake line pressure is applied and held at the target value, the compressibility during a dynamometer brake application should be on the increasing brake line pressure curve.

The stiffness model developed and used in this work is based on compressibility measurements. Similar to most FEM approaches, the contact stiffness is treated separately from the bulk stiffness (cp. chapter 2). Consequently, the overall pad normal stiffness consists of two springs in a series, one representing the contact stiffness and the other the bulk stiffness of the friction material. According to equation 2.1 (cp. p. 9) the contact stiffness c_c depends linear on the normal force N

$$c_c = \lambda_c \cdot N$$

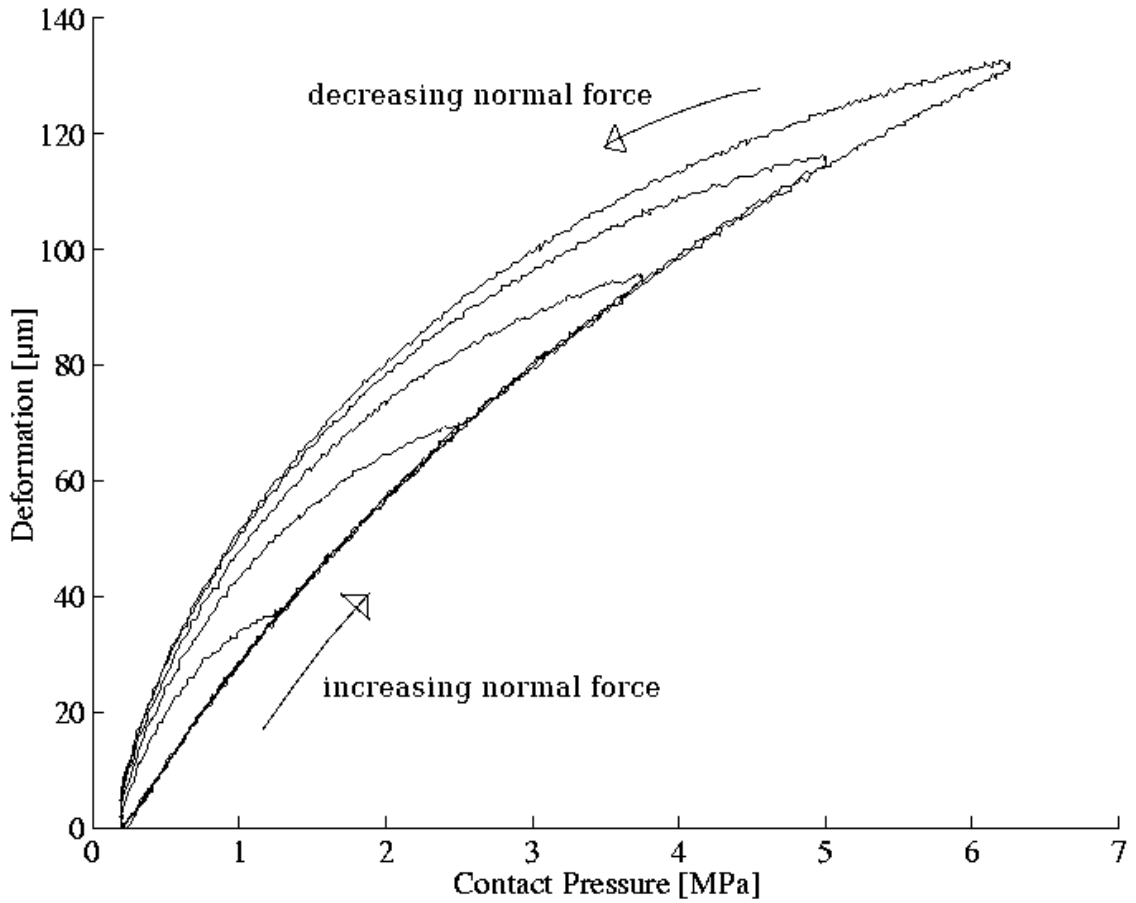

Figure 4.12.: *Deformation κ versus normal force N curves of a brake pad sample for different maximum normal forces. A deformation testing system similar to the one descried by Schmalfuß [81] with small samples described by Kemmer [58] was used with small dwell time at the maximum force*

while the bulk stiffness may also be normal force dependent, but with an additional pressure independent term $c_{b,0}$, as shown in equation 4.7:

$$c_b = \lambda_b \cdot N + c_{b,0} \tag{4.7}$$

The resulting overall pad normal stiffness c results in equation 4.8 and the compliance d is presented in equation 4.9:

$$c = -\frac{dN}{dz} = \left(\frac{1}{c_c} + \frac{1}{c_b}\right)^{-1} = \frac{\lambda_c \cdot \lambda_b \cdot N^2 + \lambda_c \cdot c_{b,0} \cdot N}{(\lambda_c + \lambda_b) \cdot N + c_{b,0}} \tag{4.8}$$

$$d = \frac{1}{c} = -\frac{dz}{dN} = \frac{1}{c} = \frac{1}{\lambda_c \cdot N} + \frac{1}{\lambda_b \cdot N + c_{b,0}} \tag{4.9}$$

The compressibility $\widehat{\kappa}$, resulting from the model, as function of the normal force is the integral of the compliance as shown in equation 4.10:

$$\widehat{\kappa}(N) = \int_{N_{\text{preload}}}^{N} d(N') \quad dN' \tag{4.10}$$

Using the Nelder-Mead simplex algorithm of Matlab, the values of λ_c, λ_b and $c_{b,0}$ were calculated for each brake pad by minimizing the sum of squared errors (SSE) between measured deformation $\kappa(N)$ and modeled compressibility $\widehat{\kappa}(N)$, using

$$SSE = \sum_i \left(\kappa(N_i) - \widehat{\kappa}(N_i)\right)^2$$

Because the Nelder-Mead algorithm only estimates local minima of the sum of squared errors, the optimization was done many times with varying initial values of λ_c, λ_b and $c_{b,0}$. To ensure the physical constraints $\lambda_c > 0$, $\lambda_b \geq 0$ and $c_{b,0} > 0$ the sum of squared errors was continuously increased as one or more values were violating the constraints. The normal force on both brake pads is equal and the solid brake disc can be assumed to be fixed between the pads and to be nearly incompressible. So, the resulting stiffness c for the model can be calculated from the pads' modeled stiffnesses c_{pad1} and c_{pad2} according to

$$c = \frac{c_{\text{pad1}} \cdot c_{\text{pad2}}}{c_{\text{pad1}} + c_{\text{pad2}}} \tag{4.11}$$

However, due to the series connection of the two stiffnesses, the resulting combined model stiffness is in the range of half the pads' stiffnesses. For better comparability of the combined model stiffness to the stiffness values of each single brake pad it is convenient to use the pad equivalent stiffness for analyses and diagrams. This pad equivalent stiffness lies between both pad stiffnesses and is equivalent to $2 \cdot c$ (from equation 4.11). If both stiffnesses are as close as in this work, the average value of both pads' stiffnesses is a useful approximation. As the resulting error from this approximation is negligible compared to measurement errors and uncertainties resulting from model limitations, the average value of both pads' stiffnesses was used as model stiffness.

Table 4.7.: *Stiffness model coefficients*

FM	*Pad 1*					*Pad 2*				
	κ_6 $[\mu m]$	λ_c $[mm^{-1}]$	λ_b	$c_{b,0}$ $[GN/m]$	R^2 [%]	κ_6 $[\mu m]$	λ_c $[mm^{-1}]$	λ_b	$c_{b,0}$ $[GN/m]$	R^2 [%]
A	64	130	4	0.402	99.9	63	148	5	0.373	99.9
B	66	245	0	0.318	99.9	65	196	0	0.347	99.9
C	84	149	10	0.193	99.9	83	108	4	0.286	99.9
D	71	146	0	0.386	99.9	67	182	3	0.205	100
E	75	156	10	0.229	99.9	83	153	13	0.172	99.9
F	53	142	0	0.576	99.7	54	140	0	0.578	99.7
G	63	192	8	0.293	99.9	62	162	4	0.368	99.9
H	38	238	0	0.704	99.7	38	260	0	0.675	99.6
I	112	110	5	0.157	100	124	486	9	0.074	100
J	43	257	0	0.550	99.8	41	445	3	0.476	99.8
K	100	175	9	0.128	99.9	103	419	8	0.113	100
L	86	5000	8	0.129	99.9	88	320	9	0.143	100
M	83	62	0	0.501	99.9	83	159	7	0.210	100
N	63	294	4	0.292	99.9	65	163	4	0.330	99.9
O	113	5000	7	0.093	100	113	136	5	0.147	99.9
P	52	313	15	0.278	99.9	50	159	2	0.541	99.9
Q	123	5000	7	0.084	100	123	495	7	0.088	100
R	64	295	5	0.270	99.9	66	5000	7	0.200	99.9
S	79	5000	9	0.132	99.4	79	5000	16	0.095	99.9
T	65	190	7	0.285	99.9	65	295	6	0.259	99.9

Model Results

Figure 4.13 shows the measured and modeled compressibility (a), the average resulting stiffness model used for analysis (b) and the particular contact, bulk and overall stiffness versus normal force plots (c,d) for both pads of friction material E, as an example. For better clarity the deformation versus normal force curves of both brake pads are plotted into the same diagram (figure 4.13 (a)), applying an offset of 20 μm to pad number one. Table 4.7 summarizes the model's parameters, coefficients of determination R^2 and compressibility measurement values κ_6 (6th cycle) for all brake pads used in dynamometer testing.

The coefficient of determination for all stiffness models is above 99.4 %, which in-

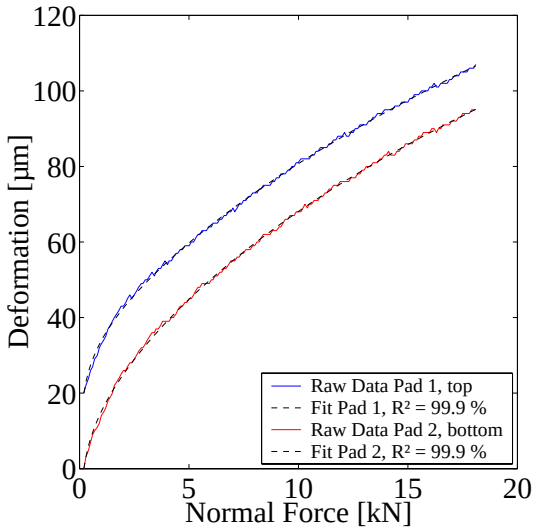

(a) Compressibility: measurement (solid) and model (dashed line)

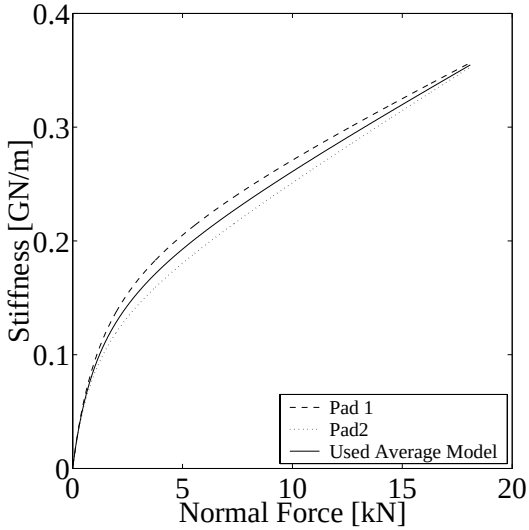

(b) Stiffness models of pad 1 (dashed), pad 2 (dotted) and resulting stiffness for analysis (solid line)

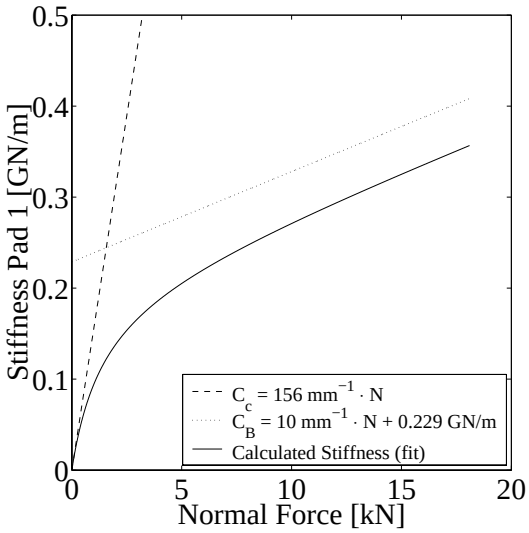

(c) Modeled stiffness of brake pad 1: contact (dashed), bulk (dotted) and resulting (solid line)

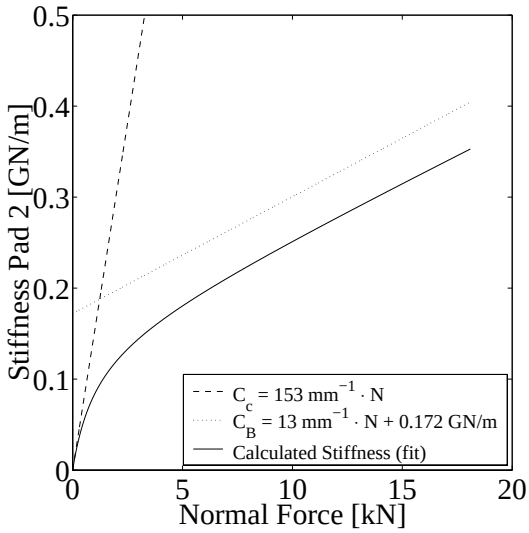

(d) Modeled stiffness of brake pad 2: contact (dashed), bulk (dotted) and resulting (solid line)

Figure 4.13.: *Summary of the stiffness model calculations for the brake pads of friction material E. The maximum applied normal force of 18.1 kN corresponds to a brake line pressure of 100 bar and a contact pressure of 5.02 MPa.*

dicates, that the pressure dependent stiffness behavior of the used friction materials can very well be described with the three chosen parameters and confirms the model approach choice. In figure 4.13 (a) the matching measurement and modelled curves are shown.

The compressibility testing of both sets of friction materials was conducted with two different preloads. For the friction materials A - H a preload corresponding to 1.1 bar brake line pressure was used, while for the friction materials I - T the common normal force (corresponding to 5 bar brake line pressure) was used. However, the first set of compressibility tests showed, that the calculated stiffness model parameters do not significantly change between models based on data with 1.1 bar or 5 bar brake line pressure preload. To be able to compare the compressibility values for both sets of tests, the deformations shown in table 4.7 are based on a brake line pressure difference between 5 bar and 100 bar for all friction materials.

Interpretation of Results

The usual values of the linear slope of contact stiffness versus normal force λ_c lie between 60 mm^{-1} and 500 mm^{-1} (table 4.7). For some friction materials (L.1, O.1, Q.1, R.2, S.1 and S.2) the value of λ_c rises toward infinity during the parameter optimization. For numerical reasons another constraint was added to the parameter optimization to ensure $\lambda_c \leq 5000$ mm^{-1}. This maximum value is large enough to minimize the effect of the contact to the overall compliance (cp. equation 4.9).

Concluding these friction materials do have a very stiff contact is wrong. However, a closer look on the specific cases has to be taken, to be able to interpret the stiffness model results. Different cases have to be considered:

1. For an arbitrary large but finite value of $\lambda_c > 0$ and with $\lambda_b \geq 0$, $c_{b,0} > 0$ the stiffness goes toward zero for vanishing normal force:

$$\lim_{N \to 0} c = 0$$

   So even for very large values of λ_c, the physically plausible stiffness curve results.

2. If a normal force $N > 0$ is applied, $\lambda_b \geq 0$ and $c_{b,0} > 0$ the compliance d converges to (cp. eq. 4.9)

$$\lim_{\lambda_c \to \infty} d = \frac{1}{\lambda_b \cdot N + c_{b,0}}$$

as λ_c goes toward infinity. In this case, the overall stiffness has an asymptotic behavior for $\lambda_c \cdot N \gg 0$:

$$c \rightarrow \lambda_b \cdot N + c_{b,0} \tag{4.12}$$

So for large values of λ_c this asymptotic behavior occurs even for very small normal forces.

3. If λ_b went toward infinity and $N > 0$, $\lambda_c > 0$, $c_{b,0} > 0$ and $\lambda_b \cdot N \gg 0$, the stiffness would show an asymptotic behavior, in the same manner as above

$$c \rightarrow \lambda_c \cdot N$$

but without an offset.

As all tested friction materials trend toward an asymptote, which has an offset at $N = 0$, the optimization algorithm never leads to $\lambda_b \rightarrow \infty$. So brake pads with $\lambda_c = 5000\,\text{mm}^{-1}$ have a linear stiffness behavior at higher normal forces *and* their asymptotes have an offset at $N = 0$, which is $c_{b,0}$. For $N > 0$ equation 4.8 can be written as

$$c = \frac{N}{N} \cdot \frac{\lambda_c \cdot \lambda_b \cdot N + \lambda_c \cdot c_{b,0}}{(\lambda_c + \lambda_b) + \dfrac{c_{b,0}}{N}}$$

and for normal forces $N \gg \dfrac{c_{b,0}}{(\lambda_c + \lambda_b)}$ the stiffness model is asymptotic to a straight line:

$$c \approx \frac{\lambda_c \cdot \lambda_b}{\lambda_c + \lambda_b} \cdot N + \frac{\lambda_c \cdot c_{b,0}}{\lambda_c + \lambda_b} \tag{4.13}$$

If the true but unknown values of λ_c and λ_b, single or both, are large or $c_{b,0}$ is small, the parameter optimization leads to $\lambda_c = 5000\ \text{mm}^{-1}$. By comparing equations 4.12 and 4.13, it can be seen, that in this case the values of λ_b and $c_{b,0}$ will not represent the bulk stiffness coefficients.

It can be concluded, that if the pad normal stiffness increases linear with normal force even for very small (positive) normal forces, the parameter optimization adjusts by $\lambda_c \rightarrow \infty$. In this case, the resulting values of λ_b and $c_{b,0}$ are not only determined by the bulk stiffness, but are associated with both, bulk and contact stiffness. Consequently, the large contact stiffness value has numerical reasons and is not necessarily due to a very stiff contact. As can be seen from the coefficient of determination R^2 values in table 4.7, the models with $\lambda_c = 5000\ \text{mm}^{-1}$ represent the compressibility measurements no worse than the other models - in these cases only the clear distinction between contact and bulk stiffness parameters cannot be made.

Model Limitations

Every model has limitations. Knowing the model limitations is crucial for interpreting the results. Therefore a closer look on the limitations of the model will be taken in this paragraph:

- As the model is based on measured data, it is prone to measurement errors. Fortunately, these errors and their propagation onto the model are easily quantifiable. As the Gaussian error propagation calculation is quite complex, it is done in appendix A. The results can be seen in figure 4.14: The absolute stiffness error σ_c of the majority of the tested brake pads slightly decreases with increasing brake line pressure and is for most pads below 15 MN/m. However, as shown is figure 4.14 (a) some brake pads show higher stiffness errors with different brake line pressure dependences. Below 10 bar the error for one friction material rises at very low brake line pressure up to 43 MN/m, while the error above 10 bar brake line pressure is below 28 MN/m for all tested friction materials. Figure 4.14 (b) shows the relative stiffness error, which is decreasing with increasing brake line pressure for all tested friction materials. Except for two brake pads the relative stiffness error is below 15 %, below 10 % above brake line pressures of 10 bar and below 5 % above 35 bar. The relative stiffness error is within tolerable limits, even if it should be kept in mind, that both tested pads of friction material S shows a relative stiffness error up to 30 % for low brake line pressures.

- During compressibility testing the brake pad is pressed against a piston adapter. Besides possible errors due to different radii or materials, the piston adapter reflects the situation in the brake assembly during brake applications only for the piston side pad, while no finger-side adapters exist. Nevertheless, the finger-side nominal contact area is (more or less) inverse to the piston-side nominal contact area. Assuming a (in z-direction) symmetric backplate, the pad deformation shape would be nearly inverse to the piston side, differing mainly because of different normal stiffnesses in x- and y-direction and a different behavior of the lateral stiffnesses under compression or tension.

- The contact is determined by the surfaces of both objects in contact and by the possible intermediate medium. The compressibility measurements use an opposing object different from the brake disc and a normal force preload to eliminate the

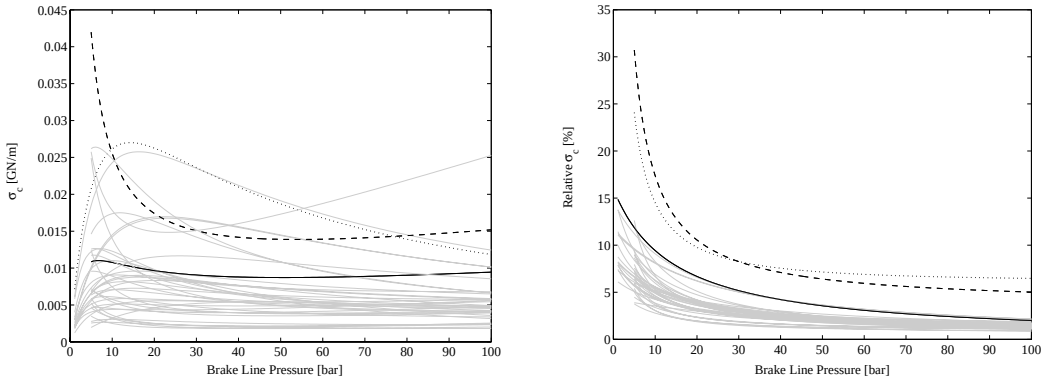

(a) Stiffness error (as calculated according to appendix A) of pad S.1 (dashed), pad H.2 (dotted) and pad P.1 (solid line), other pads plotted light gray color

(b) Relative stiffness error of pad S.1 (dashed), pad S.2 (dotted) and pad H.2 (solid line), other pads plotted light gray color

Figure 4.14.: *Absolute and relative stiffness error*

contact effects on stiffness. As it can be seen, 5 bar brake line pressure preload is not sufficient to avoid contact influences on the overall normal stiffness. Thus, the contact stiffness value for the model is based on the machined pad surface against a very smooth steel plate. It might neither reflect the real condition during a brake application nor the stiffness change due to contact change by formation of friction films and layers, third body particles, etc. A measurement of the contact stiffness during brake application is not possible yet and no appreciable models exist. Nevertheless, the contact can be assumed to become stiffer with decreasing surface roughnesses (e. g. during run-in) and softer due to the formation of the tribofilms and third body layer. Kemmer [58] showed for a single friction material, that many brake applications at high brake line pressure generated small third body particles. In his simulations, the small particles lead to the formation of a stiffer contact.

- The model does not consider effects of the velocity between pad and disc. While the bulk stiffness most likely has no velocity dependence, the velocity might influence the contact stiffness. However, Kemmer [58] made calculations of the disc velocity influence on the contact stiffness of the third body layer and found none.

- The temperature influence is not considered in the stiffness model. In most cases the compliance of the brake pad increases as the (disc) temperature increases. Mea-

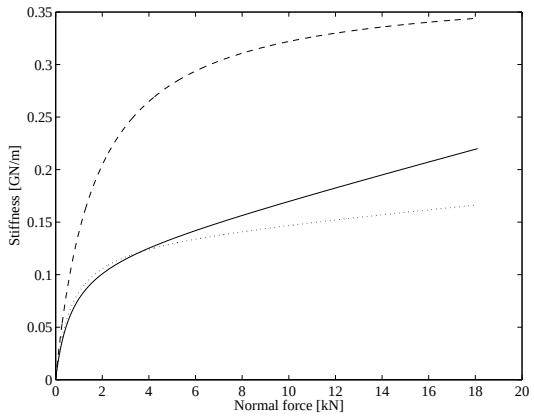

(a) Compressibility: 6th cycle at ambient temperatures (dashed), first (dotted) and second cycle (solid line) of hot compressibility

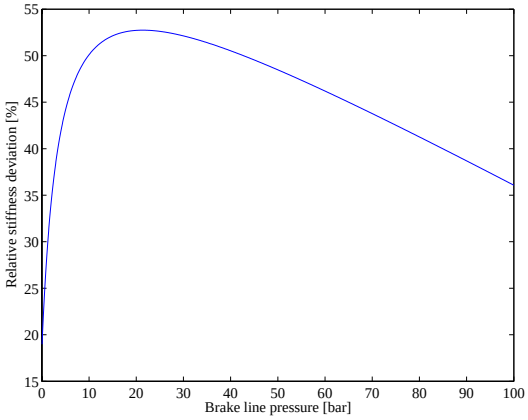

(b) Relative stiffness deviation between ambient temerature and 400 °C (2nd cycle)

Figure 4.15.: *Comparison of ambient and hot compressibility. A brake pad with friction material B was used*

suring hot compressibility changes the friction material irreversible, mainly due to chemical reactions and conversions. Because of the irreversible nature of hot compressibility testing, the brake pads cannot be tested before the dynamometer tests without modifying the friction material permanently. However, to estimate a general temperature tendency, a hot compressibility test has been conducted using a pad, which was not used during dynamometer testing. The calculated stiffness from the deformation versus normal force curves of a friction material B-type pad is shown in figure 4.15. It can be seen that the deviation at small brake line pressures is very small, has a maximum at 24 bar and decreases for higher brake line pressures. The pad becomes softer at higher temperatures. And it re-stiffens a bit for the second hot compressibility cycle, which might be due to plastic deformation and further compaction of the heat affected brake pad zone. The relative stiffness deviation due to the temperature is below 53 % and the general trend can be assumed to be similar for all tested friction materials. So even if the absolute deviation between model and reality at higher disc temperatures is not negligible, the relative deviations between the friction materials at higher temperatures can be assumed to be minor.

- The stiffness, calculated from the model, is for very low frequencies (quasi-static). It has been shown (cp. chapter 2.2.4), that the stiffness increases with frequency and the stiffening, due to normal force increase, also can be seen at higher frequencies. This suggests, that the model trends might also be valid at higher frequencies, even if the absolute values may differ. However, the normal stiffness at squeal relevant frequencies has not been measured and the preservation of the quasi-static normal force trends on stiffness has not been shown yet.

In conclusion it can be stated that even with this model's errors and limitations a clear squeal dependence on stiffness will most likely be observable. The calculated stiffness is qualified to estimate whether there is an important stiffness influence. If no stiffness influence on squeal can be found in this work, quite likely no important stiffness influence exists.

5. Squeal Propensity Regression Model Concepts

The squeal propensity regression models are of prime importance for this work. Prior to actually building squeal propensity models in chapter 6, the general methodology is discussed in this chapter. After presenting the different timescales on which analysis and models are done, data pooling functions are introduced. Using these functions, characteristic values are built on each timescale. They are used for the squeal propensity models. As the regression model function is the same for most models presented in this work, the general modeling approach is discussed. The chapter closes by introducing a measure to rate the quality of the different models. This is needed to judge if significant squeal propensity models can be built, to visualize model chances and limitations and to rank them according to their usefulness.

5.1. Timescales

As presented in chapter 3.2, during dynamometer testing data is measured on the so-called real-time timescale. Unfortunately, not all interesting parameters possibly related to brake noise can be measured during dynamometer testing, e. g. the pad normal stiffness.

The pad normal stiffness is measured once for each brake pad prior to dynamometer testing. A single compressibility value per test is measured, or in other words, the stiffness is measured on the 'one value per test' timescale.

To compare, analyze and build squeal propensity models, data from the considered parameters has to be modeled on the same timescale. This can be done by pooling the real-time data, e. g. using the average of the real-time friction coefficient values $\bar{\mu}_{\mathrm{rt}}$ as the friction coefficient value for the test $\mu_{\mathrm{tt}} = \bar{\mu}_{\mathrm{rt}}$, or by using models to calculate the expected real-time behavior. The particular indices state the timescale of the parameter.

Table 5.1.: *Analysis pattern for different timescales*

Parameter	*Timescale*		
		One value per	
	Real-Time	*Brake Application*	*Test*
brake line pressure	measurement	$\Gamma_{\text{ba,i}}(p)$	
vehicle velocity	measurement	$\Gamma_{\text{ba,i}}(v)$	
disc temperature	measurement	$\Gamma_{\text{ba,i}}(T)$	
friction coefficient	measurement	$\Gamma_{\text{ba,i}}(\mu)$	$\Gamma_{\text{tt,i}}(\mu)$
squeal frequency & SPL	measurement	$SI(\text{freq})$	$SI(\text{freq})$, dom. freq.
pad normal stiffness	$\Gamma_{\text{rt,i}}(\kappa_6, p)$	$\Gamma_{\text{ba,i}}(\kappa_6, \bar{p}_{\text{ba}})$	measurement

The transition between timescales for one parameter is done by mappings Γ, which are discussed more closely in the next section. As these data mappings include data pooling as well as models (like the stiffness model, presented in section 4.4.2), they are not one-to-one mappings. In general, they calculate an unique output based on a set of input parameters in a deterministic way - they are functions from a computer science point of view: a set of instructions to generate the output value based on the input values. Although some mappings are also functions in a mathematical sense, most of them are not.

In addition to the real-time and the test timescale, a third timescale is commonly used for brake tribology: reporting 'one value per brake application'. As on this brake application timescale no data is recorded, the real-time and the test data have to be transferred, using the data mappings $\Gamma_{\text{ba,i}}$. The durations vary between different brake applications, although this timescale is commonly used for dynamometer tests. As a result, different amounts of real-time data are mapped onto one value for different brake applications. For a model on the brake application timescale each brake application is considered equally weighted. This leads to a data weighting which differs from the models on the other timescales.

Table 5.1 summarizes the three timescales for all parameters analyzed. On the (one value per) test timescale not all data mappings are appropriate. As the same dynamometer test procedure is used the controlled parameters (pressure, velocity) do not differ between tests and the disc temperature is strongly coupled to the friction coefficient for the test timescale. The squeal frequencies and sound pressure levels are transferred from the real-time timescale to the other timescales by clustering the registered brake noise by squeal frequency and calculating the squeal propensities for each frequency interval separately.

Intervals in which noise occurred more often will further be called dominant frequency intervals. The stiffness' data mapping function is the stiffness model, presented in chapter 4.4.2.

5.2. Data Mapping Functions and Characteristic Values

5.2.1. Mapping Functions

In general, two sorts of data mapping functions Γ are used: data pooling functions, which calculate one value for a 'larger' timescale (e. g. averaging real-time values per brake application), and data models like the stiffness model, which generate data on a 'shorter' timescale.

The data mapping functions are rules how to project the parameter onto the mapped value, like using the maximum value per brake application. Each different data mapping has an index onto which timescale the data is mapped and a number identifying the mapping. A complete list of all data mappings used in this work is shown in table 5.2.

The first seven data mappings Γ_1 to Γ_7 map the real-time data, e. g. the friction coefficient, onto a brake application (index ba) or onto the test (index tt). It is obvious that no data mappings for this purpose on the real-time scale exist. Also, each data mapping with the same index number generates the same type of output - only for a different timescale. As an example, $\Gamma_{\text{ba,1}}(\mu_{\text{rt}})$ calculates the average friction value per brake application, while $\Gamma_{\text{tt,1}}(\mu_{\text{rt}})$ calculates the mean friction coefficient for the whole test. Both calculations are using the real-time 'measured' friction coefficient μ_{rt}.

The mean parameter value calculation $\Gamma_{\text{ba,1}}$ is more precise if the parameter is constant, but might be misleading if the parameter changes drastically during the brake application.

The maximum and minimum parameter values (Γ_2 and Γ_3) most often occur at the end or beginning (of a stop brake application) and might scatter on a larger scale, compared to the mean value, as they are only based on a single data point.

Mappings four and five estimate a specific parameter value from the parameter distribution per brake application. As for mapping Γ_4 the parameter value below which half the parameter values lie (median) is taken, Γ_5 estimates the parameter value below which 75 % of all parameter values lie. The latter parameter mapping is to test whether higher

Table 5.2.: *Parameter mapping functions used to calculate characteristic values on the 'one parameter value per brake application' and 'one parameter value per test' timescales*

Mapping Function			*Input*	*Output*
rt	*per ba*	*per tt*		
	$\Gamma_{ba,1}$	$\Gamma_{tt,1}$	one real-time parameter, like p, v, T, M or μ	Mean value
	$\Gamma_{ba,2}$	$\Gamma_{tt,2}$		Maximum value
	$\Gamma_{ba,3}$	$\Gamma_{tt,3}$		Minimum value
	$\Gamma_{ba,4}$	$\Gamma_{tt,4}$		Parameter value, below which 50 % of the parameter values lie (median)
	$\Gamma_{ba,5}$	$\Gamma_{tt,5}$		Parameter value, below which 75 % of the parameter values lie
	$\Gamma_{ba,6}$	$\Gamma_{tt,6}$		Center of a Gaussian curve, fitted onto the parameter's distribution
	$\Gamma_{ba,7}$	$\Gamma_{tt,7}$		Standard deviation of the fitted Gaussian curve
	$\Gamma_{ba,8}$	$\Gamma_{tt,8}$	real-time parameter, threshold	Percentage of data points, which lie above the threshold parameter value
$\Gamma_{rt,9}$			real-time p, v, T	Slope of Friction coefficient vs. vehicle velocity from model (cp. ch. 6.1.1)
$\Gamma_{rt,10}$	$\Gamma_{ba,10}$	$\Gamma_{tt,10}$	real-time p or $\Gamma_{ba,1}(p)$, κ_6	Modeled stiffness (cp. ch. 4.4.2); for ba timescale $\Gamma_{ba,1}(p)$ is taken
$\Gamma_{rt,11}$	$\Gamma_{ba,11}$	$\Gamma_{tt,11}$	real-time p or $\Gamma_{ba,1}(p)$, κ_6	Average modeled stiffness for both pads $(\Gamma_{ba,1}(\Gamma_{10}(\text{pad1}), \Gamma_{10}(\text{pad2})))$
$\Gamma_{rt,12}$	$\Gamma_{ba,12}$	$\Gamma_{tt,12}$	noise frequency and SPL, cluster interval	Squeal propensity calculation (cp. ch. 4.4.1), varying by cluster range

parameter values (e. g. for the friction coefficient) influence the squeal propensity more.

For mappings six and seven, a Gaussian curve is fitted onto the parameter distribution by minimizing the squared sum of errors by Matlab's Nelder-Mead algorithm. Γ_6 estimates the parameter value at the maximum of the Gaussian curve (the middle of the curve), while Γ_7 calculates the standard deviation of the fitted Gaussian curve. It should be noted that drag brake applications often show a Gaussian distributed friction coefficient value, while the friction coefficient of a stop brake application is not Gaussian distributed in most cases.

Γ_8 calculates the percentage of data points which are above a threshold value. This leads to a more independent measure of the parameter distribution and takes into account, that a friction coefficient threshold might exist below which no squeal is generated (as reported for the friction coefficient by Bergman et al. [9]).

$\Gamma_{\mathrm{rt},9}$ calculates the slope of the friction coefficient versus velocity curve

$$\frac{\partial \widehat{\mu}(\mathrm{p_{rt}}, \mathrm{v_{rt}}, \mathrm{T_{rt}})}{\partial \mathrm{v_{rt}}}$$

from the friction coefficient model $\widehat{\mu}(\mathrm{p_{rt}}, \mathrm{v_{rt}}, \mathrm{T_{rt}})$ using the real-time values of pressure, velocity and temperature. The friction coefficient model is presented in chapter 6.1.2.

The stiffness model presented in chapter 4.4.2 is used for a single pad by Γ_{10} and for both pads of a test by Γ_{11} - the latter averaging the particular model results for each pad as described in chapter 4.4.2.

To calculate comparable squeal propensities (Γ_{12}) on all timescales, the number of real-time data with registered noise is always divided by the overall amount of data within that cluster. The clustering is done for parameter intervals (e. g. friction coefficient and stiffness) on the real-time timescale and for each brake application or for each test. In all cases, the squeal propensity calculation is the same and is done as described in chapter 4.4.1, only the data clustering varies on different timescales.

5.2.2. Characteristic Values

Using the data mapping functions shown in table 5.2, various characteristic values α_{i} have been calculated. The characteristic values related to the friction coefficient α_μ and stiffness α_{c} are estimated on the brake application timescale α_{ba} and on the test timescale α_{tt}. In general, the index i of the characteristic value determines its type, similar to the mapping functions. They are summarized in tables 5.3 and 5.4. As the tables are formally correct but quite abstract, they can be read as follows:

- The first seven characteristic values are the output of the first seven data mappings: the mean parameter value is α_1, the maximum value α_2, and so on.
- Characteristic values eight to 16 are calculated by Γ_8 using nine threshold values. The threshold values for the friction coefficient are 0.2, 0.3, ..., 0.9, while they are 0.05 GN/m, 0.1 GN/m, ..., 0.4 GN/m for the stiffness. In both cases the ninth threshold is the average value as calculated by Γ_1.

Table 5.3.: *Real-time friction coefficient μ_{rt}, real-time stiffness $c_{rt} = \Gamma_{rt,11}(p_{rt}, \kappa_6)$ or stiffness measurement related characteristic values α for $\widehat{SI}(\mu,c)$ models on different timescales*

No.	*Timescale*			
	per brake application		*per test*	
	$\alpha_{\mu,ba,No}$	$\alpha_{c,ba,No}$	$\alpha_{\mu,tt,No}$	$\alpha_{c,tt,No}$
1	$\Gamma_{\text{ba,1}}(\mu_{\text{rt}})$	$\Gamma_{\text{ba,1}}(c_{\text{rt}})$	$\Gamma_{\text{tt,1}}(\mu_{\text{rt}})$	$\Gamma_{\text{tt,1}}(c_{\text{rt}})$
2	$\Gamma_{\text{ba,2}}(\mu_{\text{rt}})$	$\Gamma_{\text{ba,2}}(c_{\text{rt}})$	$\Gamma_{\text{tt,2}}(\mu_{\text{rt}})$	$\Gamma_{\text{tt,2}}(c_{\text{rt}})$
3	$\Gamma_{\text{ba,3}}(\mu_{\text{rt}})$	$\Gamma_{\text{ba,3}}(c_{\text{rt}})$	$\Gamma_{\text{tt,3}}(\mu_{\text{rt}})$	$\Gamma_{\text{tt,3}}(c_{\text{rt}})$
4	$\Gamma_{\text{ba,4}}(\mu_{\text{rt}})$	$\Gamma_{\text{ba,4}}(c_{\text{rt}})$	$\Gamma_{\text{tt,4}}(\mu_{\text{rt}})$	$\Gamma_{\text{tt,4}}(c_{\text{rt}})$
5	$\Gamma_{\text{ba,5}}(\mu_{\text{rt}})$	$\Gamma_{\text{ba,5}}(c_{\text{rt}})$	$\Gamma_{\text{tt,5}}(\mu_{\text{rt}})$	$\Gamma_{\text{tt,5}}(c_{\text{rt}})$
6	$\Gamma_{\text{ba,6}}(\mu_{\text{rt}})$	$\Gamma_{\text{ba,6}}(c_{\text{rt}})$	$\Gamma_{\text{tt,6}}(\mu_{\text{rt}})$	$\Gamma_{\text{tt,6}}(c_{\text{rt}})$
7	$\Gamma_{\text{ba,7}}(\mu_{\text{rt}})$	$\Gamma_{\text{ba,7}}(c_{\text{rt}})$	$\Gamma_{\text{tt,7}}(\mu_{\text{rt}})$	$\Gamma_{\text{tt,7}}(c_{\text{rt}})$
8	$\Gamma_{\text{ba,8}}(\mu_{\text{rt}}, 0.2)$	$\Gamma_{\text{ba,8}}(c_{\text{rt}}, 0.05\ \text{GN/m})$	$\Gamma_{\text{tt,8}}(\mu_{\text{rt}}, 0.2)$	$\Gamma_{\text{tt,8}}(c_{\text{rt}}, 0.05\ \text{GN/m})$
9	$\Gamma_{\text{ba,8}}(\mu_{\text{rt}}, 0.3)$	$\Gamma_{\text{ba,8}}(c_{\text{rt}}, 0.1\ \text{GN/m})$	$\Gamma_{\text{tt,8}}(\mu_{\text{rt}}, 0.3)$	$\Gamma_{\text{tt,8}}(c_{\text{rt}}, 0.1\ \text{GN/m})$
10	$\Gamma_{\text{ba,8}}(\mu_{\text{rt}}, 0.4)$	$\Gamma_{\text{ba,8}}(c_{\text{rt}}, 0.15\ \text{GN/m})$	$\Gamma_{\text{tt,8}}(\mu_{\text{rt}}, 0.4)$	$\Gamma_{\text{tt,8}}(c_{\text{rt}}, 0.15\ \text{GN/m})$
11	$\Gamma_{\text{ba,8}}(\mu_{\text{rt}}, 0.5)$	$\Gamma_{\text{ba,8}}(c_{\text{rt}}, 0.2\ \text{GN/m})$	$\Gamma_{\text{tt,8}}(\mu_{\text{rt}}, 0.5)$	$\Gamma_{\text{tt,8}}(c_{\text{rt}}, 0.2\ \text{GN/m})$
12	$\Gamma_{\text{ba,8}}(\mu_{\text{rt}}, 0.6)$	$\Gamma_{\text{ba,8}}(c_{\text{rt}}, 0.25\ \text{GN/m})$	$\Gamma_{\text{tt,8}}(\mu_{\text{rt}}, 0.6)$	$\Gamma_{\text{tt,8}}(c_{\text{rt}}, 0.25\ \text{GN/m})$
13	$\Gamma_{\text{ba,8}}(\mu_{\text{rt}}, 0.7)$	$\Gamma_{\text{ba,8}}(c_{\text{rt}}, 0.3\ \text{GN/m})$	$\Gamma_{\text{tt,8}}(\mu_{\text{rt}}, 0.7)$	$\Gamma_{\text{tt,8}}(c_{\text{rt}}, 0.3\ \text{GN/m})$
14	$\Gamma_{\text{ba,8}}(\mu_{\text{rt}}, 0.8)$	$\Gamma_{\text{ba,8}}(c_{\text{rt}}, 0.35\ \text{GN/m})$	$\Gamma_{\text{tt,8}}(\mu_{\text{rt}}, 0.8)$	$\Gamma_{\text{tt,8}}(c_{\text{rt}}, 0.35\ \text{GN/m})$
15	$\Gamma_{\text{ba,8}}(\mu_{\text{rt}}, 0.9)$	$\Gamma_{\text{ba,8}}(c_{\text{rt}}, 0.4\ \text{GN/m})$	$\Gamma_{\text{tt,8}}(\mu_{\text{rt}}, 0.9)$	$\Gamma_{\text{tt,8}}(c_{\text{rt}}, 0.4\ \text{GN/m})$
16	$\Gamma_{\text{ba,8}}(\mu_{\text{rt}}, \Gamma_{\text{ba,1}}(\mu_{\text{rt}}))$	$\Gamma_{\text{ba,8}}(c_{\text{rt}}, \Gamma_{\text{ba,1}}(c_{\text{rt}}))$	$\Gamma_{\text{tt,8}}(\mu_{\text{rt}}, \Gamma_{\text{tt,1}}(\mu_{\text{rt}}))$	$\Gamma_{\text{tt,8}}(c_{\text{rt}}, \Gamma_{\text{tt,1}}(c_{\text{rt}}))$
17	$\Gamma_{\text{ba,6}}(\mu_{\text{rt}})$ $+2 \cdot \Gamma_{\text{ba,7}}(\mu_{\text{rt}})$	$\Gamma_{\text{ba,6}}(c_{\text{rt}})$ $+2 \cdot \Gamma_{\text{ba,7}}(c_{\text{rt}})$	$\Gamma_{\text{tt,6}}(\mu_{\text{rt}})$ $+2 \cdot \Gamma_{\text{tt,7}}(\mu_{\text{rt}})$	$\Gamma_{\text{tt,6}}(c_{\text{rt}})$ $+2 \cdot \Gamma_{\text{tt,7}}(c_{\text{rt}})$
18	$\Gamma_{\text{ba,1}}(\Gamma_{\text{rt,9}}(p_{\text{rt}}, v_{\text{rt}}, T_{\text{rt}}))$		$\Gamma_{\text{tt,1}}(\Gamma_{\text{rt,9}}(p_{\text{rt}}, v_{\text{rt}}, T_{\text{rt}}))$	$\kappa_6(\text{pad1})$
19	$\Gamma_{\text{ba,2}}(\Gamma_{\text{rt,9}}(p_{\text{rt}}, v_{\text{rt}}, T_{\text{rt}}))$		$\Gamma_{\text{tt,2}}(\Gamma_{\text{rt,9}}(p_{\text{rt}}, v_{\text{rt}}, T_{\text{rt}}))$	$\lambda_c(\text{pad1})$
20	$\Gamma_{\text{ba,3}}(\Gamma_{\text{rt,9}}(p_{\text{rt}}, v_{\text{rt}}, T_{\text{rt}}))$		$\Gamma_{\text{tt,3}}(\Gamma_{\text{rt,9}}(p_{\text{rt}}, v_{\text{rt}}, T_{\text{rt}}))$	$\lambda_b(\text{pad1})$
21				$c_{\text{b,0}}(\text{pad1})$

- α_{17} is the parameter value of the fitted Gaussian's curve mean Γ_6 plus two times the Gaussian standard deviation Γ_7, as a measure for the upper parameter limit. This value is more robust to measurement errors compared to α_2, however only sensible for drag brake applications or on the test timescale.

- Additionally, three characteristic values based on the friction coefficient models (chapter 6.1.2, table 6.4) are calculated - namely the mean ($\alpha_{\mu,18}$), maximum ($\alpha_{\mu,19}$) and minimum ($\alpha_{\mu,20}$) value of $\partial\widehat{\mu}/\partial v$ ('negative slope').

Table 5.4.: *Additional characteristic values α_c for $\widehat{SI}(\mu,c)$ models based on stiffness measurement for models on the 'one value per test' timescale*

No.	*per test* $\alpha_{c,tt,No}$	*No.*	*per test* $\alpha_{c,tt,No}$	*No.*	*per test* $\alpha_{c,tt,No}$
22	κ_6(pad2)	28	$\Gamma_{tt,1}(\lambda_b$(pad1,pad2))	34	$\Gamma_{rt,11}$(50 bar,κ_6)
23	λ_c(pad2)	29	$\Gamma_{tt,1}(c_{b,0}$(pad1,pad2))	35	$\Gamma_{rt,11}$(60 bar,κ_6)
24	λ_b(pad2)	30	$\Gamma_{rt,11}$(10 bar,κ_6)	36	$\Gamma_{rt,11}$(70 bar,κ_6)
25	$c_{b,0}$(pad2)	31	$\Gamma_{rt,11}$(20 bar,κ_6)	37	$\Gamma_{rt,11}$(80 bar,κ_6)
26	$\Gamma_{tt,1}(\kappa_6$(pad1,pad2))	32	$\Gamma_{rt,11}$(30 bar,κ_6)	38	$\Gamma_{rt,11}$(90 bar,κ_6)
27	$\Gamma_{tt,1}(\lambda_c$(pad1,pad2))	33	$\Gamma_{rt,11}$(40 bar,κ_6)	39	$\Gamma_{rt,11}$(100 bar,κ_6)

- On the test timescale, there are additional characteristic values for the stiffness based on the compressibility measurements (and derived models thereof). Stiffness based characteristic values 18 to 21 are all taken from the 6th cycle of the compressibility measurement for pad number one in the test. More precisely, they are the compressibility κ_6 ($\alpha_{c,tt,18}$), calculated coefficients of linear stiffness increase for the contact λ_c ($\alpha_{c,tt,19}$) and the bulk stiffness λ_b ($\alpha_{c,tt,20}$), and the normal force independent part of the pad bulk stiffness $c_{b,0}$ ($\alpha_{c,tt,21}$).

- Similarly, $\alpha_{c,tt,22}$ to $\alpha_{c,tt,25}$ are for pad number two and values $\alpha_{c,tt,26}$ to $\alpha_{c,tt,29}$ are the average values of the measurement or calculations of both pads.

- The last stiffness based characteristic values for the test timescale ($\alpha_{c,tt,30}$ - $\alpha_{c,tt,39}$) are the calculated stiffnesses (averaged from both pads) $\Gamma_{rt,11}$ at brake line pressures of 10 bar, 20 bar, ..., 100 bar.

On the real-time timescale, mostly the measured parameter values are taken. Only one characteristic value is calculated, using the stiffness model of both pads:

$$c_{rt} = \alpha_{c,rt,40} = \Gamma_{rt,11}(p_{rt}, \kappa_6)$$

To be consistent on all timescales, the measured real-time parameter values are also treated as characteristic values for $i = 40$, so e. g. $\alpha_{\mu,rt,40} = \mu_{rt}$.

5.3. Squeal Propensity Modeling Approach

In this work, squeal propensity models are used to investigate the influences of the tribosystem parameters on the squeal propensity. Therefore, in chapter 6 numerous models based on the characteristic values of friction coefficient and pad normal stiffness are built. The characteristic values have been presented in the previous section.

All squeal propensity models are polynomial regression models, resulting from a least squares fit. For each model up to one characteristic value for each investigated parameter is considered. Three types of squeal propensity models are used:

1. Single parameter based models, used to investigate the squeal propensity dependence on the friction coefficient have the form

$$\widehat{SI}_i(\mu) = \zeta_1 \cdot \alpha_{\mu,i} + \zeta_2 \tag{5.1}$$

2. The main focus of this work's investigations is on $\widehat{SI}(\mu, c)$-models. These models are first order polynomial regression models with an interaction term, resulting in a form like

$$\widehat{SI}_{i,j}(\mu, c) = \zeta_1 \cdot \alpha_{\mu,i} + \zeta_2 \cdot \alpha_{c,j} + \zeta_3 \cdot \alpha_{\mu,i} \cdot \alpha_{c,j} + \zeta_4 \tag{5.2}$$

3. On the real-time timescale the impact of brake line pressure, vehicle velocity, disc temperature and brake torque on the squeal propensity is investigated. This is done by building $\widehat{SI}(p_{\text{rt}}, v_{\text{rt}}, T_{\text{rt}}, M_{\text{rt}})$ models. These models are based on a third order full factorial polynomial regression (including interaction terms), where all statistically insignificant terms have been removed.

5.4. Model Quality Rating Measure

In general, it is always possible to fit the squeal propensity onto a polynomial function and obtain squeal propensity trends from the model's coefficients. However, in some cases, the trends found will not represent the data.

Statistics provides methods of determining how well a regression model represents the data and what the propensity is, that a certain modeled parameter dependence is generated by chance. Although the deeper field of statistics is far beyond the scope of this work, some commonly used methods will be presented here.

The coefficient of determination R^2 is a commonly used measure of how well the data is represented by the model. It is calculated as 1 reduced by the ratio of the squared parameter deviation between model and measurement (called squared model residual) and the squared measured parameter deviation from the parameter's average value. The latter is usually called total error. As each mathematical function can be represented by an infinite order polynomial, it is obvious that R^2 can be increased only by adding additional terms. These terms do not necessarily need to be statistically significant or represent true parameter dependences.

The adjusted coefficient of determination R^2_{adj} 'adjusts' R^2 using the number of model degrees of freedom and the number of data points to be modeled. Using this adjustment, the R^2_{adj} cannot be forced to reach 1 only by adding polynomial terms to the fitting function. Moreover, the adjusted coefficient of determination is always smaller than R^2, and the gap is a measure of how well the model function (collectivity of model coefficients) represents the data. A small gap between R^2 and R^2_{adj} indicates well chosen parameters, of course only for R^2 values near one.

In addition, statistics uses different tests to estimate the significance of data dependences or the whole model. The significance in this context is the propensity, that a modeled dependence of a polynomial term is generated by chance and does not represent the modeled data. Commonly in statistics, a threshold significance is set and regression function terms with higher significance value are not considered for the overall model. This threshold significance also defines the confidence level - the propensity of a data point to be within the estimated error bounds (for normal distributed residuals). Although these methods have been used on the models described in the next chapter, they are not shown explicitly. For further information the reader is referred to Mendenhall and Sincich [65], where all methods are discussed extensively and the used formulae are stated.

In this work different squeal propensity models based on approximately 10^5 real-time data points per test have to be compared to models, built on one value per test. These very different amount of modeled data favors the use of the adjusted coefficient of determination rather than R^2. But beside using the statistical measures described above, a Quality Rating Measure, which is usable on all timescales and can be calculated for all models in the same way, is needed. As one value per test is the least common basis, a single model quality rating value per test has to be estimated.

The overall squeal propensity, calculated for each dynamometer test on a large amount of (real-time) data is a quite robust measure. In addition, each model is able to calculate

the overall squeal propensity for each test. As an example, the real-time regression models calculate a squeal propensity (between 0 % and 100 %) for each data point and the overall squeal propensity is the average squeal index for all data points of a friction material test. The test timescale based models intrinsically calculate the test's squeal propensity. For a brake application timescale based $\widehat{SI}$-model the overall squeal propensity calculation has to weight each brake application's squeal propensity by the number of data points of that brake application.

Naturally, the main purpose of the squeal propensity model is to calculate the squeal propensity with satisfactorily precision. If this is possible for the whole test using the investigated tribosystem parameters, it would prove both, the tribological influence and the possibility to calculate the squeal propensity.

Consequently, this work's standard Model Quality Rating Measure (MQRM) is the difference ΔSI between the the overall 'measured' squeal propensity SI_{measured} and the overall calculated squeal index from the model $\widehat{SI}_{\text{model}}$ for each test (as shown in equation 5.3):

$$\Delta SI = SI_{\text{measured}} - \widehat{SI}_{\text{model}} \tag{5.3}$$

It has to be stated that ΔSI is in percentage points, as it is calculated from two percentage values. A $\Delta SI = 3$ % for a particular friction material test is an absolute deviation between measured and calculated squeal propensity of 0.03, an absolute difference of three percentage points, and is not relatively based on another squeal propensity.

For each model a single ΔSI value per friction material is calculated. To rank the models, the ΔSI standard deviation $\sigma_{\Delta SI}$ and the maximum deviations for a friction material (maximum and minimum ΔSI) are considered. The model's usefulness is primarily judged by the standard deviation of ΔSI, however maximum and minimum ΔSI are used to finely differentiate models with similar ΔSI standard deviation.

In general, the model's usefulness has to be evaluated to investigate the tribological influences and the data pooling effects on the squeal propensity. In a first step, the ΔSI values for all friction material tests are calculated based on the (constant) average overall squeal propensity. The squeal propensity average is as $\zeta_4 = 5.51$ % and has been calculated by the following 0th order polynomial model:

$$\widehat{SI}_{\text{worst case}}(\alpha_\mu, \alpha_c) = 0 \cdot \alpha_\mu + 0 \cdot \alpha_c + 0 \cdot \alpha_\mu \cdot \alpha_c + \zeta_4$$

This ‘worst case’ model does not consider any tribological influences and also has only very limited capability to calculate the overall squeal propensity for each test. Its standard deviation $\sigma_{\Delta SI}$ is 4.87 percentage points with a ΔSI span of 18.20 percentage points. The maximum deviations are 12.70 percentage points (maximum ΔSI) and -5.50 percentage points (minimum ΔSI). Throughout this work, each model is judged whether its ΔSI is significantly smaller. If such models based on friction coefficient and stiffness characteristic values exist, the tribological influence can be shown.

6. Data Analysis and Evaluation of Squeal Propensity Models

In this chapter, data analyses and squeal propensity models on all three timescales are presented. Each section deals with one timescale and within each section, at first the data analyses and then the squeal propensity models are presented. Each section closes with a discussion of the results.

6.1. Real-Time Timescale

All data generated on the real-time timescale is directly related to dynamometer testing. As a lot of data has been generated during dynamometer testing, the next subsection is more extensive than similar subsections dealing with the other timescales.

6.1.1. Data Analysis

In this subsection, the dominant frequency intervals will be estimated and the squeal propensity correlation to a single measured parameter, like brake line pressure, vehicle velocity, disc temperature, brake torque or friction coefficient, will be shown. In addition, the squeal propensity versus calculated real-time stiffness will be discussed. Subsequently, the squeal propensity versus friction coefficient *and* stiffness is shown.

The analyses presented in this subsection focus on all measurement brake application data from all tests to show general trends. For each individual test the analysis result plots are generated in the described way and presented in appendix B.2.

Dominant Frequency Intervals

For squeal (propensity) investigations, the brake noise has to be quantified. For all investigations in this work, brake noise is quantified by its frequency if the sound pressure level

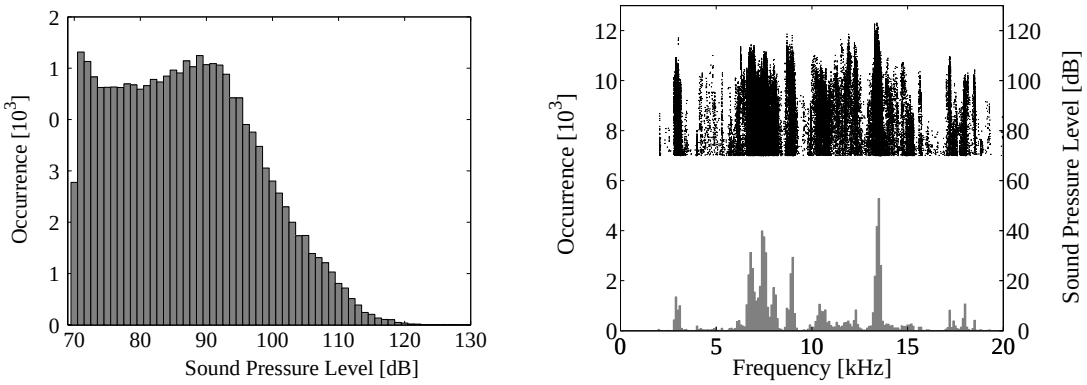

Figure 6.1.: *Noise frequency and sound pressure level result summary for all tests*

exceeds 70 dB at that frequency. Consequently, only brake noise with a sound pressure level of 70 dB or higher is considered for the squeal propensity calculation.

Figure 6.1 shows the frequency and sound pressure level distributions for all data points from the tests of all friction materials. In the left hand diagram, the sound pressure level histogram of all measured squeals is shown. The sound pressure level (SPL) occurrence is constant between 71 dB and 95 dB. The amount of squeals with higher SPLs decreases nearly monotonic. The maximum registered sound pressure level was 123.0 dB at 13.4 kHz. The visible smaller amount at 70 dB is due to the effective smaller interval: the interval is from 69.5 dB to 70.5 dB but only noises with SPL above 70 dB are analyzed.

On the upper half of the right hand diagram, each dot represents a registered squeal on the real-time timescale, indicating the squeal frequency and the sound pressure level. The frequency space is nearly covered, meaning that squeal events at almost all frequencies between 2 kHz and 20 kHz occurred. However, the histogram in the lower half shows that some frequencies occur more often than others. Every frequency, which occurs in at least 0.2 % of all data poins (approx. 3000 data points) is further called dominant frequency. This limit was found to represent the squeal histogram quite well. In the current case the main frequency at which the most squeals have been detected is 13.5 kHz with more than fifteen thousand detected squeal events. For each dominant frequency the neighboring frequency histogram bins are checked to find the whole dominant frequency interval. The dominant frequency intervals for all data points from the measurement brake applications of all friction material tests are summarized in table 6.1, further referred to by their mean

Table 6.1.: *Dominant frequency intervals for the all measurement brake application test data*

Frequency				*No. of Registered Squeals*	
Interval		*Mean*	*Peak*	*Absolute*	*Relative*
From [*kHz*]	*To* [*kHz*]	*At* [*kHz*]	*At* [*kHz*]		[*%*]
2.8	3.1	3.0	2.9	3595	0.23
6.6	7.1	6.9	6.8	11629	0.76
7.2	7.7	7.5	7.4	14909	0.97
7.8	8.2	8.0	8.0	5225	0.34
8.7	9.1	8.9	9.0	7652	0.50
13.2	13.7	13.5	13.5	15458	1.01

frequency.

Even though a lot of different squeal frequencies occurred throughout all tests, not all squeal frequencies were generated during every test. Table 6.2 summarizes the most frequent occurred squeal frequencies for each friction material test, rudimentarily arranged by frequency. The squeal index shown in table 6.2 is calculated from the measurement brake applications only, not to bias the data with the large amount of stop brake applications at high velocities and medium pressure. For the four friction materials with the highest noise propensities (SI > 9.5 %), squeal at one or more dominant squeal frequency occurred. Especially friction materials A and B emit noise within nearly all of the dominant squeal frequency intervals.

Squeal Dependence on Single Parameters

Figure 6.2 shows a summary of the squeal dependence on the brake application number. In the upper plot a point is drawn for each measured friction coefficient during the specific brake application. The color of each point indicates noise: if brake noise at a frequency between 2 kHz and 20 kHz and with a SPL equal or above 70 dB occurred, the point is drawn black, otherwise light gray. In the middle plot, a point is drawn at the particular frequency for each detected squeal with a sound pressure level above 70 dB. In the lower plot the squeal propensity is shown.

In figure 6.2 each separate brake application forms a cluster for squeal propensity calculation, this means cluster number one consists of all data from the first brake application

Table 6.2.: *Frequently registered brake noise frequency summary for dynamometer testing of each particular friction material*

FM	*SI* [%]	*Frequently Registered Noise Frequency* [*kHz*]											
A	18.2	3.0				7.6	8.0	9.1	10.6				18.5
B	10.4	3.1			7.4	7.8			10.2		12.0	13.5	
C	7.1									11.4	12.3	13.4	17.2
D	7.4					7.5							
E	7.1	2.8			7.2	7.5	8.0				13.3	13.6	18.0
F	2.9					7.4			9.9			13.6	19.3
G	0.1			6.5	7.2								
H	15.2											13.4	
I	0.1							9.0	10.4				
J	9.6			6.9				8.9				13.5	
K	0.2		5.3	7.0	7.3			8.8					
L	3.7		6.2		7.1	7.5							
M	3.2			6.8				8.7					17.4
N	5.1			6.7	7.2			9.0					
O	4.7			6.8	7.3								
P	1.5					7.5	8.2	8.9				13.6	
Q	< 0.05				7.2								
R	5.4			6.6		7.5		8.9					
S	4.7					7.7		9.0				13.5	
T	5.5			6.8			8.0					13.4	

of all conducted tests.

The three vertical dotted lines separate the four different parts of the test procedure: run-in section, drag section, stop section and pressure section (cp. chapter 4.2.3). Noise at some frequencies, e. g. in the dominant frequency intervals around 8.9 kHz and 13.5 kHz, occurs almost throughout the whole test procedure - also during run-in at velocities above 30 km/h. In addition, the middle diagram of figure 6.2 shows noise occurring at some other frequencies only during specific (parts of) sections. In the bottom diagram it can be seen that the overall squeal propensity per brake application during the run-in and the stop sections is significantly lower than during the drag and pressure sections. Within the drag brake application section, the maximum and the minimum friction coefficient is lower at high temperatures. The average squeal index decreases with increasing temperature and

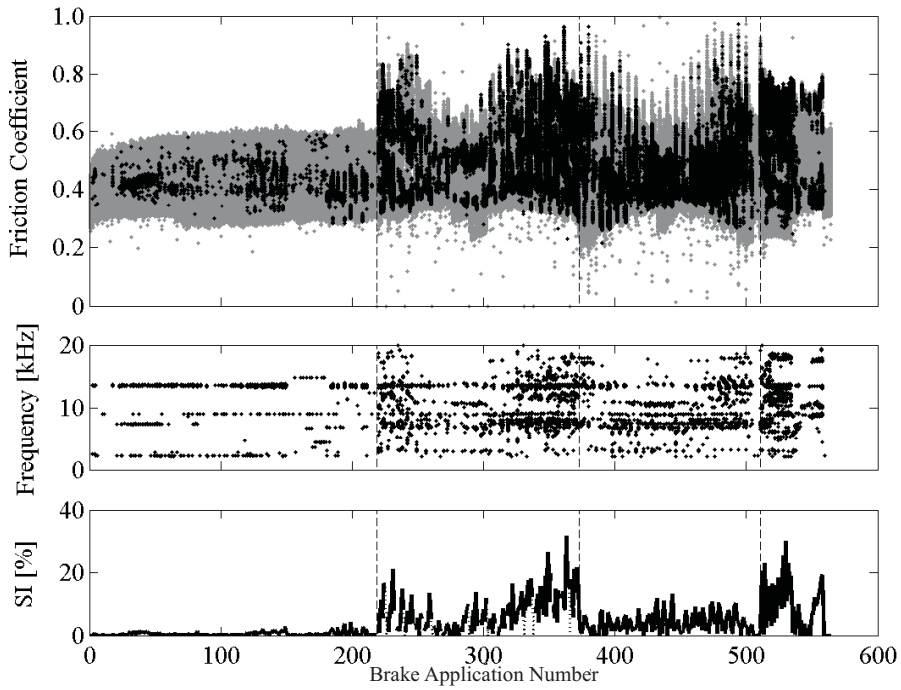

Figure 6.2.: *Friction coefficient and noise occurrences during all test procedures as function of brake application number*

is higher during the second half of the section, after the maximum temperature has been reached. Superimposed on this general trend are visible (nearly periodic) SI maxima, which are due to velocity and pressure dependences of the specific brake application. The increase of the squeal index with increasing pressure is visible in the last part of the test program - the pressure section. There the squeal propensity is higher during the first brake applications, which have the smaller initial temperature.

To find squeal dependences on controlled and measured parameters, the analysis of the real-time data is done the same way for all parameters. The whole data is plotted versus one measured parameter at a time and each parameter cluster may consist data points having very different values for the other, not explicitly shown parameters. As a consequence a seen parameter influence on the squeal propensity might not be solely due to that parameters influence, e. g. a velocity effect can also be a friction coefficient effect, as the friction coefficient is closely linked to the velocity for most materials. Also, as the squeal propensity most likely not depends solely on pressure, temperature, velocity or brake torque, the main assumption of the error calculation (cp. section 4.4.1) is violated, so no error estimation can be done. In the following, the diagrams are discussed, for the

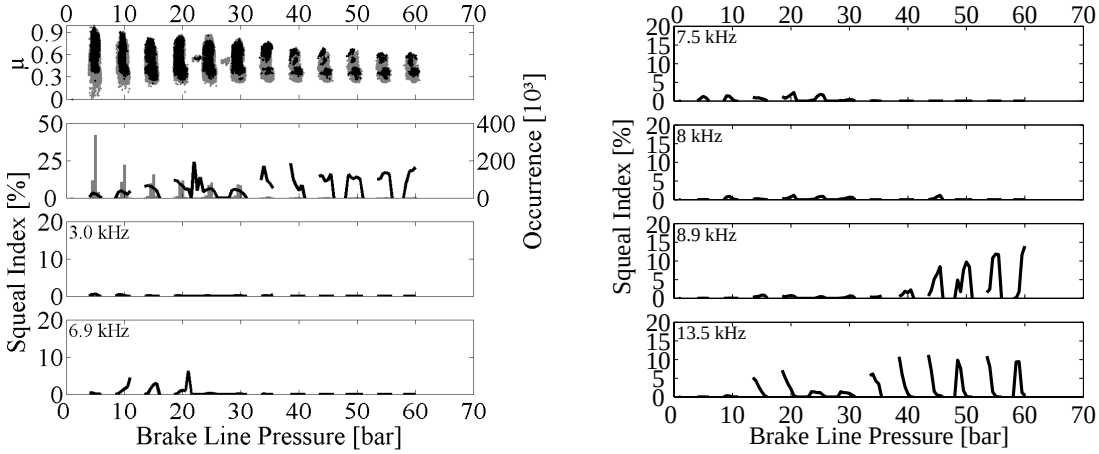

Figure 6.3.: *Squeal dependence on brake line pressure for measurement brake application data from all tests*

brake line pressure, as an example.

The squeal dependence on pressure is presented in figure 6.3. The top diagram on the left hand side shows a dot for each friction coefficient. The dot is black one, if brake noise between 2 kHz and 20 kHz was registered with a SPL equal or above 70 dB. If no squeal occurred, the dot is light gray. With increasing pressure, the deviation of friction coefficient values decreases, mainly due to a decrease of the maximum value. For target pressure values below or equal to 30 bar the friction coefficients with registered noise form a connected area, mainly at higher friction coefficient values within a pressure level. Above 30 bar brake line pressure, two or even three different areas are visible, one of them still at high friction coefficients for each pressure level.

The diagram second from the top on the left hand side combindes the number of data points within each cluster and the related squeal propensity. The histogram is plotted in light gray and related to the right axis. The squeal propensity for brake noise between 2 kHz and 20 kHz, further also called overall squeal propensity, is represented by a black line (scaled on the left axis). The cluster intervals for all parameters have the same lengths (for each parameter) and are equidistant. For the pressure, the data at each target level is divided into three to five clusters with an interval length of 0.5 bar each (fig. 6.3). Within each set of intervals for a target pressure level, the squeal propensity is not constant but mostly lower for the outer clusters. Between target pressures of 5 bar and 20 bar the average squeal propensity increases with increasing target pressure level. Between 20 bar

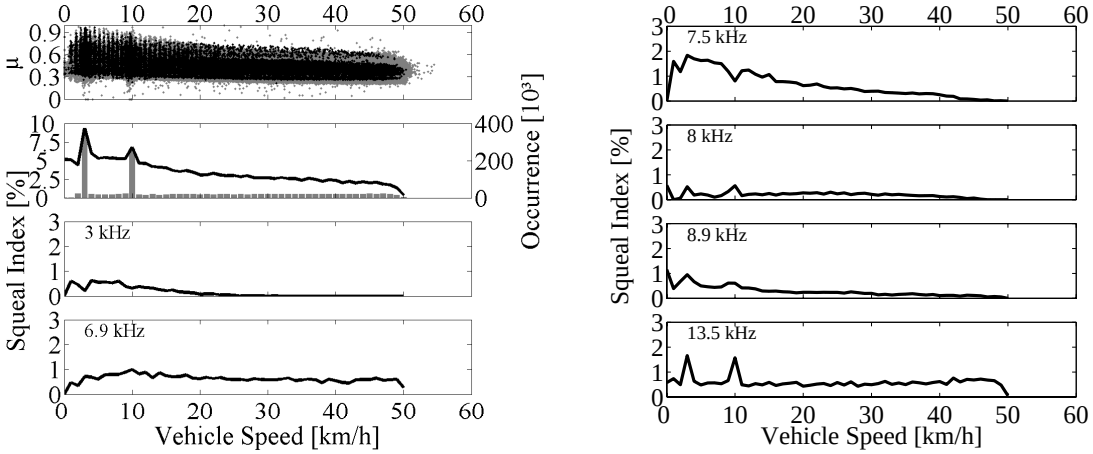

Figure 6.4.: *Squeal dependence on vehicle velocity for measurement brake application data from all tests*

and 30 bar and 35 bar to 60 bar it is nearly constant, but with a visibly higher SI value above 30 bar.

The remaining diagrams of figure 6.3 present the separate squeal propensities for brake noise within each of the dominant frequency intervals. For the calculation of these squeal propensities only the number of registered squeals within the particular dominant squeal frequency interval are divided by the overall number of data points within each cluster. It is clearly visible that the brake noise at different frequencies depends variedly on the brake line pressure: While the 6.9 kHz squeal mainly occurs between 10 bar and 20 bar, the 8.9 kHz and 13.5 kHz squeals show a visible pressure dependence - they increase or are higher at higher brake line pressures.

Figure 6.4 shows the velocity influence on the squeal propensity. The velocity is clustered into 1 km/h intervals for squeal propensity calculation. The amount of high friction coefficient values increases with decreasing vehicle velocity, while the lower friction coefficient bound is approximately constant. The overall squeal index increases with decreasing velocity (above 2 km/h) and is significantly higher at 3 km/h and 10 km/h, the velocities of the drag brake applications. The squeal propensity increases with decreasing velocity for squeal within the majority of all dominant frequency intervals. Around 6.9 kHz and around 13.5 kHz squeal is also generated for higher vehicle velocities with no significant propensity increase at low velocities. However, squeal at 13.5 kHz shows a significantly larger propensity during drag brake applications.

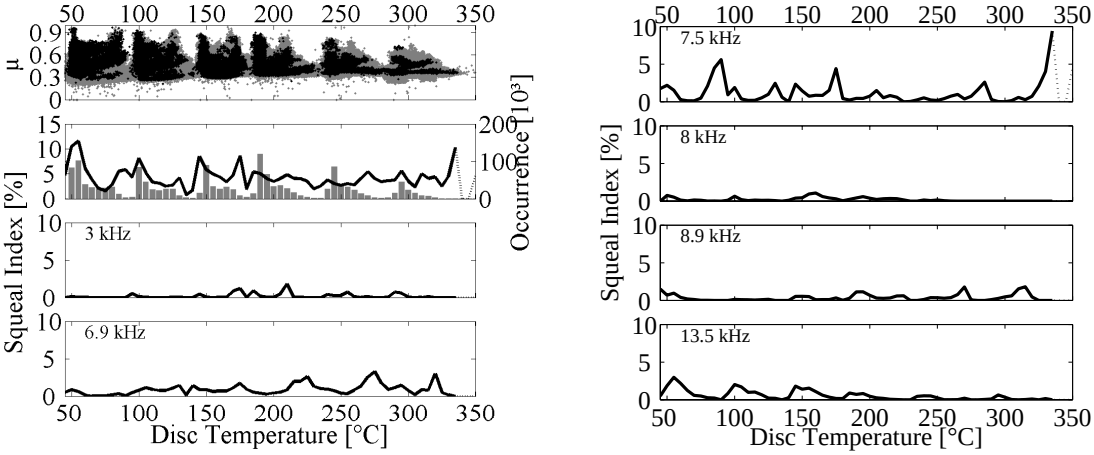

Figure 6.5.: *Squeal dependence on disc temperature for measurement brake application data from all tests*

The disc temperature influence is shown in figure 6.5. Below 250 °C the lower limit of friction coefficient values increases with increasing temperature, while the upper coefficient of friction limit decreases. Within each initial temperature block (below 300 °C) high friction coefficients occur at the temperature edges: at minimum temperature, mainly during drag brake applications, and at the end of the stop brake applications (maximum temperature). The temperature cluster size is 5 °C for this analysis. The overall squeal index is a superposition of a constant 5 % value and peak values up to 12 % around 55 °C, 100 °C, 145 °C, 175 °C and 335 °C, but no general trend or dependence can be found. This is also true for squeals at the dominant frequency intervals.

In general, the black line for the squeal propensity is only drawn, where at least 50 data points are within that cluster. If a squeal index is calculated for a cluster with less than 50 data points only a dotted line is drawn to indicate a possible weaker statistical relevance. At very high temperatures less than 50 data points are within the 5 °C cluster intervals, which is indicated by the dotted squeal propensity curve. The shown SI trends there might not be statistically significant, but generated nearly by chance.

The result of the analysis with brake torque as parameter, clustered in 100 Nm intervals, is shown in figure 6.6. The friction coefficient versus brake torque plot shows a regular pattern, because the coefficient of friction is proportional to the brake torque at each constant brake line pressure. Below 500 Nm more brake noise is generated at higher friction coefficients, while above 500 Nm no clear trend is visible. Below 80 Nm, the

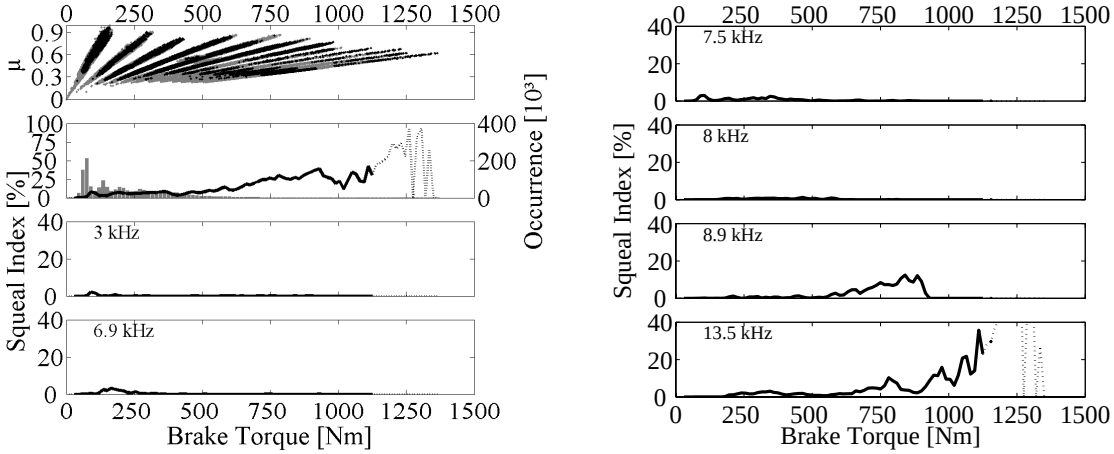

Figure 6.6.: *Squeal dependence on brake torque for measurement brake application data from all tests*

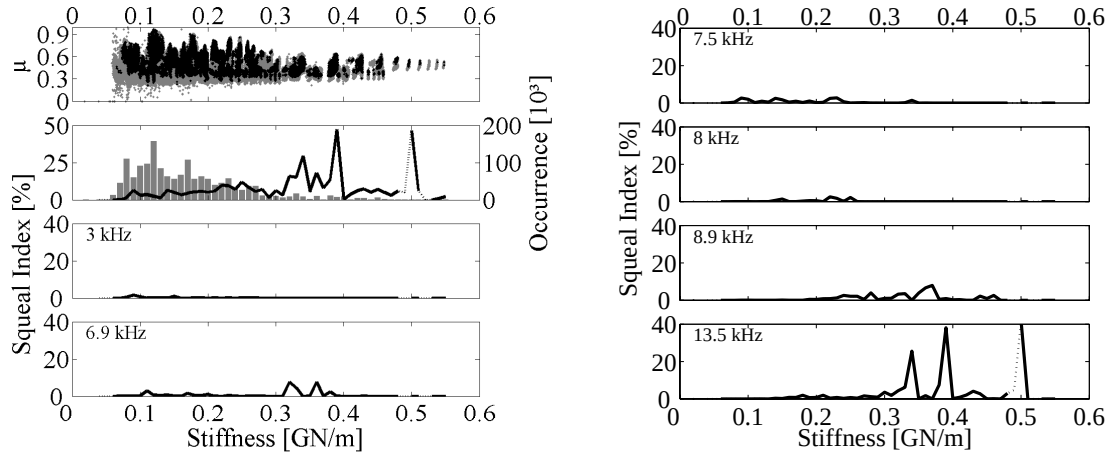

Figure 6.7.: *Squeal dependence on stiffness for measurement brake application data from all tests*

overall squeal propensity is near zero. Between 80 Nm and 500 Nm it is almost constant at approximate 8 %. Squeal in the dominant frequency intervals around 8.9 kHz and 13.5 kHz shows an increasing propensity for higher brake torques. However, for the 8.9 kHz squeal, no squeal occurred for brake torques higher than 850 Nm. And the propensity calculation of the 13.5 kHz squeal above 1100 Nm is based on clusters each consisting of 50 data points or less.

In figure 6.7 the dependence of squeal on the real-time stiffness, calculated from the

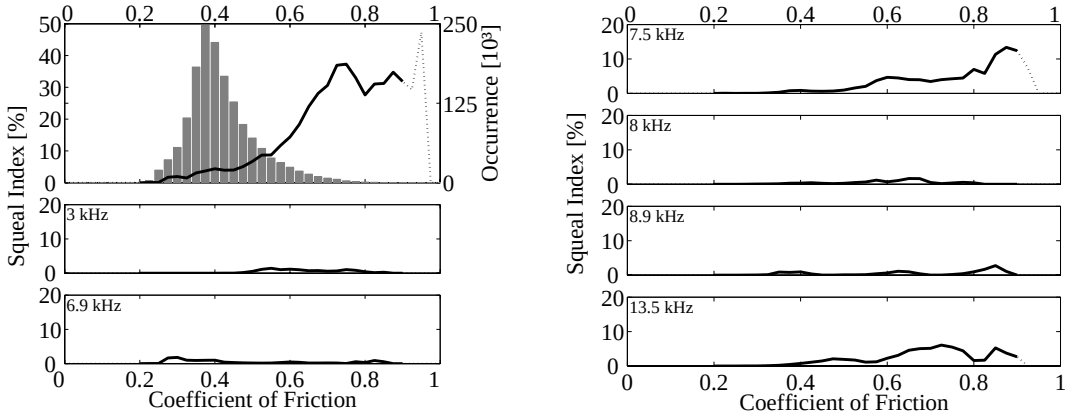

Figure 6.8.: *Squeal dependence on friction coefficient for measurement brake application data from all tests*

stiffness model (cp. chapter 4.4.2) is shown for an interval size of 0.01 GN/m. The stiffness model is mainly brake line pressure dependent, so the friction coefficient trends are basically the same as for the brake line pressure: the friction coefficient span decreases with increasing stiffness. All frequencies considered, the squeal propensity slightly increases with increasing stiffness below 0.25 GN/m and has two squeal propensity peaks around 0.4 GN/m and 0.5 GN/m. For the different dominant squeal frequencies no general trends can be seen. The 8.9 kHz and the 13.5 kHz squeal propensities show higher SI values at higher stiffnesses and the peak values in the overall squeal propensity is mainly due to the 13.5 kHz squeal.

At last, figure 6.8 shows the squeal dependence on the friction coefficient. The cluster interval of the friction coefficient values is 0.025 wide. The distribution of the friction coefficient values is nearly Gaussian around a peak value at 0.375, with an asymmetric larger amount of higher friction coefficient values. The overall squeal dependence raises from 0 % at 0.25 to 38 % at 0.75 and further (through a local minimum of 27 % at 0.8) to a maximum of over 45 % in the statistically weak area above 0.9. A clear trend of incresing overall squeal propensity with increasing friction coefficient is visible. Additionally, squeal around 7.5 kHz and 13.5 kHz shows higher squeal propensities for high friction coefficient values.

In conclusion to all these presented analyses of single parameter influences on the squeal propensity, the friction coefficient proved to be the most important one. As this has been expected, yet always counter-examples exist, a closer look on the squeal propensity

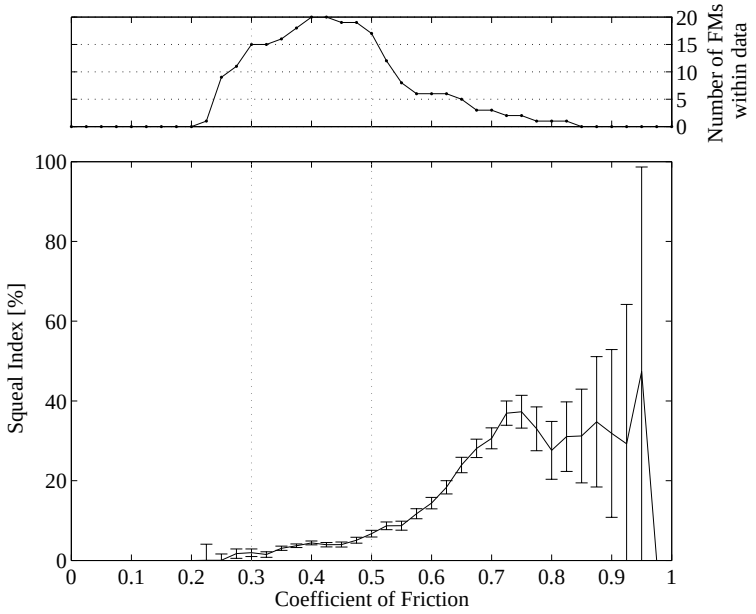

Figure 6.9.: *Squeal propensity dependence on friction coefficient for all data points from measurement brake applications (bottom). Top diagram: Number of friction materials which have more than 500 data points within that cluster.*

dependence on the friction coefficient is taken in the next paragraph.

Friction Coefficient Influence on the Squeal Propensity

As the friction coefficient has shown to be the most important single tribological parameter influence on brake squeal, the assumptions of the squeal propensity error calculation (cp. section 4.4.1) are most likely fulfilled. Using this error estimation, the squeal propensity dependence on the friction coefficient with error bounds is shown in the bottom plot of figure 6.9. It can be seen that the increasing squeal propensity trend with increasing friction coefficient is significant. However, the top diagram shows the number of different friction materials, which have at least 500 data points within that particular friction coefficient cluster. The amount of 500 data points lead to an estimated SI error of $\varepsilon \leq 10$ percentage points for each FM and cluster (using $\Psi = 95$ %). Only within the friction coefficient interval between 0.3 and 0.5 at least 2/3 of all tested friction materials contribute with equal or more than 500 data points to the overall SI(μ) calculation. Within this interval the squeal propensity rise with increasing friction coefficient is weak. The large increase of the squeal index for friction coefficients equal or above 0.6 is only based

on up to six friction materials. Assuming the friction materials influence is only taken into account if it has at least 500 data points in the specific interval.

Figure 6.10 shows the squeal index dependence on the friction coefficient for all friction materials including all data points from measurement brake applications and ε (using $\Psi = 95$ %), calculated for all intervals with data points (left) or for all intervals with at least 500 data points (right). It can be seen that only the European Metallic friction materials A - E and H contribute to the SI increase for high friction coefficients, while the trends between 0.3 and 0.5 are nonuniform.

Also, using ε as an error estimate, there are (statistically significant) counter-examples from single friction material tests to this global SI(μ) trend, shown in figure 6.9. As an example, friction material C has, based on a confidence level of 95 %, an SI of below 3 % in the $\mu = 0.5$ interval. The overall SI at the $\mu = 0.5$ interval is approximately 6.7 % $\pm\, 0.9$ percentage points (also $\Psi = 95$ %). In the same manner, the squeal propensity at particluar friction coefficient intervals for $0.3 \leq \mu \leq 0.5$ significantly differs from the overall SI trend for the friction materials B, G, H, I, J, and O. So even if it is possible that friction material C represents an unlikely case of the 5 % uncertainity or the global trend is not as plotted (also 5 % chance), the squeal propensity deviations of seven friction material tests form counter-examples.

A more complicated picture results from analyzing the squeal at each dominant frequency interval separately. Table 6.3 shows the number registered noise during measurement brake applications for each friction material, for noise at frequencies within a particular dominant frequency interval. Only during the tests of friction materials A, B, D, E noise at each dominant frequency interval has been registered and the particular squeal propensities for each dominant frequency interval are very low. For the dominant frequency intervals around 7.5 kHz, 8.9 kHz and 13.5 kHz more than 50 squeal events have been registered during the measurement brake applications for more than the half of all tested friction materials (cp. table 6.3). Also it can be seen that some friction materials have significantly more registered noise events at particular dominant frequency intervals than others, e. g. the 8.0 kHz squeal was mainly measured during testing of the T friction material.

The error bounds of the SI vs. friction coefficient plots for squeal at dominant frequency intervals are the same as for the overall SI, because in both cases all data from the measurement brake applications of all tests is considered. Figure 6.11 shows the squeal propensity dependence on the friction coefficient for noise around 7.5 kHz and

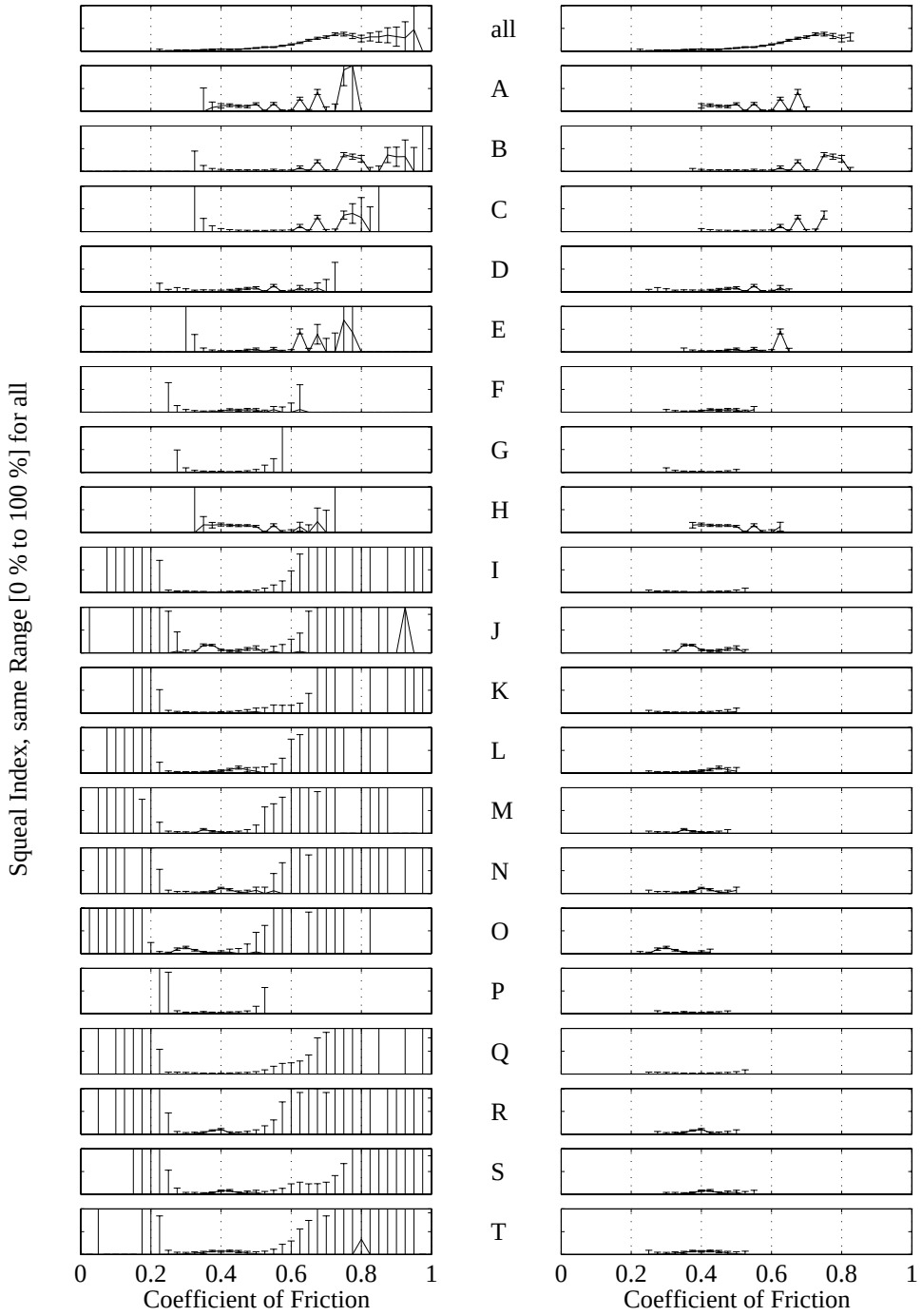

Figure 6.10.: *Squeal propensity dependence on friction coefficient for each friction material with error bars for all data from measurement brake applications. Left diagram is based on the whole data set and a vertical line indicates statistically meaningless areas with ε = 100 %, while for the diagram on the right hand side only intervals with more than 500 data points are considered.*

Table 6.3.: *Number of data points during measurement brake applications for which noise with a frequency in a dominant frequency interval was registered (zeros have been omitted for better readability, so no number indicates no noise)*

Domimant Frquency [kHz]						
	3.0	6.9	7.5	8.0	8.9	13.5
FM	*Number of data points with detected noise*					
A	2520	16	2017	1177	764	267
B	377	229	1052	135	58	696
C		15	244	19	23	1944
D	56	14	3581	498	12	35
E	642	404	1152	409	64	749
F			687	51	5	1051
G		6	35			
H		27	247	17	61	7363
I					31	
J		2523	4	33	1661	964
K		48	65		58	
L		508	1821	46		
M		657			1158	12
N		2083	164		1789	63
O		3478	523			19
P		30	135	65	374	280
Q			6			
R		929	2470		692	12
S			593	10	818	1716
T		662	113	2765	84	287
O	*Number different FM with number of noise occurrences O*					
$O > 0$	4	16	18	12	16	15
$O \geq 10$	4	15	16	12	15	15
$O \geq 50$	4	9	15	7	12	11
$O \geq 100$	3	9	14	5	7	10
$O \geq 500$	2	7	9	2	6	7

noise around 13.5 kHz. In the statistical relevant friction interval between 0.4 and 0.5 approximate 10 friction materials had a significant amount of measurements where noise at 7.5 kHz occurred. The squeal propensity for squeal at 7.5 kHz in this friction coefficient

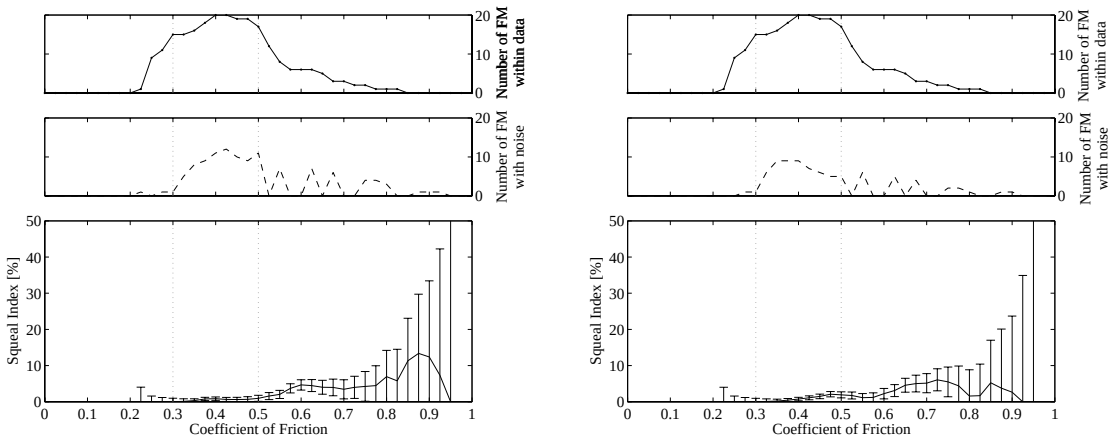

(a) 7.5 kHz **(b)** 13.5 kHz

Figure 6.11.: *7.5 kHz and 13.5 kHz squeal propensity dependence on friction coefficient for all data points from measurement brake applications (bottom). Top diagram: Number of friction materials which have more than 500 data points within that cluster. Middle diagram: Number of friction materials during the testing of which at least 200 squeal noises were registered (within the dominant frequency interval)*

range was nearly constant and below 2 % including the error (for $\Psi = 95\ \%$), while friction material D showed a significant higher SI e. g. at $\mu = 0.5$. Same counter examples to the general trend can be found for the 13.5 kHz squeal, which is mainly dominated by the H friction material. The behavior of brake noise with frequcencies around 13.5 kHz is significantly different between tests of friction material H and the general trend, which is formed by all other tests for the friction coefficient interval $[0.3\ 0.5]$.

Squeal Dependence on Friction Coefficient and Stiffness

To investigate the squeal propensity dependence on the friction coefficient and the stiffness, the two-dimensional μ-c parameter space is divided into equally spaced rectangular areas, each with an equal surface area. Each data point is part of exactly one interval, but because of the impossibility to control the friction coefficient and the stiffness the data point density over the whole μ-c parameter space is not constant. Figure 6.12 (a) shows the intervals and the grayscales indicate the number of data points which are within each interval for all measurement brake application data points from all tests. This diagram is

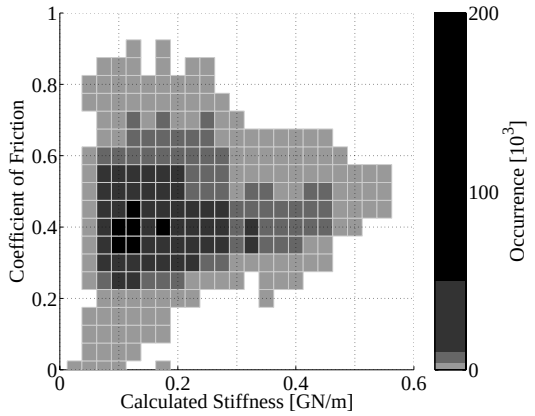

(a) Number of data points per interval

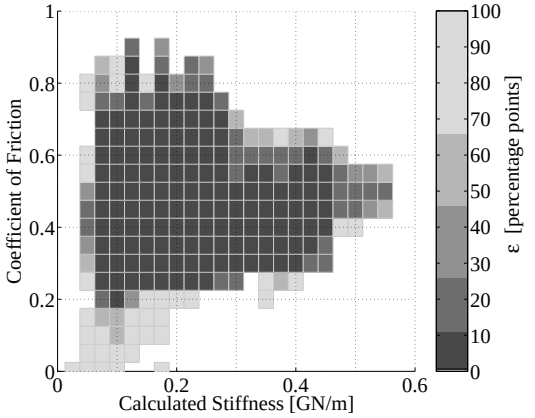

(b) Absolute squeal propensity error ε per interval

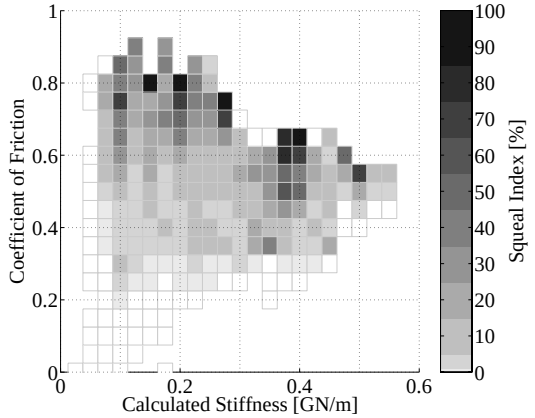

(c) Squeal propensity as function of friction coefficient and stiffness

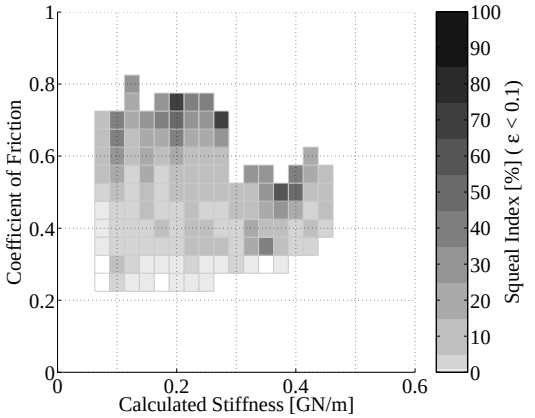

(d) Squeal propensity only shown for intervals with $\varepsilon < 10$ percentage points

Figure 6.12.: *Squeal propensity dependence on friction coefficient and stiffness on the real-time timescale, part 1*

similar to a two-dimensional histogram where the ‘color’ indicates the bin height. To calculate a squeal propensity in the same manner as done for the single parameter analysis, data clustering is necessary. The interval width has to be chosen large enough to ensure the needed amount of data points for the statistical analysis within the interval, but should not be too large as all data points in an interval have to (be assumed to) have the same squeal propensity. The interval size chosen is 0.05 for the friction coefficient and for the

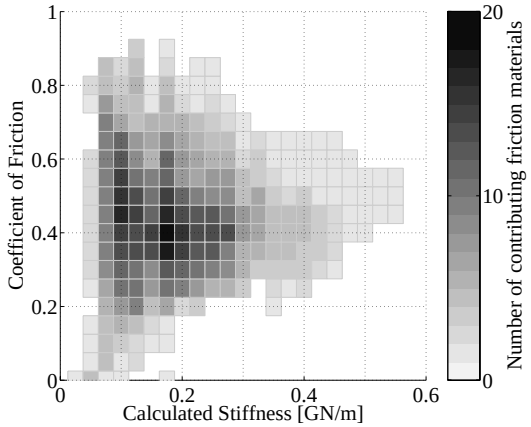

(a) Number of contributing friction materials per interval

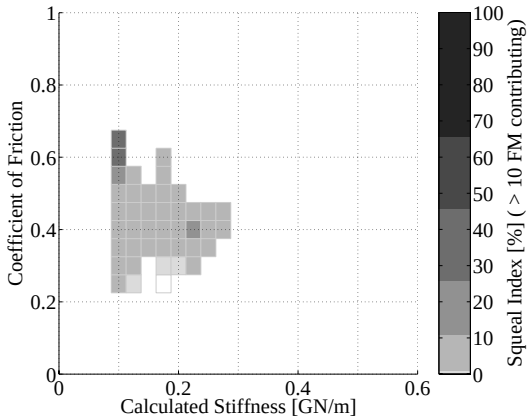

(b) Squeal propensity of all intervals with at least 10 contributing friction materials

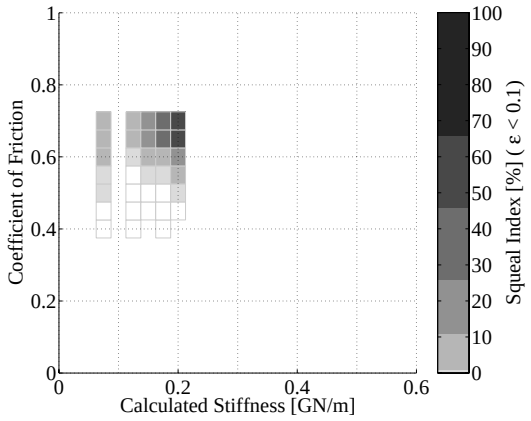

(c) Squeal propensity of friction material C (only intervals with $\varepsilon < 10$ percentage points shown)

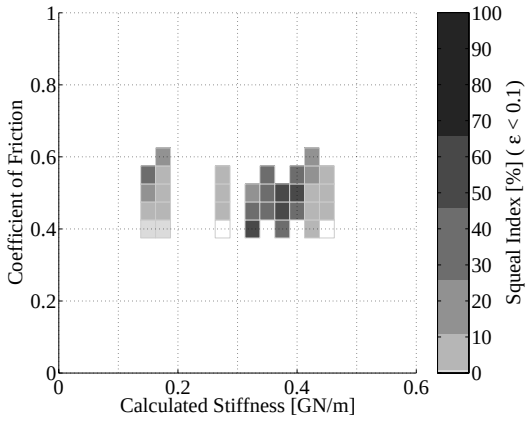

(d) Squeal propensity of friction material H (only intervals with $\varepsilon < 10$ percentage points shown)

Figure 6.13.: *Squeal propensity dependence on friction coefficient and stiffness on the real-time timescale, part 2*

stiffness it is 0.025 GN/m. It will be used for all further μ-c parameter based analyses.

The squeal propensity for each interval displayed in the same way as the distribution, is shown in figure 6.12 (c). The darker color of the upper right intervals indicate that a higher squeal propensity is calculated for intervals with higher friction coefficient *and* higher stiffness. However, as seen in figure 6.12 (a) these intervals have a small amount

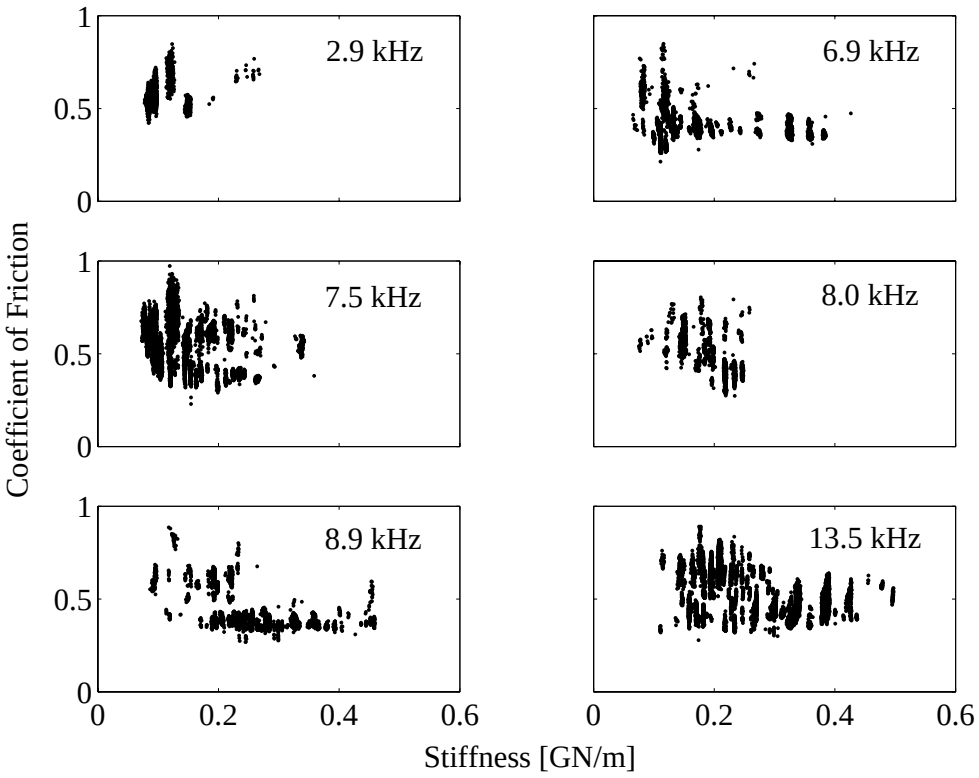

Figure 6.14.: *Friction coefficient and stiffness influence on the noise frequency for the measurement brake application data from all tests*

of data points leading to larger uncertainties in the squeal propensity estimation. Based on the error consideration of chapter 4.4.1, the absolute deviation ε between measured squeal propensity and true but unknown squeal propensity is shown for each interval in figure 6.12 (b) for a confidence level of Ψ = 95 %. Not showing all intervals where $\varepsilon > 0.1$ (which corresponds to 10 percentage points) figure 6.12 (d) also shows the trend of higher squeal propensity for intervals with high friction coefficient *and* high stiffness.

Similar to the single squeal propensity versus friction coefficient trend discussed in the last paragraph, not all μ-c intervals contain data points from all friction material tests. Figure 6.13 (a) shows the number of different friction materials which have data points falling into the particular interval. It can be seen that for the outer intervals only a few friction materials form the 'general' trend. If only intervals, which have data points from at least 10 tests with different friction materials, are considered, the diagram shown in figure 6.13 (b) results. Only a weak friction coefficient and stiffness influence on the squeal

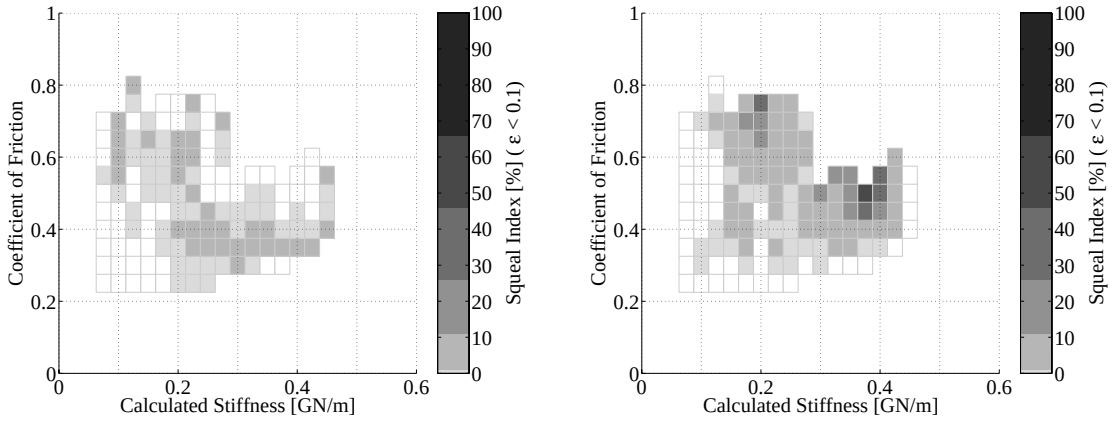

(a) Brake noise around 8.9 kHz

(b) Brake noise around 13.5 kHz

Figure 6.15.: *Squeal propensities as function of friction coefficient and stiffness for noise within two dominant frequency intervals*

propensity can be seen for this parameter range, and the friction coefficient influence on the squeal propensity is slightly stronger than the stiffness influence.

Most of the friction material dynamometer testing results show a correlation between friction coefficient, stiffness and squeal propensity, e. g. as shown for friction material C in figure 6.13 (c). However, different friction materials cover different μ-c parameter ranges and this leads to (partly large) deviations in squeal propensity for particular intervals. So even as the squeal propensity increases with increasing friction coefficient and stiffness during the most friction material tests, their squeal propensity values for most intervals differ - between each other and compared to the global trend. Additionally, squeal was only generated in a narrow brake line pressure band and independently on the friction coefficient during tests of some friction materials - falsifying the general trend from a scientific point of view, as shown for friction material H in figure 6.13 (d).

To investigate the influence of the tribological parameters μ and c on the squeal frequency, in figure 6.14 a dot indicates a squeal noise which occurred at a specific friction coefficient and stiffness. From the separate plots for each dominant frequency interval no clear trends can be seen. No general μ-c parameter range emits noise only at one dominant frequency, but noise at nearly all dominant frequencies was found throughout the largest part of the parameter space.

A closer look at the squeal propensities of squeal at two dominant frequency intervals

is presented in figure 6.15. Noise at 8.9 kHz was registered during tests with 16 different friction materials while the 13.5 kHz noise was emitted during tests of 15 friction materials. It is unclear, if the remaining friction materials are not capable of producing squeal at that particular frequencies at all, their true (but unknown) squeal propensities for these frequencies are too low or if these noises were only covered by noise at a different frequency. So, for this analysis only data from tests is considered, where noise at these frequencies was registered.

While for the 8.9 kHz squeal no significant and coherent trend can be estimated, noise around 13.5 kHz increases with increasing friction coefficient and stiffness (at least for c $\leq$ 0.425 GN/m), as shown in figure 6.15. If only squeal within a single dominant frequency interval is investigated, the general valid trend for all noise between 2 kHz and 20 kHz of increasing squeal propensity with increasing friction coefficient and stiffness in most cases cannot be found. So, while the overall squeal propensity *for noise between 2 kHz and 20 kHz* increases with increasing μ and c, this need not to be true for brake noise at a particular frequency.

Friction Coefficient Models

A supplemental result of the real-time noise data analysis is the estimation of the friction coefficient dependence on brake line pressure, disc temperature and vehicle velocity. This is done for each friction material, using multiple parameter regression models. These models are not squeal propensity models, so they are presented in this subsection as result of the real-time timescale analysis. The models are used on the brake application and test timescales to calculate the $\partial\widehat{\mu}/\partial v$ 'negative slope' characteristic values. For the friction coefficient model only the measurement brake applications are used, because the parameters in the data set should be balanced. Further, all brakings with no applied brake line pressure have been excluded, because no friction coefficient can be estimated there. The used models are quadratic in each parameter and include linear interaction terms. The models result from minimizing the difference between calculated μ from measurements and the predicted $\widehat{\mu}$ with a least squares fit. The modeled friction coefficient from this regression analysis has a form like

$$\widehat{\mu} = \zeta_1 \cdot p^2 + \zeta_2 \cdot p + \zeta_3 \cdot v^2 + \zeta_4 \cdot v + \zeta_5 \cdot T^2 + \zeta_6 \cdot T + \zeta_7 \cdot p \cdot v + \zeta_8 \cdot p \cdot T + \zeta_9 \cdot v \cdot T + \zeta_{10}$$

and the model coefficients are presented in table 6.4. For the regression analysis the adjusted multiple coefficient of determination R^2_{adj} is between 61 % and 80 %, which is

Table 6.4.: *Coefficients of the $\widehat{\mu}$(p,v,T) regression models*

FM	*Coefficient for*									
	1	p^2 $[10^{-6}$ $bar^{-2}]$	p $[10^{-3}$ $bar^{-1}]$	v^2 $[10^{-6}$ $(h/km)^2]$	v $[10^{-3}$ $h/km]$	T^2 $[10^{-6}$ $1/°C^2]$	T $[10^{-3}$ $1/°C]$	$p \cdot v$ $[10^{-6}$ bar^{-1} $h/km]$	$p \cdot T$ $[10^{-6}$ bar^{-1} $1/°C]$	$v \cdot T$ $[10^{-6}$ h/km $1/°C]$
A	0.64	41.1	-1.2	28.7	-6.1	-1.8	0.3	-23.9	-4.1	5.9
B	0.79	63.7	-3.0	72.5	-10.3	-1.2	-0.1	-10.8	-1.4	7.0
C	0.72	-10.1	1.7	-74.8	0.0	1.2	-1.2	-15.6	-9.1	9.1
D	0.52	-55.3	2.6	-61.0	-2.2	-6.2	1.0	36.3	-6.0	16.9
E	0.59	50.2	-1.8	5.7	-4.1	-1.5	0.1	-19.6	-2.5	7.4
F	0.32	18.5	0.6	-58.3	0.9	-3.1	1.5	-22.1	-12.2	-2.0
G	0.33	34.2	-0.3	18.5	-1.9	-2.1	1.0	-28.3	-2.7	3.5
H	0.52	62.2	-1.7	-58.0	0.1	-1.6	0.3	-24.5	-5.6	7.3
I	0.46	78.0	-6.0	58.4	-7.3	-2.0	0.6	22.5	1.1	18.9
J	0.49	77.9	-5.8	32.6	-5.1	-2.2	0.5	2.8	0.8	12.7
K	0.54	92.7	-8.4	76.3	-9.1	-1.2	0.0	48.1	9.1	20.1
L	0.48	90.1	-6.8	59.4	-7.3	-0.8	0.2	20.9	2.9	18.8
M	0.34	13.7	-1.8	45.8	-5.5	-3.3	1.2	16.7	-2.1	11.7
N	0.42	62.1	-5.3	45.8	-5.4	-2.6	0.9	3.7	1.5	13.3
O	0.40	29.3	-2.8	51.5	-7.1	-0.8	0.2	31.3	4.3	18.5
P	0.32	31.7	-1.6	33.6	-3.6	-3.8	1.5	-6.2	-2.0	5.4
Q	0.46	81.3	-6.6	63.0	-7.8	-2.7	0.7	18.6	0.8	21.4
R	0.39	76.7	-5.2	32.8	-3.7	-2.0	0.8	8.9	0.3	6.6
S	0.55	90.1	-7.6	63.4	-7.9	-1.5	0.1	25.7	3.5	18.9
T	0.39	72.6	-5.0	59.8	-6.4	-3.3	1.2	20.2	-2.4	13.3

only sufficient for general trends. The mean square error $\sigma_{\widehat{\mu}}$ is between 0.02 and 0.065 and includes the statistical errors of the parameters and deviations due to history effects. Both, statistical parameters and the number of data points for each model are listed in table 6.5 for all friction materials.

The coefficients of the regression models do not deliver a straight forward view on the dependences of the friction coefficient on the three parameters. Figures 6.16 and 6.17 show the general trends of the friction coefficient as function of the brake line pressure, vehicle velocity and disc temperature for all friction materials in several plots. Each three plots in a row correspond to a particular friction material and show the results from the

Table 6.5.: *Number of measurement points (only measurement brake application data), R^2_{adj} and statistical errors of the $\widehat{\mu}$(p,v,T) regression analysis*

FM	*Measurement Points*	R^2_{adj} [%]	$\sigma_{\widehat{\mu}}$	*FM*	*Measurement Points*	R^2_{adj} [%]	$\sigma_{\widehat{\mu}}$
A	68212	78.0	0.035	K	84219	62.1	0.033
B	66877	69.4	0.063	L	82866	64.7	0.032
C	65476	64.7	0.050	M	84563	70.6	0.026
D	71699	79.8	0.042	N	81389	70.8	0.027
E	71392	66.1	0.037	O	88411	72.8	0.024
F	75749	62.6	0.036	P	68967	74.8	0.022
G	75712	68.0	0.023	Q	80892	70.6	0.032
H	70547	42.6	0.040	R	81567	66.9	0.025
I	81488	69.9	0.030	S	79066	62.3	0.033
J	79501	61.2	0.029	T	79814	68.7	0.031

$\widehat{\mu}$-model as a function of the specific parameter. Due to the interaction terms in the model the friction coefficient versus parameter curves depend also on the other two parameters. Therefore three lines are drawn in each plot: the solid line represents the $\widehat{\mu}$-model using the mean values of the specific parameter range for the other two parameters. These values are $\tilde{p}$ = 32.5 bar, $\tilde{v}$ = 25 km/h and $\tilde{T}$ = 200 °C and should not be mistaken for the average parameter values during a test procedure run. The dashed and the dotted lines indicate maximum and minimum values possible within the model. These curves do not result for a constant set of the other two parameters. Instead, the other parameters are varied at each parameter value within its parameter range to find the maximum and minimum. So, they indicate the boundaries for all possible $\widehat{\mu}$-model curves.

Each friction material has its own trends, but some similarities are visible for most friction materials. The friction coefficient minimum most often is in the middle of the pressure range and at high temperatures. Some materials (e. g. A or B) show a significant higher friction coefficient at low vehicle velocities, but this is not a general trend.

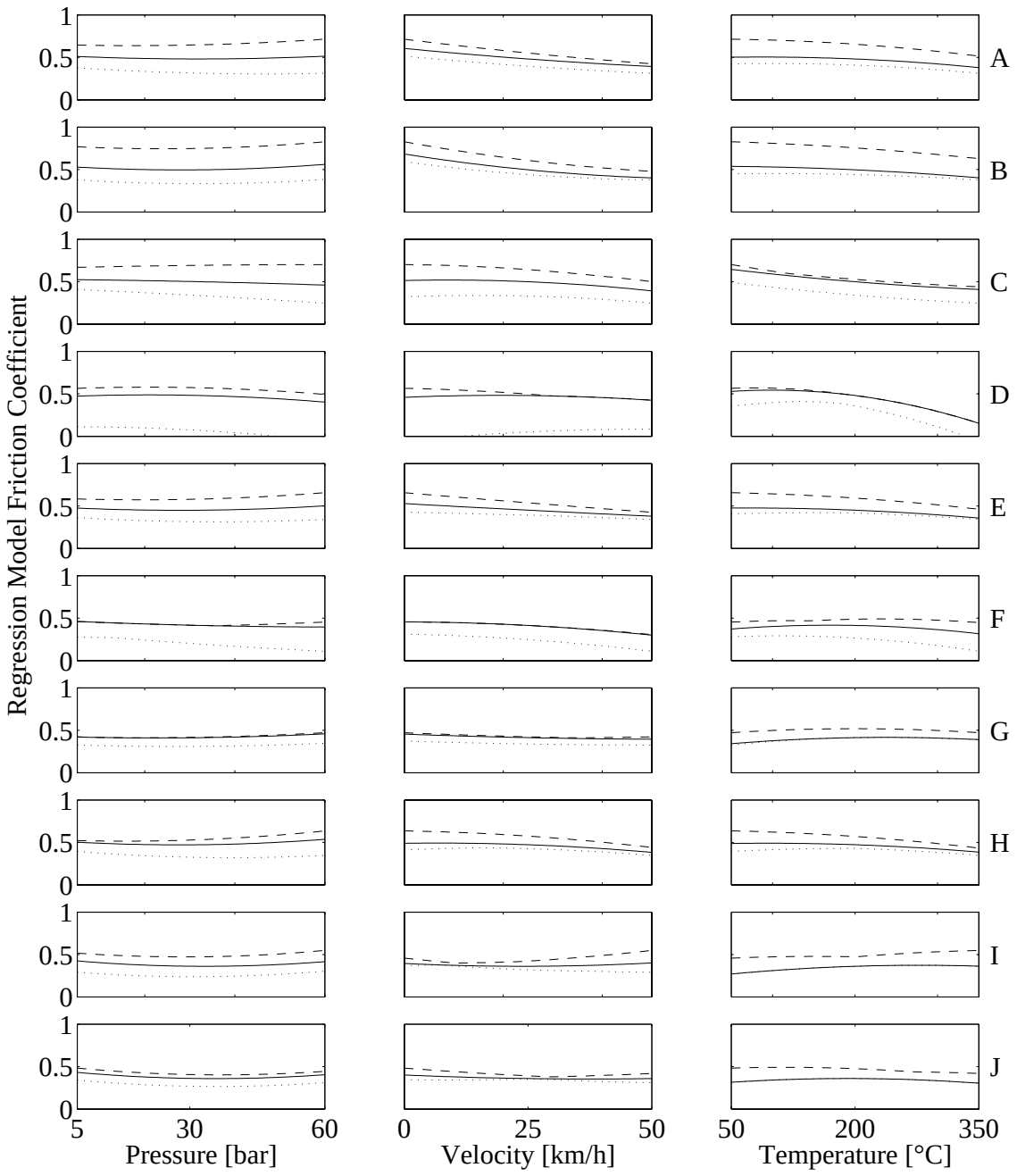

Figure 6.16.: *Solid line: Dependence of the friction coefficient on brake line pressure, vehicle velocity and disc temperature for friction materials A - J. The dashed and the dotted lines indicate maximum and minimum values possible with the model, possibly including improper model extrapolation.*

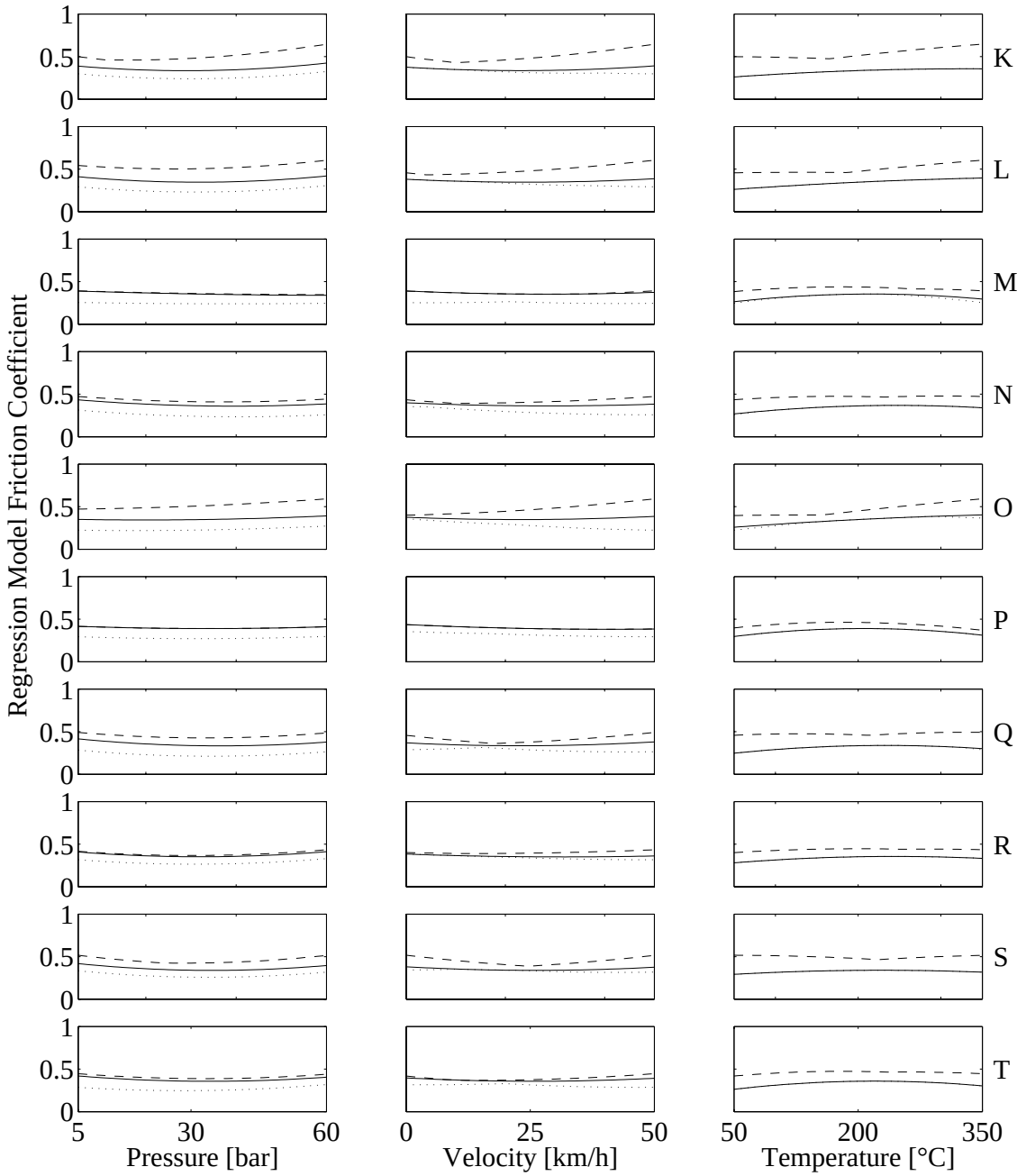

Figure 6.17.: *Solid line: Dependence of the friction coefficient on brake line pressure, vehicle velocity and disc temperature for friction materials K - T. The dashed and the dotted lines indicate maximum and minimum values possible with the model, possibly including improper model extrapolation.*

6.1.2. Model Evaluation of Squeal Propensity

In the same manner as for the analysis of the real-time data, squeal propensity models based on a different number of parameters can be built. As a result of the real-time data analysis, the single parameter dependent squeal propensity models are based on the friction coefficient, while the two parameter dependent models focus on friction coefficient and pad normal stiffness.

Further, the squeal propensity modeled consists of all squeal frequencies between 2 kHz and 20 kHz, because the squeal propensities for noise at particular dominant frequency intervals are very low and no tribological reason why noise at a specific frequency was generated only during some tests could be found. Without knowing the reasons for squeal generation at frequencies within a particular dominant frequency interval, the ΔSI measure cannot be applied and the modeled squeal propensities for noise at particular squeal frequencies are quite meaningless.

In the last paragraph the squeal propensity is modeled based on the measured brake line pressure, vehicle velocity, disc temperature and brake torque.

Single Parameter Dependent Squeal Propensity Models

As described in chapter 5.3, the solely friction dependent models are linear regression models (cp. equation 5.1) based on the characteristic value $\alpha_{\mu,\mathrm{rt},40}$, which is the real-time friction coefficient μ_{rt}. For modeling, the data is clustered into 0.05 wide intervals and a squeal propensity versus friction coefficient curve similar to the one shown in figure 6.9 results for all frequencies between 2 kHz and 20 kHz. If no data from unpressurized drag brake applications and no intervals with less than 50 data points are considered, the calculated model

$$\widehat{SI}(\mu) = 55.4\,\% \cdot \mu_{\mathrm{rt}} - 15.5\,\%$$

results. The model has a R^2_{adj} of 87.6 % and a standard error $\sigma_{\widehat{SI}}$ of approximately 4.9 percentage points. Applying the Model Quality Rating Measure presented in chapter 5.4 for each friction material, the difference ΔSI between the measured squeal propensity SI_{measured} and the modeled squeal index $\widehat{SI}_{\mathrm{model}}$ is calculated according to equation 5.3. The $\Delta\ SI$ values lie between -7.8 percentage points and 4.2 percentage points with a standard deviation $\sigma_{\Delta SI} = 3.50$ percentage points. $\sigma_{\Delta SI}$ is significantly better than the 'worst case' standard deviation of 4.87 percentage points.

By building the model on the equal weighted friction coefficient intervals, a case might occur in which all data for one interval is measured during the same test with a single friction material. In this case, this friction material would be determining the model more than other friction materials, especially if the particular interval is at the lower or upper ends.

A second $\widehat{SI}(\mu)$-model was built on the SI(μ) data. For this regression model, the squeal propensity for each interval was weighted by the number of data points in it. Because each test of a friction material has approximately the same amount of data points, all friction materials will contribute in a similar manner to the model. The resulting model

$$\widehat{SI}_{\text{wt}}(\mu) = 47.1\,\% \cdot \mu_{\text{rt}} - 14.4\,\%$$

has a R^2_{adj} of 75.3 % and an absolute standard error $\sigma_{\widehat{SI}_{\text{wt}}}$ of approximately 2.5 percentage points.

The ΔSI values lie between -4.9 percentage points and 7.4 percentage points, with a standard deviation of 3.48 percentage points, so the weighted model has a lower R^2_{adj}, but a similar $\Delta\ SI$ standard deviation value. The weighting of the data points lowers the calculated squeal propensity which decreases the error for friction materials with low measured squeal propensities, while it increases the error for tests with high measured SI.

Two Parameter Dependent Squeal Propensity Models

Similar to the squeal propensity models as function of the friction coefficient, squeal propensity models depending on the friction coefficient and pad normal stiffness have been built and are shown in table 6.6. All $\widehat{SI}(\mu, c)$-models presented in this paragraph are first order polynomial regression models with an interaction term, as presented in equation 5.2:

$$\widehat{SI}(\mu, c) = \zeta_1 \cdot \mu_{\text{rt}} + \zeta_2 \cdot c_{\text{rt}} + \zeta_3 \cdot \mu_{\text{rt}} \cdot c_{\text{rt}} + \zeta_4$$

They use the characteristic values $\alpha_{\text{rt,40}}$ - the real-time friction coefficient μ_{rt} and the real-time stiffness c_{rt}, calculated from the stiffness model $\Gamma_{\text{rt,11}}$.

Model number one was calculated based on all μ-c intervals with μ > 0, c > 0 (to exclude the unpressurized drag brake applications), which consists of at least 50 measured data points - not to bias the model with intervals where misleading squeal propensities could have been measured by chance. The resulting model has an adjusted coefficient of determination R^2_{adj} of 50.6 % which indicates that the capability of a linear interaction

Table 6.6.: *Real-time timescale squeal propensity models as function of friction coefficient and stiffness*

Models					
Number		*1*	*2*	*3*	*4*
ζ_1 [10^{-2}]		46.8	33.3	197.3	-3.9
ζ_2 [m/TN]		0	53.2	2296.2	-853.5
ζ_3 [m/TN]		517.8	710.3	-3417.0	2810.3
ζ_4 [10^{-2}]		-17.4	-14.6	-97.7	1.2
R^2_{adj} [%]		50.6	57.7	(89.3)	[57.9]
SI_{model} *deviations*					
Pad	Measured SI [%]	ΔSI [percentage points]			
A	18.21	5.69	7.29	-7.41	8.19
B	10.35	-5.29	-3.48	-22.71	-2.88
C	7.07	-5.1	-2.66	-20.63	-0.80
D	7.36	-1.66	-0.27	-10.62	0.04
E	7.1	-1.55	0.11	-9.48	1.21
F	2.85	-3.74	-3.74	-7.22	-2.86
G	0.11	-5.61	-5.29	-7.38	-4.64
H	15.2	2.29	1.47	-6.65	1.38
I	0.06	-2.59	-1.53	-2.13	-1.56
J	8.79	1.03	-0.21	-4.14	1.57
K	0.24	-1.76	-1.09	-1.25	-1.26
L	3.54	0.7	1.18	1.38	1.33
M	3.04	0.65	1.15	1.74	1.23
N	5.07	0.97	0.97	0.80	1.76
O	4.56	3.47	3.91	4.39	3.54
P	1.44	-3.43	-3.82	-4.58	-2.75
Q	0.01	-2.78	-1.74	-2.59	-1.75
R	5.39	1.14	0.87	1.25	1.78
S	4.44	-0.12	0.57	-0.77	1.03
T	5.31	0.59	0.76	-0.58	1.51
Minimum ΔSI [percentage points]		-5.61	-5.29	-22.71	-4.64
Maximum ΔSI [percentage points]		5.69	7.29	4.39	8.19
$\sigma_{\Delta SI}$ [percentage points]		3.02	2.87	7.04	2.81

model to fit the squeal propensities of the particular intervals is not satisfactory. For that model, the single stiffness influence had shown to be statistically not significant,

consequently the model was built without that term, considering the stiffness influence only through the $\mu \cdot c$ term. The largest absolute ΔSI is 5.69 percentage points for friction material A, which is a relative deviation of about 31 % and is within two times the standard deviation $\sigma_{\Delta SI} = 3.02$ percentage points. The model is able to provide the general trend of increasing squeal propensity with increasing friction coefficient and stiffness. This SI rise also correlates with the measured squeal propensity trend for most friction materials. The standard deviation of ΔSI is smaller than for the solely friction coefficient dependent squeal propensity models.

Model two considers only intervals, where μ > 0, c > 0 and SI > 0. The latter is to prevent the model failing in handling a sharp bend, as the measured data is not continuously differentiable at SI = 0. All intervals are weighted by the number of data points which lie within the particular interval. The model is built on the whole (remaining) data and the values of each data point are mapped to the μ, c, and SI values of the interval it belongs to. Compared to model number one, model two has an improved R^2_{adj} of 57.7 % and also a reduced standard deviation of ΔSI of 2.87 percentage points. Even if the trends (and coefficients) of both models are quite similar, the maximum absolute deviation between measurement and model of friction material A increases to 7.29 percentage points.

As the squeal propensity measurement is inaccurate due to the finite number of measured data points, the error estimation presented in chapter 4.4.1 is considered in building SI model number three. The model was calculated minimizing the sum of squared deviations between model and measured squeal index for each interval by Matlab's Nelder-Mead algorithm. To include the estimated error ε only the squared deviations of intervals are considered, which show a larger SI deviation between measurement and model as the error value ε for that interval. For all intervals in which not a single noise has been registered, the model may have (virtual) squeal propensities below zero without the squared deviation to be considered. This was done to overcome the sharp bend problems already discussed for the second model above. So, a 'virtual' negative squeal propensity is possible for all intervals without a registered squeal, possibly leading to a better fit. The stated adjusted coefficient of determination R^2_{adj} differs from the previously used one for models one and two. As only data points which lie outside the calculated error bounds for the interval are considered to reduce R^2_{adj}, the value of 89.3 % leads to two conclusions: First, it is not possible to build a linear model, where the deviation between measured and calculated squeal propensity is within the ε error bounds for all intervals. And second, the error of the measured squeal propensity for each interval might be larger than calculated by ε as

the chosen confidence level of 95 % leads to a model, which has more than 5 % residuals larger than ε. All in all, model three states a clear friction coefficient dependence of the squeal propensity, while high values of $\mu \cdot c$ tend to reduce the squeal propensity. As this trend contradicts the dependences of most friction materials, the ΔSI values are larger as for the first two models, resulting in a standard deviation $\sigma_{\Delta SI}$ of 7.04 percentage points and calculating a squeal propensity of approximately 33 % for friction material B, which is more than three times the measured value.

For the forth model Matlab's Nelder-Mead algorithm was used to find a model, which shows the smallest ΔSI values for every friction material. For this purpose the modeled squeal propensities and ΔSI values for each friction material were calculated during each iteration of the algorithm. The algorithm minimized the squared ΔSI values, using a ΔSI value based R^2_{adj} for maximization. Obviously, this R^2_{adj} differs from the two different R^2_{adj} used in models one and two or three. It can be seen that even though the standard deviation of ΔSI can be reduced to 2.81 percentage points, the best value for the adjusted coefficient of determination is 57.9 %. Model number four also shows increasing squeal propensity with increasing $\mu \cdot c$, but the solely μ- and c-dependent trends decrease the squeal propensity.

In conclusion to all models it can be stated that models one, two and four are able to calculate the general trends for the squeal propensity, but with a considerable model error. Especially friction materials A, B, F, G, O and P show similar deviations for all models. These friction materials show high, low and middle squeal propensities, so no general trend of model error on the squeal propensity can be found. As the deviations of model three which show different individual dependencies of the SI on μ and c, are significantly larger compared to the other models, the general trend of increasing squeal propensity with increasing $\mu \cdot c$ seems probable.

Multiple Parameter Dependent Squeal Propensity Models

In addition to single and two parameter dependent squeal propensity models, models that are also depending directly on brake line pressure, velocity or temperature seem suitable. By adding additional parameters, the parameter space becomes multidimensional, resulting in significantly smaller amounts of data in a particular (multidimensional) data cluster. The amount of data within a cluster defines the deviation between measured and true, but unknown, squeal propensity - so a certain amount of data is needed in each considered

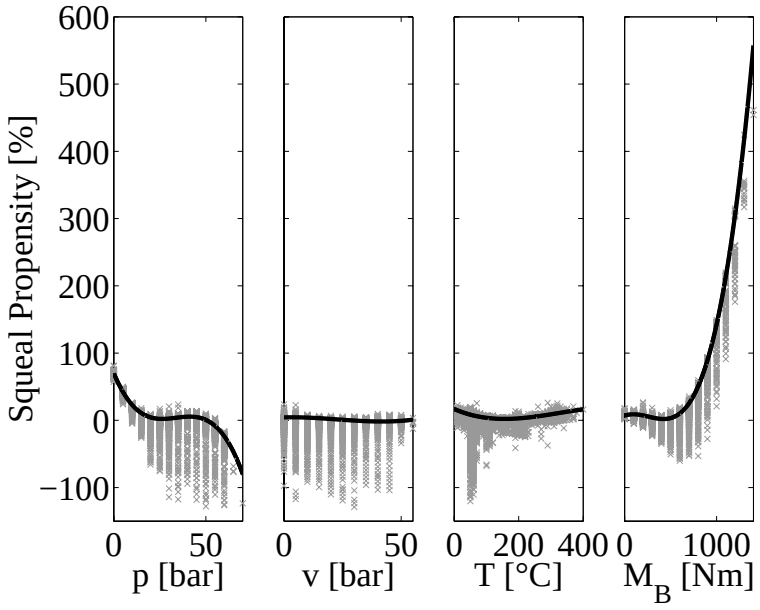

Figure 6.18.: *Adjusted response plot of the overall $\widehat{SI}(p, v, T, M)$ regression model*

data interval (cp. chapter 4.4.1). From conducting the various parameter combinations (Brake application numer, μ, c, p, v, T, M), no model with significantly lower ΔSI and $\sigma_{\Delta SI}$ resulted. Consequently, only the squeal propensity model solely dependent on the measurands brake line pressure, vehicle velocity, disc temperature and brake torque is presented in this paragraph.

An adjusted response plot of the $\widehat{SI}(p, v, T, M)$-model for all friction materials and all frequencies is presented in figure 6.18. In an adjusted response plot, the solid line represents the dependence on the particular parameter predicted by the model, each using the average values for the other parameters. The measured data is plotted as points around the solid line, the distance indicating the particular data point's residual. In this way it is possible to visualize the trend from the model, as well as the errors of the model for each data point.

The $\widehat{SI}(p, v, T, M)$-model is basically a full factorial third order polynomial regression with interaction terms. From the model six terms were removed, whose likelihood that the relationship for these terms could happen by chance was too high. An adjusted coefficient of determination less than 50 % resulted ($R^2_{\text{adj}} = 47.8$ %) and also not satisfactory ΔSI values. The absolute value of the squeal propensity as shown in figure 6.18 exceeds the reasonable parameter range between 0 % and 100 % in both directions.

These modeled $\widehat{SI}$ values outside the reasonable squeal propensity range origin from a (partly inappropriate) model extrapolation of the modeled parameter space, e. g. no very high brake torques result at medium brake line pressure and vehicle velocity. However, general trends and dependences are visible: the squeal propensity rises with decreasing brake line pressure and increasing brake torque while only weak depencences (with large scatter) exist on disc temperature and vehicle velocity. The brake line pressure and brake torque dependences indicate the friction coefficient based trends.

6.1.3. Discussion

Based on the SAE J2521 standard, a sound pressure level threshold of 70 dB was used. Noise with sound pressure levels below this threshold is not considered for further analysis. Squeal at all dominant frequencies and at most of the other frequencies detected during the conducted tests has sound pressure levels between 70 dB and 95 dB (and above). If the sound pressure level threshold for the analysis had been chosen higher, similar results to what is shown would result.

Throughout all tests a lot of different squeal frequencies have been recorded, nearly covering the whole frequency space between 2 kHz and 20 kHz. This leads to the conclusion that each particular vibrating system was different, on one hand because of the different brake parts used and on the other hand because of changes during the test procedure. These latter changes might include direct parameter changes like another applied brake line pressure.

The adjusted multiple coefficient of determination R^2_{adj} of the $\widehat{\mu}(p, v, T)$-models of each friction material is between 61 % and 80 %, which is sufficient to estimate general trends. The particular friction coefficient behavior of each tested friction material is different, although some trends show up more often. For most friction materials the friction coefficient has its lowest value in the medium brake line pressure range at high temperatures. Friction materials A and B show a large increase of the friction coefficient with decreasing vehicle velocity, also at high absolute friction coefficients. Both materials have an overall squeal propensity for the test of more than 10 %, emitting squeal at many different frequencies at these low vehicle velocities. In a similar way, the $\widehat{\mu}(p, v, T)$-models can be linked also to the squeal propensity for other friction materials: E. g. tests with friction material D generated squeal only below disc temperatures of 220 °C and the model friction coeffient shows a significant lower value at higher temperatures during the

dynamometer testing of this friction material. The pressure dependence of the friction coefficient is very weak for most tested friction materials, leading to the conclusion that a pressure dependence of the squeal propensity is most likely a friction coefficient effect.

For the analysis of the squeal dependence on single parameters like brake line pressure, vehicle velocity, disc temperature, brake torque, pad normal stiffness and friction coefficient, three different trends can be separated:

1. Friction material dependent trends:

    - The brake system, equipped with a different friction material emits squeal at different frequencies and with different squeal propensities, because the overall system changes (slightly) as the friction material is changed.
    - The dependences of squeal on p, v, T, M at a specific frequency might be different for different friction materials. This is especially true for the temperature dependences. That might be the reason why no general relationship between squeal propensity and temperature has been found. On the other hand, the temperature strongly affects the tribosystem, the condition of the friction films and the chemistry, and therefore has also an effect on the friction coefficient. The squeal propensity dependence on the other parameters was also different for each tested friction material, but in most cases (e. g. for squeal at the dominant frequencies) shows similar tendencies.

2. Squeal at different frequencies shows different squeal propensity dependences (mainly) on brake line pressure, brake torque, vehicle velocity, pad normal stiffness and friction coefficient, independent of the used friction material. For squeal at the dominant frequencies, the following general trends for brake noise at different squeal frequencies are found:

    - The squeal at 3 kHz occurs with a higher propensity at low brake line pressures, vehicle velocities, brake torques and at high friction coefficients.
    - The 6.9 kHz squeal has a higher squeal index at brake line pressures between 10 bar and 20 bar, low brake torques and friction coefficients. Also the squeal index is nearly independent of the vehicle velocity in this case.
    - Squeal at 7.5 kHz occurs more often at low velocities, low brake torques, brake line pressures below 30 bar and high friction coefficients.

- The 8.0 kHz squeal occurs mainly at high friction coefficients and more often during drag brake applications than during stop brake applications.
- The squeal at 8.9 kHz has a higher squeal index at high brake line pressures and stiffnesses, low vehicle velocities (slightly more often during drag than during stop brake applications) and high brake torques, as long as the brake torque is below 850 Nm.
- The 13.5 kHz squeal occurs more often during drag brake applications at high brake torques, friction coefficients and stiffnesses.

3. General trends for squeal at all frequencies between 2 kHz and 20 kHz and for all friction materials have also been found. The $\widehat{SI}(p, v, T, M)$ regression model shows a higher overall squeal propensity at low brake line pressures and high brake torques. The general trend of the squeal propensity to increase with decreasing vehicle velocity (cp. figure 6.4) results from a high friction coefficient at low velocities and is mainly a friction coefficient effect and only to a minor extent based on the vehicle velocity itself. In general, the friction coefficient is shown to have the most important single tribological influence on the squeal propensity. A linear model of the squeal propensity versus friction coefficient shows a significant squeal propensity and friction coefficient relationship

$$\widehat{SI}(\mu_{\text{rt}}) = 55.4\,\% \cdot \mu_{\text{rt}} - 15.5\,\%$$

with an adjusted coefficient of determination R^2_{adj} of 87.6 %. By weighting the intervals by the number of contributing data points a slightly different model

$$\widehat{SI}_{\text{wt}}(\mu_{\text{rt}}) = 47.1\,\% \cdot \mu_{\text{rt}} - 14.4\,\%$$

with a R^2_{adj} of 75.3 % results. Both models have similar maximal deviations ΔSI around 7.6 percentage points and also similar standard deviations of ΔSI around 3.5 percentage points. These models are clearly better than the worst case described in chapter 5.4, but they are not capable of estimating the squeal propensities for particluar friction material tests with satisfactory precision. As the friction material tests reveal strongly different friction coefficient distributions during different tests, the statistics (and the squeal propensity calculation) is based on different populations. In other words, the strong increasing squeal propensity trend at high friction

coefficients is only supported by data points from little more than one quarter of all friction material tests. The other friction materials did not cover this parameter space, so it is not possible to draw valid general conclusions. Even worse, there are statistical significant counter-examples (even considering the SI measurement error bounds). So the squeal propensity cannot be solely dependent on the friction coefficient. However, the tested European Metallic friction material class shows a quite clear trend of increasing SI with increasing (high) friction coefficients.

Beside all discussed limitations the friction coefficient is the most dominant single tribological parameter to effect the squeal propensity (at least for very high values), while brake line pressure, vehicle velocity, disc temperature, brake torque and stiffness by itself only play minor roles for global SI trends.

The general trends for the dominant frequency intervals have the same limitations as the global SI trends: Even if they show squeal propensity trends, which are mainly correlated to the friction coefficient, counter-examples exist. From a tribological point of view it is still unclear why squeal at a particular frequency occurs.

Most of the friction material dynamometer testing results show a correlation between friction coefficient, stiffness and squeal propensity. The entire data supports the hypothesis of an increasing squeal propensity with increasing friction coefficient and stiffness. This is still true if only data clusters with tolerable measurement error ε values are considered. However, there are friction materials (e. g. friction material H) which show significantly different trends. Also, for different friction materials squeal propensity values for most μ-c intervals differ between each other and compared to the global trend. Even as the squeal propensity rises with increasing friction coefficient and stiffness during the most friction material tests. If only intervals are considered, which consist of data points from at least 10 tests with different friction materials, a weak friction coefficient and stiffness influence on the squeal propensity can be seen. In this case the friction coefficient influence on the squeal propensity is slightly stronger as the stiffness influence.

The investigation of the influence between the squeal frequency and the tribological parameters μ and c shows no clear trends. No general μ-c parameter range emits noise only within a single dominant frequency interval, but noise at nearly all dominant frequencies is found throughout the largest part of the parameter space. While the propensity for squeal at 13.5 kHz increases with increasing friction coefficient and stiffness (at least for

c $\leq$ 0.425 GN/m), this general trend is not valid for the 8.9 kHz squeal as well as for squeal within the majority of the dominant frequency intervals.

The squeal propensity models built on noise within each dominant frequency interval could not explain why during some tests no noise at a particular dominant frequency interval has been generated. In conclusion, judged by ΔSI values, the models are not appropriate and not shown in this work. No correlation between the investigated parameters of the tribosystem and the squeal frequency has been found. In conclusion, only squeal propensity models, for which noise at all frequencies between 2 kHz and 20 kHz has been considered, are presented.

The majority of the squeal propensity as function of friction coefficient and stiffness models are able to calculate the squeal propensity trend for most friction materials quite well, even as the $\sigma_{\Delta SI}$ values are between 2.81 and 3.02 percentage points. So compared to the 'worst case' squeal propensity model as well as compared to the single friction coefficient dependent models the SI calculation capability of the

$$\widehat{SI}(\mu_{\text{rt}}, c_{\text{rt}}) = -3.9 \cdot 10^{-2} \cdot \mu_{\text{rt}} - 0.85\, m/GN \cdot c_{\text{rt}} + 2.8\, m/GN \cdot \mu_{\text{rt}} \cdot c_{\text{rt}} + 1.2 \cdot 10^{-2}$$

model is noticeably improved. All SI models with small $\sigma_{\Delta SI}$ values rely on an increasing squeal propensity with increasing $\mu \cdot c$, while the model with decreasing squeal propensity with increasing $\mu \cdot c$ shows significant larger deviations of ΔSI. This supports $\mu \cdot c$ as tribological dominant parameter. However, the low adjusted coefficients of determination, the large standard deviations of ΔSI and the continuously high ΔSI for some particular friction materials also form counter-examples to the global SI trend. So it is most likely that other parameters, which differ between the different friction material tests, e. g. structural changes or damping differences, have also a significant influence.

6.2. Brake Application Timescale

Reducing measured 'real-time' data to one value per brake application is very common in brake dynamometer testing. No data is explicitly generated on this timescale, but the squeal propensity for each brake application can be analyzed and is presented in the next subsection. To be comparable throughout this work on all timescales, the squeal propensity is always calculated the same way: using the real-time data as introduced in chapter 4.4.1. This means the squeal propensity of a brake application is the ratio between the number of real-time data points with registered brake noise and the overall number of

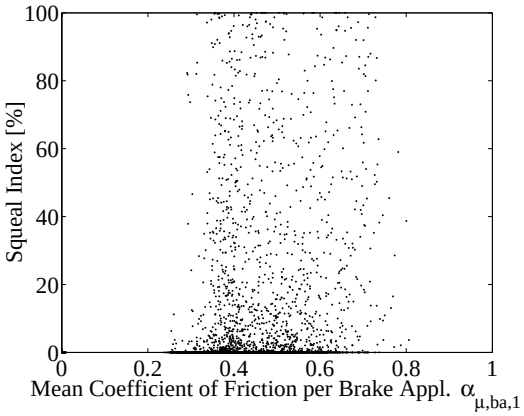

(a) Squeal propensity of all friction material tests versus the mean friction coefficient $\alpha_{\mu,\text{ba},1}$

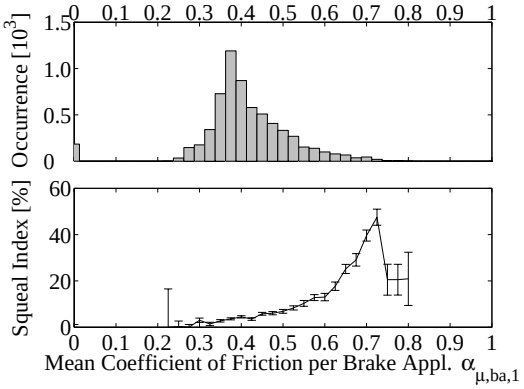

(b) Squeal propensity of all friction material tests as function of the *clustered* mean friction coefficient $\alpha_{\mu,\text{ba},1}$

Figure 6.19.: *Squeal propensity dependence on friction coefficient on the brake application timescale*

real-time data points for the brake application. On the brake application timescale, brake duration dependent amounts of real-time data are mapped onto a single value. So, caution must be taken when calculating combined squeal propensities for different brake applications or the whole test. When brake applications are combined in this section, each contributing squeal propensity is weighted by the amount of real-time data points during that particular brake application. This results in a real-time timescale equal squeal propensity calculation. For all noise data on this timescale, all squeal frequencies between 2 kHz and 20 kHz are used, if the noise sound pressure level is equal to or exceeds 70 dB. The reasons for doing that have been already discussed for the real-time timescale.

6.2.1. Data Analysis

On the real-time timescale each data point only contains the information whether it squeals or not. A brake application data point contains squeal propensity information, due to the real-time data clustering on each brake application.

As an example, the squeal propensity versus the mean friction coefficient $\alpha_{\mu,\text{ba},1}$ is shown in figure 6.19 (a). In the interval of $0.25 \leq \alpha_{\mu,\text{ba},1} \leq 0.7$, squeal propensities between 0 % and 100 % occur for very similar $\alpha_{\mu,\text{ba},1}$ values and no clear trend is visi-

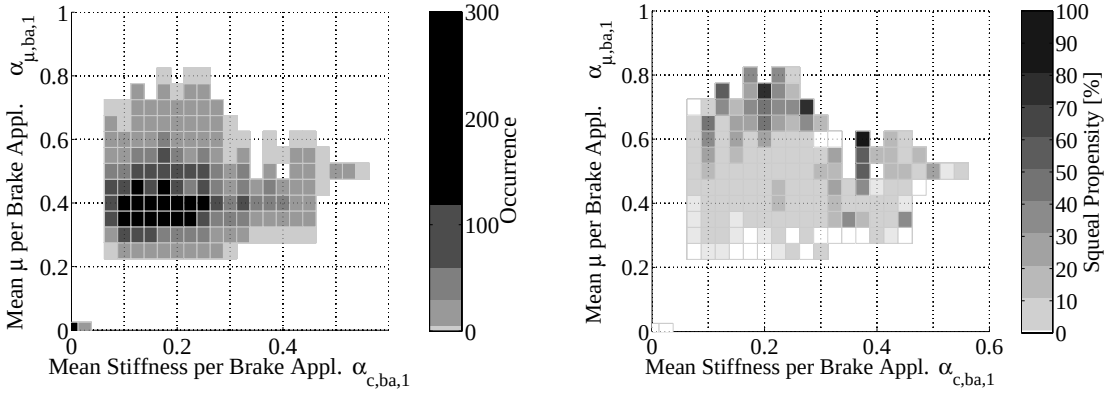

(a) Number of data points within each interval

(b) Squeal propensity for each interval

Figure 6.20.: *Squeal propensity dependence on mean friction coefficient $\alpha_{\mu,ba,1}$ and mean stiffness $\alpha_{c,ba,1}$ on the brake application timescale*

ble. The calculated squeal propensity for each brake application is only based on some hundred data points leading to squeal propensity errors of 10 percentage points $\leq \varepsilon \leq$ 23 percentage points based on the error estimation described in chapter 4.4.1.

By clustering the brake application data in the same way as on the real-time timescale figure 6.19 (b) results. It shows the mean friction coefficient $\alpha_{\mu,\mathrm{ba,1}}$ distribution and an increasing squeal propensity with increasing mean friction coefficient - very similar to the real-time correlation. The plotted error bars in the bottom diagram are calculated based on the real-time data points within each interval. Similar to the trends on the real-time timescale, the squeal propensity versus friction coefficient correlation is detectable. Most conclusions from the real-time timescale can also be found here: In the low and medium friction coefficient range a lot of different friction material tests contribute to the data and the squeal propensity increase is weak. For the high squeal propensity slope at high friction coefficients only a small amount of friction material tests is responsible.

As the squeal propensity versus $\alpha_{\mu,\mathrm{ba,i}}$ or $\alpha_{\mathrm{c,ba,j}}$ trends strongly depend on the particular characteristic value, the correlation analysis is done by the regression models in the next section. As an example of the squeal propensity dependence on two characteristic values, one based on the friction coefficient and the other based on stiffness, figure 6.20 is shown here. In the same manner as on the real-time timescale the parameter space is divided into intervals of equal area. Within each interval, all data points are clustered and the resulting

squeal propensity is calculated. Figure 6.20 (a) shows the distribution of the mean friction coefficient $\alpha_{\mu,\text{ba,1}}$ and mean stiffness $\alpha_{\text{c,ba,1}}$ values in the parameter space. The right hand diagram (figure 6.20 (b)) visualizes a high squeal propensity for intervals at high mean friction coefficient and high mean stiffness. Even though there is a large area in the middle of the covered parameter space in which the squeal propensity is nearly constant.

6.2.2. Model Evaluation

For the first set of regression models no further data clustering is applied to the brake application data. Considering all noise between 2 kHz and 20 kHz with a sound pressure level equal or above 70 dB, linear squeal propensity models with interaction terms were built. They use each combination of one friction coefficient based characteristic value $\alpha_{\mu,\text{ba,i}}$ and one stiffness based characteristic value $\alpha_{\text{c,ba,j}}$, resulting in 340 regressions.

In the first set of regression analysis the maximum adjusted coefficient of determination R^2_{adj} was below 6.5 % and the calculated squeal indices for the particular friction materials had no correlation with the measured squeal propensities and did not even reflect general trends.

So, for a second set of regression models, all brake applications with average brake line pressure equal to zero (no valid friction and stiffness values) and all brake applications without squeal occurrence were excluded. The reasons for the latter have been already discussed for the real-time timescale models. By excluding these brake applications, the amount of considered brake applications for the regression was reduced to below 20 % of all brake applications. The maximum R^2_{adj} of the second model set was below 4.8 % and again, no model was able to calculate the general measured SI trends for the different friction material tests.

For the third set of regression models the characteristic values were clustered as described and shown for the real-time timescale (e. g. figure 6.20). Additionally, all intervals without noise or with μ = 0 or c = 0 were not considered for the models. The regression models in this set have adjusted coefficients of determination R^2_{adj} between 0 % and nearly 100 %, leading to standard deviations of the model quality rating measure ΔSI as shown in figure 6.21. However, there need not necessarily be a correlation between a good model with small ΔSI and a well fitted model with a high R^2_{adj}.

In figure 6.21 all standard deviations of ΔSI for the third set of regression models are plotted, supplemented by the ΔSI standard deviations of single μ or c dependent

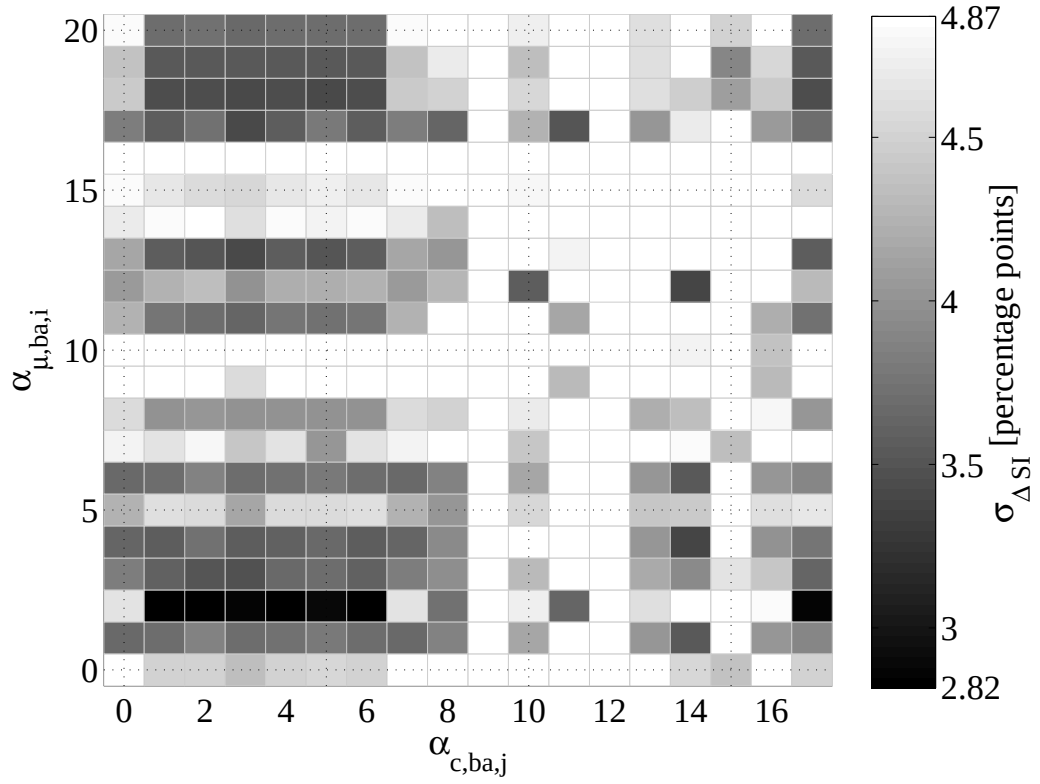

Figure 6.21.: *Standard deviation of ΔSI values for the third set of squeal propensity models based on clustered data on the brake application timescale*

models in the first column and row, respectively. The solely friction coefficient characteristic value dependent models are in most cases slightly better than the solely stiffness characteristic value based ones. But the best models are based on friction coefficient and stiffness characteristic values. The most promising characteristic values for squeal propensity models are the combination of the maximum friction coefficient $\alpha_{\mu,\mathrm{ba},2}$ and one of the following stiffness values: the mean, maximum, minimum, median stiffness, the center of Gaussian fitted stiffness, the center of the Gaussian fitted stiffness plus two times the standard deviation or the stiffness value, below which 75 % of all values lie ($\alpha_{\mathrm{c,ba},1}$ to $\alpha_{\mathrm{c,ba},6}$ or $\alpha_{\mathrm{c,ba},17}$). The constant target brake line pressure during a brake application leads to a nearly constant stiffness, so all these values are very similar and differences can be expected to be insignificant.

The best model on the brake application timescale is based on the maximum friction coefficient $\alpha_{\mu,\mathrm{ba},2}$ and the stiffness value $\alpha_{\mathrm{c,ba},6}$, where the center of a fitted Gaussian curve

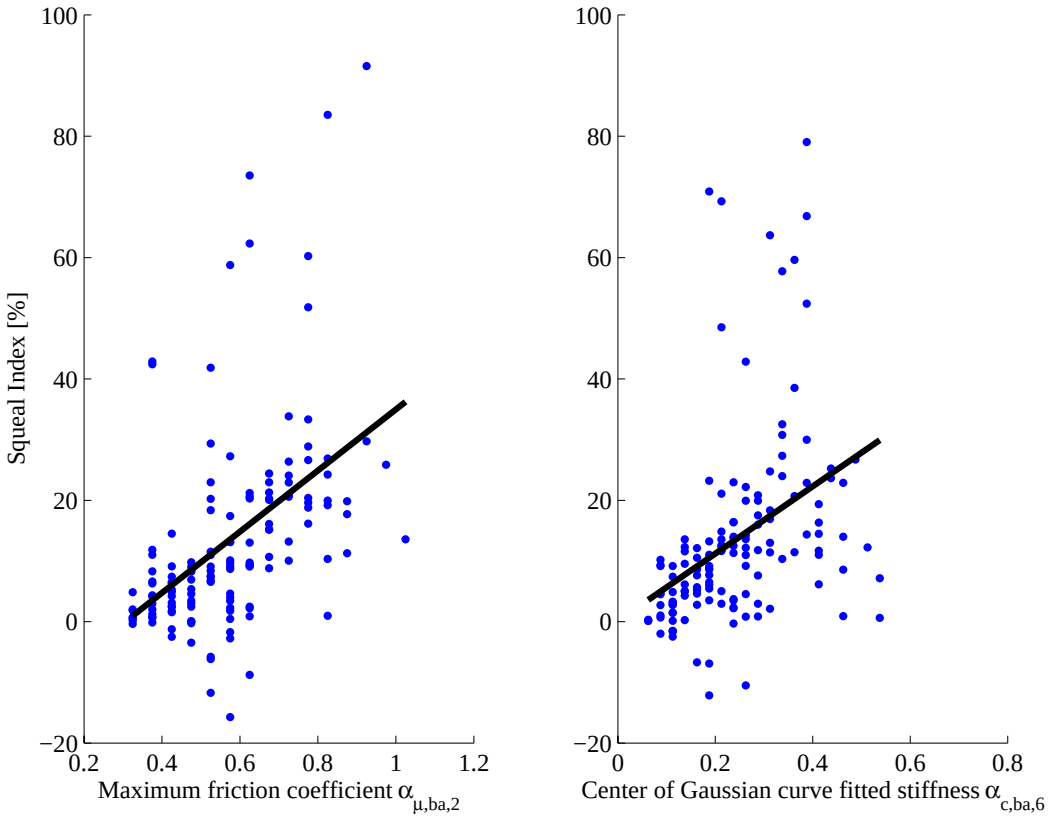

Figure 6.22.: *Adjusted response plot for the best $\widehat{SI}$ model on the brake application timescale: $\widehat{SI}(\alpha_{\mu,ba,2}, \alpha_{c,ba,6})$*

lies:

$$\widehat{SI}_{\text{ba}} = -0.13 \cdot \alpha_{\mu,\text{ba},2} - 0.96 \cdot m/GN \cdot \alpha_{\text{c,ba},6} + 2.65 \cdot m/GN \cdot \alpha_{\mu,\text{ba},2} \cdot \alpha_{\text{c,ba},6} + 0.08$$

It has a squeal propensity standard deviation $\sigma_{\Delta SI}$ of 2.82 percentage points, all ΔSI values lie between -5.78 percentage points and 7.01 percentage points - while the fit's R^2_{adj} is only 22.0 %. In the adjusted response plots (figure 6.22) it can be seen that the model reflects the general measured trends with significant scatter and some outliners. Figure 6.22 visualizes an increasing squeal propensity with incresing $\alpha_{\mu,\text{ba},2}$ and $\alpha_{\text{c,ba},6}$. This is due to the large coefficient of the $\alpha_{\mu,\text{ba},2} \cdot \alpha_{\text{c,ba},6}$ interaction term.

On the other hand, the model based solely on $\alpha_{\text{c,ba},16}$ (percentage of data points, which have a higher stiffness value than the average stiffness value for that brake application) has an adjusted coefficient of determination $R^2_{adj} \approx 99.4\,\%$. The model's SI calculation for each test is worse ($\sigma_{\Delta SI} \approx 5.07$ percentage points) than the 0th order polynomial

('worst case') model presented in chapter 5.4.

6.2.3. Discussion

Three different sets of linear regression models have been tested. Each model is built on one of the 20 friction coefficient based characteristic values, one of the 17 stiffness based characteristic values and the interaction term of both characteristic values.

Models built on brake application data without further data clustering are not able to calculate squeal propensities, which correlate with the measured trends. The model's standard deviations, maximum and minimum ΔSI are significant larger as for the real-time data based models. And the 'squeal propensity versus a single friction coefficient based characteristic value' plots (e. g. figure 6.19 (a)) show no clear correlation.

If the data is clustered in the same way as done on the real-time timescale, trends are visible. Some of the resulting models are equally capable of calculating the squeal propensities for each friction material test, compared to the real-time data based models. Considering these two findings, it can be concluded that

- the squeal propensity measurement during a brake application is still very error prone
- models built on this data are not good enough to reflect global trends
- the squeal propensity scatter between brake applications with similar friction coefficient and stiffness based characteristic values is too large to be calculated accurately.

Models built on clustered data use much more reliable squeal propensities and are able to calculate the overall squeal propensity for each test with a real-time model equivalent precision. Of course, these models are still not capable of calculating an accurate squeal propensity for a particular brake application.

To generate a suitable model, judged by ΔSI values near zero, one needs meaningful characteristic values which are fitted well, measured by a high R^2_{adj}. However, the use of a meaningful characteristic value is more important than the quality of the fit: The weak fitted model ($R^2_{adj} \approx 22\ \%$) has a ΔSI standard deviation equal to the real-time models, while the very well fitted models using insignificant characteristic values are not even able to reflect general measured SI trends.

There are meaningful characteristic values and it is likely that some data pooling functions are capable of maintaining measured squeal propensity dependences.

In most cases the standard deviation of ΔSI is higher, if the model is only based on a single characteristic value from one parameter. So even as some friction coefficient based characteristic values form quite good models, the best models are based on the maximum friction coefficient $\alpha_{\mu,\mathrm{ba},2}$ and the stiffness, e. g. the mean stiffness, as the stiffness is nearly constant during a brake application due to the constant brake line pressure.

6.3. Test Timescale

The third timescale presented in this chapter is the reduction of real-time data or measurement of one value per test. Besides the compressibility measurements on this timescale, the characteristic values presented in chapter 5.2.2 are used for plots and models. In brake industry it is common practice to reduce the real-time friction coefficients of an AK Master dynamometer test to one so-called 'nominal' friction coefficient, which is used for brake performance issues. Is it also suitable to reduce real-time data to one value per test for brake squeal tests? The answer to this question is presented in this section. As for the brake application timescale before, squeal noise at frequencies between 2 kHz and 20 kHz is considered for analysis if the sound pressure level is equal to or exceeds 70 dB.

6.3.1. Data Analysis

As the compressibility measurement can be attributed to the test timescale, it is the first presented analysis. In figure 6.23 (a) the squeal propensity for each test is indicated by the shade of gray in the $\alpha_{\mathrm{c,tt},26}$-$\alpha_{\mu,\mathrm{tt},12}$ paramter space. $\alpha_{\mathrm{c,tt},26}$ is the average compressibility of the pad pairs and $\alpha_{\mu,\mathrm{tt},12}$ is the percentage of friction coefficient values, which exceed 0.5. The highest squeal propensities (friction materials A and B) occurred for low compressibility and high $\alpha_{\mu,\mathrm{tt},12}$ values, as indicated by the dark dots. For tests with $\alpha_{\mu,\mathrm{tt},12} < 10$ % only a weak trend of increasing squeal propensity with decreasing compressibility is visible.

In figure 6.23 (b) the squeal propensity versus $\alpha_{\mu,\mathrm{tt},12}$ and the maximum stiffness per test $\alpha_{\mathrm{c,tt},2}$ is shown. The stiffness model monotonically increases with increasing brake line pressure. The maximum stiffness per test is the stiffness value at 60 bar, which is related to the measured compressibility. The squeal propensity is high for high $\alpha_{\mathrm{c,tt},2}$ *and*

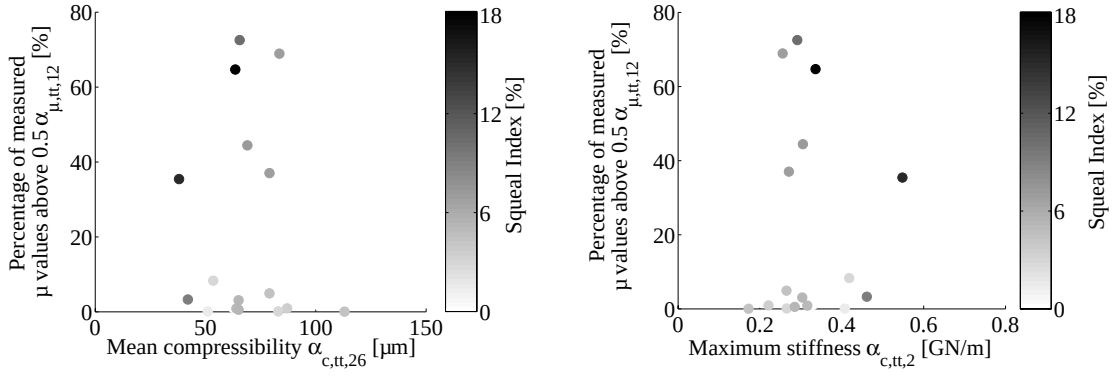

(a) Squeal propensity dependence on $\alpha_{\mu,\mathrm{tt},12}$ and $\alpha_{\mathrm{c,tt},26}$

(b) Squeal propensity dependence on $\alpha_{\mu,\mathrm{tt},12}$ and $\alpha_{\mathrm{c,tt},2}$

Figure 6.23.: *Squeal propensity dependence on friction coefficient and stiffness based characteristic values on the test timescale*

$\alpha_{\mu,\mathrm{tt},12}$ values and decreases to medium $\alpha_{\mathrm{c,tt},2}$ and $\alpha_{\mu,\mathrm{tt},12}$ values. Again, for very low $\alpha_{\mu,\mathrm{tt},12}$ values there are a couple of tests for which no clear trend is visible.

6.3.2. Model Evaluation

Linear regression models for the squeal propensities of noise at the whole frequency range have been built. Per test, each model uses one value of the friction coefficient based characteristic values $\alpha_{\mu,\mathrm{tt,i}}$, one value of the the stiffness based ones ($\alpha_{\mathrm{c,tt,j}}$) and the product of both values. The set of models is completed by single parameter dependent models. As all models on this timescale try to minimize the ΔSI values, the adjusted coefficient of determination R^2_{adj} is directly linked to the standard deviation of ΔSI. The fits are completely different from the models on the other timescales, so the model's R^2_{adj} can not be compared. The adjusted coefficients of determination R^2_{adj} lie between 0.0 % and 77.0 % which indicates that there is a relationship between the squeal index and the characteristic values based on stiffness and friction coefficient. Some characteristic values are more related to the squeal propensity than others. Figure 6.24 summarizes the standard deviations $\sigma_{\Delta SI}$ for all models built on this timescale.

Each characteristic value (either friction coefficient or stiffness based) has its own potential in contributing to a well correlated squeal propensity model. This can be seen by the line type structure of the diagram in figure 6.24. The intersections are superpositions

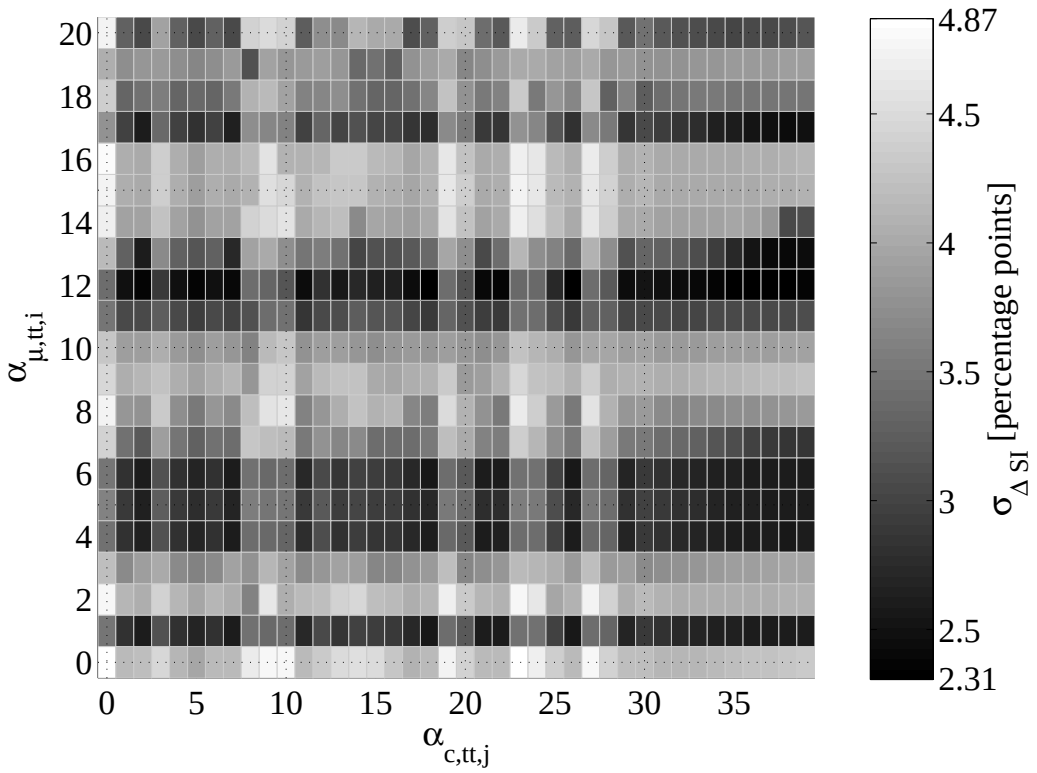

Figure 6.24.: *Standard deviation of ΔSI for all squeal propensity models built on the test timescale*

of the individual potentials. There are also interaction effects which lead to higher or lower $\sigma_{\Delta SI}$ values as expected for the two characteristic values: e. g. the model based on $\alpha_{\mu,\text{tt},17}$ and $\alpha_{\text{c,tt},7}$ is better than expected.

The $\widehat{SI}$ models solely based on friction coefficient characteristic values (whose $\sigma_{\Delta SI}$ are shown in the first column in figure 6.24) are in most cases better than the ones solely based on stiffness characteristic values (related $\sigma_{\Delta SI}$ shown in the first row in figure 6.24). There are many models based on combinations of a stiffness and a friction coefficient characteristic value, which are significantly better than the single parameter dependent models.

Good models are built on the mean, median friction coefficient, Gaussian fit mean, Gaussian fit mean plus two times the standard deviation and the 75 % threshold friction coefficient values as well as on the percentage of friction coefficients above 0.4, 0.5 and 0.6. The stiffness based characteristic values which contribute to the best models are:

the stiffness value below which 75 % of all values (for that test) lie, the mean value of the Gaussian fit plus two times the standard deviation, the percentage of data points with stiffness greater than 0.15 GN/m and the compressibility and calculated normal force independent part of the pad bulk stiffness for both pads and their average value. For some models with small $\sigma_{\Delta SI}$ the models become better by using the calculated stiffness at higher brake line pressures ($\alpha_{\text{c,tt,31}}$ to $\alpha_{\text{c,tt,39}}$).

One of the best models on the test timescale is based on the percentage of friction coefficient values above 0.5 $\alpha_{\mu\text{,tt,12}}$ and the mean compressibility $\alpha_{\text{c,tt,26}}$:

$$\widehat{SI}_{\text{tt}} = 0.48 \cdot \alpha_{\mu\text{,tt,12}} - 0.0004 \cdot \mu m^{-1} \cdot \alpha_{\text{c,tt,26}} - 0.0051 \cdot \mu m^{-1} \cdot \alpha_{\mu\text{,tt,12}} \cdot \alpha_{\text{c,tt,26}} + 0.061$$

It has ΔSI values between -3.88 percentage points and of 4.38 percentage points and a standard deviation $\sigma_{\Delta SI} = 2.33$ percentage points. It is better than the models built with the real-time data, although similarities are visible: the largest ΔSI occurs for friction materials A and B and the squeal propensity of friction material O's test is not calculated satisfactorily.

6.3.3. Discussion

For estimating the characteristic values on the test timescale, the whole real-time data from the measurement brake applications of each test is used to calculate a single value.

The real-time measured squeal propensity trends have been maintained by the data pooling of some characteristic values, because the $\widehat{SI}$ models on the test timescale show small ΔSI values (absolute as well as for the standard deviation). In summary there are 183 models with standard deviations $\sigma_{\Delta SI}$ below 3.0 percentage points. Some of the best relationships between the squeal propensity and the estimated characteristic values are found for the mean friction coefficient $\alpha_{\mu\text{,tt,1}}$ and the percentage of data points above μ = 0.5 $\alpha_{\mu\text{,tt,12}}$. This reflects the found tendency, that the friction materials with high friction coefficients show higher squeal propensities and supports the friction coefficient threshold for squeal as found by Bergman and Eriksson (cp. chapter 2.3.3). From the characteristic values based on the stiffness, the following ones are part of the models with highest R^2_{adj} and smallest $\sigma_{\Delta SI}$: the compressibility (first pad $\alpha_{\text{c,tt,18}}$, second pad $\alpha_{\text{c,tt,22}}$ and both pads $\alpha_{\text{c,tt,26}}$) and the stiffness (model) values at brake line pressures between 50 bar and 100 bar ($\alpha_{\text{c,tt,34}}$ to $\alpha_{\text{c,tt,39}}$).

There are good squeal propensity models based on test timescale characteristic values. This indicates, that it is possible to reduce the real-time data without loosing significant

trends. The data reduction onto a single value per test makes it easier to fit linear regression models: A squeal propensity of zero only occurs on this timescale only in the special case of zero registered noise events throughout a whole test.

Models based on the compressibility or stiffnesses at high brake line pressures show better correlations to the measured squeal data than the contact stiffness related characteristic values. This might have some of the following reasons:

- The contact stiffness is not important
- The contact stiffness model is not accurate enough to show the trends
- Mainly the overall stiffness, including contact and bulk, is influencing the squeal propensity.

However, the characteristic values of the stiffness model on the test timescale do correlate with the measured SI trends. And additionally conducted tests with very unbalanced parameters (e. g. only drag brake applications at low pressures) suggest an influence of the contact stiffness on the squeal propensity. So, it seems highly likely that the reasons are a combination of model inaccuracy and overall stiffness based influence.

Models based on some characteristic values on the test timescale are capable of calculating the squeal propensity for each test to a better extent than the real-time data based models. But one has to keep in mind that the real-time data is needed to generate the test timescale characteristic values. This result supports the assumptions of the squeal propensity error ε, the stiffness model limitations and the measurement errors: It indicates, that on a larger scale (and for a balanced dynamometer test procedure) these errors and uncertainties play minor roles, and that better results on the other timescales might result from more precise measurements and models.

In this subsection only the results on the test timescale have been discussed. So in this chapter all analyses and models on all investigated timescales have been presented. In the next chapter these findings are summarized and reviewed in respect to the goals of this work.

7. General Discussion

The main focus of this work is on clarifying two questions: Is it possible to describe squeal behavior with the most squeal relevant parameters of the pad/disc tribosystem, which are the friction coefficient μ and the normal stiffness c of the brake pad? And on which timescale must dependencies be reported to find the best correlations? The whole picture is composed of different parts, whose results and conclusions will be brought together in this chapter.

1. Based on the data analyses, the following can be stated:

    - During the whole test program, squeal at nearly every frequency between 2 kHz and 20 kHz occurred. Noise within some (so-called dominant) frequency intervals was detected significantly more often. As squeal within the dominant frequency intervals occurred at the whole friction coefficient and stiffness parameter range, no influence of these parameters on the squeal frequency could be found. It is likely that non-tribosystem parameters define the squeal frequency, as during different friction material dynamometer tests noise at different frequencies was generated. Of course, the pad stiffness influences non-tribological parameters like the ‘structure’ to some extent, but no correlation between stiffness and squeal frequency could be found experimentally. So for the squeal propensity calculations discussed in this chapter, noise at all frequencies between 2 kHz and 20 kHz is considered if its sound pressure level is equal to or exceeds 70 dB.
    - The most important single tribosystem parameter for the brake squeal propensity is the friction coefficient. As it strongly depends on the vehicle velocity, a found squeal propensity dependence on vehicle velocity can also be credited to a major extent to the friction coefficient. The stiffness also has an influence on the brake squeal propensity. It can be expected that a real-time pad

stiffness measurement or a more sophisticated model would result in a better visible stiffness impact of squeal propensity.

- Most tested European Metallic type friction materials show significant correlations between friction coefficient and squeal propensity, but this is not true for all tested friction materials. A trend of high squeal propensities for high friction coefficients is only supported by a minority of friction material tests. The friction coefficient cannot be controlled properly and the resulting friction coefficient distributions for most tests are quite different. Very high friction coefficients have been measured only during the majority of tests. Also, counter-examples to the global SI versus friction coefficient trend exist.
- For the majority of the friction material tests, the squeal propensity increases with increasing friction coefficient and stiffness values. The different tests cover different areas in the μ-c parameter space and even as the local trends form a global trend of increasing SI with μ and c, counter-examples to this global trend exist. Nevertheless, the majority of friction materials shows a local trend of increasing squeal propensity with increasing friction coefficient and stiffness. Additional parameters most likely exist, which are responsible for the weak correlation between some local trends and the global trend. By replacing the pads to investigate different areas in the μ-c parameter space, other unrecognized parameters were changed and it might not have been possible to keep the structure of the system as constant as needed. μ and c are important, but are not that dominant as to rule out all other parameters.
- The introduced stiffness model has proven to be sufficient to show basic stiffness influences on the squeal propensity. Some influence of the calculated stiffness could be found for many of the tested friction materials and the $\widehat{SI}$ models using characteristic values based on the stiffness model do reflect the $\widehat{SI}(\kappa)$ trends.

2. For data pooling and the use of characteristic values on the different timescales the following can be stated:

   - Whether squeal propensity trends from the real-time measured data can also be found on other timescales mainly depends on two things: the used characteristic value and the timescale. The latter defines the extent of data reduction.

Although characteristic values like the percentage of friction coefficient values above 0.5 $\alpha_{\mu,12}$ contributes to good $\widehat{SI}$ models on the brake application and on the test timescale, there is no unique global quality measure for them. Most characteristic values are timescale-sensitive and the best $\widehat{SI}$ models on each timescale depend on different characteristic values. However, the 'better' ones on each timescale form a picture, which coincides with trends on the real-time timescale: the maximum friction coefficient $\alpha_{\mu,\mathrm{ba},2}$ is important but also prone to measurement errors. These errors are less important on the brake application timescale, as some hundred maximum friction coefficients are calculated from each test data. $\alpha_{\mu,12}$ indicates the position of the friction distribution to be important for brake squeal. In the same manner the (e. g. mean) stiffness $\alpha_{\mathrm{c},1}$ is important on the brake application and test timescales. The fact that the compressibility $\alpha_{\mathrm{c,tt},26}$ or the stiffness at high brake line pressures (e. g. $\alpha_{\mathrm{c,tt},37}$) builds better $\widehat{SI}$ models indicates the limitations of the stiffness model. In conclusion, it is possible to keep squeal propensity trends through data pooling, but not all data pooling is equally appropriate. Measurement uncertainties and model limitations might additionally have to be considered when choosing data pooling functions.

- On the brake application timescale, no adequate characteristic values could be found unless the brake application data points were further clustered. The clustered data reflects the real-time squeal propensity trends for some characteristic values, so it is likely that for a proper squeal propensity measurement the amount of data generated during a single brake application is not sufficient.
- By reducing the measured real-time data to one value per test, characteristic values were generated which seem to be more robust to measurement errors and which are able to overcome the stiffness model's limitations. For the models, measurements and characteristic values of this work, data reduction to the test timescale is favorable over the brake application timescale.

3. For the squeal propensity models, the following can be stated:

   - It is possible to build squeal propensity models on all timescales. The models are able to reflect the general measured trends for squeal at all frequencies between 2 kHz and 20 kHz. The best model is able to calculate the squeal

propensities for every test with an error standard deviation $\sigma_{\Delta SI} \approx 2.32$ percentage points which is less than half of the constant 'worst case' (0th order polynomial) model (4.87 percentage points). As these model errors occur on all timescales, they can most likely be attributed to the presence of other unconsidered parameters influencing the squeal propensity. From the compressibility measurements an energy dissipation per cycle can be calculated from the area of the force-deformation hysteresis. Even if no sinusoidal force excitation is applied, the energy dissipation is related to the quasi-static damping value. To compare these energy dissipations, they are based on the total energy input per cycle. The lower relative energy dissipation of 17.9 % for friction material A might be a cause for the higher squeal propensity, compared to friction material B with similar friction coefficient and stiffness values, but an energy dissipation of 20.6 % per cycle. Unfortunately this energy dissipation cannot explain the behavior of some other friction materials (e. g. friction material O). Further, it is unclear if the quasi-static damping is related to the squeal propensity or how the damping changes for higher frequencies and different friction materials.

- On all timescales the single parameter dependent models using friction coefficient based characteristic values are better than the models solely based on stiffness characteristic values. Models, showing the smallest ΔSI values are based on one friction coefficient *and* one stiffness based characteristic value. This is true for the best models on all timescales. Additionally, these models are strongly influenced by the interaction term, indicating the impact of the combined parameters on the squeal propensity.
- To model the squeal propensity on the brake application or test timescale with 'reduced' characteristic values, a weakly fitted model using meaningful characteristic values produces better results than a highly significant fit based on characteristic values which are not representative. On these timescales building good models is more difficult than on the real-time timescale. However, these models are less influenced by measurement (or stiffness model) errors and might therefore produce slightly better $\widehat{SI}$ calculations.
- Quite good models result (mainly on the test timescale) if the minimum $\partial\widehat{\mu}/\partial v$ 'negative slope' $\alpha_{\mu,20}$ is used in addition to some of the stiffness based char-

acteristic values. This result seems quite reasonable: In literature it has been often stated that a negative friction coefficient versus velocity slope leads to negative damping and squeal. In the conducted experiments the largest negative $\alpha_{\mu,\text{tt},20}$ value occurred at very low velocities and therefore for very high friction coefficients. It is likely that this result can not be attributed to the negative slope value.

- In table 7.1 the best $\widehat{SI}$ models on all timescales based on friction coefficient and stiffness characteristic values are shown. The best squeal propensity model is built on the test timescale: It is based on the percentage of friction coefficient values above 0.5 $\alpha_{\mu,\text{tt},12}$ and the stiffness at 80 bar brake line pressure $\alpha_{\text{c,tt},37}$. The $\widehat{SI}$ model using $\alpha_{\mu,\text{tt},12}$ and the mean compressibility of both pads $\alpha_{\text{c,tt},26}$ comes in second. On one hand this supports the statement of a friction coefficient threshold for brake squeal (made by Bergman et al. [9]), even if it cannot be seen clearly for all friction materials. On the other hand it supports the compressibility influence on the squeal propensity. It can be assumed that a more sophisticated stiffness model might lead to a clearer squeal propensity dependence on the overall stiffness, including both bulk and contact. The best real-time and brake application timescale $\widehat{SI}$ models have similar ΔSI values. They are visibly worse compared to the ones of test timescale models. The brake application timescale $\widehat{SI}$ model is based on the maximum friction coefficient $\alpha_{\mu,\text{ba},2}$ and the (Gaussian fitted) mean stiffness $\alpha_{\text{c,ba},6}$. The real-time models differ in considered μ-c intervals and data weighting: the second model weights each interval by the number of contributing data points while the first model only considers intervals consisting of at least 50 data points and with SI, μ and c greater than zero.

  In figure 7.1 it can be seen that the models mainly show SI deviations for similar friction material tests. In the top left diagram, the absolute ΔSI values for each model and test is shown, while the other plots each represent a single model: they show the modeled squeal propensity versus the measured SI, so in a perfect model all markers should lie on the dashed line. The vertical distance between marker and line represents the ΔSI value for the particular test as shown in table 7.1. The friction material test for each marker can be estimated by comparing the axis values of each marker to the measured SI

Table 7.1.: *Selected squeal propensity models as function of friction coefficient and stiffness on all timescales*

Models					
Timescale	*real-time*		*brake application*	*test*	
Number	*1*	*2*	*3*	*4*	*5*
Parameter 1	μ_{rt}	μ_{rt}	$\alpha_{\mu,\text{ba},2}$	$\alpha_{\mu,\text{tt},12}$	$\alpha_{\mu,\text{tt},12}$
Parameter 2	c_{rt}	c_{rt}	$\alpha_{\text{c,ba},6}$	$\alpha_{\text{c,tt},37}$	$\alpha_{\text{c,tt},26}$
ζ_1 $[10^{-2}]$	46.8	33.3	-13.3	-15.5	48.4
ζ_2 [m/TN] or $[\mu m^{-1}]$	0	53.2	-961.3	63.8	-4.2 $\cdot 10^{-4}$
ζ_3 [m/TN] or $[\mu m^{-1}]$	517.8	710.3	2646.8	880.1	-5.2 $\cdot 10^{-3}$
ζ_4 $[10^{-2}]$	-17.4	-14.6	7.7	0.9	6.4
R^2_{adj} [%]	50.6	57.7	(22.0)	[76.6]	[76.6]
SI_{model} *deviations*					
Pad	Measured SI [%]	ΔSI [percentage points]				
A	18.21	5.69	7.29	7.00	4.08	4.38
B	10.35	-5.29	-3.48	-5.64	-0.54	-3.88
C	7.07	-5.1	-2.66	-1.43	-2.39	0.51
D	7.36	-1.66	-0.27	-0.77	0.61	-1.82
E	7.10	-1.55	0.11	-0.03	-0.33	1.20
F	2.85	-3.74	-3.74	-4.82	-2.95	-3.01
G	0.11	-5.61	-5.29	-5.77	-3.24	-3.81
H	15.20	2.29	1.47	-0.34	-1.94	0.22
I	0.06	-2.59	-1.53	-3.55	-2.15	-1.13
J	8.79	1.03	-0.21	-1.43	3.93	3.30
K	0.24	-1.76	-1.09	-3.66	-2.19	-1.81
L	3.54	0.70	1.18	-1.36	0.98	0.79
M	3.04	0.65	1.15	-0.86	0.22	0.14
N	5.07	0.97	0.97	-0.6	1.96	1.25
O	4.56	3.47	3.91	0.79	2.40	2.94
P	1.44	-3.43	-3.82	-4.11	-2.37	-2.81
Q	0.01	-2.78	-1.74	-4.19	-2.08	-0.86
R	5.39	1.14	0.87	-1.69	2.45	1.66
S	4.44	-0.12	0.57	-2.02	1.14	1.01
T	5.31	0.59	0.76	-1.41	1.87	1.21
Characteristic ΔSI values [percentage points]					
Minimum ΔSI		-5.61	-5.29	-5.77	-3.24	-3.88
Maximum ΔSI		5.69	7.29	7.00	4.08	4.38
$\sigma_{\Delta SI}$		3.02	2.87	2.82	2.32	2.33

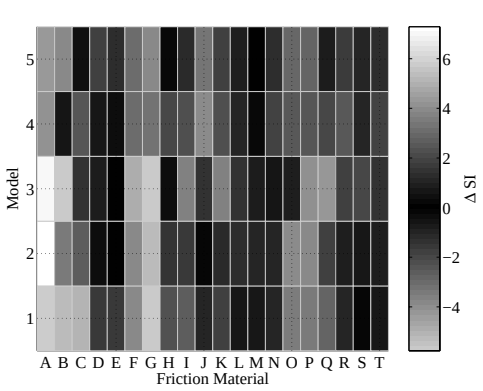

(a) Model's ΔSI overview

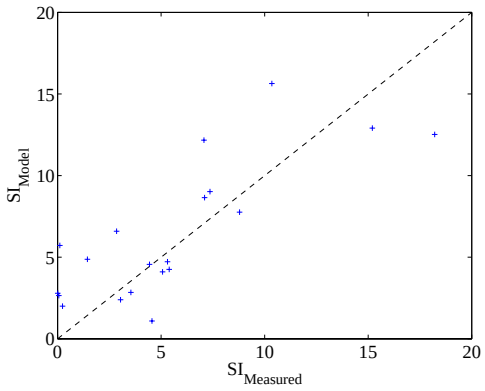

(b) Model 1

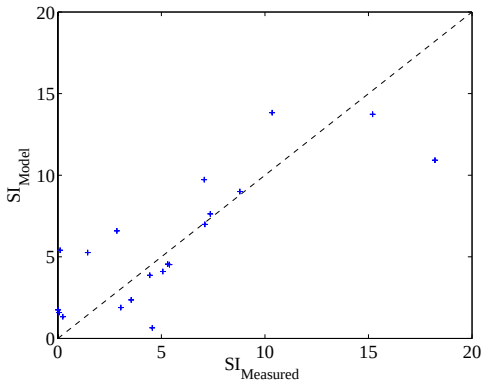

(c) Model 2

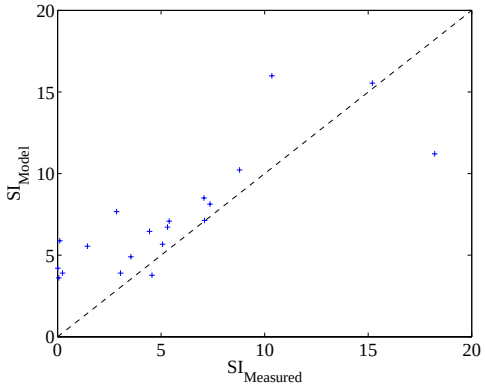

(d) Model 3

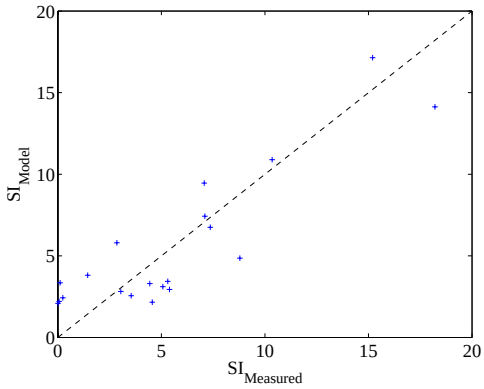

(e) Model 4

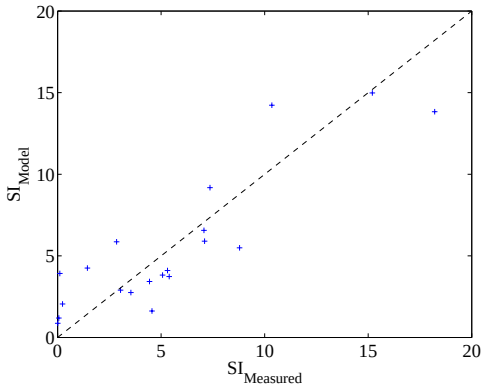

(f) Model 5

Figure 7.1.: *Visualization of selected squeal propensity models of table 7.1*

value in table 7.1 - the markers have not been labeled for better readability.

For the test of friction material A all models calculate a lower squeal propensity than measured. For friction material B's test they calculate a higher $\widehat{SI}$, even as model four quite matches the measured squeal propensity. Additionally, all models calculate a higher $\widehat{SI}$ for the tests of friction materials F, G and P and only the brake application timescale model is able to calculate the squeal propensity of friction material O's test satisfactorily. Again, this behavior indicates at least one additional unrecognized parameter which influences the squeal propensity. This might lead to an impossibility to generate nearly perfect squeal propensity models solely based on friction coefficient and stiffness.

For the sake of completeness the coefficients of the regression models are also shown in table 7.1. But they are not normalized, are multiplied with different characteristic values (using different units) and should not be compared. The same is true for the shown R^2_{adj} values, as they reflect different model building on the different timescales.

In conclusion, the most important results of this work are:

- It is possible to describe the squeal behavior, mainly the squeal propensity, to a certain extent with the friction coefficient and the pad's normal stiffness - or characteristic values calculated thereof. Both parameters influence the propensity of brake squeal generation.

- Most likely there are other parameters influencing the squeal propensity. It has to be expected that it is not possible to keep all those other relevant parameters constant during the experiments.

- It is possible to reduce the measured real-time data to a single value per brake application or one value per test without loosing measured squeal propensity trends. The best models are built on the test timescale, probably because data on this timescale is less prone to measurement errors and less dependent on the stiffness model. Also a friction coefficient threshold for squeal generation can be modeled best on that timescale.

8. Summary and Outlook

The goal of this work was to investigate the influence of tribosystem parameters on disc brake squeal. From theoretical considerations of the excitation mechanism in the literature as well as from conducted experiments, the friction coefficient and the pad stiffness normal to the friction interface are the most promising candidates for these parameters. Yet they had never been experimentally investigated. To study only tribosystem parameter influences, the parameters which are not part of the tribosystem (e. g. component resonant frequencies) were kept as constant as possible for the conducted experiments.

In a first step, 20 different friction materials have been tested, using the identical brake with six identically constructed brake discs on the same brake dynamometer. The measured friction coefficient proved to have the best single correlation to the brake squeal propensity for squeal at frequencies between 2 kHz and 20 kHz. Different squeal propensity vs. friction coefficient trends for different friction materials result and counter-examples to the general trend exist. The general trend of a rising squeal propensity with increasing friction coefficient is mainly supported by the European Metallic type friction materials, which also tend to generate very high friction coefficient values during dynamometer testing.

As the pad normal stiffness is not measurable with sufficient precision during dynamometer testing, a stiffness model based on compressibility measurements has been developed. Using this model, a clear trend of an increasing squeal propensity with increasing friction coefficient and increasing stiffness can be found for most tests. Analog to the solely friction coefficient dependent trend, the local trends for the friction materials add up to a similar global trend, but also produce counter-examples.

Some facts suggest the existence of other squeal propensity influencing parameters. Squeal at many different frequencies has been registered throughout the tests and no tribological explanation for the squeal frequency could be found. Also counter-examples to the general squeal propensity trend exist. As it is most unlikely to leave all resonant

frequencies of the system unchanged during the experiments, the other squeal propensity influencing parameters might belong to the structural system. Also parameters like damping or the chemical composition of the friction materials might lead to a shift of squeal propensity dependences between two tests. The latter for example by generating different particles, tribological films or layers, which might influence the contact (stiffness) significantly.

By building linear regression models based on the friction coefficient and the stiffness, it is possible to calculate the squeal propensity for each test. The deviations between measurement and model are in a suitable range to reproduce the measured trends, but it is not possible to calculate the squeal propensity with a very high precision. This might also indicate the existence of additional parameters. However, the models are a helpful tool to investigate different data mapping functions. These functions have been used to calculate a single characteristic value per brake application or per test. Characteristic values are based on the friction coefficient and stiffness. The correlation between the squeal propensity and these characteristic values shows that the measured squeal propensity trends can be maintained in spite of data pooling. Using specific characteristic values for squeal propensity models on the brake application or test timescales, the squeal propensity models are as good as the measurement data based squeal propensity models.

Some of the squeal propensity models with the smallest deviation between measured and calculated squeal propensity for each test are built on the test timescale: They are based on the percentage of friction coefficient values above 0.5 during the test and on the compressibility of the brake pads or modeled stiffness at brake line pressures above 50 bar. This supports the assumptions that higher friction coefficient values drastically lead to more brake squeal and that the squeal propensity is dependent on the pad normal stiffness. It also shows the introduced stiffness model to be sufficient to show basic dependences and that with an improved model more clear trends could become visible.

The experimental results indicate that the brake squeal phenomenon can only be solved if both, tribological and structural parameters are considered simultaneously. FEM has proven to be a highly sophisticated tool to investigate brake squeal, so additional effort should be conducted to incorporate the needed tribological concepts. Further effort should be taken in measuring and modeling the elastic properties of friction materials at a squeal relevant frequency range, e. g. estimating the damping at squeal relevant frequencies.

A. Stiffness Model Error Analysis

Every model has limitations and models based on measurement data additionally have errors. Errors due to the deformation measurement, the normal force application or due to the stiffness model itself, may occur. The stiffness model error σ_{model} already consists of the statistical deformation measurement error, the error due to the applied normal force during the compressibility testing and the error due to the model assumptions. This model error σ_{model} is a deformation error, because the model fits the deformation versus normal force curve. By using the Gaussian error propagation, the stiffness error σ_c can be calculated from the model error. Therefore, in a first step the compliance error σ_d is calculated from the model error and in a second step the error propagation onto the stiffness model is conducted.
The compliance error σ_d is

$$\sigma_d = \sqrt{\left(\frac{\partial d}{\partial z}\right)^2 \cdot \sigma_{\text{model}}^2} = \left| \sigma_{\text{model}} \cdot \frac{\partial d}{\partial z} \right| \tag{A.1}$$

The absolute differential in pad normal direction dz is defined as (cp. [21])

$$dz = \frac{\partial z}{\partial N}\, dN + \sum_j \frac{\partial z}{\partial \chi_j}\, d\chi_j$$

where $d\chi_j$ represents the other parameters on which the stiffness depends, like vehicle velocity, interface temperature, etc. The stiffness in the used model only depends on normal force, so the partial and absolute deviations

$$\frac{\partial z}{\partial \chi_j} = 0, \forall j \Leftrightarrow \frac{dz}{dN} = \frac{\partial z}{\partial N}$$

are the same. For $dz \neq 0$ and $\partial z \neq 0$ the modeled stiffness is

$$c = -\frac{dN}{dz} = -\frac{\partial N}{\partial z}$$

and for $\partial N \neq 0$ equation A.2 results form equation A.1:

$$\sigma_d = \left| \sigma_{\text{model}} \cdot \frac{\partial d}{\partial z} \right| = \left| \sigma_{\text{model}} \cdot \frac{\partial d}{\partial N} \cdot \frac{\partial N}{\partial z} \right| = \left| \sigma_{\text{model}} \cdot c \cdot \frac{\partial d}{\partial N} \right| \tag{A.2}$$

Using the functions $f = f(N)$ and $g = g(N)$ according to

$$\begin{aligned} f &= \lambda_c \cdot \lambda_b \cdot N^2 + \lambda_c \cdot c_{b,0} \cdot N \\ f' &= \frac{\partial f}{\partial N} = 2 \cdot \lambda_c \cdot \lambda_b \cdot N + \lambda_c \cdot c_{b,0} \\ g &= (\lambda_c + \lambda_b) \cdot N + c_{b,0} \\ g' &= \frac{\partial g}{\partial N} = \lambda_c + \lambda_b \end{aligned} \tag{A.3}$$

the compliance (cp. equations 4.8 and 4.9 on page 71) is

$$d = \frac{g}{f} = \frac{1}{c}$$

and the resulting compliance error σ_d is shown in equation A.4:

$$\begin{aligned} \sigma_d &\overset{A.2}{=} \left| \sigma_{\text{model}} \cdot c \cdot \frac{\partial d}{\partial N} \right| \overset{A.3}{=} \left| \sigma_{\text{model}} \cdot \frac{f}{g} \cdot \frac{f \cdot g' - f' \cdot g}{f^2} \right| \\ &= \left| \sigma_{\text{model}} \cdot \left(\frac{g'}{g} - \frac{f'}{f} \right) \right| \end{aligned} \tag{A.4}$$

According to the Gaussian error propagation, the resulting stiffness error is

$$\sigma_c = \sqrt{\left(\frac{\partial c}{\partial d} \right)^2 \sigma_d^2} = \left| \frac{1}{d^2} \cdot \sigma_d \right| = \left| \, c^2 \cdot \sigma_d \, \right| \overset{A.4}{=} \left| \sigma_{\text{model}} \cdot c^2 \cdot \left(\frac{g'}{g} - \frac{f'}{f} \right) \right| \tag{A.5}$$

The stiffness error is proportional to the model error, the squared (normal force dependent) stiffness and a factor which depends on the model parameters and the normal force. This results in different stiffness errors for the different brake pads and for different normal forces. Figure 4.14 (p. 78) shows the stiffness errors for all tested pads.

B. Complete Data Analysis Diagrams

In this chapter figures of additional measurement data and the complete analysis plots are presented to complete the whole view. In the previous chapters only adequate examples have been discussed to shorten the presentation. Remarks or cross references to previous chapters are made in each subsection.

B.1. Disc Out-Of-Plane Deflection Shapes

The first figures in this chapter show out-of-plane deflection shapes for disc number six which were measured in free-free condition using a Ploytec 1-D scanning LDV. They provide a general impression of the deflection shapes, resulting at the different resonant frequencies for the used discs in free-free condition. Some deflection shapes are not easy to identify and illustrate in two dimensions. Especially above 7 kHz vibration frequency, as there they are a superposition of vibrations with circumferential and nodal diameters. So, figures with a quasi-three-dimensional view are presented here to try to overcome this limitation.

B.2. Complete Dynamometer Testing Data Analysis Diagrams

The later plots in this section, exemplarily shown in the previous chapters, are here to complete the analysis plots for all friction materials. So it is possible to show a complete overview of each result, without enlarging the presented work to an inadequate extend. For conclusions and additional descriptions see chapter 6, as all data has been analyzed the same way as described there.

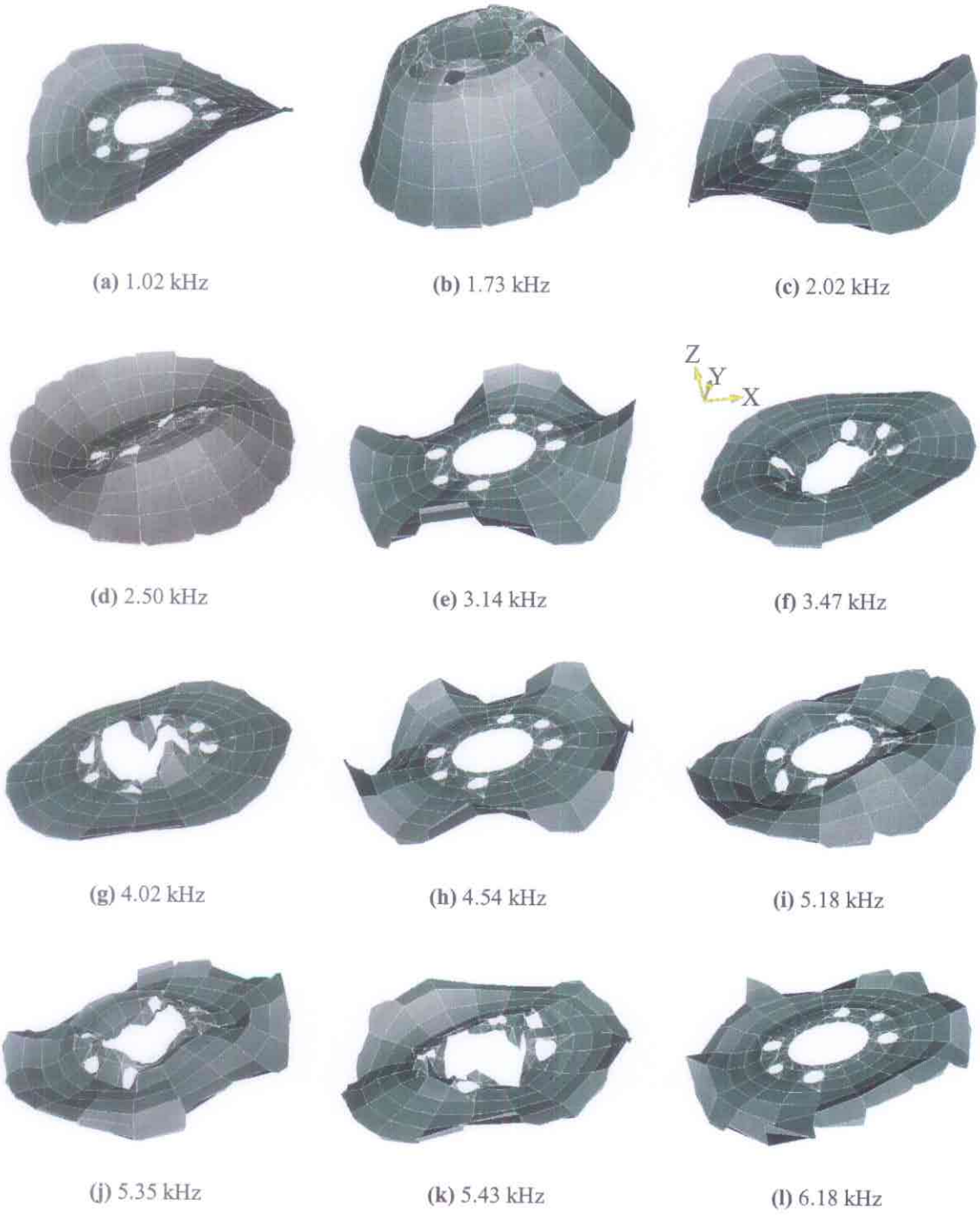

(a) 1.02 kHz (b) 1.73 kHz (c) 2.02 kHz

(d) 2.50 kHz (e) 3.14 kHz (f) 3.47 kHz

(g) 4.02 kHz (h) 4.54 kHz (i) 5.18 kHz

(j) 5.35 kHz (k) 5.43 kHz (l) 6.18 kHz

Figure B.1.: *Disc out-of-plane deflection shapes in the frequency range 1.0 kHz to 6.2 kHz*

Figure B.2.: *Disc out-of-plane deflection shapes in the frequency range 6.3 kHz to 12.5 kHz*

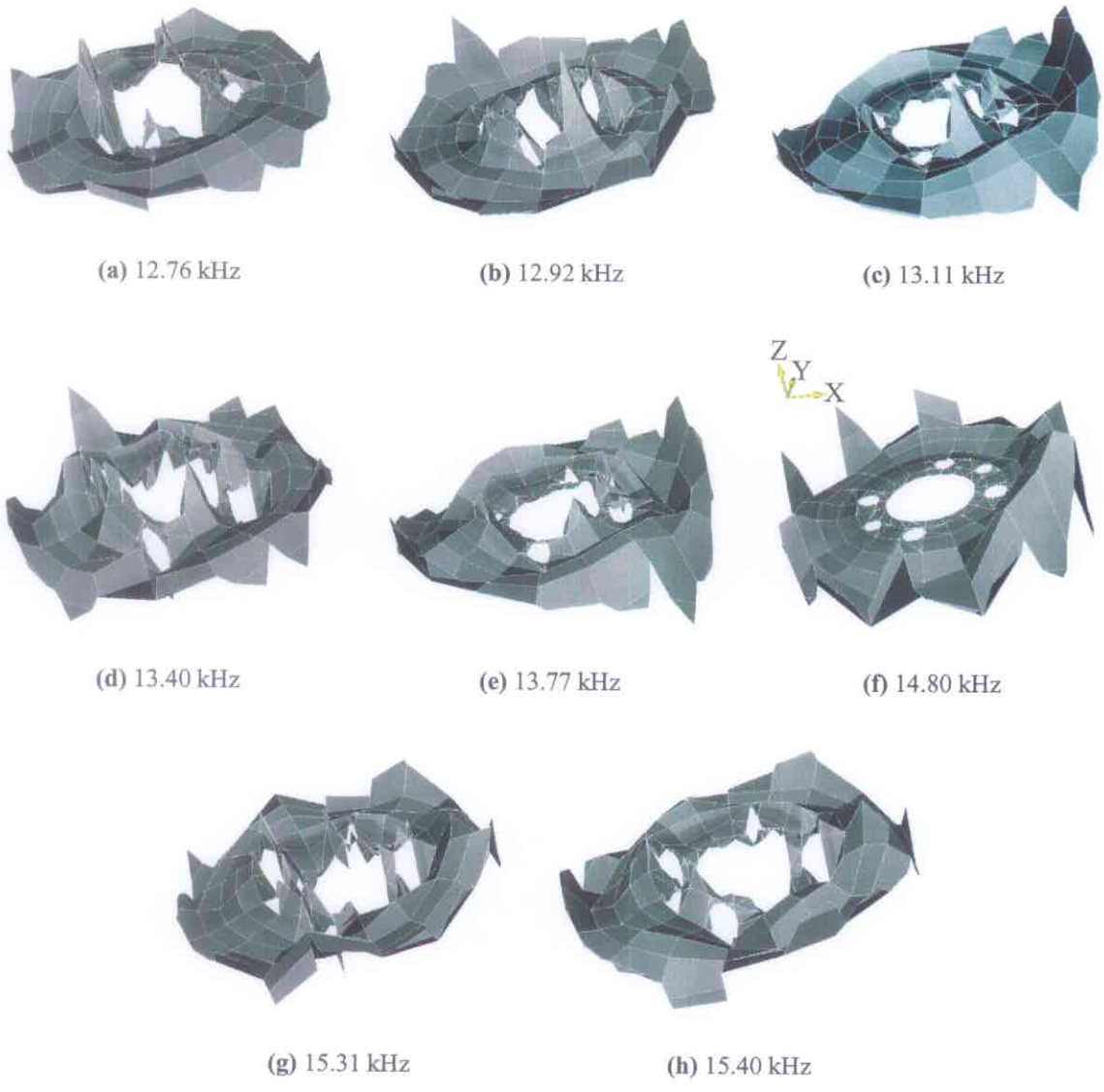

(a) 12.76 kHz (b) 12.92 kHz (c) 13.11 kHz

(d) 13.40 kHz (e) 13.77 kHz (f) 14.80 kHz

(g) 15.31 kHz (h) 15.40 kHz

Figure B.3.: *Disc out-of-plane deflection shapes in the frequency range above 12.5 kHz*

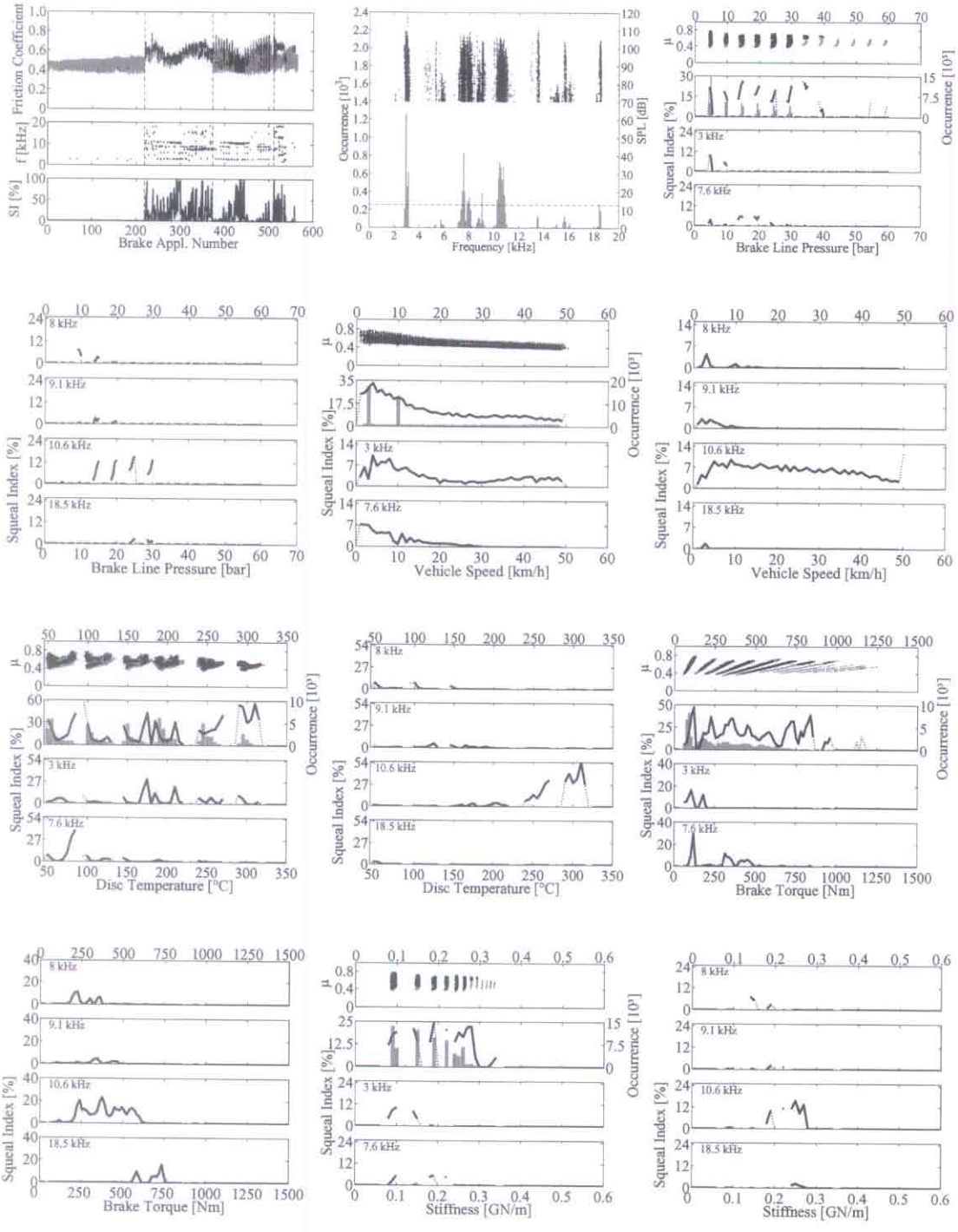

Figure B.4.: *Squeal dependences during tests of friction material A, part 1*

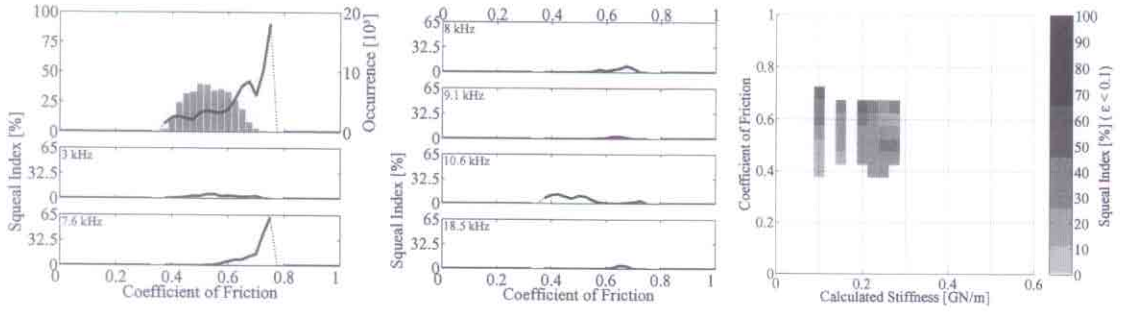

Figure B.5.: *Squeal dependences during tests of friction material A, part 2*

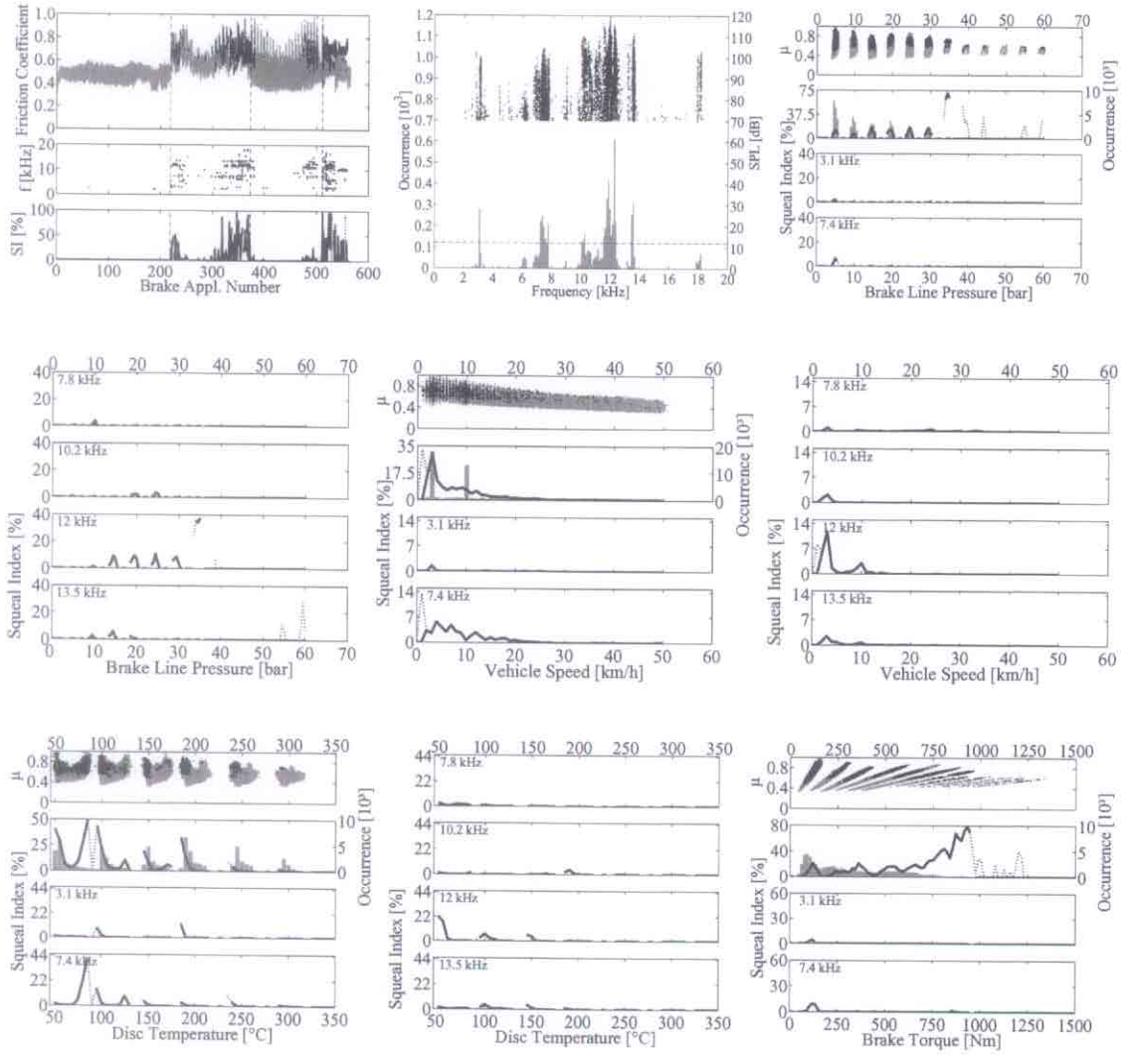

Figure B.6.: *Squeal dependences during tests of friction material B, part 1*

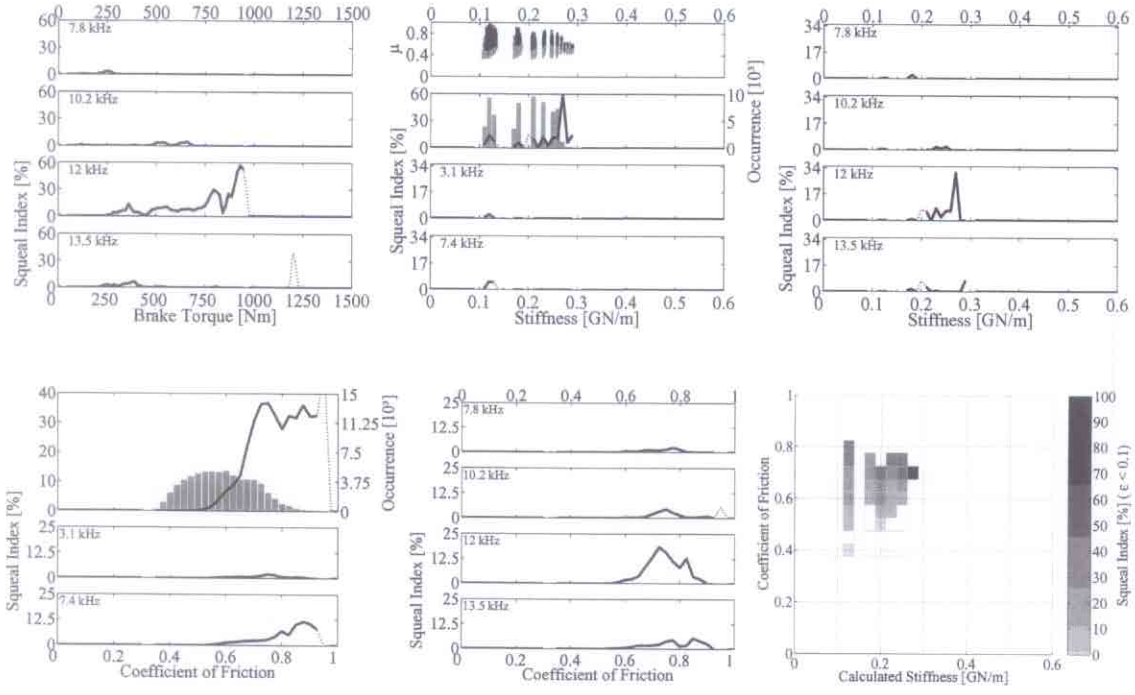

Figure B.7.: *Squeal dependences during tests of friction material B, part 2*

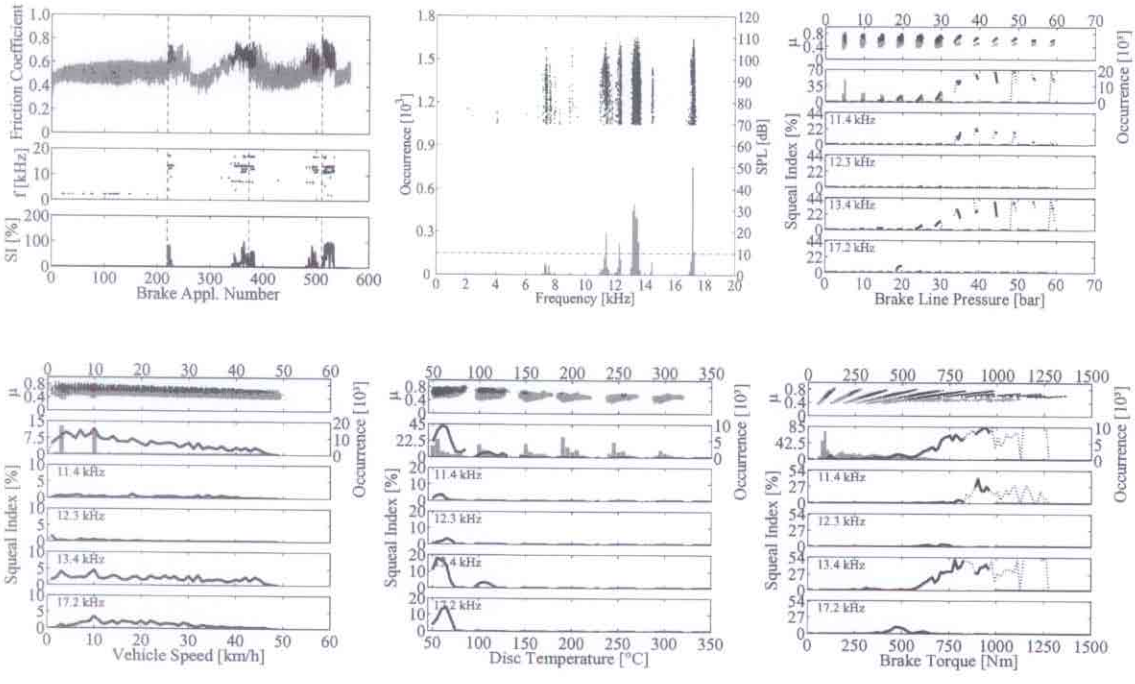

Figure B.8.: *Squeal dependences during tests of friction material C, part 1*

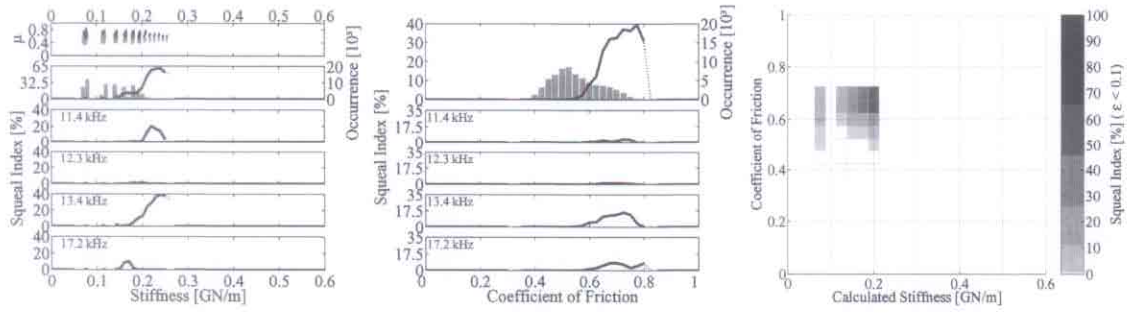

Figure B.9.: *Squeal dependences during tests of friction material C, part 2*

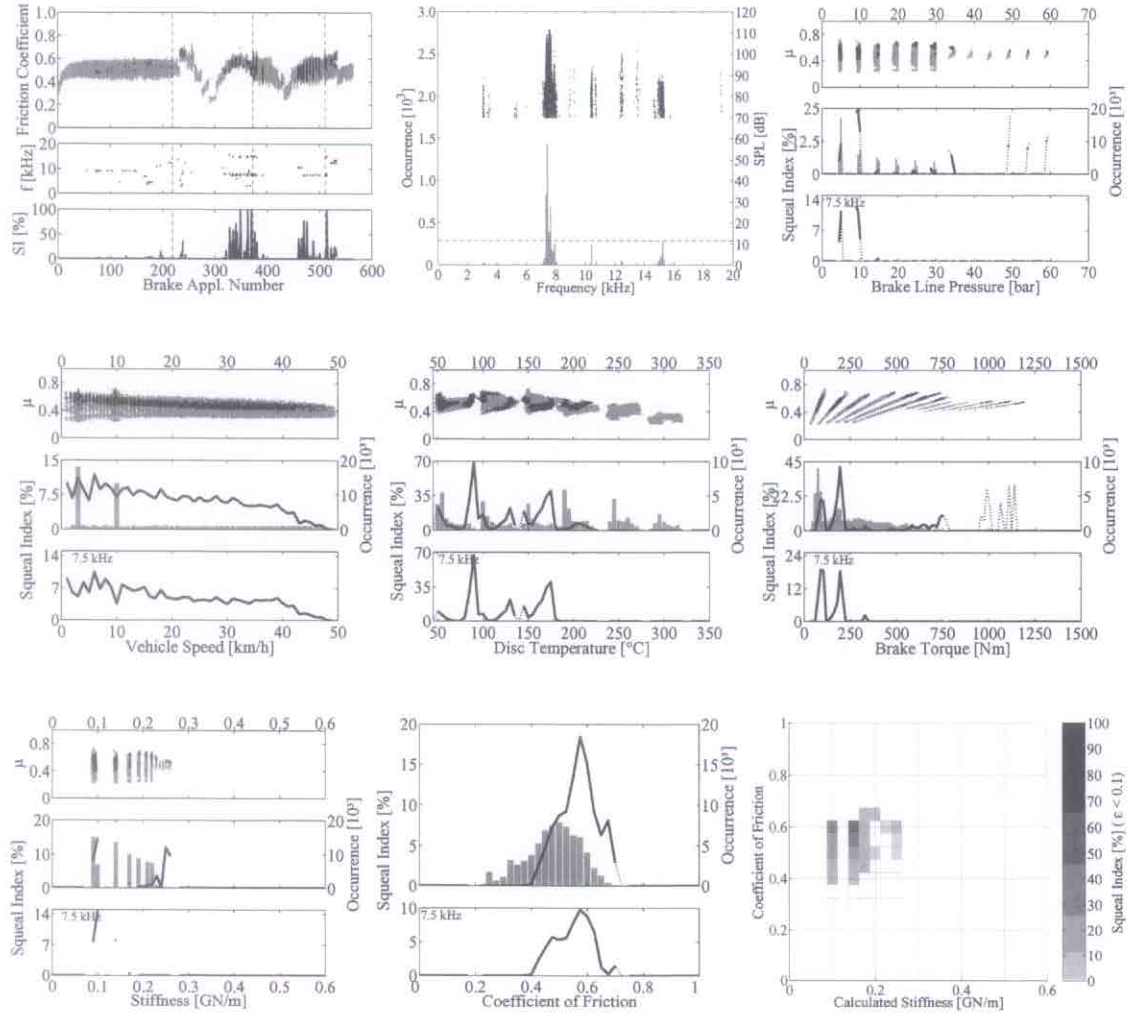

Figure B.10.: *Squeal dependences during tests of friction material D*

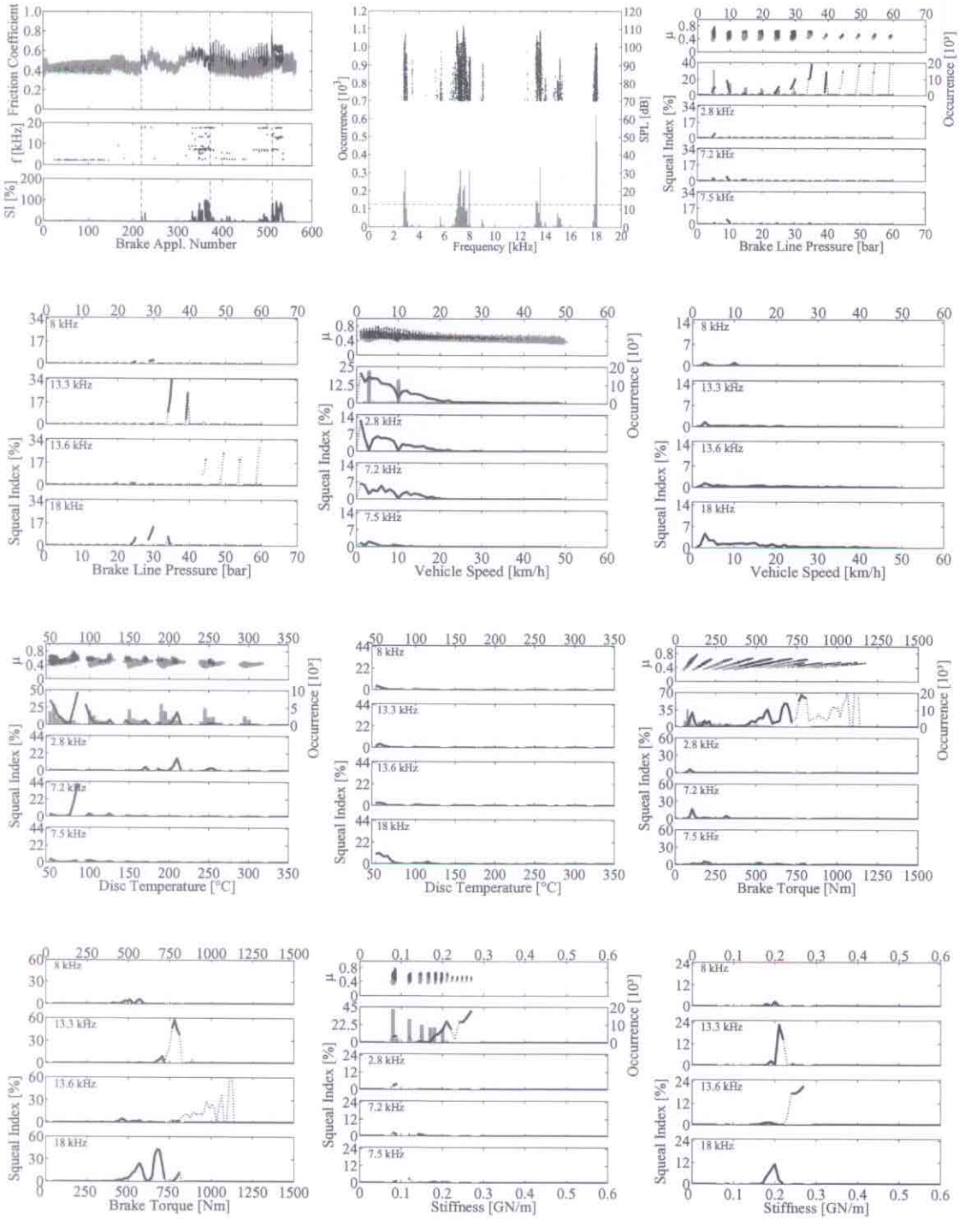

Figure B.11.: *Squeal dependences during tests of friction material E, part 1*

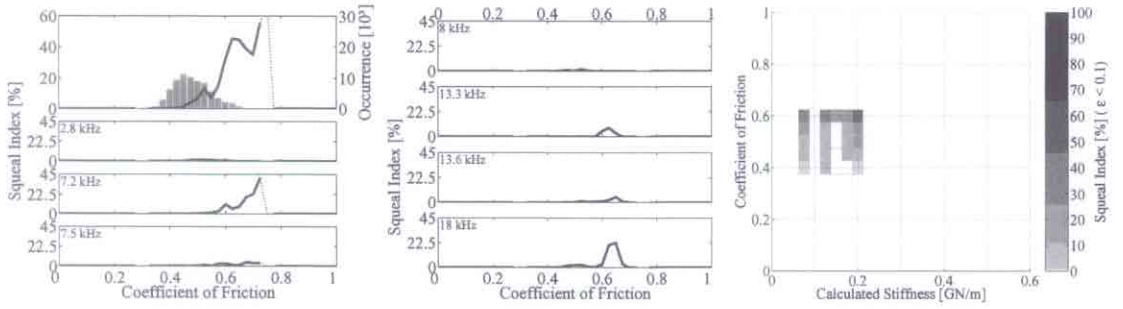

Figure B.12.: *Squeal dependences during tests of friction material E, part 2*

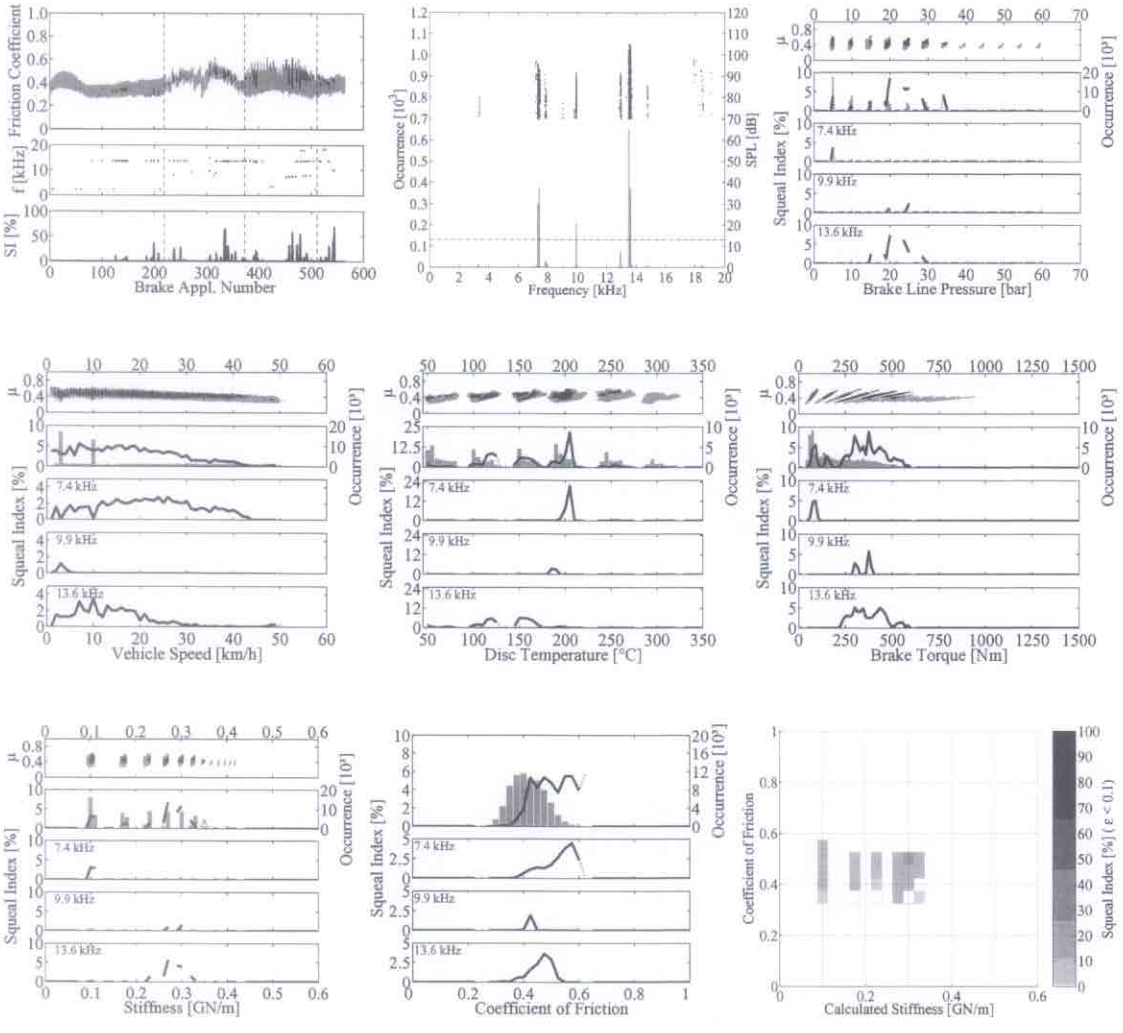

Figure B.13.: *Squeal dependences during tests of friction material F*

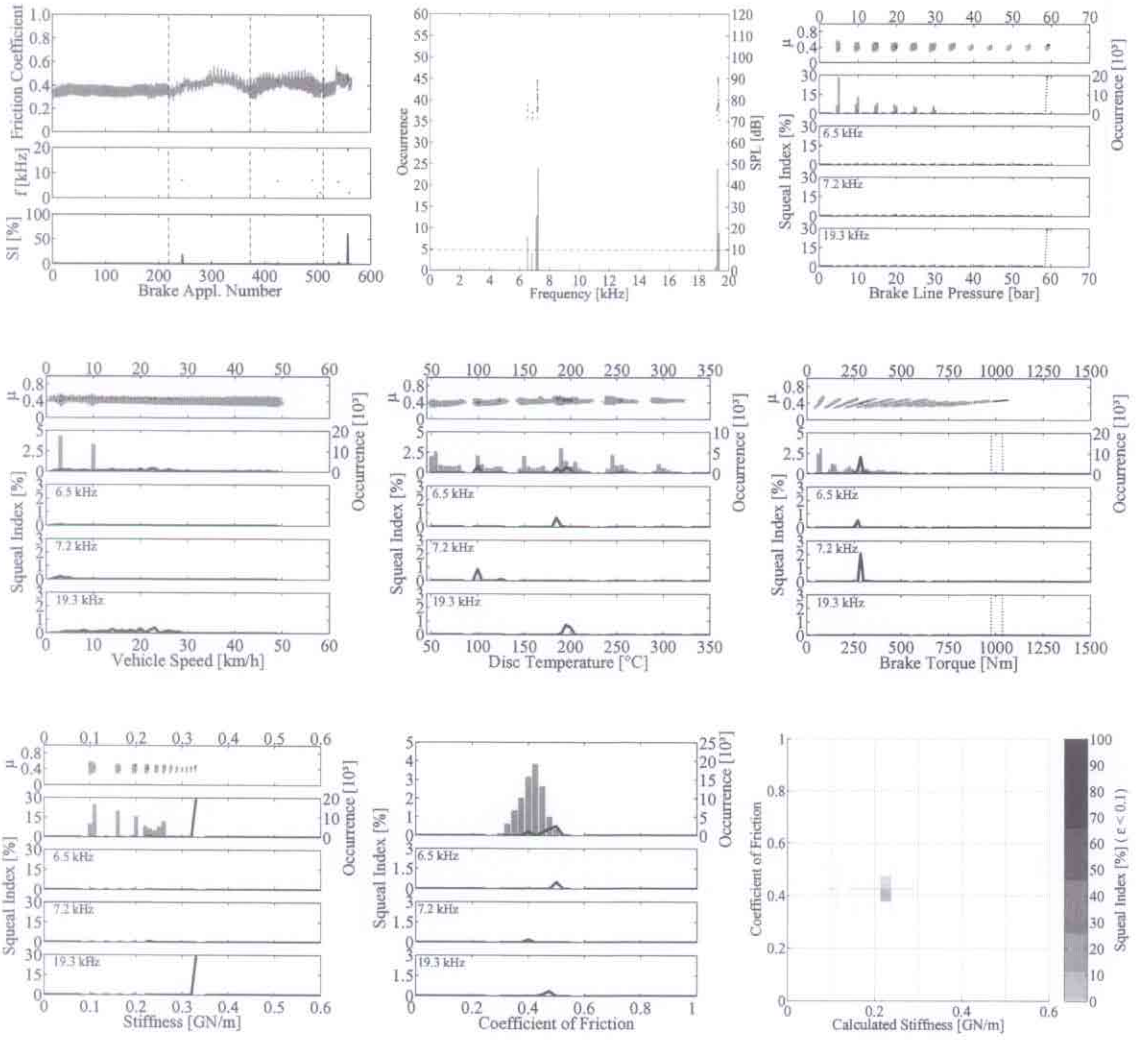

Figure B.14.: *Squeal dependences during tests of friction material G*

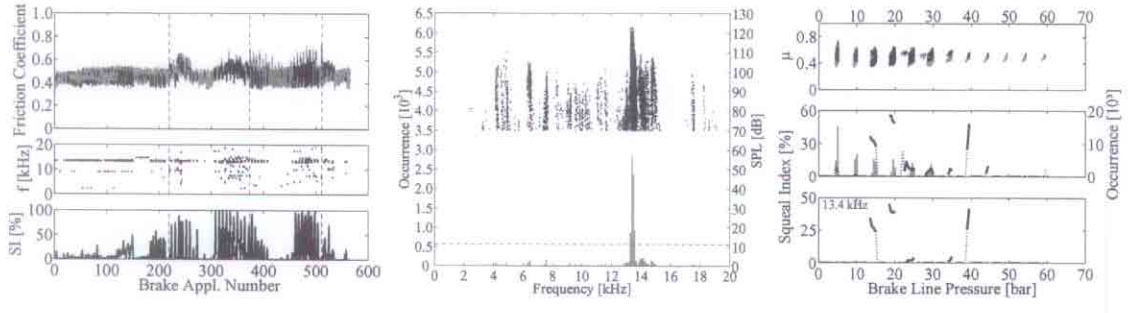

Figure B.15.: *Squeal dependences during tests of friction material H, part 1*

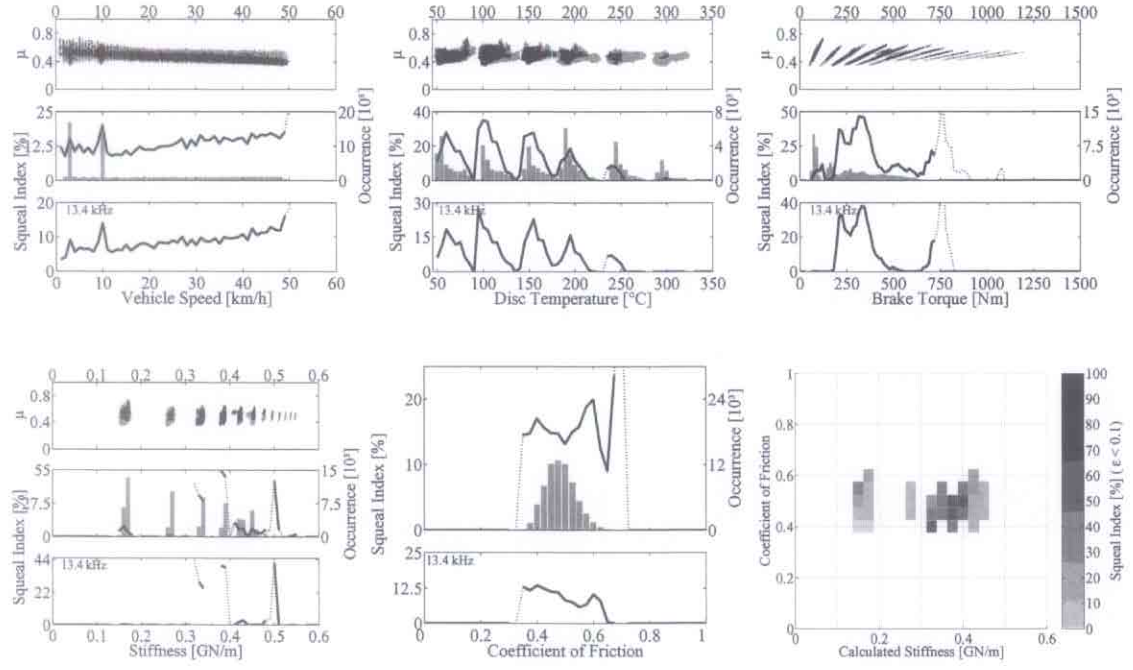

Figure B.16.: *Squeal dependences during tests of friction material H, part 2*

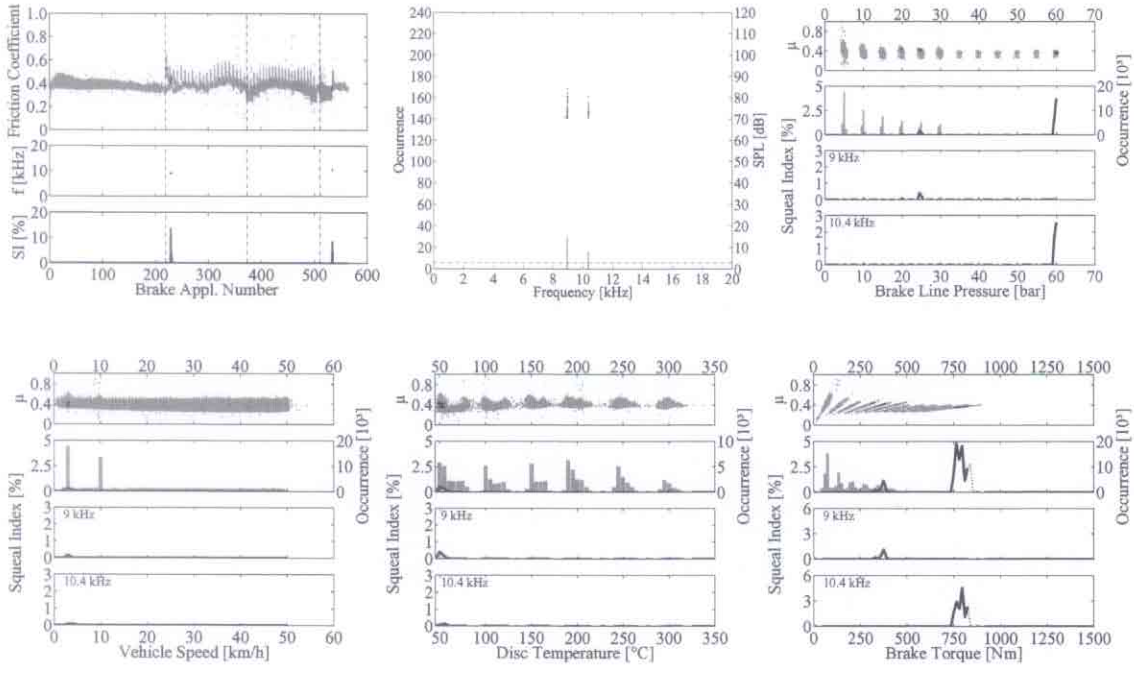

Figure B.17.: *Squeal dependences during tests of friction material I, part 1*

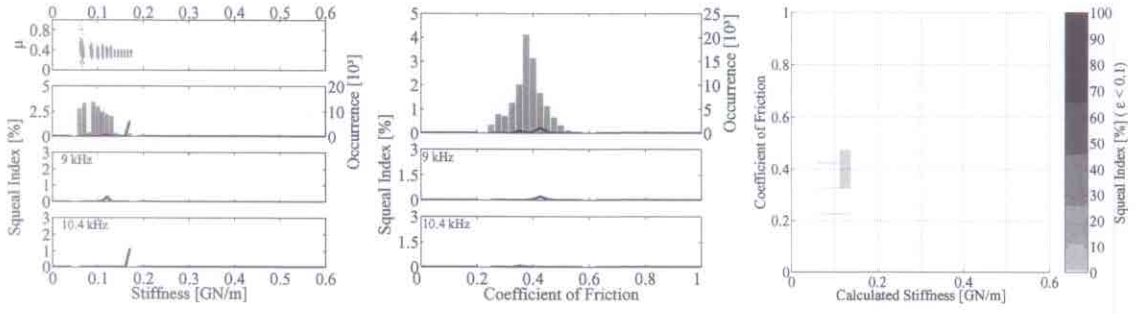

Figure B.18.: *Squeal dependences during tests of friction material I, part 2*

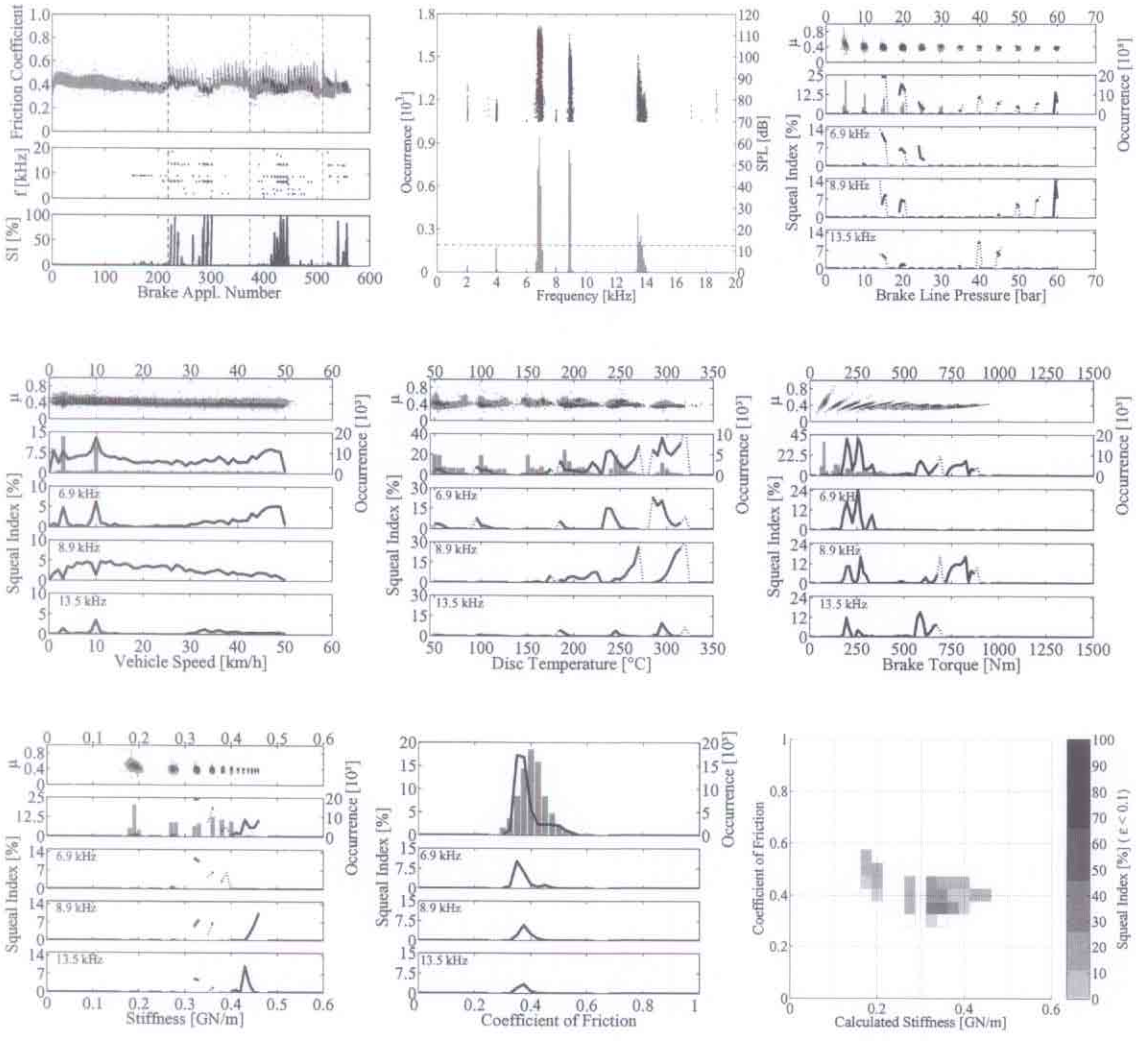

Figure B.19.: *Squeal dependences during tests of friction material J*

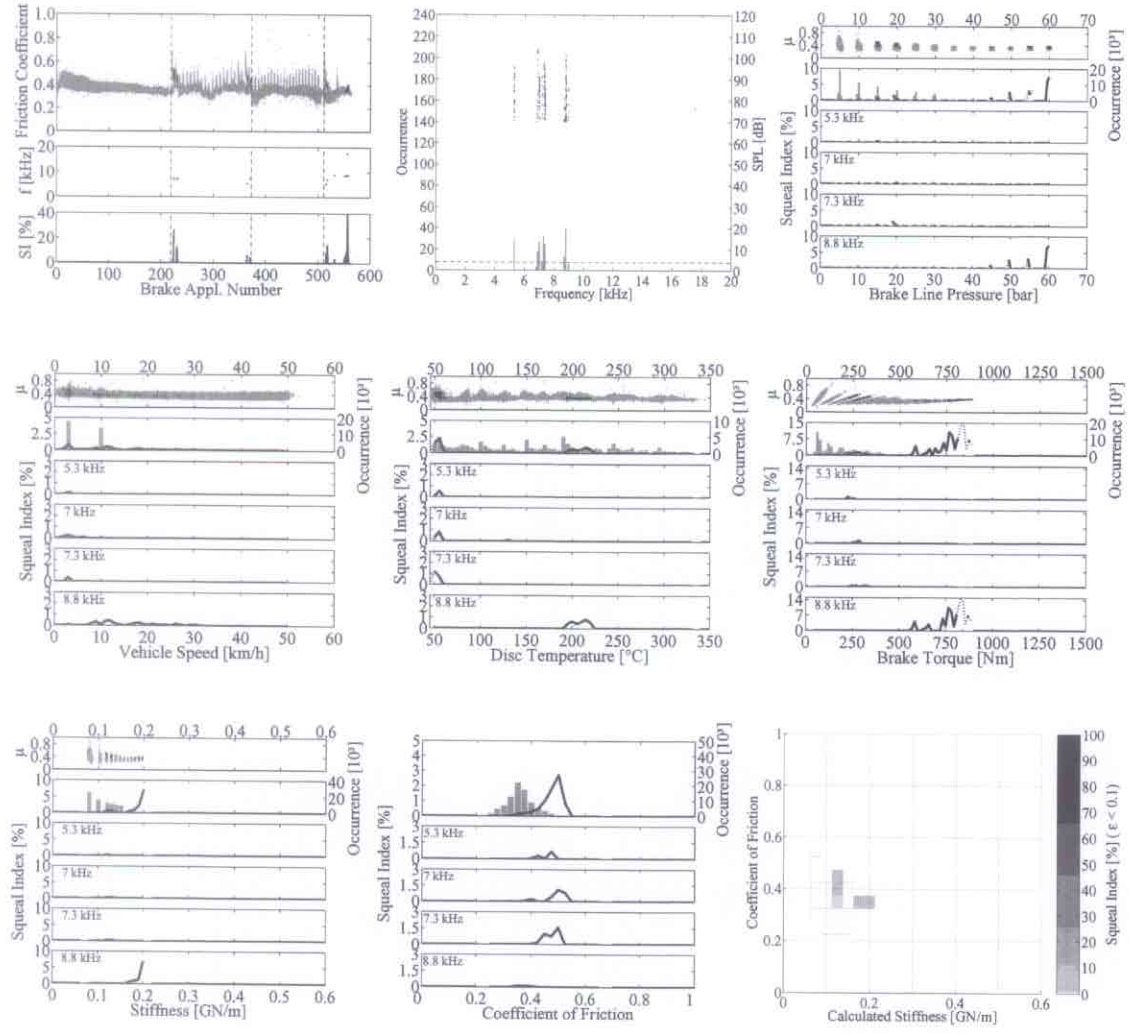

Figure B.20.: *Squeal dependences during tests of friction material K*

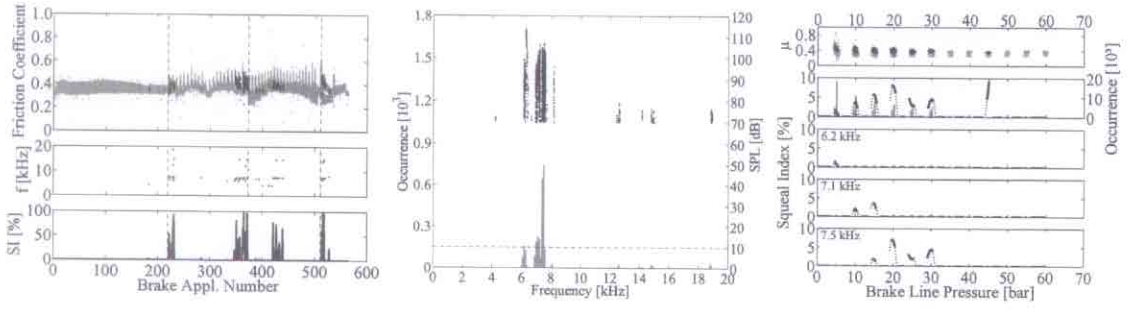

Figure B.21.: *Squeal dependences during tests of friction material L, part 1*

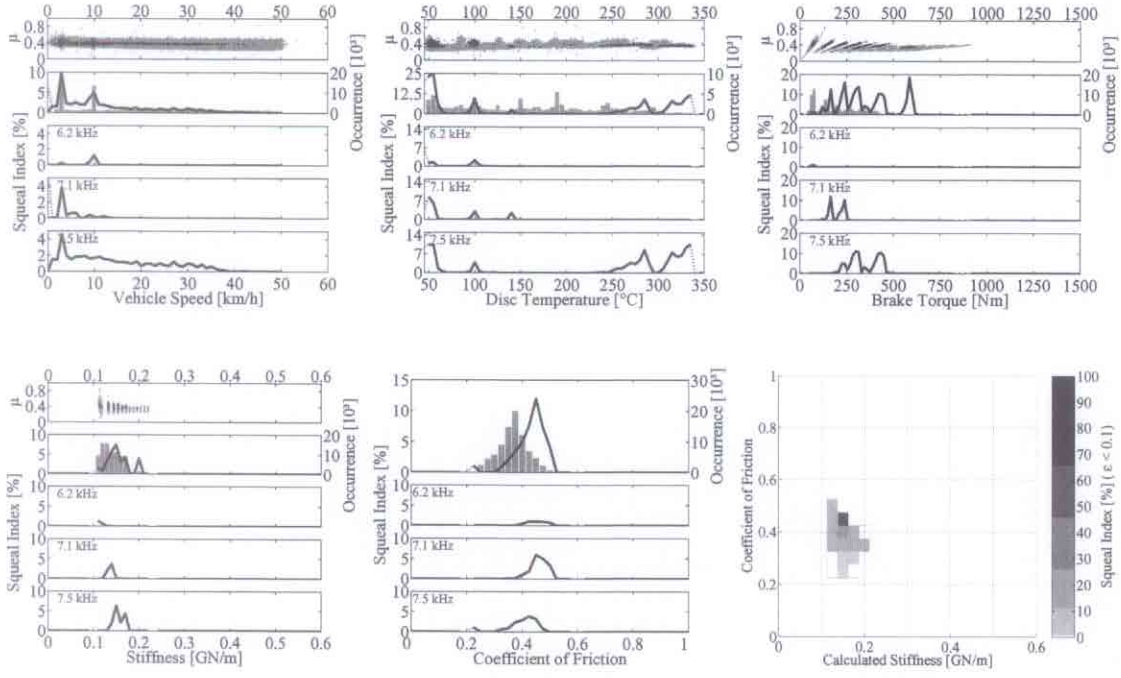

Figure B.22.: *Squeal dependences during tests of friction material L, part 2*

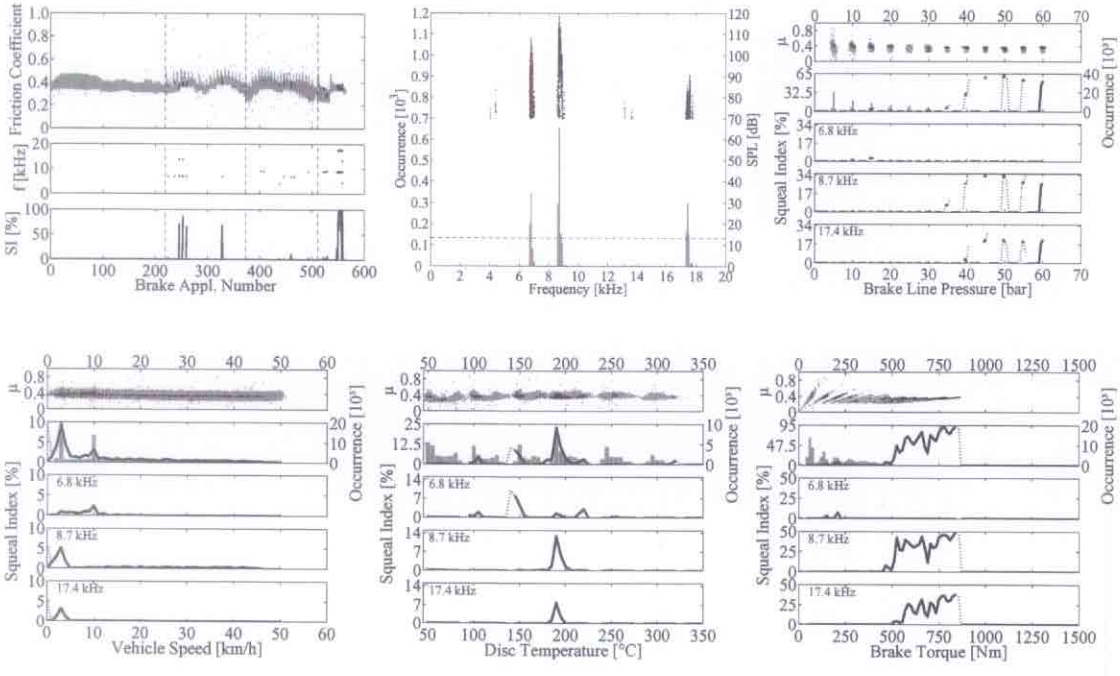

Figure B.23.: *Squeal dependences during tests of friction material M, part 1*

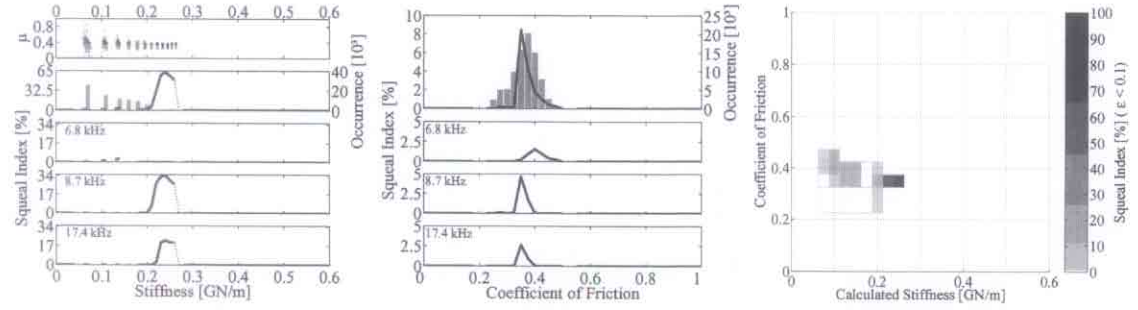

Figure B.24.: *Squeal dependences during tests of friction material M, part 2*

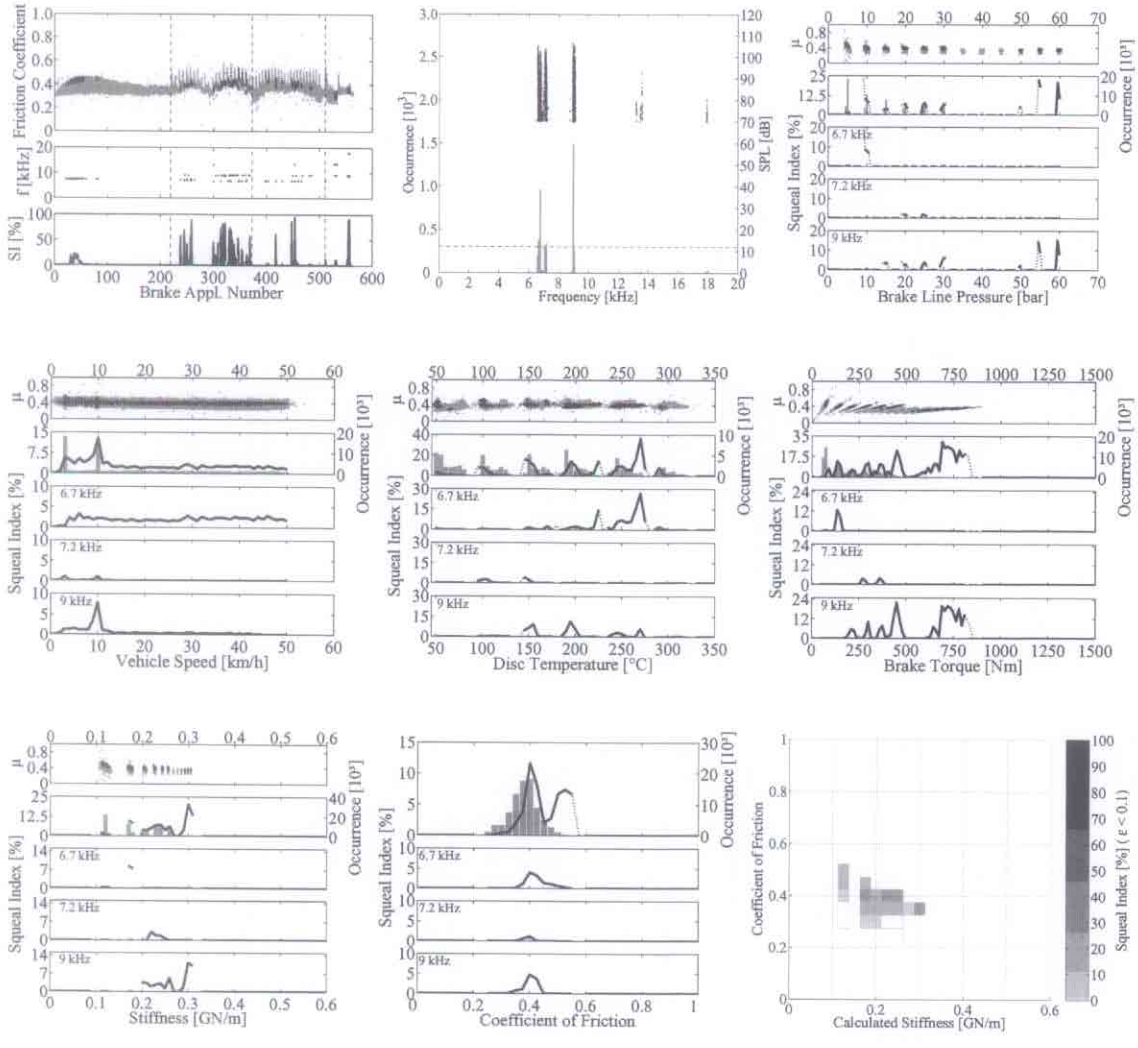

Figure B.25.: *Squeal dependences during tests of friction material N*

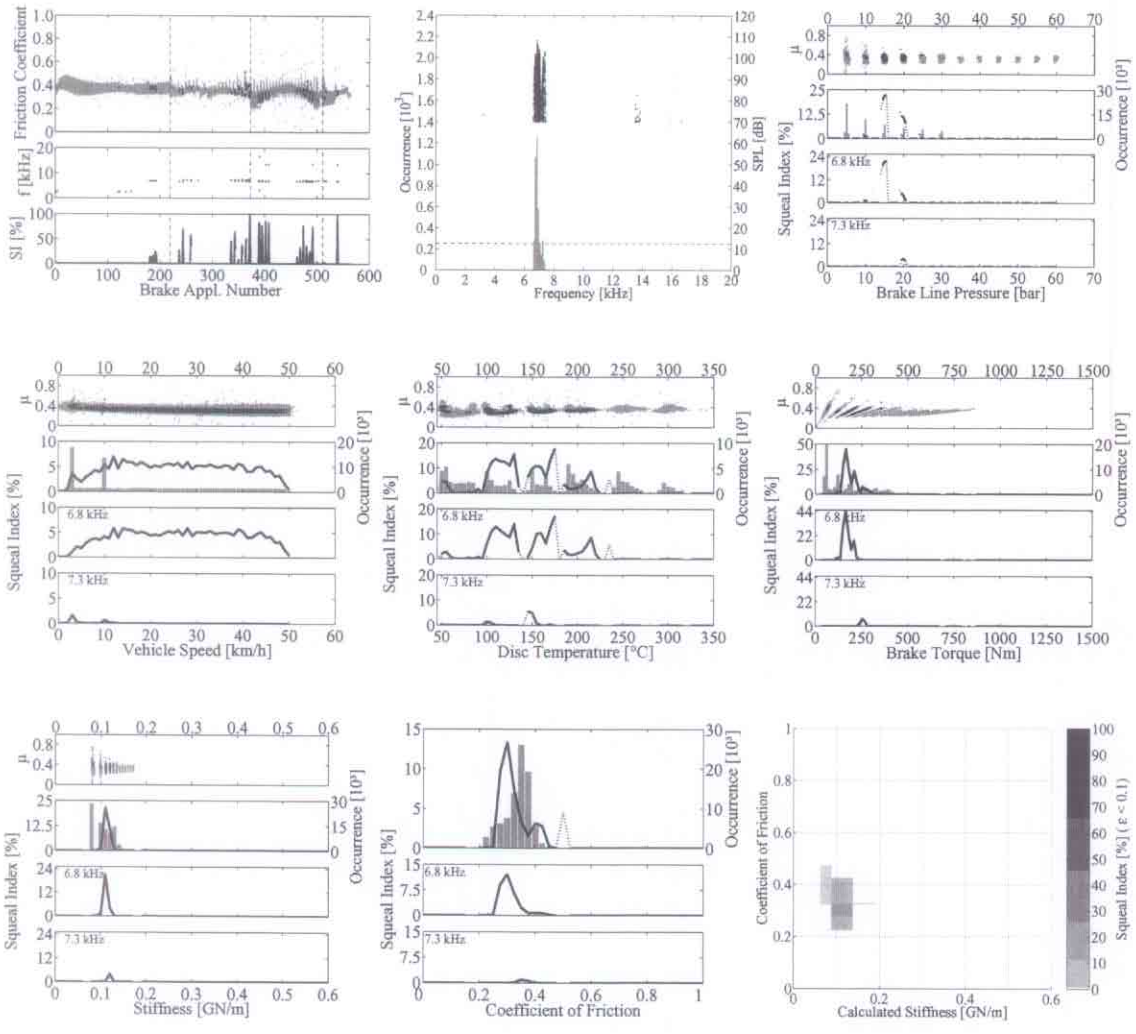

Figure B.26.: *Squeal dependences during tests of friction material O*

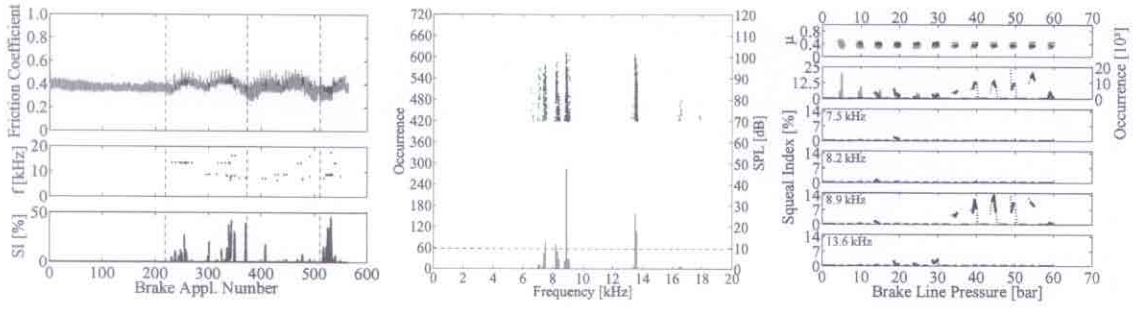

Figure B.27.: *Squeal dependences during tests of friction material P, part 1*

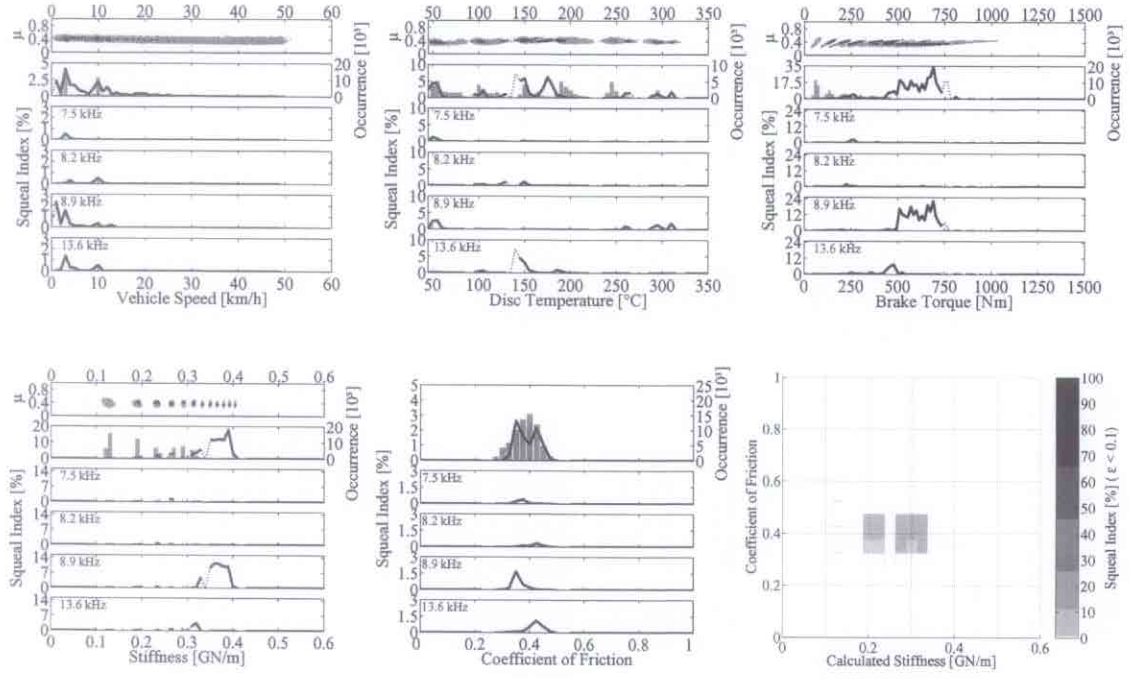

Figure B.28.: *Squeal dependences during tests of friction material P, part 2*

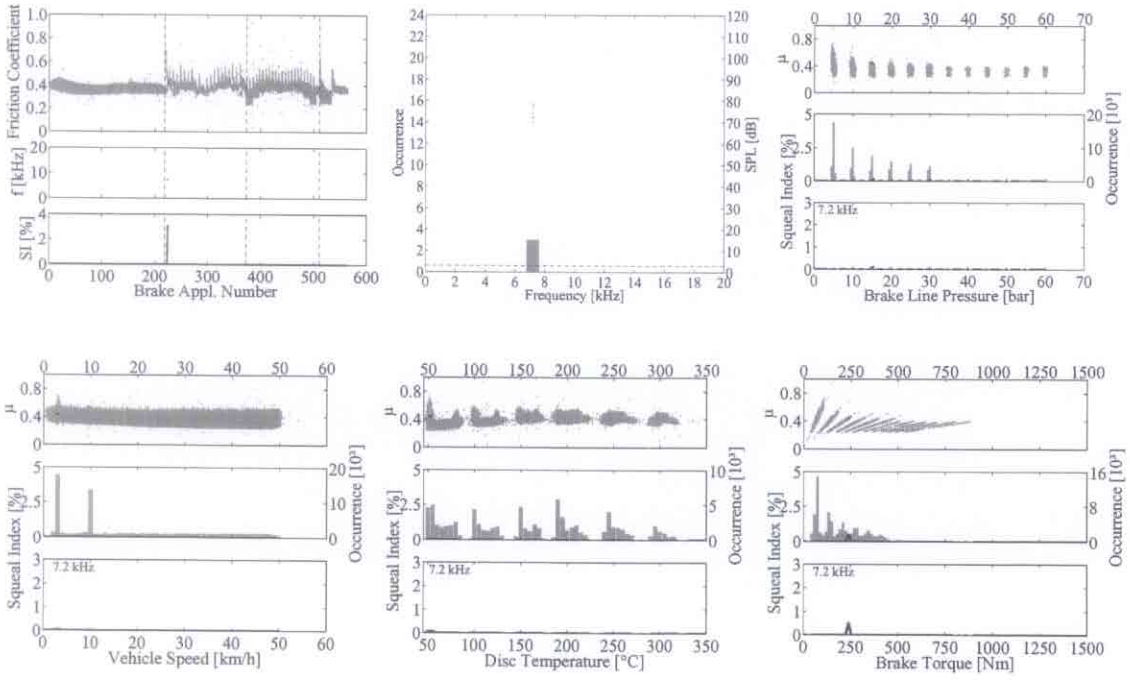

Figure B.29.: *Squeal dependences during tests of friction material Q, part 1*

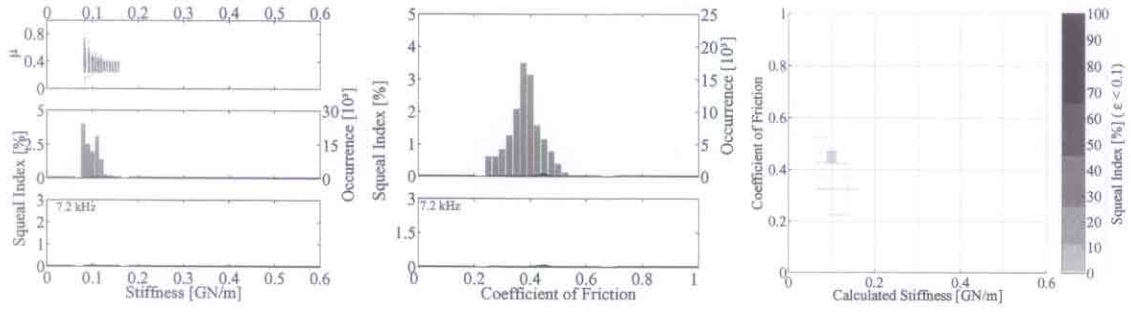

Figure B.30.: *Squeal dependences during tests of friction material Q, part 2*

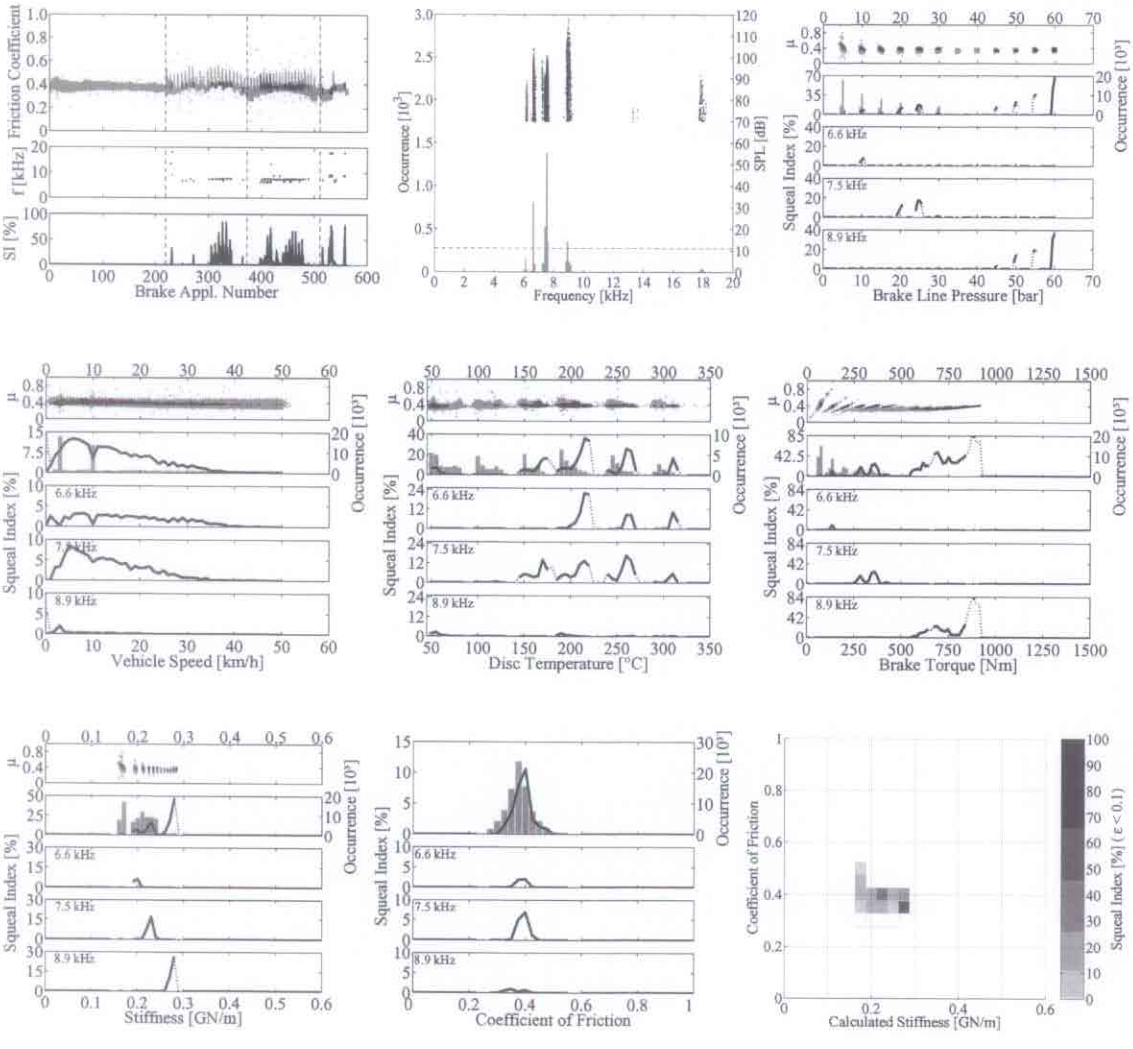

Figure B.31.: *Squeal dependences during tests of friction material R*

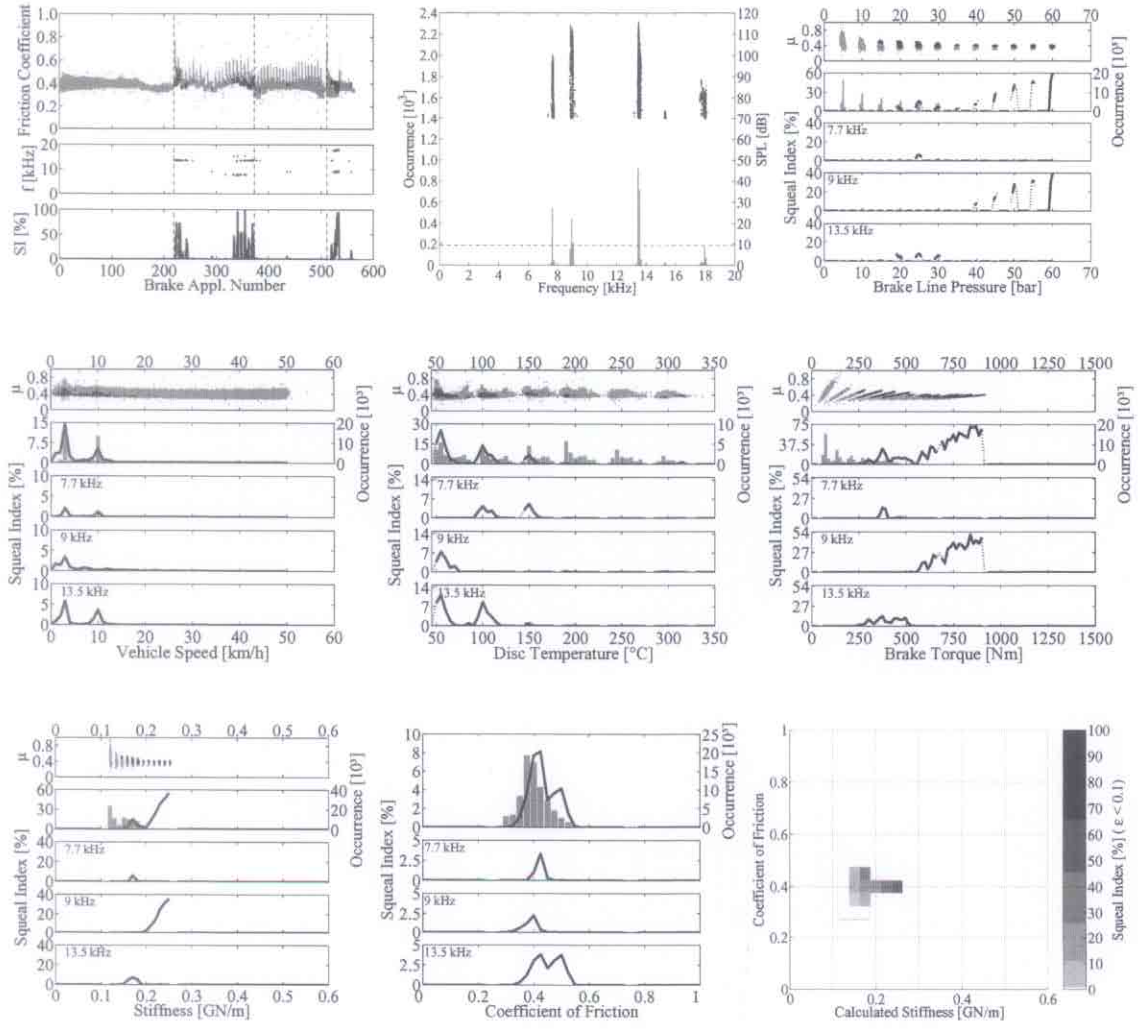

Figure B.32.: *Squeal dependences during tests of friction material S*

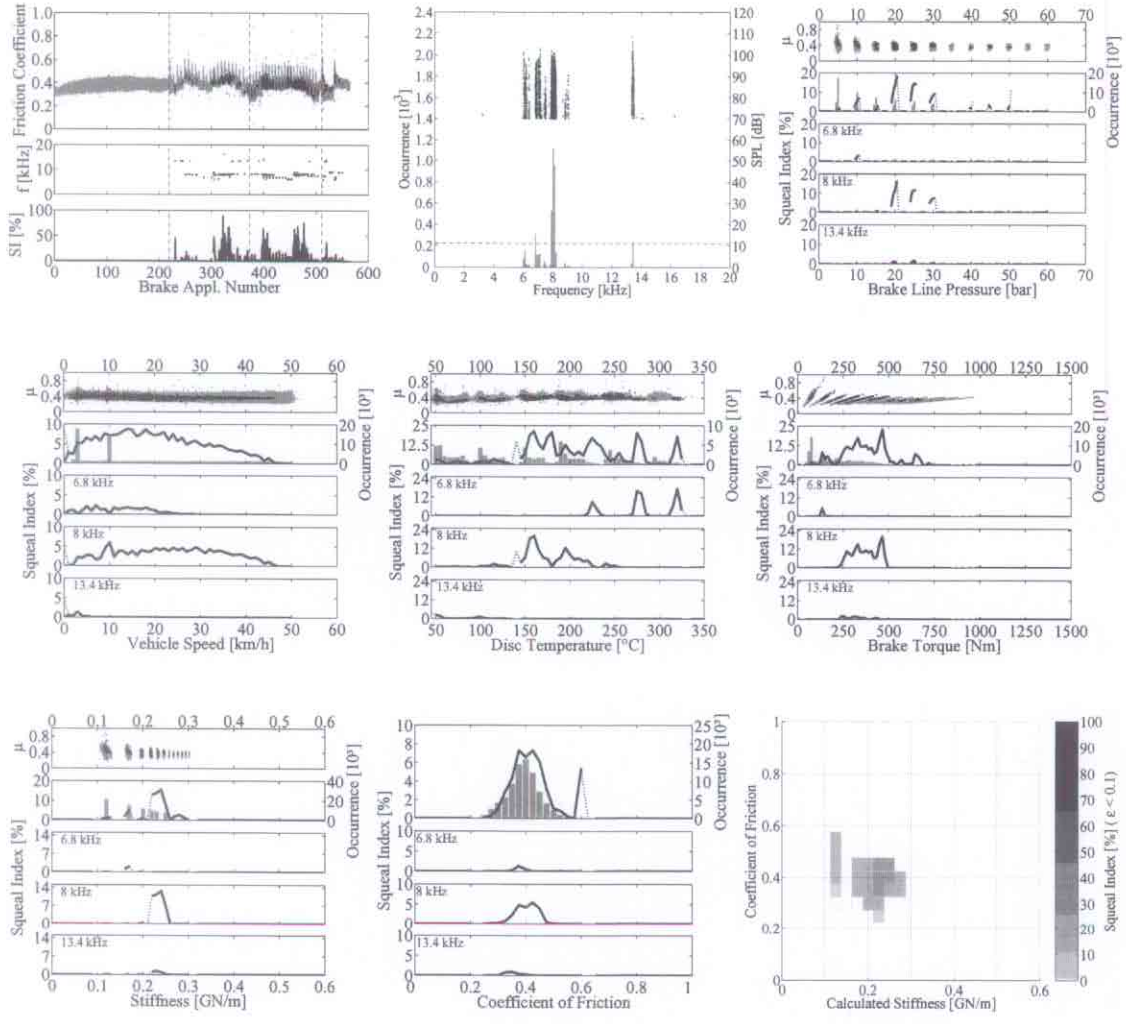

Figure B.33.: *Squeal dependences during tests of friction material T*

C. Deutsche Kurzfassung

C.1. Fragestellung

C.1.1. Motivation

Das Phänomen des Bremsenquietschens wird seit annähernd 70 Jahren untersucht. In dieser Zeit wurden beachtliche Fortschritte erzielt, jedoch existiert bis heute kein allgemeingültiges und umfassendes Verständnis.

Viele experimentelle Arbeiten deuten auf den Reibkoeffizient zwischen Bremsbelag und Bremsscheibe als wichtigsten tribologischen Einflussparameter auf das Bremsenquietschen hin - allerdings gibt es in den meisten Fällen auch Gegenbeispiele zu aufgezeigten Trends. Diese legen nahe, dass der Reibkoeffizient nicht der einzige Parameter des tribologischen Systems (Tribosystems) bestehend aus Bremsbelag und -scheibe sein kann, der die Quietschentstehung bei Kraftfahrzeugbremsen beeinflusst.

Betrachtet man den Anregungsmechanismus des Bremsenquietschens im Tribosystem Belag/Scheibe, so führt die Kopplung mehrerer Freiheitsgrade zu einer reiberregten Schwingung, die sich im Bezugssystem der Bremsscheibe folgendermaßen beschreiben lässt:

Eine Oszillation der Auslenkung in axialer Richtung führt zu einer oszillierenden Normalkraft am Reibkontakt. Diese führt weiterhin zu einer oszillierenden Tangentialkraft, zu einer oszillierenden Tangentialauslenkung die wiederum zu einer oszillierenden Normalbewegung führt. Aus dieser Überlegung ergeben sich vier Kopplungsparameter. Die Kopplungen zwischen Tangentialkraft und -bewegung sowie die Kopplung zwischen der tangentialen und der axialen Auslenkung werden durch strukturmechanische Parameter bestimmt. Die Kopplungen innerhalb des Tribosystems sind die axiale Steifigkeit zwischen axialer Auslenkung und Kraft sowie der Reibkoeffizient als Kopplungsparameter zwischen der axialen und der tangentialen Kraft. Diese Überlegungen sind auch z. B. anhand des von Hamabe et al. [49] vorgestellten Modells, das durch Allgaier [3] ausführlich

diskutiert wird, nachvollziehbar.

Die Steifigkeit des Tribosystems in axialer Richtung wird (für das hier verwendete System) maßgeblich durch die Belagsteifigkeit normal zur Bremsscheibenoberfläche beeinflusst. Dennoch wurden bisher die Einflüsse des Reibkoeffizienten und der normalen Belagsteifigkeit auf das Bremsenquietschen nicht systematisch durch Experimente an einem Original-Bremssystem untersucht.

Da die Auftretenswahrscheinlichkeit des Bremsenquitschens normalerweise relativ gering ist, müssen während den Experimenten viele Versuche mit denselben bzw. ähnlichen Parameter-Sätzen durchgeführt werden. Dies führt zu sehr großen und unübersichtlichen Datenmengen. Um diese Daten beherrschbar und darstellbar zu machen ist es gebräuchlich, diese auf Minimal-, Maximal- oder Mittelwerte zu reduzieren. Beispielsweise wird bei Untersuchungen zur Funktionalität des Bremssystems oft ein sogenannter nominaler Reibwert angegeben, der sich als Mittelwert aus den Mittelwerten einzelner Teile eines bestimmten Prüfprogramms zusammensetzt. Obwohl das Reibverhalten innerhalb eines Bremsvorgangs und bei Vergleich verschiedener Bremsungen sehr unterschiedlich ist, gilt der nominale Reibwert als Indikator für das Reibverhalten des Belag-Scheibe-Tribosystems. In Bezug auf die Quietschentstehung wurde bisher nicht erforscht, ob signifikante Trends erhalten bleiben, wenn man die gemessenen Daten auf z. B. einen Wert pro Bremsung oder einen Wert pro Versuch reduziert.

C.1.2. Stand der Technik

Im Folgenden werden einige Literaturstellen vorgestellt, die für das Verständnis dieser Zusammenfassung hilfreich sind. Diese Auswahl gibt einen sinnvollen und strukturierten Überblick. Auf eine ausführliche Beschreibung des Stands der Technik wird hier bewusst verzichtet, da es den Rahmen der vorliegenden Kurzfassung sprengen würde.

- Nach Blau [15] wird der Faktor zwischen der Reibkraft F_r und der Normalkraft N üblicherweise als Reibwert μ bezeichnet.

- Das Reibverhalten eines Bremssystems hängt sowohl von direkten Einflussgrößen wie dem Bremsdruck, der Fahrzeuggeschwindigkeit oder der Temperatur im Reibkontakt ab, wie auch, laut Kemmer [58], von der Vorgeschichte. Als Vorgeschichte wird in diesem Zusammenhang die Gesamtheit der vorangegangenen Bremsungen bezeichnet. Diese verändern den Zustand des Tribosystems, der sich wieder-

um auf das (Reib-) Verhalten auswirkt [58]. Durch die Vorgeschichtenabhängigkeit des Reibverhaltens können unterschiedliche Reibwerte und Reibwertverläufe bei denselben Kontrollparameterwerten für Bremsdruck, Fahrzeuggeschwindigkeit und Scheibentemperatur resultieren.

- Der in dieser Arbeit verwendete Kompressibilitätstester wird hauptsächlich für Untersuchungen des „Pedalgefühls“ verwendet, wie z. B. durch Hecht-Basch et al. [50]. Der Kompressibilitätstester eignet sich nicht ohne weiteres zur Bestimmung des E-Moduls von Bremsbelägen, misst allerdings die druckabhängige Belagsteifigkeit unter realitätsnahen Bedingungen. Diese ist für die Kopplung zwischen der normalen Deformation und der Normalkraft am Reibkontakt maßgeblich verantwortlich. Augsburg et al. [5] ermittelten eine zunehmende normale Belagsteifigkeit mit zunehmender mittlerer Normalkraft und zunehmender Frequenz einer Normalkraftoszillation. Das nicht-lineare Verhalten der Belagsteifigkeit zeigt außerdem ein Hysterese-Verhalten.

- Thomas and Sayles [88] zeigen eine linear von der Normalkraft abhängende Kontaktsteifigkeit für elastische Rauheiten, deren Höhen Gauss-verteilt sind. Sie stützen sich auf das Kontaktmodell von Greenwood and Williamson [47] und werden von Sherif [82] bestätigt, der für elastische Kontaktsituationen einen prinzipiellen Anstieg der Kontaktsteifigkeit mit zunehmender Normalkraft zeigt. Dabei untersucht Sherif [82] sowohl das Kontaktmodell von Greenwood und Williamson als auch das von Onions und Archard und folgerte, dass die Veränderung der Kontaktsteifigkeit in beiden Fällen einer sich versteifenden Feder ähnele.

- Es gibt verschiedene Arten von Schwingungen des Bremssystems. Laut Wallaschek et al. [95] werden sie danach benannt, wie sie sich anhören, z. B. bezeichnet Muhen oder Heulen Bremsgeräusche bei Frequenzen unterhalb von 1 kHz. Bei selbsterregten Schwingungen mit Frequenzen zwischen 1 kHz und 20 kHz spricht man üblicherweise von Bremsenquietschen [95]. In dieser Arbeit wurde Quietschen bei Frequenzen zwischen 2 kHz und 20 kHz untersucht.

- Stellvertretend für die vielen (experimentellen) Arbeiten der vergangenen Jahre zum Thema Bremsenquietschen sollen an dieser Stelle noch die Arbeiten von Bergman [7] und Eriksson [34] erwähnt werden, die in ihren hier zitierten Dissertationen zusammengefasst sind. Unter anderen fanden sie für Ihre Bremsenkonfigurati-

on einen kritischen Reibwert, unterhalb dessen kein Bremsenquietschen gemessen wurde [9] und dass Bremsenquietschen innerhalb von weniger als 0,1 s einsetzt, sofern die Kontaktbedingungen dies unterstützen [36].

C.1.3. Zielsetzung

Das Ziel der Arbeit ist die Frage zu klären, ob es möglich ist das Quietschverhalten mit den dominanten Parametern des Tribosystems zu beschreiben. Aufgrund der oben gezeigten Überlegungen sind diese Tribosystem-Parameter der Reibkoeffizient μ und die Belagsteifigkeit c normal zur Bremsscheibenoberfläche und somit auch normal zur Reibkraft.

Zur Klärung dieser zentralen Frage wurden Experimente an einem Bremsenprüfstand durchgeführt, der mit Geräuschmesstechnik ausgerüstet ist. Da bei Speicherung der „Echtzeit“-Daten große Datenmengen erzeugt werden, ist es in der Bremsenindustrie üblich, Datenreduktionen zur Speicherung, Auswertung und Darstellung der Daten durchzuführen. Bisher ist ungeklärt, ob es einen Zusammenhang zwischen solch reduzierten Parametern, wie z. B. einem mittleren Reibwert, und dem Quietschverhalten gibt. Die Untersuchung, ob gefundene Zusammenhänge zwischen reduzierten Parametern und dem Quietschverhalten bei Reduktion auf einen Wert pro Bremsung oder einen Wert pro Versuch aussagefähiger sind als die „Echtzeit“-Daten-Trends bildet die zweite Säule der Arbeit.

Durch diese Zielsetzung beschäftigt sich die Arbeit, größtenteils auf experimentelle Weise, mit dem Phänomen des Bremsenquietschens und ergänzt dadurch die häufig durchgeführten Simulationen, z. B. anhand der Methode der Finiten Elemente. Bei solchen Simulationen liegt der Fokus auf den strukturmechanischen Einflüssen auf das Quietschverhalten und es werden häufig sehr eingeschränkte Annahmen über das Tribosystem gemacht, z. B. ein konstanter oder rein geschwindigkeitsabhängiger Reibwert. Bei der vorliegenden Arbeit wurde versucht, die Struktur des schwingenden Bremssystems so konstant wie möglich zu halten, um den Einfluss der Tribosystem-Parameter auf das Bremsenquietschen zu untersuchen.

C.2. Methodischer Ansatz

C.2.1. Vorgehen

Zur Klärung der in der Zielsetzung vorgestellten Fragen wurden Experimente an einem Bremsenprüfstand durchgeführt. Da die zu untersuchenden Größen Reibwert und Belagsteifigkeit nicht direkt veränderbar sind, wurde ein Prüfprogamm entwickelt, das genügend Bremsungen enthält um eine statistisch aussagefähige Datenbasis zu liefern. Es basiert auf einer Standard-Bremsgeräusch-Prüfprozedur, gewährleistet eine gute und größtenteils gleichmäßige Abdeckung des kontrollierbaren Parameterraums aus Bremsdruck, Fahrzeuggeschwindigkeit und Scheibentemperatur und enthält eine geringe Anzahl von Bremsvorgängen, um das System durch Verschleiss geringstmöglich zu verändern.

Die Veränderung der untersuchten Reibwert- und Belagsteifigkeitsbereiche wurde durch die Verwendung unterschiedlicher Bremsbeläge erreicht sowie durch die unvermeidbare Variation von Reibwert und Belagsteifigkeit während der Bremsenprüfstandsversuche. Fünf Reibmaterialien waren Original- bzw. Ersatzteile für das untersuchte Bremssystem, dazu zu drei Reibmaterialien von amerikanischen Sports-Utility-Vehicles, die zurechtgeschnitten wurden um im getesteten Bremssystem verwendet werden zu können. Des Weiteren wurden 12 Reibmaterialien speziell für die Versuche von einem Belaghersteller entwickelt und gefertigt.

Aufgrund der Multidimensionalität des Quietschverhaltens und seiner Abhängigkeiten ist eine Präzisierung des Begriffes „Quietschverhalten“ notwendig. In der vorliegenden Arbeit wird das Quietschverhalten durch die Quietschfrequenz, den zugehörigen Schalldruckpegel sowie die Auftretenshäufigkeit repräsentiert. Um das Quietschverhalten handhabbar zu machen wurde ein in der Bremsenindustrie gängiger Schalldruckpegel-Grenzwert von 70 dB festgelegt, oberhalb dem ein Bremsgeräusch als Quietschen registriert wurde. Dies ermöglicht die Berechnung einer Quietschwahrscheinlichkeit (SI) in Abhängigkeit von verschiedenen Größen für verschiedene Frequenzintervalle.

Während der Reibwert messtechnisch gut zugänglich ist, ist es nicht möglich die Belagsteifigkeit während der Versuche mit ausreichender Genauigkeit zu messen. Daher wurden vor den Geräuschversuchen Kompressibilitätsmessungen an allen Bremsbelägen durchgeführt. Basierend auf diesen Messungen wurde ein Bremsdruck-abhängiges Belagsteifigkeitsmodell entwickelt, mit dessen Hilfe die Belagsteifigkeit während der Geräuschversuche berechnet werden kann.

Während der Geräuschversuche wurden Bremsdruck, Bremsmoment, Fahrzeuggeschwindigkeit und Scheibentemperatur mit einer Abtastrate von 25 Hz erfasst. Die Aufzeichnung der Bremsgeräusche erfolgte mit 51,2 kHz, allerdings wurden jeweils 40 ms zusammen ausgewertet, so dass Quietschgeräusche ebenfalls mit 25 Hz „gemessen“ wurden. Der Reibwert wurde aus Bremsmoment und Bremsdruck berechnet. Dieser Datensatz, bei dem 25 Datenpunkte pro Sekunde während eines Bremsvorganges gemessen wurden, wird in der Arbeit „Echtzeit“-Daten genannt. Die Zeitskala, auf der diese Daten erfasst wurden heißt Echtzeit-Zeitskala. Kompressibilitätsversuche ergeben z. B. für den Fall der Belagsdeformation bei Bremsdruckänderung von der 5 bar Vorlast auf die 100 bar Maximallast einen Wert pro Bremsbelag und Geräuschversuch. Diese Messungen finden auf der sogenannten Versuch-Zeitskala statt und die Daten werden Versuch-Zeitskala-Daten genannt. Die dritte, in der Arbeit untersuchte Zeitskala ist die Bremsung-Zeitskala. Obwohl auf dieser Zeitskala keine Daten gemessen werden ist es in der Bremsenindustrie üblich, einen Wert pro Bremsung anzugeben, z. B. einen mittleren Reibwert.

Um zu überprüfen, ob die Quietschwahrscheinlichkeit (SI) vom Reibwert μ und/oder der Belagsteifigkeit c abhängt, wurden $\widehat{SI}$-Regressionsmodelle in Abhängigkeit von μ und c für Daten auf allen Zeitskalen berechnet. Um die Güte aller Modelle auf allen Zeitskalen bewerten zu können, wurde ein Maß eingeführt welches es ermöglicht für jedes Modell die Anwendbarkeit zur $\widehat{SI}$-Berechnung und die Nützlichkeit der Datenreduktionen zu beurteilen.

In den folgenden Unterkapiteln wird auf besondere Aspekte der Methodik und deren Umsetzung gesondert eingegangen.

C.2.2. Experimente

Um die Struktur des Bremssystems so einfach, reproduzierbar und unverändert wie möglich bei allen Versuchen zu halten, wurde auf den Aufbau des Achsschenkels verzichtet und der Bremssattel direkt mit dem Aufnehmer verschraubt. Angaben auf fahrzeugbezogene Werte beziehen sich somit jeweils auf das Originalfahrzeug, dessen Bremssystem für die Versuche benutzt wurde. Die Angabe einer Fahrzeuggeschwindigkeit ist gleichbedeutend mit der Angabe der Rotationsgeschwindigkeit der Bremsscheibe im Originalfahrzeug, die am Prüfstand verwendet wurde.

Für die Gesamtheit der Versuche wurde stets derselbe Bremssattel eines europäischen Wagens der Kompaktklasse verwendet. Der Scheibenverschleiss durch die Versuche der

20 verschiedenen Reibmaterialien machte den Einsatz von sechs baugleichen unbelüfteten Graugussscheiben nötig. Um die strukturelle Ähnlichkeit der verwendeten Beläge und Scheiben zu überprüfen wurden die Resonanzfrequenzen der Teile durch Frequecy Response Functions (FRF) gemessen. Diese waren nicht identisch, wichen aber in den meisten Fällen nur unwesentlich voneinander ab. Die Messungen zeigten lediglich bei zwei der amerikanischen SUV-Reibmaterialien starke Abweichungen, die sehr wahrscheinlich aufgrund eines radialen Schlitzes in der tangentialen Mitte des Reibmaterials zustande kamen, den nur diese Reibmaterialien aufwiesen. Zusammenfassend läßt sich feststellen, dass bei den Bremsscheiben und den Bremsbelägen geringe Abweicheungen der Resonanzfrequenzen beobachtet wurden, die allerdings unvermeidbar waren.

Für die Aufbereitung und Auswertung der Daten wurden selbstentwickelte Progamme in MATLAB verwendet, die teilweise auf Programme anderer Autoren aufbauen. Diese mathematische Programmiersprache bot die Möglichkeit die Rohdatenverarbeitung, Quietscherkennung, Auswertung und Darstellung innerhalb eines „Programmes“ zu realisieren. Auf diese Weise ist sichergestellt, dass jeder Schritt nachvollziehbar ist und keine ungewünschte Datenreduktion oder Filterung stattfindet. Neben Dateneinlese- und Konvertierungsprogrammen wurden so auch die in der Arbeit dargestellten Schaubilder erzeugt und die Quietschwahrscheinlichkeits-Regressionsmodelle berechnet. Außerdem wurde eine eigene Geräuscherfassungs-Routine entwickelt, die zur Quietscherkennung auch den Hintergrund-Geräuschpegel berücksichtigt. Ein Geräusch wurde nur als Quietschen gekennzeichnet, wenn sich sowohl im Mikrofonsignal wie auch im Signal des Beschleunigungsaufnehmers, der am Bremssattel befestigt war, ein Peak ergab deren Frequenzen innerhalb von 50 Hz lagen und der Schalldruckpegel gleich oder größer als 70 dB war.

C.2.3. Berechnung der Quietschwahrscheinlichkeit

Es ist prinzipiell nicht möglich, die Quietschwahrscheinlichkeit SI *direkt* zu messen. Die Quietschwahrscheinlichkeit kann aufgrund der Häufigkeit der beiden diskreten Ereignissen „quietscht“ oder „quietscht nicht“ berechnet werden. Dieser Vorgang ist vergleichbar mit der Berechnung der Wahrscheinlichkeit, dass eine geworfene Münze Kopf oder Zahl zeigt, indem man sie sehr oft wirft. Daraus wird ersichtlich, dass auch zur präzisen Berechnung der Quietschwahrscheinlichkeit eine große, statistisch unabhängige Anzahl von Datenpunkten unter gleichen Bedingungen benötigt wird.

Die zu untersuchenden Einflussgrößen auf das Bremsenquietschen unterliegen entweder Messungenauigkeiten (z. B. μ) oder können nur begrenzt genau geregelt werden (z. B. Bremsdruck). Deshalb müssen Daten in Intervallen zur Quietschwahrscheinlichkeitsberechung zusammengefasst werden. Da innerhalb dieser Intervalle die Quietschwahrscheinlichkeit als konstant angenommen wird, dürfen die Intervall nicht zu groß gewählt werden.

Die Quietschwarscheinlichkeitsberechnung erfolgt, indem man die Anzahl der Datenpunkte, bei denen Quietschen detektiert wurde durch die Gesamtanzahl der Datenpunkte des Intervalls teilt. Um auf allen Zeitskalen dieselbe SI-Berechnung zu gewährleisten wurden stets die Echtzeit-Daten als Basis für die Berechnung verwendet, auch wenn die Daten „anschließend“ auf z. B. einen Wert pro Bremsung reduziert wurden. Im Falle einer Quietschwahrscheinlichkeit pro Bremsung müssen zur Berechnung der Gesamtquietschwahrscheinlichkeit eines Versuches die Einzelwahrscheinlichkeiten mit der Anzahl der Echtzeit-Datenpunkte pro Bremsung gewichtet werden.

Es ist offensichtlich, dass die SI-Berechnung genauer wird je mehr Daten innerhalb eines Intervalls zur Verfügung stehen. Unter folgenden Voraussetzungen kann eine Fehlerabschätzung der Quietschwahrscheinlichkeit durchgeführt werden: Es gibt genau eine Quietschwahrscheinlichkeit pro Intervall (oder die SI-Variationen innerhalb eines Intervalls ist vernachlässigbar), die Quietschwahrscheinlichkeit hängt vom gewählten (Satz von) Parameter(n) ab und die SI-Verteilung ist statisch.

Laut Benoullis Gesetz der großen Zahl konvergiert die Häufigkeit der Quietschereignisse gegen die wahre (aber unbekannte) Quietschwahrscheinlichkeit, wenn die Anzahl der Datenpunkte n gegen unendlich geht. Für Werte von n, die kleiner als unendlich sind, erlaubt das schwache Gesetz der großen Zahlen eine Größenabschätzung des zu erwartenden Unterschieds zwischen berechneter SI und wahrer Quietschwahrscheinlichkeit. Danach ist mit einer Aussagewahrscheinlichkeit Ψ die Abweichung der berechneten und der tatsächlichen Quietschwahrscheinlichkeit größtenfalls gleich

$$\varepsilon \leq \sqrt{\frac{1}{4 \cdot n \cdot (1 - \Psi)}} \tag{C.1}$$

In der Arbeit wurde eine Aussagewahrscheinlichkeit von $\Psi = 95$ % verwendet, was bedeutet, dass z. B. für $n = 500$ Datenpunkte in einem Intervall die berechnete Quietschwahrscheinlichkeit SI mit 95 %iger Wahrscheinlichkeit nur um $\varepsilon = \pm$ 10 Prozentpunkte von der wahren Quietschwahrscheinlichkeit SI_{real} abweicht.

C.2.4. Belagsteifigkeitsmodell

Um SI-Modelle auf allen Zeitskalen berechnen zu können, müssen entweder die Echtzeit-Daten reduziert oder die Versuchsdaten modellmäßig erweitert werden. Zur Berechnung der Echtzeit-Daten für die Belagsteifigkeit in normaler Richtung wurde die Belagdeformation d als Funktion der Normalkraft N (die sich aus dem Bremsdruck p ergibt) für jeden Belag durch Kompressibilitätsversuche gemessen. Betrachtet man den Bremsbelag modellmäßig als zwei Federn in Reihenschaltung, so bietet sich eine Trennung des Kontakts und des Restbelags ohne Kontakt an. Im vorliegenden Modell wurde die Kontaktsteifigkeit c_c als eine sich linear versteifende Feder angenommen, was zu

$$c_c = \lambda_c \cdot N \tag{C.2}$$

führt, während die Steifigkeit des Restbelags zusätzlich zur Normalkraft-abhängigen Komponente auch eine drucklose Grundsteifigkeit $c_{b,0}$ hat:

$$c_b = \lambda_b \cdot N + c_{b,0} \tag{C.3}$$

Mit diesen Annahmen ergibt sich die Belagsteifigkeit c zu

$$c = -\frac{dN}{dz} = \left(\frac{1}{c_c} + \frac{1}{c_b}\right)^{-1} = \frac{\lambda_c \cdot \lambda_b \cdot N^2 + \lambda_c \cdot c_{b,0} \cdot N}{(\lambda_c + \lambda_b) \cdot N + c_{b,0}} \tag{C.4}$$

Durch Minimierung der quadratischen Fehlersumme der Nachgiebigkeitsabweichungen wurde für jeden Bremsbelag ein $c(N)$-Modell berechnet. Das hohe Bestimmtheitsmaß R^2 von über 99,4 % deutet an, dass die Kompressibilitätskurve als Funktion der Normalkraft sehr gut durch die in Gleichung C.4 gegebene Formel dargestellt werden kann. In den meisten Fällen liegt der Koeffizient λ_c der Kontaktsteifigkeitszunahme mit zunehmender Normalkraft zwischen $62\ mm^{-1}$ und $500\ mm^{-1}$. Die drucklose Grundsteifigkeit $c_{b,0}$ der Beläge lag zwischen 0,074 GN/m und 0,704 GN/m.

Jedes Modell hat Grenzen und Modelle, die auf Messdaten beruhen haben zusätzlich noch Unsicherheiten. Während die Unsicherheiten für die meisten Bremsbeläge in tolerierbaren Größenordnungen sind, bestehen die Grenzen des Modells z. B. darin, dass lediglich der Haupteinflussparameter Bremsdruck im Modell berücksichtigt wird. Die Hauptlimitationen des Modells sind:

- Die Kompressibilitätsmessungen finden mit planparallel-geschliffenen Bremsbelagoberflächen statt, die gegen einen Stahl-Scheibenersatzkörper gedrückt werden.

Diese Oberflächenkonfigurationen geben nicht die während der Versuche herrschenden Bedingungen wieder. Außerdem werden ggf. auftretende Änderungen im Kontakt, wie sie z. B. von Kemmer [58] gezeigt wurden, nicht berücksichtigt.

- Obwohl der Druckeinfluss auf die Belagsteifigkeit als dominant bezeichnet werden kann, verändert sich die Belagsteifigkeit durch Temperatureinfluss irreversibel. Daher war es nicht möglich, diesen Einfluss zu ermitteln, ohne die Bremsbeläge dauerhaft zu verändern. Aufgrund einer Abschätzung durch Versuche an einem der getesteten Belagmaterialien ergibt sich eine relative c-Abweichung zwischen Raumtemperatur und 400 řC von ca. 53 %. Da angenommen werden kann, dass Bremsbeläge generell bei höheren Temperaturen geringere Steifigkeiten aufweisen, werden die Unterschiede zwischen den verschiedenen Reibmaterialien voraussichtlich deutlich geringer sein als der Unterschied zum Modell.

- Die berechneten Belagsteifigkeiten gelten für den quasi-stationären Fall. Für höhere Frequenzen ist zu erwarten, dass die Steifigkeiten generell ansteigen. Andererseits legen Ergebnisse wie z. B. die von Augsburg et al. [5] nahe, dass selbst bei höheren Frequenzen die Belagsteifigkeit mit zunehmender Normalkraft zunimmt.

Es darf dennoch erwartet werden, dass auch mit diesem Grundmodell der Belagsteifigkeit generelle Abhängigkeiten und Einflüsse auf das Bremsenquietschen nachgewiesen werden können.

C.2.5. Modellierung der Quietschwahrscheinlichkeit

Zur Untersuchung der Einflüsse von Reibkoeffizient und Belagsteifigkeit auf die Quietschwahrscheinlichkeit wurden $\widehat{SI}$-Regressionsmodelle auf allen Zeitskalen gebildet.

Um die Echtzeit-Daten, hauptsächlich den Reibwert, für andere Zeitskalen zu reduzieren, wurden Funktionen benutzt, die in mathematischem Sinn als Projektionen bezeichnet werden. Die wichtigsten dieser Projektionen sind der Mittel-, Minimal- und Maximalwert, der Median, der Parameterwert, unterhalb dem 75 % der Werte liegen, der Mittelwert und die Standardabweichung einer auf die Daten angepassten Gausskurve sowie der Prozentsatz der Werte, die oberhalb eines Schwellenwertes liegen.

Mit Hilfe dieser Projektionen wurden für jede Zeitskala ein oder mehrere Kennwerte für jeden Parameter berechnet. Während auf der Echtzeit-Zeitskala der „gemessene“

Reibwert und die Steifigkeit, berechnet durch das im vorherigen Kapitel vorgestellte Modell, die einzigen Kennwerte waren, gab es auf der Bremsung-Zeitskala 20 reibwertbezogene ($\alpha_{\mu,\text{ba,i}}$) und 17 steifigkeitsbezogene Kennwerte $\alpha_{\text{c,ba,j}}$. Auf der Versuch-Zeitskala waren es 39 belagsteifigkeitsbezogene Kennwerte $\alpha_{\text{c,tt,j}}$.
Die berechneten $\widehat{SI}$-Regressionsmodelle hatten auf allen Zeitskalen entweder die Form

$$\widehat{SI}_i(\mu) = \zeta_1 \cdot \alpha_{\mu,i} + \zeta_2 \tag{C.5}$$

für Einzelparametereinflüsse, jedoch meistens die Form

$$\widehat{SI}_{i,j}(\mu, c) = \zeta_1 \cdot \alpha_{\mu,i} + \zeta_2 \cdot \alpha_{c,j} + \zeta_3 \cdot \alpha_{\mu,i} \cdot \alpha_{c,j} + \zeta_4 \tag{C.6}$$

wenn reibwertbasierte *und* steifigkeitsbasierte Kennwerte berücksichtigt wurden.

Es ist generell möglich ein Polynom an jede beliebige Funktion anzupassen und anhand der Koeffizienten z. B. aus Gleichung C.6 Trends für die $\widehat{SI}$-Anhängigkeiten abzuleiten. Die Statistik liefert Berechungsverfahren und Kennwerte zur Beurteilung, wie gut ein Datensatz durch ein Modell wiedergegeben wird, beispielsweise das Bestimmheitsmaß R^2 bzw. das angepasste Bestimmtheistmaß R^2_{adj} oder Parameter- bzw. Modellsignifikanzen [65].

Während diese Gütemaße für die Echtzeit-Zeitskala durchaus sinnvoll und anwendbar sind musste für die anderen Zeitskalen, deren Vergleich und die Gütebestimmung der einzelnen Projektionen bzw. daraus resultierenden Kennwerte ein anderes Maß gefunden werden.

Die Gesamt-Quietschwahrscheinlichkeit für jeden Versuch wird der Basis von ca. 10^5 Echtzeit-Datenpunkten berechnet, die bei einem sehr ausgewogenen Prüfprogramm gemessen wurden. Daher ist anzunehmen, dass die Gesamt-Quietschwahrscheinlichkeit ein zuverlässiger SI-Wert ist. Des Weiteren ist jedes Modell in der Lage, die Gesamt-SI zu berechnen.

Als Maß für die Modellgüte wird deswegen die Abweichung ΔSI zwischen der „gemessenen“ Gesamt-Quietschwahrscheinlichkeit SI_{gemessen} und der berechneten Quietschwahrscheinlichkeit $\widehat{SI}_{\text{Modell}}$

$$\Delta SI = SI_{\text{gemessen}} - \widehat{SI}_{\text{Modell}} \tag{C.7}$$

benutzt.

Beide Quietschwahrscheinlichkeiten werden üblicherweise in Prozent angegeben; die Einheit der Differenz ΔSI ist Prozentpunkte.

Pro Modell und Versuch kann auf diese Weise ein ΔSI-Wert berechnet werden, d. h. 20 ΔSI-Werte pro Modell. Um die Güte der Modelle und deren Kennwerte zu bewerten wurden (hauptsächlich) die ΔSI-Standardabweichung $\sigma_{\Delta SI}$, aber auch die Maximal- und Minimalwerte von ΔSI berücksichtigt.

Zur Beurteilung der Modellgüte wurde in einem ersten Schritt ein konstantes (nullte Ordnung Polynom-) Modell gebildet, das den „worst-case“ abdeckt:

$$\widehat{SI}_{\text{worst case}}(\alpha_\mu, \alpha_c) = 0 \cdot \alpha_\mu + 0 \cdot \alpha_c + 0 \cdot \alpha_\mu \cdot \alpha_c + \zeta_4$$

Mit der durchschnittlichen Gesamt-Quietschwahrscheinlichkeit von $\zeta_4 = 5,51$ % ergeben sich $\sigma_{\Delta SI} = 4,87$ Prozentpunkte, die minimale ΔSI zu $-5,50$ Prozentpunkte und die maximale ΔSI zu $12,70$ Prozentpunkte für dieses Modell, das keine Tribosystemparameter-Abhängigkeiten enthält.

Die Güte jedes Modells kann somit anhand der Verbesserung (Minimierung) von $\sigma_{\Delta SI}$ und Minimal- bzw. Maximalwerten von ΔSI gemessen werden, die näher bei Null liegen als für das $\widehat{SI}_{\text{worst case}}$-Modell.

C.3. Ergebnisse

C.3.1. Echtzeit-Zeitskala

Während der Gesamtheit aller dargestellten Geräuschprüfstandsversuche wurden Quietschgeräusche bei nahezu allen Frequenzen zwischen 2 kHz und 20 kHz gemessen. Dieses Ergebnis legt nahe, dass viele unterschiedlich schwingende Systeme aufgetreten sind, wahrscheinlich einerseits aufgrund der unterschiedlichen verwendeten Beläge und Scheiben und andererseits durch Systemänderungen während des Testprogramms, z. B. durch unterschiedliche Bremsdrücke.

Die Häufigkeiten des Auftretens bestimmter Quietschfrequenzen unterscheiden sich zum Teil deutlich. Quietschen trat hauptsächlich bei Frequenzen auf, die sich in sechs sogenannte dominate Frequenzintervalle einteilen lassen. Bremsgeräusche mit Frequenzen innerhalb dieser dominanten Frequenzintervalle haben unterschiedliche Abhängigkeiten ihrer Auftretenshäufigkeiten:

- Quietschen zwischen 2,8 kHz und 3,1 kHz tritt häufiger bei niedrigen Bremsdrücken, Fahrzeuggeschwindigkeiten und Bremsmomenten sowie für höhere Reibwerte auf.

- Die Quietschwahrscheinlichkeit für Bremsgeräusche zwischen 6,6 kHz und 7,1 kHz ist für Bremsdrücke zwischen 10 bar und 20 bar am größten dasselbe gilt für niedrige Bremsmomente und kleine Reibwerte. Außerdem ist die Quietschwahrscheinlichkeit nahezu unabhängig von der Fahrzeuggeschwindigkeit.

- Quietschen bei Frequenzen zwischen 7,2 kHz und 7,7 kHz tritt häufiger für niedrige Geschwindigkeiten und Bremsmomente bei Bremsdrücken unterhalb von 30 bar sowie hohen Reibwerten auf.

- Die SI für Quietschen zwischen 7,8 kHz und 8,2 kHz ist bei hohen Reibwerten und während Schleppbremsungen größer.

- Quietschen zwischen 8,7 kHz und 9,1 kHz tritt häufiger bei hohen Bremsdrücken und Belagsteifigkeiten, kleinen Fahrzeuggeschwindigkeiten und höheren Bremsmomenten auf, solange diese unterhalb von 850 Nm sind.

- Die Quietschwahrscheinlichkeit für Bremsgeräusche zwischen 13,2 kHz und 13,7 kHz ist während Schleppbremsungen größer als während Stoppbremsungen und steigt mit höheren Bremsdrücken, Bremsmomenten, Reibkoeffizienten und Belagsteifigkeiten.

Die Untersuchung des Reibwert- und Belagsteifigkeitseinflusses auf die Quietschfrequenz zeigte keinen eindeutigen Trend. Es gibt keinen Bereich im μ-c-Parameterraum, bei dem Bremsgeräusche nur innerhalb eines dominanten Frequenzintervalles registriert wurden. Quietschen mit Frequenzen in fast allen dominanten Frequenzintervallen wurde für den größten Teil des μ-c-Parameterraumes beobachtet.

Da keine experimentellen Hinweise auf einen Einfluss der Tribosystem-Parameter μ und c auf die Quietschfrequenz gefunden werden konnten, wurde für die Quietschwahrscheinlichkeits-Modelle ausschließlich die Gesamt-SI für alle Bremsgeräusche zwischen 2 kHz und 20 kHz betrachtet.

Der wichtigste Einzeleinfluss-Parameter ist der Reibwert da z. B. in den Auswertungen sichtbare Fahrzeuggeschwindigkeitseinflüsse höchstwahrscheinlich in einem höheren Reibwert bei kleineren Geschwindigkeiten begründet liegen.

Bildet man ein $\widehat{SI}$-Regressionsmodell ausschließlich mit dem gemessenen Reibwert als Parameter, so ergibt sich

$$\widehat{SI}(\mu_{\mathrm{rt}}) = 55.4\,\% \cdot \mu_{\mathrm{rt}} - 15.5\,\%$$

mit einem angepassten Bestimmtheitsmaß R^2_{adj} von 87,6 %. Die maximalen ΔSI-Absolutwerte liegen bei 7,8 Prozentpunkten und es ergibt sich eine ΔSI-Standardabweichung von 3,50 Prozentpunkten.

Obwohl dieses Modell besser ist als das konstante („worst case“) Modell, ist es nicht in der Lage, die Gesamt-Quietschwahrscheinlichkeiten der einzelnen Versuche ausreichend zu berechnen. Der Hauptgrund hierfür liegt in den teilweise sehr unterschiedlichen Reibwertverteilungen der einzelnen Versuche. Diese führen dazu, dass sich der beobachtbare Trend erhöhter Quietschwahrscheinlichkeit mit steigendem Reibwert aus verschiedenen Grundgesamtheiten zusammensetzt. Der in Abbildung C.1 gezeigte, stark ansteigende SI-Trend für Reibwerte über 0,55 wird lediglich von etwas mehr als einem Viertel aller Reibmaterial-Versuche unterstützt (s. oberes Diagramm). Da bei den Versuchen der anderen Reibmaterialien diese hohen Reibwerte nicht (mehr als 500 mal) erreicht wurden, können keine Schlussfolgerungen über deren Quietschwahrscheinlichkeit bei Reibwerten über 0,55 gezogen werden. Alle Reibmatererialien der Versuche mit Reibwerten über 0,55 lagen innerhalb einer Reibmaterialienkategorie („European-Metallic“). Reibmaterialien dieser Kategorie zeichnen sich durch ihren Einsatz in europäischen Fahrzeugen und durch einen Eisen und Nicht-Eisenmetallanteil (nach Gewicht) zwischen 15 % und 40 % aus. Bei diesen Reibmaterialien war ein deutlicher Reibwerteinfluss auf die Quietschwahrscheinlichkeit zu sehen.

Allerdings gibt es selbst unter Berücksichtigung des zu erwartenden $[-\epsilon, \epsilon]$-Fehlerintervalls statistisch signifikante Gegenbeispiele die den Schluss nahelegen, dass der Reibwert allein nicht ausreicht, um die Quietschwahrscheinlichkeit maßgeblich zu bestimmen.

Die Mehrheit der $\widehat{SI}$-Modelle, die den gemessenen Reibwert und die berechnete Echtzeit-Belagsteifigkeit in Betracht ziehen ist in der Lage, die einzelnen Quietschwahrscheinlichkeiten bis zu einem gewissen Maß zu berechnen. Es ergeben sich Werte für die ΔSI-Standardabweichung zwischen 2,81 Prozentpunkten und 3,02 Prozentpunkten. Vergleicht man das Modell

$$\widehat{SI}(\mu_{\text{rt}}, c_{\text{rt}}) = -3.9 \cdot 10^{-2} \cdot \mu_{\text{rt}} - 0.85\, m/GN \cdot c_{\text{rt}} + 2.8\, m/GN \cdot \mu_{\text{rt}} \cdot c_{\text{rt}} + 1.2 \cdot 10^{-2}$$

mit dem Konstantwert-Modell bzw. mit dem rein Reibkoeffizient-abhängigen Modell, so ist die SI Berechnung der einzelnen Versuche sichtbar besser. Allgemein lässt sich sagen, dass alle Modelle, die eine ansteigende SI mit ansteigendem $\mu \cdot c$ zeigen, deutlich geringere ΔSI-Werte aufweisen, was $\mu \cdot c$ als Einflussparameter auf die Quietschwahrscheinlichkeit unterstützt. Auch zum allgemeinen $SI(\mu, c)$-Trend gibt es statistisch signifikante

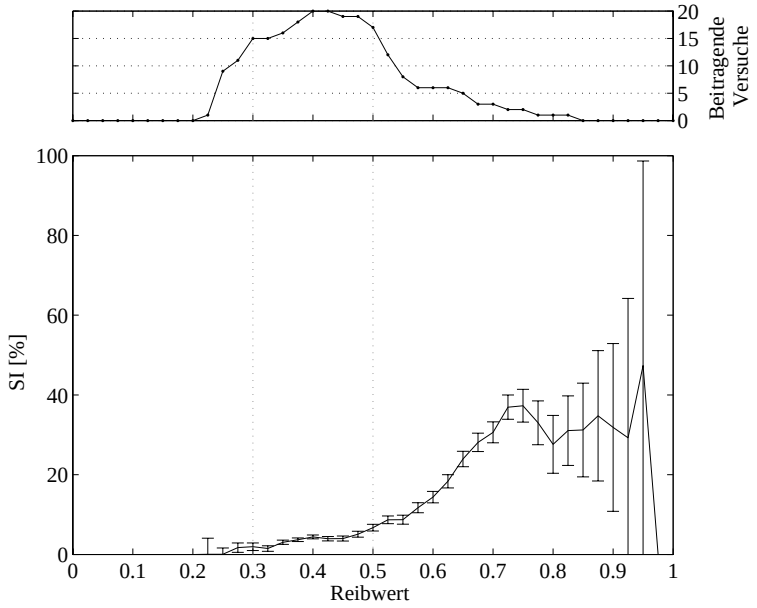

Abbildung C.1.: *Reibwerteinfluss auf die Quietschwahrscheinlichkeit (unteres Diagramm). Oberes Schaubild: Anzahl der Versuche mit verschiedenen Reibmaterialien, die mindestens 500 Datenpunkte im betreffenden Reibwert-Intervall haben*

Gegenbeispiele. Dies deutet darauf hin, dass es weitere Einflussgrößen, wie z. B. strukturmechanische Unterschiede oder Dämpfung gibt, deren Einfluss nicht verhindert oder vernachlässigt werden kann.

C.3.2. Bremsung-Zeitskala

Es wurden $\widehat{SI}$-Modelle auf drei verschiedene Arten, die sich hauptsächlich durch die berücksichtigten Daten unterscheiden gebildet. Für jede Art wurden Modelle gebildet, die alle Kombinationen der 20 reibwertbasierenden ($\alpha_{\mu,\mathrm{ba,i}}$) und 17 belagsteifigkeitsbasierenden Kennwerte $\alpha_{textc,ba,i}$ sowie die Abhängigkeiten der Quietschwahrscheinlichkeit von einzelnen Kennwerten berücksichtigen.

Fasst man die Echtzeit-Daten zu einem Wert pro Bremsung zusammen und führt keine weitere Clusterung durch, so ergeben sich große Streuungen der SI bei gleichen oder sehr ähnlichen Reibwerten (dargestellt in Abbildung C.2 (a)) bzw. Belagsteifigkeiten. SI-Regressionsmodelle mit diesen Daten sind nicht in der Lage die Quietschwahrscheinlichkeit pro Bremsung und die Gesamt-SI zu berechnen, d. h. die ΔSI-Werte dieser Modelle

sind betragsmäßig erheblich größer als für die Modelle der Echtzeit-Daten.

Werden die Bremsungskennwerte zusätzlich in derselben Weise wie für die Echtzeit-Daten in Intervalle unterteilt und jeweils die (gewichtete) mittlere Quietschwahrscheinlichkeit zur Modellbildung benutzt, ergeben sich Modelle deren ΔSI-Werte mit den Echtzeit-Daten-Modellen vergleichbar sind. Aber auch diese Modelle sind nicht in der Lage, die Quietschwahrscheinlichkeit für einzelne Bremsungen ausreichend gut zu berechnen. Diese Tatsache unterstützt die in Kapitel C.2.3 vorgestellte SI-Ungenauigkeitsabschätzung, da die Anzahl der Daten eines Bremsvorganges nicht für eine ausreichend genaue SI-"Messung" genügt, sondern die Quietschwahrscheinlichkeit erst bei Betrachtung einer größeren Datenmenge von mehreren Bremsungen mit gleichen Parametern aussagefähig wird.

Um ein gutes Modell mit geringen ΔSI-Absolutwerten anhand von Bremsung-Zeitskala-Kennwerten zu erstellen, werden aussagefähige Kennwerte benötigt, die modellmäßig gut abgebildet werden können (hohes R^2_{adj}). Dabei ist ein schlechtes Modell mit niedrigem R^2_{adj} basierend auf aussagefähigen Kennwerten besser, als ein gut angepasstes Modell, das auf aussagelosen Kennwerten beruht. Die Tatsache, dass es Modelle auf der Bremsung-Zeitskala gibt, die ähnliche ΔSI-Werte wie die Echtzeit-Daten-Modelle aufweisen, legt den Schluss nahe, dass es möglich ist, aussagefähige Kennwerte zu berechnen.

In Abbildung C.2 (b) sind die ΔSI-Standardabweichungen $\sigma_{\Delta SI}$ aller Modelle abgebildet, bei denen nur Intervalle mit SI, μ und c Werten größer Null berücksichtigt wurden. In den meisten Fällen ist ein Ein-Kennwert-basiertes Modell schlechter als ein Modell, das einen reibwertbasierten *und* einen belagsteifigkeitsbasierten Kennwert berücksichtigt. Obwohl manche rein Reibwert-Kennwert-basierende Modelle relativ niedrige $\sigma_{\Delta SI}$-Werte aufweisen basieren die besten Modelle auf dem maximalen Reibwert pro Bremsung $\alpha_{\mu,\text{ba,a}}$ und der (z. B. mittleren) Belagsteifigkeit, deren berechneter Wert sich aufgrund des konstanten Bremsdrucks während jeder Bremsung nur geringfügig ändert.

C.3.3. Versuch-Zeitskala

Die $\widehat{SI}$-Modelle mit Versuch-Zeitskala Kennwerten sind in den meisten Fällen besser als die Modelle der anderen Zeitskalen, d. h. sie haben sowohl geringere ΔSI-Absolutwerte als auch geringere ΔSI-Standardabweichungen. Insgesamt konnten mit Versuch-Zeitskala-Kennwerten 183 $\widehat{SI}$-Regressionsmodelle ermittelt werden, deren ΔSI-Standardabwei-

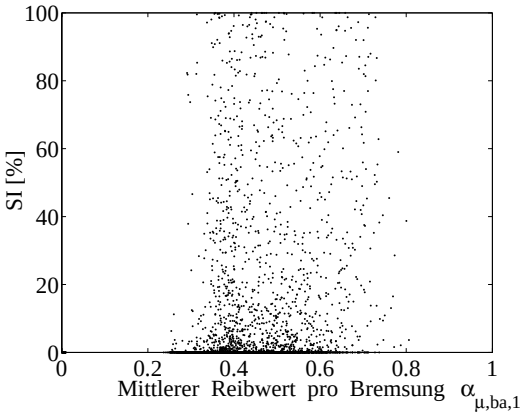

(a) Quietschwahrscheinlichkeiten aller Versuche als Funktion des mittleren Reibwerts pro Bremsung $\alpha_{\mu,\text{ba},1}$

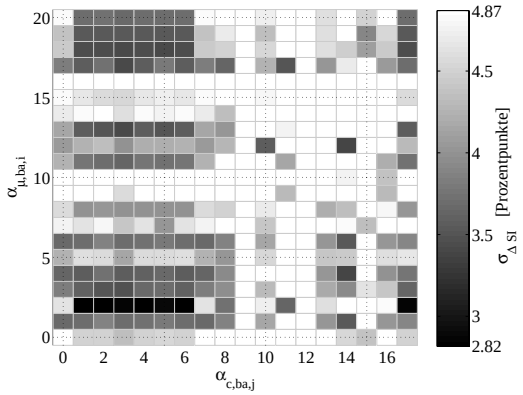

(b) ΔSI-Standardabweichung der $\widehat{SI}$-Modelle mit Bremsung-Zeitskala-Kennwerten

Abbildung C.2.: *SI-Abhängigkeiten und $\widehat{SI}$-Modellgüten auf der Bremsung-Zeitskala*

chungen $\sigma_{\Delta SI}$ kleiner als 3,0 Prozentpunkte waren. Die Werte der ΔSI-Standardabweichungen der Modelle auf der Versuch-Zeitskala sind in Abbildung C.3 dargestellt.

Einige der besten Modelle basieren auf dem mittleren Reibwert $\alpha_{\mu,\text{tt},1}$ oder dem Prozentsatz der Reibwerte über $\mu = 0,5$, was die Hypothese der Existenz eines kritischen Reibwertes für die Quietscherzeugung unterstützt. Dieser wurde von Bergman et al. [9] für ihr System gezeigt, ist aber innerhalb der gemessenen Daten der vorliegenden Arbeit nicht eindeutig belegbar. Als beste Belagsteifigkeitskennwerte zur $\widehat{SI}$-Modellbildung zeigten sich die Kompressibilitäten der beiden Bremsbeläge $\alpha_{\text{c,tt},18}$ und $\alpha_{\text{c,tt},22}$ sowie ihr Mittelwert $\alpha_{\text{c,tt},26}$, die antiproportional zu einer als konstant angenommenen Belagsteifigkeit sind und die Werte des Belagsteifigkeitsmodells bei Bremsdrücken von 50 bar bis 100 bar ($\alpha_{\text{c,tt},34}$ to $\alpha_{\text{c,tt},39}$).

Die Tatsache, dass es auch auf der Versuch-Zeitskala möglich ist, gute $\widehat{SI}$-Modelle zu erzeugen belegt, dass es möglich ist aussagefähige Kennwerte aus Messdaten zu berechnen, selbst wenn die gesamten Messdaten eines Versuches auf einen Wert pro Parameter reduziert werden. Obwohl die Modelle mit Versuch-Zeitskala-Kennwerten bessere Quietschwahrscheinlichkeitsberechnungen für die einzelnen Versuche liefern als Echtzeit-Daten-Modelle, ist die Erfassung der Echtzeit-Daten notwendig, um die Kennwerte daraus zu berechnen. Auch unterstützt diese Tatsache die Annahme der SI-Messungsunge-

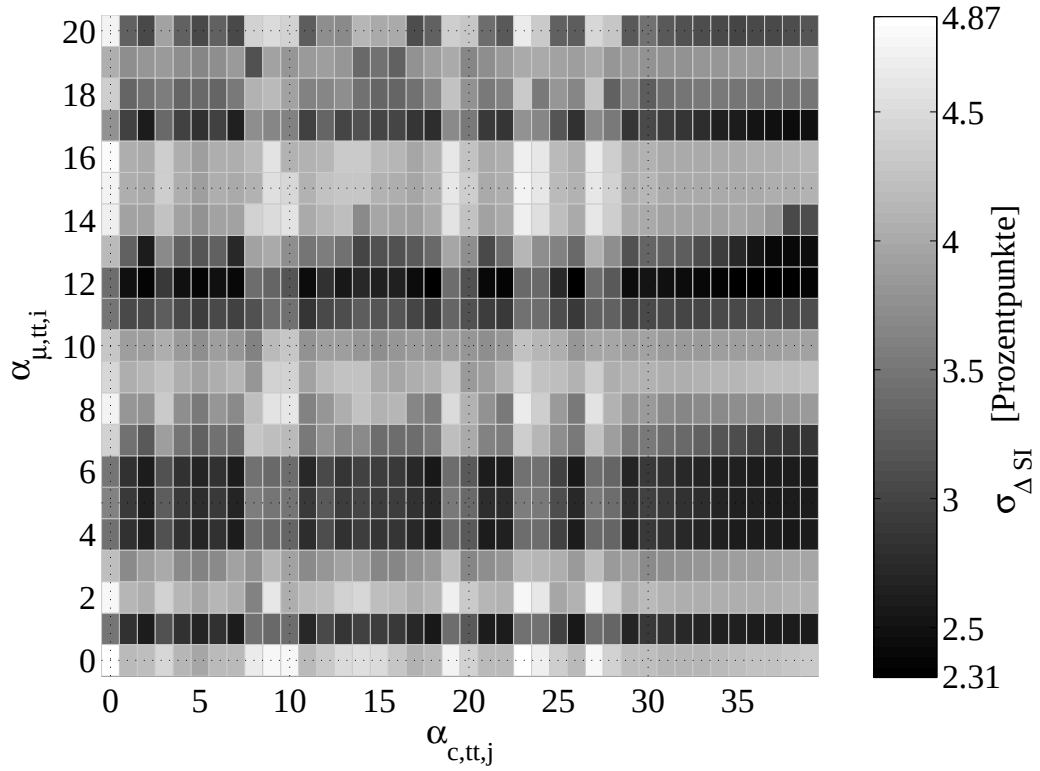

Abbildung C.3.: *ΔSI-Standardabweichung der $\widehat{SI}$-Modelle mit Versuch-Zeitskala-Kennwerten*

nauigkeit ε, die Einschränkungen des Belagsteifigkeitsmodells sowie die angenommenen Messungenauigkeiten. Diese Einflüsse treten bei einer größeren Datenmenge (für den vorliegenden Fall eines ausgeglichenen Geräuschprüfstand-Versuchsprogramms) nicht so deutlich hervor wie innerhalb der Echtzeit-Daten. Daher ist zu erwarten, dass durch präzisere Messungen und bessere Belagsteifigkeitsmodelle die $\widehat{SI}(\mu, c)$-Modelle weiter verbessert werden können.

Diese Vermutung wird zusätzlich unterstützt durch die Tatsache, dass die besten $\widehat{SI}$-Modelle (neben reibwertbedingten Kennwerten) die Kompressibilität oder Werte des Belagsteifigkeitsmodells bei hohen Bremsdrücken verwenden. Aus Versuchen mit weniger ausgeglichenen Versuchsprogammen ist ein Einfluss der Gesamt-Belagsteifigkeit d. h. auch ein Kontakteinfluss, wahrscheinlich, der aber im vorliegenden Modell nur statisch abgebildet wird. Bei einer Verbesserung des Belagsteifigkeitsmodells das eine z. B. durch Bremsdruck- oder Vorgeschichtenänderung bedingte Kontaktänderung (wie von Kemmer

[58] beobachtet) berücksichtigt, ist zu erwarten, dass auch Kontakt- bzw. Gesamtsteifigkeitskennwerte bei kleineren Drücken zu guten $\widehat{SI}$-Modellen beitragen können.

C.3.4. Zusammenfassung und Schlussfolgerungen

Die wichtigsten Ergebnisse der Datenanalysen können folgendermaßen zusammengefasst werden:

- Während der Versuche wurden Quietschgeräusche bei fast allen Frequenzen zwischen 2 kHz und 20 kHz registriert. Geräusche bei manchen Frequenzen waren deutlich häufiger. Da kein Zusammenhang zwischen der Quietschfrequenz und den untersuchten Parametern des Tribosystems gefunden werden konnte ist es wahrscheinlich, dass die Quietschfrequenz hauptsächlich von anderen Parametern (z. B. der Strukturmechanik) beeinflusst wird. Für weitere Untersuchungen (und Modelle) wurde aus diesem Grund das Quietschen frequenzunabhängig betrachtet.

- Der Reibwert ist der dominanteste Einzeleinfluss-Parameter auf die Quietschwahrscheinlichkeit, obwohl auch die Belagsteifigkeit einen Einfluss hat. Es ist zu erwarten, dass bei einem verbesserten Belagsteifigkeitsmodell dieser Einfluss deutlicher zu sehen sein wird. Trotzdem ist das vorgestellte Belagsteifigkeitsmodell ausreichend, um den grundsätzlichen Einfluss der Belagsteifigkeit auf die Quietschwahrscheinlichkeit aufzuzeigen.

- Der Trend zunehmender Quietschwahrscheinlichkeit mit zunehmendem Reibwert wird für Reibwerte über 0,55 nur von Versuchen unterstützt, die mit Reibmaterialien eines Typs („European-Metallic“) durchgeführt wurden. Da der Reibwert nicht (komplett) kontrollierbar ist kann keine Aussage über das Verhalten der meisten Reibpaarungen bei solch hohen Reibwerten gemacht werden. Zusätzlich bilden mehrere statistisch signifikant abweichende SI-Trends einzelner Versuche Gegenbeispiele zum globalen Trend.

- Für die Mehrheit der Versuche steigt die Quietschwahrscheinlichkeit SI mit dem Produkt aus Reibwert μ und Belagsteifigkeit c und auch die Gesamt-SI zeigt diesen Trend. Allerdings weichen auch hier manche Einzeltrends vom Gesamttrend derart ab, dass man sie als Gegenbeispiele bezeichnen kann. Es kann gefolgert werden, dass lokale Trends zunehmender SI mit zunehmendem $\mu \cdot c$ existieren, diese aber

von mindestens einem weiteren, nicht Tribosystem-Parameter überdeckt werden, der innerhalb der Versuchsreihe nicht konstant gehalten oder vernachlässigt werden konnte.

In Bezug auf Datenreduktion und die Berechnung von Kennwerten pro Bremsung bzw. Versuch können folgende Ergebnisse zusammengefasst werden:

- Die Auswahl eines aussagefähigen Kennwertes, der gemessene SI-Trends wiedergibt, ist abhängig von der Zeitskala. D. h. es wurde kein einzelner Kennwert gefunden, der die besten Modelle sowohl auf der Bremsungs-, als auch auf der Versuch-Zeitskala liefert, obwohl der Prozentsatz der Reibwerte über 0,5 auf beiden Zeitskalen zu guten Modellen beiträgt. Neben der Lage der Reibwertverteilung ist der Maximalwert pro Bremsung ein guter Kennwert auf der Bremsung-Zeitskala, dieser ist jedoch anfällig gegenüber Fehlmessungen oder einzelnen „Ausreißer“-Werten. Zusätzlich hängt die Quietschwahrscheinlichkeit von der Belagsteifigkeit ab. Trotz der Einfachheit des Modells ist die mittlere Steifigkeit durchaus ein guter Kennwert. Folglich ist es möglich, die Trends der Quietschwahrscheinlichkeit durch die Datenreduktion nicht zu verlieren. Es ist dabei zu beachten, dass hierfür nicht alle vorgestellten Kennwerte in selbem Maße geeignet sind.

- Auf der Bremsung-Zeitskala sind die SI-Trends nur beobachtbar, sofern die Quietschwahrscheinlichkeit aufgrund von ausreichend vielen Echtzeit-Datenpunkten berechnet wird. Eine Datenreduktion auf einen Wert pro Bremsung ohne die Kennwerte in Intervallen zusammenzufassen, liefert keine aussagefähigen Quietschwahrscheinlichkeiten. D. h. die Anzahl der Datenpunkte einer Bremsung genügt nicht für eine präzise SI-“Messung“.

- Da bei der Kennwertberechnung auch die Messfehler und Modellunzulänglichkeiten nicht so stark zum Tragen kommen, sind Versuch-Zeitskala-Kennwerte besser zur Beschreibung von SI-Trends geeignet als Kennwerte von der Bremsung-Zeitskala. Im vorliegenden Fall scheinen die Versuch-Zeitskala-Kennwerte sogar robuster gegenüber Streuungen und Fehlern zu sein, als die Echtzeit-Daten.

Die wichtigsten Ergebnisse der $\widehat{SI}$-Regressionsmodell-Untersuchungen sind:

- Auf allen Zeitskalen sind Einparamter-$\widehat{SI}$-Modelle mit Reibwert-Kennwerten besser, d. h. haben geringere ΔSI-Werte als Modelle, die mit Belagsteifigkeitskennwerten berechnet wurden. Die besten Modelle berücksichen jedoch stets einen reibwertbezogenen *und* einen steifigkeitsbezogenen Kennwert.

- Bei $\widehat{SI}$-Modellen mit Kennwerten der Bremsung- oder Versuch-Zeitskala ist ein aussagefähiger Kennwert wichtiger als gutes Modell mit hohem Bestimmtheitsmaß R^2, um Modelle mit geringen ΔSI-Werten zu erhalten.

- In Tabelle C.1 sind die Daten der besten $\widehat{SI}(\mu, c)$-Modelle aller drei Zeitskalen aufgelistet. Das $\widehat{SI}$-Modell Nummer vier, basierend auf den Versuch-Zeitskalen-Kennwerten der Belagsteifigkeit bei 80 bar Bremsdruck $\alpha_{\text{c,tt,37}}$ und dem Prozentsatz der Reibwerte über 0,5 $\alpha_{\mu\text{,tt,12}}$, ist das beste aller Modelle. $\widehat{SI}$-Modell Nummer fünf, basierend auf $\alpha_{\mu\text{,tt,12}}$ und der mittleren Kompressibilität beider Bremsbeläge $\alpha_{\text{c,tt,26}}$ ist ähnlich gut. Diese Modelle haben ΔSI-Standardabweichungen von weniger als der Hälfte des konstanten („worst case“) Modells und unterstreichen den Einfluss des Reibwertes und der Belagsteifigkeit auf die Quietschwahrscheinlichkeit. Das beste Modell aufgrund von Bremsung-Zeitskala-Kennwerten basiert auf dem maximalen Reibwert $\alpha_{\mu\text{,ba,2}}$ und dem Mittelwert einer Gausskurve $\alpha_{\text{c,ba,6}}$, die über die Steifigkeitsverteilung gelegt wurde. Die beiden Echtzeit-$\widehat{SI}$-Modelle unterscheiden sich aufgrund der berücksichtigten μ-c-Intervalle sowie der Datengewichtung: Das erste Modell berücksichtigt nur Intervalle, bei denen SI, μ und c größer als Null sind und das Intervall mindestens 50 Datenpunkte enthält, während das zweite Modell alle Intervalle mit der Anzahl der darin enthaltenen Datenpunke gewichtet.

- In Abbildung C.4 sind die ΔSI-Werte aller in Tabelle C.1 gezeigten $\widehat{SI}$-Modelle grafisch dargestellt (a), sowie die von den Modellen berechneten Quietschwahrscheinlichkeiten gegenüber den gemessenen SI aufgetragen (b) - (f). Bei einem perfekten $\widehat{SI}$-Modell würden alle Datenpunkte auf der gestrichelten Linie liegen. Die vertikale Abweichung zwischen einem Datenpunkt und der Linie zeigt den ΔSI-Wert für den betreffenden Versuch (und das betreffende Modell). Aus Tabelle C.1 und Abbildung C.4 ist ersichtlich, dass die Modelle ähnliche ΔSI-Trends für dieselben Versuche zeigen. Alle Modelle berechnen eine zu niedrige Quietschwahrscheinlichkeit für den Versuch mit Reibmaterial A und eine zu hohe SI im Fall

Tabelle C.1.: *Ausgewählte $\widehat{SI}$-Modelle basierend auf Reibwert- und Belagsteifigkeitskennwerten auf allen drei Zeitskalen*

Modelle						
Zeitskala		*Echtzeit*		*Bremsung*	*Versuch*	
Nummer		*1*	*2*	*3*	*4*	*5*
Parameter 1		μ_{rt}	μ_{rt}	$\alpha_{\mu,\text{ba},2}$	$\alpha_{\mu,\text{tt},12}$	$\alpha_{\mu,\text{tt},12}$
Parameter 2		c_{rt}	c_{rt}	$\alpha_{\text{c,ba},6}$	$\alpha_{\text{c,tt},37}$	$\alpha_{\text{c,tt},26}$
ζ_1 [10^{-2}]		46.8	33.3	-13.3	-15.5	48.4
ζ_2 [m/TN] or [μm^{-1}]		0	53.2	-961.3	63.8	-4.2 $\cdot 10^{-4}$
ζ_3 [m/TN] or [μm^{-1}]		517.8	710.3	2646.8	880.1	-5.2 $\cdot 10^{-3}$
ζ_4 [10^{-2}]		-17.4	-14.6	7.7	0.9	6.4
R^2_{adj} [%]		50.6	57.7	(22.0)	[76.6]	[76.6]
SI_{Modell} *Abweichungen*						
Reibmaterial	Gemessene SI [%]	ΔSI [Prozentpunkte]				
A	18.21	5.69	7.29	7.00	4.08	4.38
B	10.35	-5.29	-3.48	-5.64	-0.54	-3.88
C	7.07	-5.1	-2.66	-1.43	-2.39	0.51
D	7.36	-1.66	-0.27	-0.77	0.61	-1.82
E	7.10	-1.55	0.11	-0.03	-0.33	1.20
F	2.85	-3.74	-3.74	-4.82	-2.95	-3.01
G	0.11	-5.61	-5.29	-5.77	-3.24	-3.81
H	15.20	2.29	1.47	-0.34	-1.94	0.22
I	0.06	-2.59	-1.53	-3.55	-2.15	-1.13
J	8.79	1.03	-0.21	-1.43	3.93	3.30
K	0.24	-1.76	-1.09	-3.66	-2.19	-1.81
L	3.54	0.70	1.18	-1.36	0.98	0.79
M	3.04	0.65	1.15	-0.86	0.22	0.14
N	5.07	0.97	0.97	-0.6	1.96	1.25
O	4.56	3.47	3.91	0.79	2.40	2.94
P	1.44	-3.43	-3.82	-4.11	-2.37	-2.81
Q	0.01	-2.78	-1.74	-4.19	-2.08	-0.86
R	5.39	1.14	0.87	-1.69	2.45	1.66
S	4.44	-0.12	0.57	-2.02	1.14	1.01
T	5.31	0.59	0.76	-1.41	1.87	1.21
Charakeristische ΔSI*-Werte* [Prozentpunkte]						
Minimum ΔSI		-5.61	-5.29	-5.77	-3.24	-3.88
Maximum ΔSI		5.69	7.29	7.00	4.08	4.38
$\sigma_{\Delta SI}$		3.02	2.87	2.82	2.32	2.33

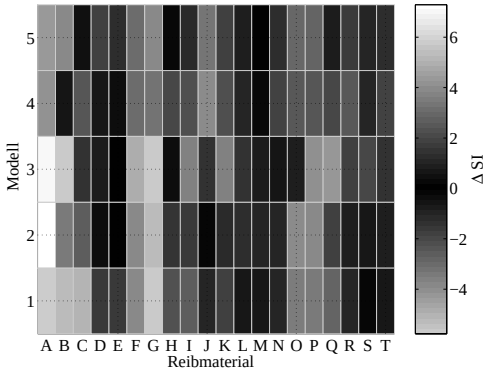

(a) ΔSI-Werte der Modelle

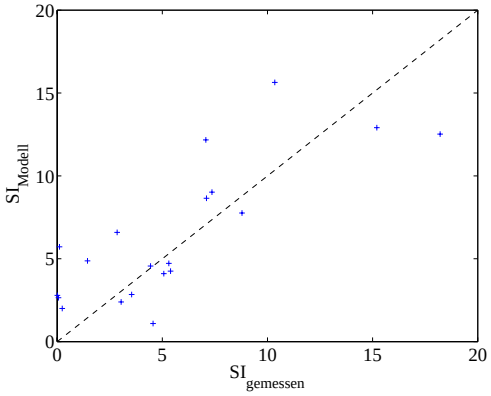

(b) Modell 1

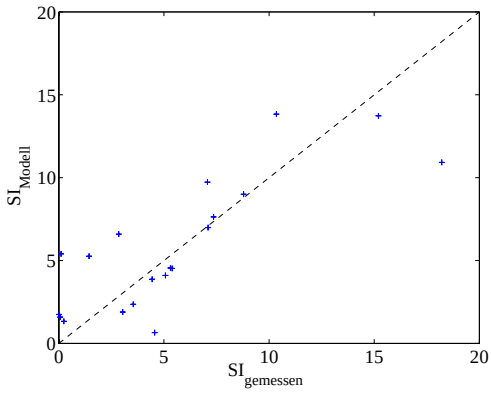

(c) Modell 2

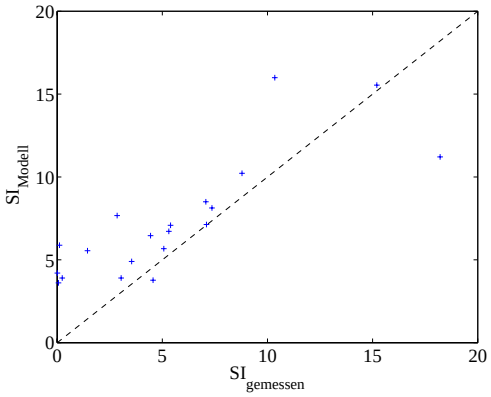

(d) Modell 3

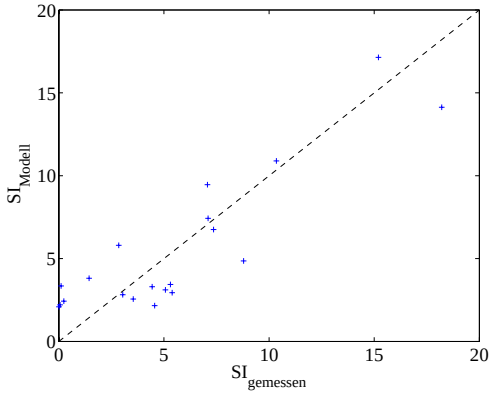

(e) Modell 4

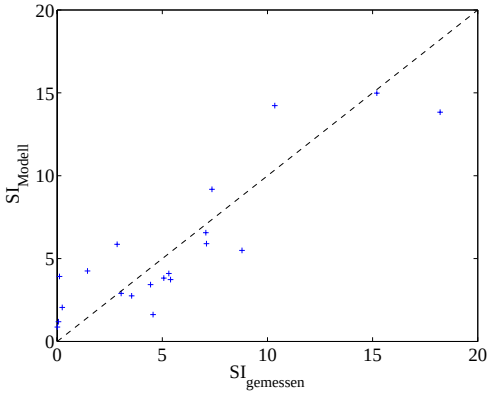

(f) Modell 5

Abbildung C.4.: *Diagramme der Quietschwahrscheinlichkeitsmodelle aus Tabelle C.1*

von Reibmaterial B, obwohl Modell vier die Quietschwahrscheinlichkeit relativ gut wiedergibt. In gleicher Weise sind die berechneten $\widehat{SI}$ für die Versuche der Reibmaterialien F, G und P zu hoch und nur Modell drei ist in der Lage, die Quietschwahrscheinlichkeit des Reibwert-O-Versuchs ausreichend genau zu berechnen. Dies alles deutet auf mindestens einen weiteren Parameter hin, der für ein gutes Modell zu berücksichtigen wäre.

Bezogen auf die Zielsetzung der Arbeit wurde somit folgendes festgestellt:

- Es ist möglich das Quietschverhalten, genauer: die Auftretenswahrscheinlichkeit des Bremsenquietschens bis zu einem gewissen Maß durch den Reibwert und die Belagsteifigkeit (oder durch daraus berechnete Kennwerte) zu beschreiben, da diese Parameter die Quietschwahrscheinlichkeit beeinflussen.

- Höchstwahrscheinlich existieren weitere Einfluss-Parameter auf das Bremsenquietschen, die wahrscheinlich nicht Teil des Tribosystem sind und zwischen bzw. während der durchgeführten Versuche nicht konstant gehalten werden konnten. Es ist unbekannt aber unwahrscheinlich, dass es möglich ist diese Parameter generell konstant zu lassen um die Quietschwahrscheinlichkeit ausschließlich mit μ und c beschreiben zu können.

- Es ist möglich eine Datenreduktion der gemessenen Echtzeit-Daten durchzuführen, um pro Parameter einen Kennwert pro Bremsung bzw. pro Versuch zu berechnen *ohne* gemessene SI-Trends zu verlieren. Die besten $\widehat{SI}$-Modelle wurden mit Versuch-Zeitskala-Kennwerten berechnet, möglicherweise weil diese Kennwerte weniger anfällig für Messfehler oder Unzulänglichkeiten des Belagsteifigkeitsmodells sind.

- Die experimentellen Ergebnisse legen nahe, dass das Phänomen des Bremsenquietschens nur komplett verstanden werden kann, wenn sowohl Tribosystem- wie auch strukturmechanische Parameter in Betracht gezogen werden. Da die Methode der Finiten Elemente ein weit entwickeltes Hilfsmittel zur Untersuchung des Bremsenquietschens darstellt, sollte darüber nachgedacht werden, wie tribologische Konzepte darin verankert werden können. Außerdem sollten weitere Anstrengungen unternommen werden, die elastischen Eigenschaften von Bremsbelägen im quietschrelevanten Frequenzbereich zu messen und simulationstechnisch abzubilden.

Bibliography

[1] M. K. Abdelhamid. Towards smarter measurement systems. In *Proceedings of the IMAC-XXI, A Conference on Structural Dynamics*, Februray 2003.

[2] I. L. M. Ahmed, P. S. Leung, and P. K. Datta. Contact analysis of the disc brake by finite element methods. *European Conference on Vehicle Noise and Vibration, IMechE, London, UK*, 2002.

[3] R. O. Allgaier. *Experimentelle und numerische Untersuchungen zum Bremsenquietschen*. PhD thesis, Universität Stuttgart, 2001.

[4] G. Amontons. De la resistance caus'ee dans les machines. *Memoires de l'Académie Royale A, Paris*, pages 257 – 282, 1699.

[5] K. Augsburg, H. Günther, H. Abendroth, and B. Wernitz. Comparison between different investigation methods of quasi-static and dynamic brake pad behaviour. *SAE 2003-01-3340*, 2003.

[6] H.-J. Bargel and G. Schulze. *Werkstoffkunde*. VDI-Verlag GmbH, ISBN 3-18-400823-1, pages 230 - 231, 5th edition, 1988.

[7] F. Bergman. *Tribological nature of squealing disc brakes*. PhD thesis, University of Uppsala, Sweden, 1998.

[8] F. Bergman, M. Eriksson, and S. Jacobson. The effect of Cu_2S solid lubricant addition, and varying density, on the occurrence of brake squeals for one low-metal, organic type friction material. In *The 17th Annual SAE Brake Colloquium and Engineering Display*, pages 137 – 143. SAE, 1999.

[9] F. Bergman, M. Eriksson, and S. Jacobson. Influence of disc topography on generation of brake squeal. *Wear*, 225-229:621 – 628, 1999.

[10] F. Bergman, M. Eriksson, and S. Jacobson. A software-based measurement system for test and analysis of automotive brake squeal. *TriboTest*, 5(3):265 – 275, 1999.

[11] F. Bergman, M. Eriksson, and S. Jacobson. The effect of reduced contact area on the occurrence of brake squeals for an automotive brake pad. *Proc Instn Mech Engrs Part D, J. of Automobile Engineering*, 214:561 – 568, 2000.

[12] F. Bergman, L. Gudmand-Høyer, M. Eriksson, and S. Jacobson. The effect of Cu_2S, PbS, Sb_2S_3 solid lubricants on the occuuence of brake squeals for three automotive brake pad matrix types. In *Nordtrib '98, Proc. of the 8th Int. Conf. on Tribology, Vol. 2*, pages 665 – 672, 1998.

[13] P. J. Blau. Compositions, functions, and testing of friction brake materials and their additives. Technical Report ORNL/TM-2001/64, Oak Ridge National Laboratory, September 2001.

[14] P. J. Blau. Experimental aspects of friction research on the macroscale. In B. Bhushan, editor, *Fundamentals of Tribology and Bridging the Gap between Macro- and Micro/Nanoscales*, pages 261 – 278. Luwer Academic Publishers, 2001.

[15] P. J. Blau. The significance and use of the friction coefficient. *Tribology International*, 34:585 – 591, 2001.

[16] Bosch. *Automotive Handbook*. Robert Bosch GmbH, ISBN 0-7680-1513-8, 6th edition, 2004.

[17] F. P. Bowden and D. Tabor. *The Friction and Lubrication of Solids*. Oxford University Press, ISBN 0-19-850777-1, Reprint 1986.

[18] J. Brecht. Properties of friction materials. In *Fortschritts-Berichte VDI, Reihe 12: Verkehrstechnik/Fahrzeugtechnik, Band 556*, pages 1 – 23, October 2003.

[19] J. Brecht, A. Elvenkemper, J. Betten, U. Navrath, and J. B. Multhoff. Elastic properties of friction materials. *SAE 2003-01-333*, 2003.

[20] B. Breuer and K. H. Bill. *Bremsenhandbuch*, chapter 23 & 25, pages 350 – 357. Vieweg & Sohn Verlag, ISBN 3-528-03952-3, 2003.

[21] I. N. Bronstein, K. A. Semendjajew, G. Musiol, and H. Mühlig. *Taschenbuch der Mathematik*. Verlag Harri Deutsch, ISBN 3-8171-2002-8, 2nd edition, 1995.

[22] R. J. Canali and A. Tamagna. Evaluation of properties of disc and pad materials and their relation with disc brake noise - an experimantal investigation. *SAE 2002-01-2604*, pages 163 – 171, 2002.

[23] D. Chan and Stachowiak. Review of automotive brake friction materials. *Proceedings of the Institution of Mechanical Engineers D, Journal*, 218, no. D9:953 – 966, 2004.

[24] F. Chen, M. K. Abdelhamid, P. Blaschke, and J. Swayze. On automotive disc brake squeal part III: Test and evaluation. *SAE 2003-01-1622*, 2003.

[25] F. Chen, R. L. Quaglia, and C. A. Tan. On automotive disc brake squeal part I: Mechanisms and causes. *SAE 2003-01-0683*, 2003.

[26] C. A. Coulomb. Theorie des machines simples, en ayant egard au frottement de leurs parties, et la roideur des cordages. 161 - 331, Memoires de Mathematiques et de hysique de l'Académie des Sciences, Paris, 1785 10.

[27] D. A. Crolla and A. M. Lang. Brake noise and vibration - the state of the art. In *Proceedings of the 18th Leeds-Lyon Symp. on Vehicle Tribology, Tribology Series 18, Leeds*, pages Paper VII (i), pages 165 – 174. Dowson, D. and Taylor, C. M. and Godet, M., 1991.

[28] H. Czichos and K.-H. Habig. *Tribologie-Handbuch*. Friedr. Vieweg & Sohn, ISBN 3-528-16354-2, 2nd edition, 2003.

[29] L. da Vinci. *Notebooks and manuscripts, prepared in the late 1400s*. as described in [32].

[30] R. Deike, A. Engels, F. Hauptvogel, P. Henke, K. Röhring, W. Siefer, H. Werning, and D. Wolters. Gußeisen mit Lamellengraphit - Eigenschaften und Anwendung. *Konstruieren und Giessen*, 2:19 – 41, 25. Jahrgang, 2000.

[31] S. Dörsch. *Periodische Veränderung lokaler Kontaktgrößen in Reibpaarungen trockenlaufender Bremsen*. PhD thesis, VDI Verlag Düsseldorf, 2004.

[32] D. Dowson. *History of tribology*. Professional Engineering Publishers, London, ISBN 1-86058-070-X, 2nd edition, 1998.

[33] K. B. Dunlap, M. A. Riehle, and R. E. Longhouse. An investigative overview of automotive disc brake noise. *SAE 1999-01-0142*, pages 1 – 8, 1999.

[34] M. Eriksson. *Friction and contact phenomena of disc brakes related to squeal*. PhD thesis, University of Uppsala, Sweden, 2000.

[35] M. Eriksson, F. Bergman, and S. Jacobson. Surface characterisation of brake pads after running under silent and squealing conditions. *Wear*, 232:163 – 167, 1999.

[36] M. Eriksson, F. Bergman, and S. Jacobson. A study of initialization and inhibition of disc-brake squeal. In D. Barton and Earle S., editors, *Brakes 2000 Automotive braking - Technologies for the 21st Century, Leeds, UK*, pages 29 – 38. Professional Engineering Publishing, 2000.

[37] M. Eriksson, F. Bergman, and S. Jacobson. On the nature of tribological contact in automotive brakes. *Wear*, 252/1-2:26 – 36, 2002.

[38] M. Eriksson and S. Jacobson. Tribological surfaces of organic brake pads. *Tribology International*, 33:817 – 827, 2000.

[39] M. Eriksson and S. Jacobson. Friction behaviour and squeal generation of disc brakes at low speeds. *Proc Instn Mech Engrs Part D, J. of Automobile Engineering*, 215:1245 – 1256, 2001.

[40] M. Eriksson, J. Lord, and S. Jacobson. Wear and contact conditions of brake pads - dynamical in-situ studies of pad on glass. *Wear*, 249:272 – 278, 2001.

[41] M. Eriksson, A. Lundqvist, and S. Jacobson. A study of the influence of humidity on the friction and squeal generation of automotive brake pads. *Proc Instn Mech Engrs Part D, J. of Automobile Engineering*, 215:329 – 342, 2001.

[42] D. J. Ewins. *Modal Testing: Theory and Practice*. Research Studies Press, London, 1984.

[43] P. Filip, Z. Weiss, and D. Rafaja. On friction layer formation in polymer matrix composite materials for brake applications. *Wear*, 252:189 – 198, 2002.

[44] J. Flint and J. Hultén. Lining-deformation-induced modal coupling as squeal generator in a distributed parameter disc brake model. *Journal of Sound and Vibration*, 254(1):1 – 21, 2002.

[45] GfT. Arbeitsblatt 7, Tribologie. Technical report, Gesellschaft für Tribologie, 2002.

[46] Y. Goto, T. Amago, K. Chiku, T. Matsushima, and Y. Ishihara. Experimental identification method for interface contact stiffness of FE model for brake squeal. In D. C. Barton and A. Blackwood, editors, *Braking 2004, Vehicle Braking and Chassis Control*. Professional Engineering Publishing Ltd., London, ISBN 1-86058-464-0, July 2004.

[47] J. A. Greenwood and J. B. P. Williamson. Contact of nominally flat surfaces. *Proc. Royal Soc. London*, pages 300 – 319, 1966.

[48] L. Gudmand-Høyer, A. Bach, G. T. Nielsen, and P. Morgen. Tribological properties of automotive disc brakes with solid lubricants. *Wear*, 232:168 – 175, 1999.

[49] T. Hamabe, K. Yamazaki, H. Yamada, H. Matsui, S. Nakagawa, and M. Kawamura. Study of a method for reducing drum brake squeal. *SAE 1999-01-0144*, pages 53 – 60, 1999.

[50] R. Hecht-Basch, P. Sanders, D. Hartsock, and C. Evans. Correlation of lining properties with brake pedal feel. *SAE 2002-01-2602*, 2002.

[51] M. Hiller. Nanotribologische Untersuchungen mit dem Rasterkraftmikroskop. Master's thesis, Universität Karlsruhe (TH), 2002.

[52] J. Hultén. Some drum brake squeal mechanisms. *Proceedings of the 1995 Noise and Vibration Conference, Vol. 1, SAE Paper 951280*, pages 377 – 388, 1995 (also or as long version in [53]).

[53] J. Hultén. *Drum Brake Squeal*. PhD thesis, Chalmers University of Technology, 1998.

[54] R. A. Ibrahim. Friction-induced vibration, chatter, squeal and chaos. *Applied Mechanics Reviews*, 47(7):209 – 253, 1994.

[55] International Standard. Road vehicles - brake linings - compressive strain test method. *ISO 6310*, 2001.

[56] H. P. Jost. *Lubrication (Tribology) Education and Research - A report on the presentposition and industry's needs*. Her Majesty's Stationery Office, London, 1966.

[57] M. Kaido and Y. Sasaki. Harmonization activities on ISO and JIS standards (compressibility) for brake linings in Japan. *SAE 2001-01-3152*, 2001.

[58] H. A. Kemmer. *Investigation of the Friction Behavior of Automotive Brakes through Experiments and Tribological Modeling*. PhD thesis, Universität Paderborn / Robert Bosch GmbH, Schriftenreihe ISBN 3-00-011230-8, 2002.

[59] N. M. Kinkaid, O. M. O'Reilly, and P. Papadopoulos. Automotive disc brake squeal. *Journal of Sound and Vibration*, 267:105 – 166, 2003.

[60] A. M. Lang and T. P. Newcomb. The vibration characteristics of squealing brakes. *FISITA Congress, Paper 905170*, pages 250 – 257, 1990.

[61] Y. S. Lee, P. C. Brooks, D. C. Barton, and D. A. Crolla. A study of disc brake squeal propensity using a parametric finite element model. *ImechE Conference on Vehicle Noise and Vibration*, pages 191 – 201, 1998.

[62] G. D. Liles. Analysis of disc brake squeal using finite element methods. *SAE 891150*, pages 249 – 257, 1989.

[63] K. Magnus and K. Popp. *Schwingungen*. B. G. Teubner GmbH, ISBN 3-519-42301-4, 2002.

[64] K. Mao, Y. Sun, and T. Bell. Contact mechanics of engineering surfaces: State of the art. *Surface Enigneering*, Vol. 10(No. 4):297 – 306, 1994.

[65] W. Mendenhall and T. Sincich. *A Second Course in Statistics - Regression Analysis*. Prentice Hall, USA, 5th edition, 1996.

[66] H. R. Mills. Brake squeak. Technical report, Technical Report 9000 B. Institution of Automobile Engineers, 1938.

[67] P. Mody, W. Rumold, F. Attia, and S. Ansmann. Mojacar and Los Angels City Traffic vehicle testing: A comparison & analysis of subjective ratings and objective measurements. *SAE 2002-01-2600*, 2002.

[68] J. E. Mottershead and S. N. Chan. Brake squeal - an analysis of symmetry and flutter instability. In R. A. Ibrahim and A. Soom, editors, *ASME Conf. on Friction-Induced Vibration, Chatter, Squeal and Chaos, DE-vol. 49*, pages 87 – 97, 1992.

[69] D. Nguyen and J. Taylor. Continuous process for manufacturing of friction materials. In *Bridging the Centuries with Sampe's Materials and Process Technology, Book 2, ISBN 0-938994-86-7*, pages 2307 – 2317. Society for the Advancement of Material and Process Engineering, 2000.

[70] K.-H. Oehl and H.-G. Paul. *Bremsbeläge für Straßenfahrzeuge*. Verlag Moderne Industrie, ISBN 3-478-93049-9, 2nd edition, 1991.

[71] W. Österle and D. Bettge. A comparison of methods for characterizing brake lining surfaces. *Praktische Metallgraphie*, 41:494 – 505, 2004.

[72] W. Österle, I. Dörfel, W. Gesatzke, H. Rooch, and I. Urban. A characterization of tribological contacts with FIB and TEM. *Praktische Metallographie*, 41:166 – 179, 2004.

[73] W. Österle, I. Urban, H. Kleinlein, A. Loemba, and S. Trepte. Reibschichtbildung und mögliche Einflüsse auf Reibschwingungen bei einem Bahn-Bremsbelag. In *Reibung und Schwingungen in Fahrzeugen, Maschinen und Anlagen, Tagung Hannover, ISBN 3-18-091736-9*, pages 283 – 296. VDI Verlag GmbH, Nov. 2002.

[74] H. Ouyang, Q. Cao, J. E. Mottershead, T. Treyde, and M. P. Cartmell. Modelling and simulation of the vibration and squeal of a car disc brake. In D. Barton and B. Shilton, editors, *Braking 2002, From the Driver to the Road*. Professional Engineering Publishing Ltd., London, ISBN 1-86058-371-7, July 2002.

[75] B. N. J. Persson. *Sliding Friction: physical principles and applications*. Springer-Verlag, ISBN 3-540-63296-4, 1998.

[76] S. K. Rhee, Tsang H. S., and Wang Y. S. Friction-induced noise and vibration of disc brakes. *Wear*, 133:39 – 45, 1989.

[77] J. W. Richmond, T. K. Kao, and M. W. Moore. The development of computational analysis techniques for disc brake pad design. In D. C. Barton, editor, *Advances in Automotive Braking Technology*. MEP Ltd., London and Bury St. Edmunds, ISBN 1-86058-039-4, 1996.

[78] H. Rinne. *Taschenbuch der Statistik*. Wissenschaftlicher Verlag Harri Deutsch, Frankfurt, 3rd edition, 2003.

[79] A. Rinsdorf. *Theoretische und experimentelle Untersuchungen zur Komfortoptimierung von Scheibenbremsen*. PhD thesis, Universität-Gesamthochschule Siegen, 1996.

[80] P. G. Sanders, T. M. Dalka, and R. H. Basch. A reduced-scale brake dynamometer for friction characterization. *Tribology International*, 34:609 – 615, 2001.

[81] Ch. Schmalfuß. *Theoretische und experimentelle Untersuchungen von Scheibenbremsen*. PhD thesis, Universität Karlsruhe (TH), VDI Verlag Düsseldorf, 2002.

[82] H. A. Sherif. Parameters affecting contact stiffness of nominally flat surfaces. *Wear*, 1:113 – 121, 1991.

[83] K. Shin. Analysis of friction induced disc brake noise using simple mathematical models. *Noise & Vibration Worldwide*, 35:22 – 27, 2004.

[84] H. R. E. Siller. *Non-linear modal analysis methods for engineering structures*. PhD thesis, Imerial College London, 2004.

[85] R. T. Spurr. A theory of brake squeal. *Proceedings of the Institution of Mechanical Engineers*, 1:33 – 40, 1961.

[86] U. Stolz, K.-H. Hach, and H. A. Kemmer. Untersuchungen am Tribosystem Bremsbelag/Bremsscheibe mit einem Modellprüfstand. In *Reibung und Schwingungen in Fahrzeugen, Maschinen und Anlagen*, pages 117 – 134. VDI Verlag GmbH, ISBN 3-18-091736-9, Düsseldorf, November 2002.

[87] T. R. Thomas. *Rough Surfaces*. Imperial College Press, ISBN 1-86094-100-1, 2nd edition, 1999.

[88] T. R. Thomas and R. S. Sayles. Stiffness of machine tool joints: A random process approach. *Journal of Engineering for Industry. Transactions of the ASME*, pages 250 – 256, 1977.

[89] J. K. Thompson and C. M. Fudge. One year's experience utilizing the SAE J2521 brake noise test procedure. In D. Barton and B. Shilton, editors, *Braking 2002, From the Driver to the Road*. Professional Engineering Publishing Ltd., London, ISBN 1-86058-371-7, July 2002.

[90] J. K. Thompson, B. Lowe, M. Doescher, D. Rhode, and M. Rogus. Brake squeal noise measurement repeatability between dynamometers. In D. C. Barton and A. Blackwood, editors, *Braking 2004, Vehicle Braking and Chassis Control*. Professional Engineering Publishing Ltd., London, ISBN 1-86058-464-0, July 2004.

[91] H.-J. Thun. Bremsenprüfstand mit Schwungmassensimulation. *Elekro Anzeiger*, 34 (6):49 – 53, 1981.

[92] S. Trepte. *Bewertung von Reibwerkstoffen für Fahrzeugbremsen*. PhD thesis, Otto-von-Guericke-Universität Magdeburg, 2004.

[93] A. Tuchinda. *Development of Validated Models for Brake Squeal Predctions*. PhD thesis, Imperial College London, 2003.

[94] US Working Group on Brake Noise. SAE J2521 - disc brake dynamometer squeal matrix. Technical report, SAE International, Warrendale, PA, USA, 2000.

[95] J. Wallaschek, K.-H. Hach, U. Stolz, and P. Mody. A survey of the present state of friction modelling in the analytical and numerical investigation of brake noise generation. In *ASME Design Engineering Technical Conference, Las Vegas*, 1999.

[96] K. Willner. Kontinuums- und Kontaktmechanik. *Springer-Verlag, ISBN 3-540-43529-8*, 2003.